Integrated mechanisms of cellular behavior: Cell biology and biological physics of the slime mold *Physarum polycephalum*

Dissertation submitted towards the degree
Doctor of Natural Sciences
– Dr. rer. nat. –

Dipl. Biol. Christina Oettmeier

Bremen, September 24, 2019

Referees: Prof. Dr. Hans-Günther Döbereiner
Prof. Dr. Wolfgang Marwan

Universität Bremen

For strange effects and extraordinary combinations we must go to life itself, which is always far more daring than any effort of the imagination.

—Sir Arthur Conan Doyle

Abstract

In its natural habitat, the plasmodial slime mold *Physarum polycephalum* forms extensive transport networks that can reach up to square meters in surface area. Under laboratory conditions, small spherical microplasmodia can be produced, which are only several hundred micrometers in diameter. These fragments can be used to study the reorganization of the network, the morphology of which depends on environmental factors. When nutrients are scarce, *P. polycephalum* forms fan-shaped, polarized mesoplasmodia with an internal vein system instead of a stationary network with reticulated external tubes. Mesoplasmodia are migrating, autonomous and unconnected subunits, which represent a starvation-induced foraging strategy. This thesis demonstrates that the number of mitochondria correlates with the metabolic state of the cell: In the absence of glucose, the slime mold is forced to switch to different metabolic pathways, which occur inside the mitochondria. A catabolic cue which stimulates mitochondrial biogenesis is discussed.

A detailed and quantitative ultrastructural description of the three main morphotypes, macro-, meso-, and microplasmodia, is provided in this thesis. These investigations provide the basis for physical models of the system. Furthermore, the present work discusses the unique motility mechanisms of mesoplasmodia: At the posterior end, lateral contraction waves pump endoplasm through the veins towards the extending front. The internal flow channel system forms a cascade of forks, which acts as a low-pass filter and causes the isotropic extension of the cellular front. This effect is analyzed by a lumped parameter model, based on the analogy of hydro-dynamic phenomena to electric circuits. The direction of locomotion is controlled via an asymmetry in the elasticity of the actin cortex. A softness gradient exists along the anterior-posterior axis, with the front being the most elastic.

The slime mold is capable of constructing networks optimized for transport, and exhibits other sophisticated and complex behaviors such as decision-making, efficient foraging, and memory. The structure of the cell and its dynamics are strongly interconnected. Large-scale patterns and other phenomena, which can be observed on the entire network, are based on locally occurring cellular and molecular processes. The interplay of these mechanistic interactions, and especially the resulting intracellular fluid flow, is hypothesized to underlie the information processing which is the basis of complex behavior in *P. polycephalum*. The ultrastructure of the cell is the substrate on which cellular computing takes place. Therefore, an understanding of the unique cell biology of the slime mold is necessary to study emergent phenomena such as minimal cognition.

Contents

Acknowledgements

I would like to thank **Prof. Dr. Hans-Günther Döbereiner** for supervising my PhD project, for the numerous fruitful discussions, and his enthusiasm for science in general and my work in particular. He gave me the opportunity to learn, and grow as a person and as a scientist.

I also want to thank **Prof. Dr. Wolfgang Marwan** for his interest in my work, for a very welcome positive feedback and for being the second examiner of my thesis. Thanks also for providing me with the slime mold and all the good advice.

Furthermore, I want to thank my past and present lab mates:
Dr. Erik Bernitt, **Dr. Adrian Fessel**, **Malte Ohmstede**, **Tanja Deppner** and soon-to-be doctors **Julia Lange** and **Jonghyun Lee**. It would not have been the same without you! And thanks to Julia and Adrian for proofreading.

I am also very grateful to **Anja Bammann** for her excellent lab work, shared affection for the slime molds, and constant supply of chocolate in times of need. Furthermore, I want to thank **Anna Piórecka-Ecken** for excellent secretarial work.

Finally, I owe everything to my family. None of this would have been possible without your love and support.

List of Figures

List of Tables

Chapter 1

Introduction

1.1 Preface

The giant unicellular, multi-nucleated protist *Physarum polycephalum* lacks a brain or even rudimentary neural structures. Nonetheless, the slime mold shows seemingly 'intelligent' behavior. It can, for example, solve mazes and connect multiple food sources via the shortest pathway. It makes decisions, can evaluate food sources based on their nutrient composition, and even possesses a memory, both intra- and extracellular. For all intents and purposes, the slime mold behaves in the same way as life-forms with a much higher degree of information-processing sophistication.

This raises the question of how *P. polycephalum* achieves such a complex behavioral and information-processing repertoire. A human brain, the ultimate cognitive organ, consists of approximately 86 billion neurons, which are highly interconnected by innumerable synapses. There is a profound scientific uncertainty about just how cognition and intelligence arise. Popular hypotheses are the coordination of brain waves produced by neurons in the cortex firing in synchrony [Lundqvist et al., 2018], and plasticity [Santarnecchi and Rossi, 2016], which means the response of brain activity patterns to changes. Another hypothesis is the network neuroscience theory [Barbey, 2018], which states that intelligence arises from communication of the whole brain with itself, regarding the brain as a dynamic network of interconnected elements. Intelligence and cognition emerge from the interaction among the many elements of the brain, from molecular foundations to higher-order structures. Connectivity, at both the structural and functional level, leads to emergent behavior. The understanding of connectivity in complex systems is crucial for the investigation of emergence [Turnbull et al., 2018]. Neural activity patterns, associated e.g. with learning, can arise through self-organization processes within the network of the brain [Hütt et al., 2014].

In the brain, basic neurological processes lead to conscious thought. It is a central hypothesis of this thesis that equivalent cell biological mechanisms and processes lead to

the complex behavior and basic cognition observed in the slime mold. In other words, the fact that forms of elementary cognition and learning have been discovered in non-neural organisms implicates convergent evolution. Elementary cognitive behaviors can be found throughout the phylogenetic tree, including fungi, ciliates and prokaryotes [van Duijn, 2017]. This hints at the independent, convergent evolution of cognitive phenomena, resulting in analogous structures and mechanisms. Section 6.3 provides a more in-depth discussion of the evolution of cognitive complexity. A classic example for convergent evolution is the recurrent development of flight: This capacity has independently evolved in flying insects, birds, bats, and even pterosaurs. For an informative and comprehensive overview of the convergent evolution of cognitive complexity, the reader is referred to the theme issue "Convergent minds: the evolution of cognitive complexity in nature" [Foster, 2017]. The rich cell biology and ultrastructure of *P. polycephalum*, which still has much to reveal, is organized in highly interconnected physiological networks or circuits. So, in this thesis, it is presumed that cellular cognition and intelligence are emergent properties of these non-neural networks. This biophysical and biochemical circuitry is relatively under-studied in *P. polycephalum*, and thus, this thesis delves into details of the ultrastructure and connects the metabolic and motile network. Another focus is put on the construction of a fluid dynamic model. The application of physical principles to explain behavior will lead to the understanding of general, universal principles behind such cognitive tasks as decision-making in both neural and non-neural organisms.

1.2 Thesis outline

The aim of this thesis is to contribute to the understanding of the slime mold's complex behavior in a mechanistic approach. Overarching topics are amoeboid locomotion and fluid dynamic signal processing, as well as the metabolic control of foraging. These investigations are necessary for the further studies of emergent behavior and minimal cognition. A new growth mode of *P. polycephalum*, the mesoplasmodium, has been extensively studied and established as a model system during the course of this work [Lee et al., 2018]. Mesoplasmodia are tadpole- or fan-shaped, millimeter-sized units with a stable and defined morphology, a persistent shape, and move on straight trajectories for hours.

An overview of the past research efforts on *P. polycephalum* is given in chapter 2. Here, the slime mold is introduced as a model organism, and general information about its biology, systematics and life cycle will be provided.

Chapter 3 informs about a detailed investigation of the ultrastructure of different growth forms (micro-, meso- and macroplasmodia) by transmission electron microscopy (TEM), scanning electron microscopy (SEM), light microscopy, and fluorescence microscopy of F-actin. The main focus is the cytoskeleton, and for the first time, we have described actin asters in migrating mesoplasmodia. These detailed investigations of cellular ultra-

structure and morphology are the basis for the analysis of viscoelastic and rheological measurements. Furthermore, these data also provide structural details for the many physical models that have been constructed for the understanding of locomotion. An investigation of the ultrastructure of mesoplasmodia is presented here for the first time. Micromechanical measurements of the viscoelastic properties of microplasmodia have also been performed during the course of this thesis [Fessel et al., 2017]. By micromechanical indentation, parameters such as Young's modulus, Poisson's ratio, and relaxation times associated with viscous processes were measured. Given the importance of cell mechanics in the emergence of complex behavior, these investigations essentially characterize the substrate on which fluid dynamic computing takes place.

Whereas the research presented in chapter 3 is mostly based on static, i.e., fixed samples of slime molds, the data in chapter 4 take into account the dynamics of living slime molds. Spatio-temporal analyses of oscillations were performed, and the fluid dynamics of the endoplasm was investigated. The analysis of cell speed, cell shape dynamics, and internal flow patterns lead to the construction of a novel lumped parameter model, which can explain the polarization and onset of migration of mesoplasmodia. The model is based on the electronic-hydraulic analogy. Because certain concepts in electrical circuits bear a strong similarity to fluid flow in networks of compliant tubes, the mesoplasmodium can be modeled as a circuit consisting of several low-pass filters. This filter cascade demonstrates an efficient and fast way in which signals can be processed. The model is based upon the data presented in chapter 3.

Chapter 5 is a further investigation of the newly described mesoplasmodia. They are only created during glucose deprivation, and an investigation of their mitochondria showed significantly increased numbers of mitochondria as compared to non-starved plasmodia. It is hypothesized that the number of mitochondria correlates with the metabolic state of the cell: When glucose is absent, the slime mold is forced to switch to different metabolic pathways, which occur inside mitochondria. The role of AMP-activated protein kinase (AMPK) as a metabolic switch during glucose-deprivation in *P. polycephalum* is discussed here for the first time.

In chapter 6, a synthesis of the main findings of this thesis is presented. Furthermore, the connection between cell biology and behavior is elaborated on, and the concept of a "network of networks" is presented.

Supplementary texts and figures are provided in the appendix (chapter 7). A declaration of own contribution to the presented publications within this thesis (chapters 2, 3, 4 and 5) can also be found in the appendix (section 7.4).

1.3 *Physarum polycephalum* in a nutshell

The term 'amoeba' describes a wide variety of cells or unicellular organisms which are capable of drastically altering their shape. By this definition, amoeba are a polyphyletic group, which means that they do not share a common ancestor. Instead, amoeboid organisms can be found in every major lineage of eukaryotes; among the protozoa, but also in fungi, algae, and animals. One amoeboid model organism is the giant acellular slime mold *P. polycephalum* (see figure 1.1), which is the subject of this thesis.

P. polycephalum belongs to the myxomycetes (commonly known as acellular or plasmodial slime molds), a class of eukaryotic amoebae containing approximately 900 species. They are considered as a monophyletic taxon within the Amoebozoa [Leontyev and Schnittler, 2017; Leontyev et al., 2019]. Plasmodial slime molds are closer related to the animal-fungal clade (which occurred approximately 1.54 billion years ago) than are green plants [Baldauf and Doolittle, 1997], indicating that mycetozoa can be regarded as a sister group to animals and fungi. Thus, slime molds are evolutionary ancient and primeval life forms, arriving hundreds of millions of years before animals or plants.

P. polycephalum can be found in temperate forests, where it inhabits moist, shaded areas and decaying plant matter like deadwood debris and leaf litter. The species is distributed worldwide [Schnittler et al., 2017]. During the reproductive phase, which is triggered by the activation of a phytochrome photoreceptor [Glöckner and Marwan, 2017], the slime mold develops haploid spores through meiosis and rearrangement of cellular components. These small airborne spores can be widely dispersed by wind, giving the slime mold access to a wide range of habitats. *P. polycephalum*'s complex life cycle is given in figure 2.2. During the diploid, vegetative phase, *P. polycephalum* forms planar networks (termed macroplasmodia) which can reach sizes of more than $1\,\mathrm{m}^2$ (see for example [Hausmann and Stiemerling, 1997] and [Stockem and Brix, 1994]), making it the largest known single-celled organism. Macroplasmodia with diameters of 5 to 7 cm can have millions of nuclei [Kalyanasundaram, 2004; Thiriet, 2018].

However, for many research endeavors, simpler model systems are needed. A distinctive feature of *P. polycephalum* is its capability to be fragmented. It is therefore possible to 'downscale' the organism by transferring it to liquid shaking culture. Subjected to shear forces, a macroplasmodium breaks up to form so-called microplasmodia, small spherical units ranging from 100 to 500 µm in diameter [Bernitt et al., 2010]. This feature was found to be a key asset for the research on *P. polycephalum* during this thesis, because microplasmodia are easy to cultivate and handle, but most importantly, they are reproducible and homogeneous growth forms. A macroplasmodium can also be cut into pieces, which become self-consistent organisms after a short membrane regeneration time. However, the number of nuclei and the composition of the cytoplasm are unknown and may vary between growth fronts and veins, so that random cut-outs do not represent

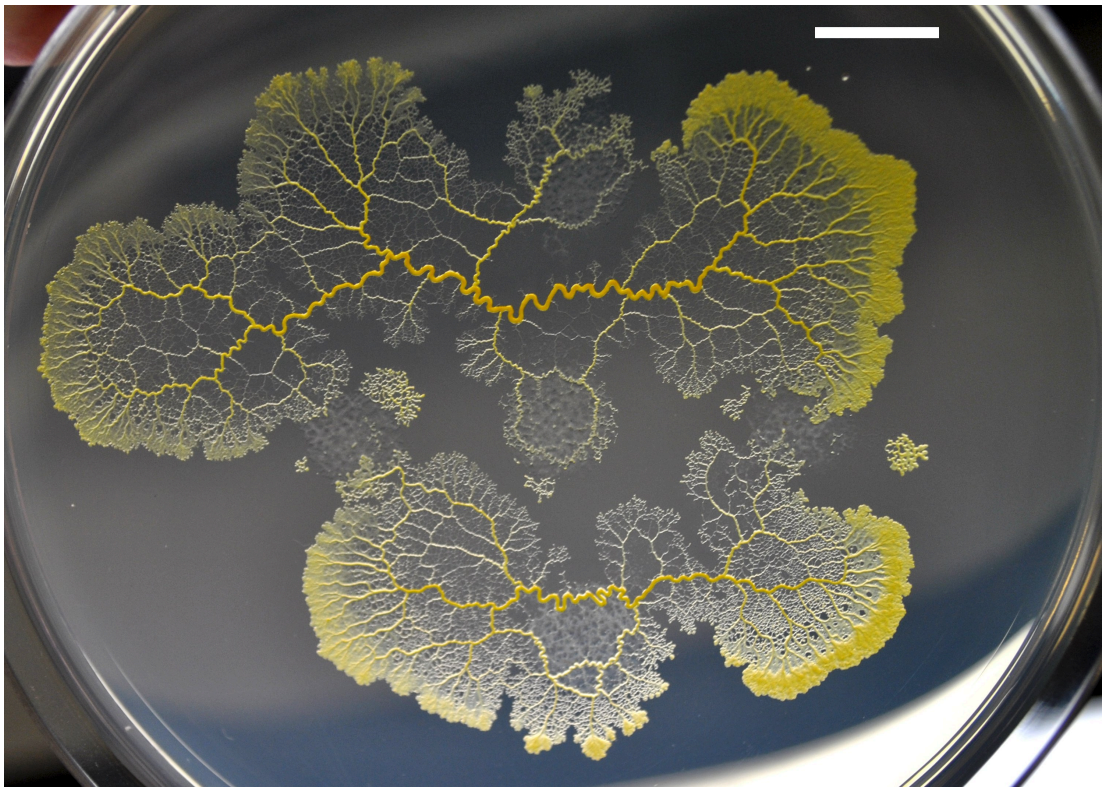

Figure 1.1: Macroplasmodium of *P. polycephalum* growing on nutrient-containing agar in a Petri dish with a diameter of 9 cm. It covers an area of $\sim$25 cm^2. The macroscopic morphology of the organism can be seen, consisting of veins in the central part and growth fronts in the periphery of the plasmodium. Scale bar = 1 cm.

the whole cell nor are they reproducible across experiments. Microplasmodia, on the other hand, have a constant protein to DNA ratio [Aldrich and Daniel, 1982a]. Thus, the value of microplasmodia lies in their suitability as reproducible starting points for experiments. A more thorough description of microplasmodia is given in section 3.4.4. Microplasmodia can be plated onto a solid agar surface and fuse with each other, thereby creating new networks or, depending on culture age and glucose availability, medium-sized migrating units, termed mesoplasmodia. For an overview of the different morphotypes, see section 3.2 and figure 3.1.

1.4 Amoeboid locomotion and 'intelligent' behavior

Like most eukaryotic cells, amoeba are characterized by a special type of movement termed amoeboid locomotion, which involves pronounced cytoplasmic fluid flow. This pattern of cell movement, which resembles the locomotory mode of free-living amoeba such as the eponymous *Amoeba proteus*, involves the formation of pseudopods, lobopods,

adhesions to the substrate, and translocation of the cell body [Rieu et al., 2009, 2015; Fukui, 2002]. Although amoeboid locomotion is a common type of movement, its exact mechanism is still unknown [Lämmermann and Sixt, 2009]. However, since many unicellular organisms as well as some cells of multicellular organisms (e.g. leukocytes) are capable of amoeboid locomotion, it is well possible that different sets of mechanisms give rise to the same phenomenon. Processes on the molecular scale play a role as well as processes on the scale of a whole cell, which usually starts at tens of micrometers. The process of amoeboid locomotion is intimately coupled with the flow of cell membranes and the cortical cytoskeleton [Grebecki, 1994; Paluch and Raz, 2013; Álvarez-González et al., 2015], but also with the flow of cytoplasm [Mogilner and Manhart, 2018; Allen and Allen, 1978]. Since *P. polycephalum* is a huge cell, ranging from a few hundred micrometers up to a square meter, there is a great wealth of large-scale fluid dynamics and cell mechanics phenomena in effect, which can usually not be found in smaller cells.

The above-mentioned processes which contribute towards locomotion are mechanical in nature or based on the mechanical properties of the cell. Cell mechanics are therefore crucial for locomotion, intracellular transport, cell division and the integration and distribution of information [Fletcher and Mullins, 2010]. Thus, in order to understand the behavior, function and emergent properties of cells, the mechanics, dynamics and interactions of the structural components need to be investigated. This includes membranes, organelles, cytoplasm and the cytoskeleton. These components interact to give rise to some fascinating emergent properties, like complex behavior, which are among the main new research topics regarding *P. polycephalum*. Despite lacking even rudimentary neuronal structures, *P. polycephalum* shows seemingly 'smart' behavior. It can, for example, solve mazes [Nakagaki et al., 2000] and connect multiple food sources via the mathematically shortest path [Nakagaki et al., 2004a]. Furthermore, the slime mold is capable of making complex decisions [Beekman and Latty, 2015], evaluates food sources based on their nutrient composition [Dussutour et al., 2010], and even possesses a memory [Reid et al., 2012, 2013]. These features are usually associated with life-forms which have a much higher degree of information-processing sophistication. The underlying functions are not neuron-based, but are emergent phenomena resulting from mechanochemical processes that are connected to the cytoskeleton and the fluid dynamics of the cytoplasm. Investigations of the ultrastructure and the dynamics of cell locomotion, a process which is intimately linked to the actomyosin cytoskeleton, reveal an alternative to neurological information processing: Sensory input from the environment is processed, and the information is then distributed as fluid dynamic oscillations throughout the network.

The slime mold carries out complex sequences of action, which often appear intentional, motivated and seem 'intelligent'. However, these reactions to external or internal stimuli, as well as the decisions the organism makes, are not in the same category as those of higher animals. Whereas the behavior of higher animals is controlled by a nervous

system, slime molds and other protozoans lack even basic neural structures. However, one cannot dismiss the observed behavior as trivial or random, because complex (and experimentally confirmed) traits such as memory, learning, and risk assessment can only occur if the cell contains a fairly sophisticated information processing machinery. Indeed, a candidate for this non-neural information processing device is a network of intracellular signaling reactions, as proposed in figure 1.2. Those protein-based biochemical circuits

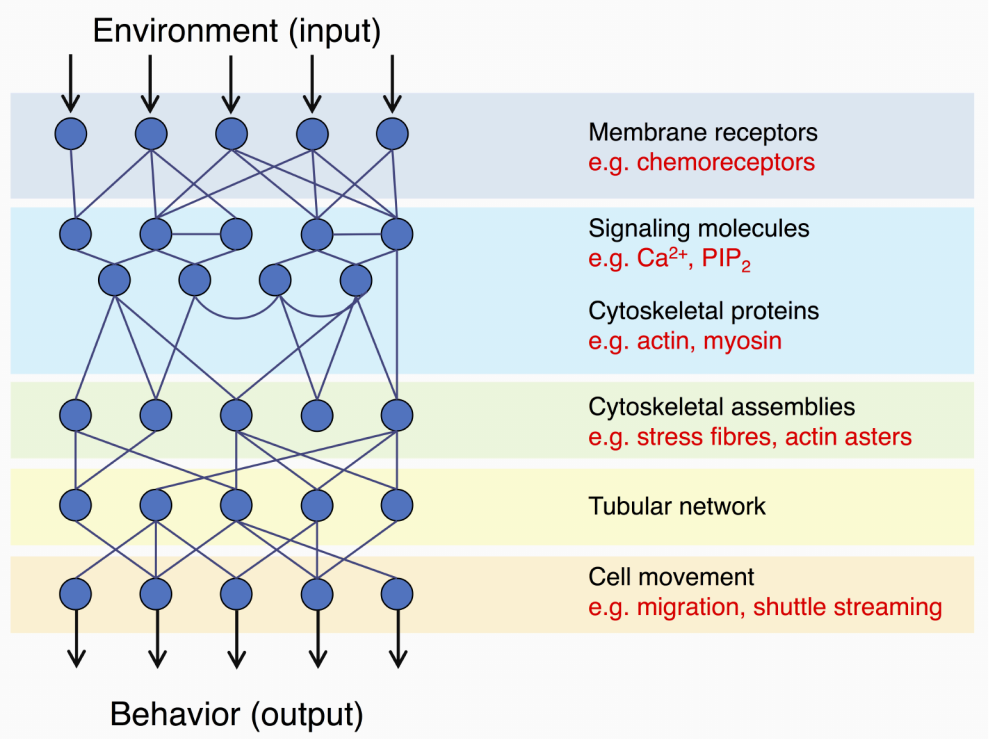

Figure 1.2: Proposed parallel network of the motile physiology of *P. polycephalum*. Signals from outside the cell are received by membrane receptors, and trigger intracellular signalling cascades, which in turn affect the cytoskeleton and its superstructures. This, in turn, generates observable behavior such as chemotactic locomotion. We have described actin asters, a special actin superstructure, for the first time in *P. polycephalum* (see chapter 3). Adapted and redrawn from [Bray, 2001].

can serve an analog function to a nervous system (this will be discussed in more detail in chapter 6). It has been speculated that the cytoskeleton plays a major role in the information-processing of *P. polycephalum* [Mayne et al., 2015]. Figure 1.2 resembles an artificial neural network, which loosely models the neurons of a brain, organized in layers. This suggests a different 'substrate' for the processing of information: Whereas in the brain this task is performed by interconnected neurons and glial cells, the slime mold makes use of its biochemical machinery and cellular components as outlined above. This thesis aims to contribute to the investigation of this substrate, see for example

chapter 3. Furthermore, and possibly unique to relatively large amoeba, is the concept of hydrodynamic signal processing, which has recently been referred to briefly [Alim et al., 2017] and which will be discussed in more detail in chapter 4 of this thesis.

A crucial question is whether it is possible that parallels exist between the cognitive capacities of protozoans and multicellular organisms. This furthers the question whether those parallels just concern the level of functional analogue, but extend in fact to the level of (molecular) mechanisms, e.g. the presence of equivalent signaling pathways. In the case of *P. polycephalum*, this would be especially interesting since slime molds are evolutionary old and primal life forms [Baldauf and Doolittle, 1997]. In addition to amoeboid locomotion, *P. polycephalum* has the potential to become a quantitative behavioral model. Its relative simplicity allows for the investigation of several functional levels, reaching from molecular networks (signaling, metabolic, structural) to cytoskeletal and organelle organization up to topological and morphological dynamics. Finally, the extensive interconnection between the motile machinery and cytoplasmic signaling pathways, which is currently not well understood, leads to the emergence of sophisticated behavior (see figure 1.2).

1.5 *P. polycephalum* as a model organism

P. polycephalum is an ideal model organism to study large-cell amoeboid locomotion, owing to the multitude of different behaviors that can be observed. Furthermore, the patterns of behavior can easily be manipulated, since the slime mold exhibits pronounced chemotaxis [Durham and Ridgway, 1976] and phototaxis [Hato et al., 1976]. The rich oscillation and flow dynamics, combined with the convenient size and relative ease with which it can be cultivated and observed, make *P. polycephalum* a versatile and fascinating model system. The development of standard molecular methods is still in its early stages, but much knowledge of the molecular biology and genetics (see section 1.7.3) of the slime mold has been gained in recent years.

Working with *P. polycephalum* means to perform cell biology on an unusual length scale: In the lab, the organism ranges from tens of micrometers to centimeters. This means that continuum mechanics, and in particular fluid dynamics, play a very different role compared to 'conventional' eukaryotic cells. An example is cell locomotion. Whereas the locomotion of vertebrate cells such as fibroblasts or keratocytes is based on the polymerization of actin from their monomeric subunits [Pollard and Cooper, 2009; Mitchison and Cramer, 1996], the locomotion of amoeba above a certain size is strongly influenced by fluid dynamics [Paluch and Raz, 2013; Bray, 2001]. This demonstrates the importance of size: Lamellipodia, for example, extend via the polymerization of actin at their front end. This protrusion pushes the membrane outward. However, this mechanism, called actin treadmilling, relies on the diffusion of actin monomers from the depolymerizing ends at the base of the actin filaments to the tips [Naoz et al.,

2008]. Transport by diffusion becomes less and less effective with increasing distances, and therefore, larger cells such as the slime mold employ more active and large-scaled mechanisms, like cytoplasmic streaming. This is driven by periodic contractions of the outer actin cortex, which cause pressure differences and a resulting flow of cytoplasm. Still, actin polymerization plays an important role in the dynamics of the cytoskeleton, as demonstrated by cytoskeletal assemblies and superstructures like actin asters (see for example chapter 3). The enormous size of the organism makes it possible to utilize methods that are not usually used in cell biology, e.g. from hemodynamics. A downside is, however, that classical cell biological methods, such as the fluorescent labeling of molecular structures, can be difficult. One technique to label, for example, cytoskeletal proteins, mitochondria, or other specific structures is to simply incubate cells with the respective probes, which passively diffuse across the plasma membrane and accumulate in the desired structures. The slime mold, however, is a large cell. An average eukaryotic cell is about 25 µm in diameter, whereas microplasmodia, the smallest viable units, start at a diameter of $\sim$ 50 µm. This means that there is a huge increase in diffusive time scales as cells approach macroscopic sizes. Furthermore, the slime mold continuously secretes copious amounts of slime [McCormick et al., 1970], a mucopolysaccharide which further impedes diffusion and forms an extracellular barrier. In section 3.3.2, techniques are presented which provide solutions to these challenges, for example the use of microinjection.

In the further course of this introduction, previous own work is presented briefly (section 1.6) and the current state of the research on *P. polycephalum* is summarized (section 1.7). An overview on past research efforts is given in chapter 2.

1.6 Previous own work

During the course of this doctoral thesis, several precursory publications have been produced. We[a] previously have characterized in detail the oscillations of microplasmodia [Bernitt et al., 2010]. Several patterns were described, among them the ubiquitous fast oscillations with periods of 1 to 2 min as well as lateral contraction waves moving along the circumference. Such lateral waves can also be found in migrating mesoplasmodia, and are described in section 4.4.2.

Furthermore, we used microplasmodia as starting points to grow networks. Plated onto agar, microplasmodia fuse and give rise to macroplasmodia in a percolation transition [Fessel et al., 2012]. Most of the previously isolated microplasmodia connect with each other to form one single giant component. We modeled this topological phase transition using the configuration model of graph theory for small link degree, and found an analytically exact solution. In a follow-up publication, we described that the slime mold does not begin to forage (i.e., expand its network) before the network is structured to

[a] In this section, 'we' includes the author of this thesis and her co-authors.

some degree [Fessel et al., 2015]. This happens at or shortly after percolation.

Moreover, we employed microplasmodia to study the viscoelasticity and nonlinear elasticity of *P. polycephalum* via microindentation [Fessel et al., 2017]. Our results suggest a characterization of microplasmodia as porous, compressible structures that act like elastic solids with high Young's modulus on short time scales, whereas on long time scales and upon repeated indentation viscous behavior dominates. We found that Young's modulus oscillates in phase with the shape oscillations of microplasmodia. This means that during contraction, structural changes take place. The actin cortex becomes denser and motor protein activity takes place, altering the mechanics and density of the actin cytoskeleton. Therefore, modeling *P. polycephalum* oscillations as a driven oscillator with constant moduli is not practicable, because the spring constant is time-dependent.

Lastly, we characterized the foraging pattern of mesoplasmodia, a novel growth mode which occurs in the absence of glucose and when microplasmodia are close to forming spherules (inactive resting stages) [Lee et al., 2018]. Instead of turning into a percolated network as described above, microplasmodia fuse locally into disconnected foraging units (termed mesoplasmodia) which, for hours, travel on straight trajectories away from their point of origin.

For all of the above-mentioned publications, I was involved in developing the research designs, performed the experiments, and contributed in writing the papers.

1.7 Present and future research on *P. polycephalum*

The investigation of the slime mold's locomotion, behavior and further emergent properties unites different scientific disciplines. The resulting perspective is interdisciplinary and creates a unique new field at the intersection of cell biology, mathematics and physics. The most important current research questions are addressed below.

1.7.1 How is intracellular fluid flow coordinated and what is its role in locomotion and signal processing?

A wide range of movement patterns can be observed in *P. polycephalum*, the most prominent being the so-called shuttle streaming, a vigorous flow of endoplasm through the organism's veins. This rhythmic and very regular pattern of contraction and relaxation, brought about by the ATP-consuming interaction of actin fibres with myosin motors, drives intracellular flow and serves to transport cytoplasm throughout the network [Nachmias and Ingram, 1970; Brix and Stockem, 1987; Kukulies et al., 1987; Ohl et al., 1991].

In addition to shuttle streaming, several highly coordinated spatio-temporal oscillatory patterns have been identified, for example the propagation of peristaltic contractions [Baranowski and Wohlfarth-Bottermann, 1982]. Standing waves have also been observed in longer veins [Ermakov and Priezzhev, 1984]. In medium sized plasmodia (with a diameter of about 5 cm), nearly synchronous and synphasic radial pulsations of all veins in the network have been reported, with contraction phases coincident to the expansion phases of the growth fronts [Grebecki and Cieslawska, 1978]. At the sheet-like growth fronts, quasi-stochastic and wave-like thickness oscillations have been observed, which eventually synchronized [Beylina et al., 1984]. Such waves sometimes circulate and form spiral patterns [Takagi and Ueda, 2010].

Starting in the early 2000's, some astonishing properties of the slime mold's networks were investigated. Their efficiency, fault tolerance, and cost were compared to those of real-world infrastructure networks [Nakagaki et al., 2004a,b; Tero et al., 2010], demonstrating a very high degree of optimization for a unicellular organism. Apart from its ability to solve mazes [Nakagaki et al., 2000], the slime mold can even tackle complex problems such as the traveling salesman problem [Zhu et al., 2013].

Current research approaches relate the observed phenomena of the network with regard to transport and information processing to the dynamics of the shuttle streaming. The organization of cytoplasmic flow in both developed networks and in small fragments is the focus now. Oscillation patterns like peristalsis have been reported early on [Baranowski and Wohlfarth-Bottermann, 1982], but have been elaborated on recently [Alim et al., 2013], especially in light of transport mechanisms which could possibly influence the distribution of chemical signals throughout the cell body [Alim et al., 2017; Zhang et al., 2017; Marbach et al., 2016]. The peristaltic wave driven by cross-sectional contractions of the network's tubes can possibly serve the purpose of signal propagation. Furthermore, the overall shape and structure of the macroplasmodial networks are a current research focus, and how plasmodia forage [Lee et al., 2018; Liu et al., 2019; Shirakawa et al., 2019], interact [Vogel et al., 2016], and the way resulting networks are optimized depending on environmental conditions and initial growth pattern [Akita et al., 2017; Takamatsu et al., 2017; Dirnberger and Mehlhorn, 2017].

On a smaller scale, cytoplasmic flow is currently investigated to find out how locomotion of smaller plasmodia is achieved [Lewis et al., 2015; Lewis and Guy, 2017; Zhang et al., 2017; Kuroda et al., 2015]. Guy et al. [2011] propose a model of pressure-driven flow through a polymer network; where an increasing flow rate increases the rate of depolymerization. Contractility, adhesion and flow are involved, as well as flow-induced channel formation. Essentially, the direction and speed of locomotion were found to rely on the coordination between contraction, flow and adhesion. Whereas a fully developed network is optimized for transport, smaller subunits (termed mesoplasmodia) exhibit prolonged, constant migration while foraging. This migration is examined in

more detail in chapter 4 of this thesis. Macroplasmodial networks consist of more stationary veins, which can be remodeled by the organism, and expand at dedicated growth fronts. The current reinforcement model [Akita et al., 2017; Schenz et al., 2017] states that veins in the network will be either abolished or reinforced, depending on the amount of cytoplasm which flows through them. Another research topic is still the origin of the primary oscillator, an unknown mechanism which causes the rhythmic contraction-relaxation pattern. So far, biochemical processes associated with respiration seem to play a role [Avsievich et al., 2017], as well as calcium [Korohoda et al., 1983], but mechanical factors are also involved [Teplov, 2017].

The motion of tiny, often artificial *P. polycephalum* fragments (i.e. protoplasmic droplets consisting of endoplasm, which have been extracted from a vein) is often described by a poroelastic model [Alonso et al., 2016; Kulawiak et al., 2018; Strychalski et al., 2015]. Here, the poroelastic medium is assumed to consist of two phases: An active viscoelastic solid, which represents the cytoskeleton, and a viscous fluid describing the cytoplasm. The intracellular free calcium concentration is presumed to drive the dynamics of the system. The poroelastic model might work well for the observed oscillations of minute protoplasmic droplets, but it is doubtful that the model can explain the behavior of large networks, where, in particular, cytoplasmic flow is responsible for many of the observed phenomena.

Applications of the observed intracellular fluid dynamics extend to the design and construction of soft robots [Umedachi et al., 2013; Onoda et al., 2017] and fluid computing. As computers shrink in size and as the need to build soft-bodied robots increases, it becomes necessary to create soft and deformable materials [Wissman et al., 2017] to replace rigid and hard components of electrical switches and circuits. Soft robots can be better at grasping and manipulating objects, and adapting to uneven and rough terrain, by being able to squeeze, climb and elongate [Mazzolai and Mattoli, 2016], much like living creatures. The idea that fluids can act as information carriers and computing substrates is not new (for a brief history of liquid computers, see the review by Adamatzky [2019]). Liquid-based computing devices can be used to implement logic gates [Adamatzky, 2015], fluid mappers and maze solvers [Fuerstman et al., 2003; Oh et al., 2012], as well as hydraulic integrators. The advantages of fluidic computing and actuating devices are their reliability, robustness, tolerance (to shock, vibration and radiation), as well as low production costs. Therefore, fluidic and microfluidic devices have mainly been investigated by engineers. However, liquid computing overlaps strongly with the biology of *P. polycephalum*, as many of its features (shuttle streaming, signal propagation, morphological changes triggered by cytoplasmic flow) are fluidic phenomena and responsible for the slime mold's learning and adaptive behavior.

1.7.2 How does an apparently simple organism coordinate sophisticated behavior?

A crucial requirement for any form of complex behavior is memory. Without memory, the cell would be unable to detect change in its environment, and the resulting behavior would be random. The absence of a memory means the inability of learning. Even very simple organisms can adapt to changing environments, raising the possibility that mechanisms for learning might have evolved before nervous systems. It has been demonstrated that *P. polycephalum* possesses a memory, both extracellular in the form of secreted slime [Reid et al., 2012; Smith-Ferguson et al., 2017] and intracellular [Saigusa et al., 2008]. As the slime mold moves through its environment, it lays tracks of extracellular slime. When it encounters these tracks again, the slime functions as external spatial memory system and the slime mold 'remembers' that it has been in the area before. By avoiding areas it has previously explored, *P. polycephalum* can escape from a U-shaped trap in the laboratory [Reid et al., 2012], and it can maximize its foraging. *P. polycephalum* is even able to distinguish between extracellular slime deposited by members of its own kind and members of other slime mold species [Reid et al., 2013].

In contrast to the design and evaluation of these straightforward experiments, the mechanism of the internal memory is not understood that well. The organism exhibits habituation [Boisseau et al., 2016; Vogel and Dussutour, 2016], meaning a decreased response to a stimulus after repeated presentations. In this case, the slime mold learned to ignore the repellents quinine or caffeine, but it could also be habituated to salt [Boussard et al., 2019]. Furthermore, *P. polycephalum* is able to detect and react to periodically occurring events [Saigusa et al., 2008], effectively showing anticipation. Ever since these phenomena have been observed, the search for a molecular basis of memory is ongoing. It could be demonstrated that slime molds, which had been habituated to salt, were able to transfer this learned behavior to other slime molds, which had never encountered the negative stimulus, via cell fusion [Vogel and Dussutour, 2016]. The transfer required the mixing of cytoplasm between two individuals, and thus it was speculated that the substrate for habituation is located in the cytoplasm. It was found that *P. polycephalum* takes up and stores the repellent [Boussard et al., 2019], a process which could be a part of the molecular mechanism of memory and learning. Physical models have been constructed which reproduce the observed phenomena [Pershin et al., 2009; Whiting et al., 2016; Ntinas et al., 2017].

A possible mechanism of memory formation is based on epigenetics [Levenson and Sweatt, 2005]. Epigenetic mechanisms cause heritable phenotype changes based on alterations in, e.g., chromatin structure, but not in DNA sequence. Epigenetic memory can be found, for example, in biennial plants [Henderson et al., 2003]. They must experience a period of cold weather after the first year in order for flowering to be triggered in the second year. In this case, exposure to cold activates epigenetic mechanisms

which involve the methylation of DNA-binding proteins and thus cause stable changes in gene expression patterns. Epigenetic processes seem to play a substantial part in the memory and learning of single-celled organisms [Zacharioudakis et al., 2007; Ginsburg and Jablonka, 2008; Perkins and Swain, 2009; De la Fuente, 2015].

A further key feature of the slime mold is its ability to make complex decisions. As mentioned above, it can find its way through a maze [Nakagaki et al., 2000], construct efficient transport networks [Tero et al., 2010; Houbraken et al., 2012], and make decisions [Beekman and Latty, 2015], for example regarding its nutrient uptake [Dussutour et al., 2010]. Astonishingly, it has even been shown to express 'irrational' behavior [Latty and Beekman, 2011a] and evaluate risks during foraging [Latty and Beekman, 2010]. Under stress, for example exposure to light or risk of starvation, *P. polycephalum* makes foraging decisions influenced by speed accuracy trade-offs resembling those of higher organisms [Latty and Beekman, 2011b].

How the decision process is executed is one of the key questions in current research. *P. polycephalum* emerges as a model system to study processes which could possibly underlie all decision-making [Beekman and Latty, 2015]. We know, however, that in the absence of a centralized information-processing organ, the observed complex behavior of *P. polycephalum* must be a result of decentralized biophysical and biochemical mechanisms. Sophisticated behavior in *P. polycephalum* is a combination of genetics (as will be discussed in section 1.7.3), epigenetics, and the motile machinery, which is extensively interconnected with cellular signaling pathways. Examples for such signaling molecules in *P. polycephalum* are calcium ions (Ca^{2+}), cyclic AMP (cAMP), phosphatidylinositol-4,5-bisphosphate (PIP_2), and protein kinases. Calcium is involved in the actomyosin contractions [Ridgway and Durham, 1976; Kessler et al., 1980; Kuroda and Kuroda, 1982]. Furthermore, calcium forms a gradient throughout the cell during migration [Natsume et al., 1992], thus establishing polarization. Another important function of calcium is its involvement in the primary oscillator, the oscillatory biochemical network governing the rhythmic contractile activity of *P. polycephalum* [Avsievich et al., 2017]. A more thorough description is given in section 2.5 and figure 2.3. The slime mold can produce and secrete cAMP [Ueda et al., 1986], which is suspected to play a role in locomotion and chemotaxis [Matveeva et al., 2010a, 2012b]. However, further studies are necessary. PIP_2, a membrane-bound, receptor-controlled phospholipid regulates the activity of proteins associated with the actin cortex. Therefore, PIP_2 and associated pathways affect the shape, autooscillatory control and motility of the plasmodium [Matveeva et al., 2008, 2012a, 2014]. Protein kinases also play a crucial role in signal transduction. Receptor tyrosine kinases (RTKs) and histidine kinases, which are mostly found in prokaryotes, plants, fungi and amoebozoa, but not in metazoa, are very abundant [Schaap et al., 2015]. Furthermore, several AMP-activated protein kinase (AMPK) orthologs have been found in the *P. polycephalum* genome [Schaap et al., 2015]. They are expressed in starving, sporulation-competent plasmodia [Glöckner and Marwan,

2017]. When activated by low ATP levels, as for example during glucose deprivation, AMPK activation stimulates mitochondrial biogenesis and enhances catabolic processes. In this thesis, the role of AMPK as a metabolic switch during glucose-deprivation in *P. polycephalum* is discussed for the first time (see chapter 5).

In summary, it becomes clear that the dynamics of these signaling molecules and pathways affect the cytoskeleton in many ways, and hence modulate its morphology and function (for example the formation of stress fibres or the softening of the actin cortex). These processes, in turn, produce manifold movements and shape changes. The rich motile physiology, coupled with intracellular signaling, has collective properties that give the slime mold a very useful circuitry to achieve motility and complex behavior. Chapter 4 of this thesis introduces yet another possible mechanism by which *P. polycephalum* can transmit and process information, namely cytoplasm-based fluid dynamic information processing. In the absence of a central nervous system, complex behavior has to be conveyed via e.g. mechanochemical processes and local interactions. This type of non-neural information processing is prominently observed in *P. polycephalum*, which forms a self-organizing vein network that serves the purpose of foraging and nutrient distribution throughout the cell body. The slime mold's oscillations are decentralized and self-organized, and a hypothesis of this work is that the resulting pulsatile flows (shuttle streaming) through its veins carry information in the form of frequency and amplitude. Durham and Ridgway [1976] have shown that local oscillations in a macroplasmodium increase when it encounters a positive chemical stimulus (for example glucose) and decrease upon contact with a repellent (salt). They hypothesized that the plasmodium behaves as a system of loosely coupled oscillators, which individually oscillate at a frequency determined by local conditions, not a fixed resonance. Coupled oscillator models explain wave patterns and wave propagation [Iima et al., 2017]. A thorough review on the subject of mechanochemical oscillations, hydrodynamic interactions and self-organization is provided by Teplov [2017]. Introducing memory into this concept, the learning abilities of *P. polycephalum* have been modeled with a memristor [Pershin et al., 2009], a hypothetical electrical component which 'remembers' how much electric charge has flowed through it in the past. In this case, an inductor and capacitor create the oscillations which mimic the biological oscillator. When memristor circuits are subjected to time-dependent input, they demonstrate learning and the anticipation of future changes of the signal. Such a circuit has been used to mimic *P. polycephalum*'s network and foraging behavior [Ntinas et al., 2017].

1.7.3 What is the genetic basis of *P. polycephalum*'s complexity?

For a comprehensive overview of the genetics and molecular phylogeny of myxomycetes, the reader is referred to the book edited by Stephenson and Rojas [2017], which also includes information on molecular biology and evolutionary pathways. When mammalian and bacterial cell culture and genetic engineering techniques advanced in the 1970s, genetic research on *P. polycephalum* was all but abandoned. Other systems were

easier to manipulate, and considered more relevant, for example the development of vaccines and other proteins, e.g. insulin and antibodies, *in vitro*. As a result, a lot of standard techniques are not applicable to *P. polycephalum*, for example the transfection with GFP-actin to render the cytoskeleton visible. The reason is that those techniques and protocols were developed for mammalian cells (which are cultivated under vastly different conditions than slime molds), and also because the slime mold has a very high genetic stability. Any nuclei transfected with foreign genetic material are detected, shut down and eliminated. Thus, modifying the genetic material of *P. polycephalum* has mostly been relegated to Mendelian genetics. Even today, a simple first step such as the isolation of DNA and RNA from any stage of the slime mold's life cycle is not straightforward: There are no commercially available nucleic acid isolation kits specifically designed for myxomycetes, so researchers have to modify existing kits and protocols, which were for example designed for the isolation of plant DNA [Walker et al., 2017]. Furthermore, the presence of highly repetitive DNA sequences has made sequence analysis and assembly unusually difficult [Miller et al., 2017].

Starting in the 1980s, molecular methods were increasingly used in myxomycete research. DNA sequencing was used for the purpose of phylogenetic investigations. At first, only a limited number of gene sequences were investigated [Baldauf and Doolittle, 1997; Baldauf, 1999]. However, as the number of available gene sequences increased, so did the research possibilities, especially in the area of taxonomy. More advanced molecular biology tools made it possible to identify species of slime molds and to shed light on the evolutionary history of myxomycetes [Leontyev et al., 2019]. It is possible to genetically transform and transfect *P. polycephalum* [Burland et al., 1993a,b], but so far, the technique has only been applied to haploid amoebae and is not commonly used.

Yet, in spite of the delay in the use of molecular methods in slime molds, advancements in molecular genetics have been made. The complete genome of *P. polycephalum* was recently reported [Schaap et al., 2015]. Furthermore, transcriptome data are now available [Glöckner et al., 2008; Bundschuh et al., 2011], and it is possible to inhibit gene function by RNA interference (RNAi), [Haindl and Holler, 2005]. Materna and Marwan [2005] were the first to investigate the effect of antisense RNA on gene expression. However, there is still a lack of established cell cycle mutants in *P. polycephalum*, and current difficulties of reproducibly creating transgenic lines have still to be overcome [Schaap et al., 2015].

The genomic analysis of *P. polycephalum* shows its extraordinary molecular richness, complexity and evolutionary distinctiveness [Schaap et al., 2015]. It appears that *P. polycephalum* possesses a higher molecular complexity than other species of the Amoebozoa that have been sequenced so far. It is intriguing, but perhaps not surprising, that genes which are involved in signaling pathways and sensory receptors are very abundant [Schaap et al., 2015]. Tyrosine kinases, which are involved in intracellular signal trans-

duction, feature heavily in the slime mold's genome. Similar receptor tyrosine kinases (RTKs) are also found in humans, and are characteristic for animal cells. Furthermore, the slime mold has many histidine kinase-based two-component signaling systems, which are not found in animals. What makes the organism even more unique is the presence of bacterial and plant type photoreceptors, for example phytochromes, as well as metabolic pathways and a cell cycle control system typically found in more complex eukaryotes. As an example, investigations of the transcriptome during developmental switching (photoreceptor-triggered activation of the sporulation pathway) shows extensive remodeling of intracellular signaling networks [Glöckner and Marwan, 2017]. In conclusion, *P. polycephalum* displays many interesting, complex and versatile features, especially in the area of cell signaling, which are the basis and prerequisite for its dynamic behavior.

The multinucleate giant cells of *P. polycephalum*, a true coenocyte, offer great opportunities as a model system. The naturally synchronous populations of nuclei [Sachsenmaier et al., 1972] provide extensive homogenous biological material for the analysis of signaling and gene expression dynamics at the single cell level. Because all nuclei are identical and highly synchronized clones, it is possible to perform genetic experiments simultaneously. In contrast to vertebrate cells, which have only one nucleus, a plasmodium can be subdivided into several identical, rapidly synchronizing units for different treatments. Furthermore, with the availability of genome and transcriptome data, reverse genetic approaches are now possible. Specific genes in mutant cell lines can thus be identified. Plasmodial mutants of *P. polycephalum* can for example be created by chemical mutagenesis [Sujatha et al., 2005]. For the reasons mentioned above, *P. polycephalum* also lends itself to epigenetic investigations, i.e. studies of heritable phenotype changes that do not involve alterations in the DNA sequence. The phenotype of a cell is not only determined by specific genes and pathways, but cell physiology complements genetics by connecting genotype and phenotype via epigenetic processes and other dynamical responses. Werthmann and Marwan [2017] have investigated and modeled the epigenetic landscape of *P. polycephalum* during the light-induced developmental switch to sporulation. Their findings show individual differences in gene expression patterns, which nonetheless ultimately lead, after an initial light stimulus, to sporulation (see also [Rätzel and Marwan, 2015]). They could model these very complex cellular responses and phenotypes with Petri nets [Marwan et al., 2011; Blätke et al., 2012; Werthmann and Marwan, 2017]. Furthermore, epigenetic processes also appear to be the structural manifestation of cellular metabolic memory [De la Fuente, 2015].

1.8 Discussion of minimal cognition and consciousness in *P. polycephalum*

1.8.1 Minimal cognition

In light of its behavioral complexity, it is tempting to attribute some kind of cellular intelligence or at least cognitive abilities to the slime mold. However, the terms 'intelligence', 'cognition' and 'consciousness' have to be used very carefully here so as not to cause confusion. Generally, intelligence implies that an organism can learn, evaluate, and make decisions towards actions that result in desired consequences. In psychology and other cognitive sciences, there is a long-standing lack of agreed definitions for key concepts such as intelligence and cognition. Both are highly theoretical constructs which can be defined broadly or narrowly, depending on the context. This is nicely highlighted by an article entitled "What is cognition?" [Bayne et al., 2019], where the eleven authors formulate their (eleven different) understandings of what cognition means, and what is required to call a particular phenomenon 'cognitive'. Hence, it is far beyond the scope of this thesis to create comprehensive definitions. The interested reader is directed towards a wealth of review articles on the subject of cellular cognition which were published in recent years, for example [Lyon, 2015; Calvo and Baluška, 2015; Godfrey-Smith, 2016; Ford, 2017; Baluška and Reber, 2019].

As Lyon states, apart from the lack of universal linguistic and conceptual definitions, many findings are ultimately calibrated against humans [Lyon, 2006]. She argues that we should probably extend the conceptions from narrowly human to include broadly biological. As an example, the capacity of problem solving can be defined to include, in humans, rational decision-making and abstract thinking. In a broader biological sense, problem solving encompasses a general adaptability and the selection of behavior under "circumstances with multiple parameters and high degrees of uncertainty" [Lyon, 2015]. In humans, the term "self-awareness" is defined by the rather complex and psychologically important concept of 'self'. However, as Lyon states, the general capacity of self-reference can also be realized in non-neural organisms. Even bacteria are capable of distinguishing themselves from one another [Gibbs et al., 2008]. Macroplasmodia of the slime mold *P. rigidum* can recognize 'self' and 'non-self', based on chemicals within their slime sheath [Masui et al., 2018]. The authors propose that the secreted slime disperses information about the individual self into the environment. Many other, simple life forms have mechanisms for recognizing 'self' from 'non-self'; prominent examples being the allorecognition of tunicates [McKitrick and Tomaso, 2010], sponges [Grice and Degnan, 2017], and corals [Rinkevich, 2004]. Interestingly, those mechanisms of self-recognition are not analogous to the immunological processes of vertebrates [Burnet, 1971; Bayne, 1990; Grosberg and Plachetzki, 2010]. This can be considered as another example for convergent evolution of cognitive mechanisms, which will be discussed in more detail in section 6.3.

Slime molds and other amoeba are not classified as intelligent in the traditional sense, because they lack any of the components which are typically required to produce intelligence, i.e. brains or nervous systems. Nevertheless, single celled organisms do possess intricate systems that are capable of sensing environmental or internal changes and are able to react to these changes. The zygomycete fungus *Phycomyces blakesleeanus* for example is in possession of a light sensing system that is as sensitive to a wide interval of light intensities as the human eye [Sanz et al., 2009]. These systems behave in a manner that is comparable to the nervous system of higher animals, and demonstrate a very high level of sophistication. Free-living protozoa have to continually monitor their abiotic and biotic environment (temperature, physical or chemical obstacles, food sources, predators, light), and be ready to react to it quickly. This, in turn, implies the presence of a minimal information-processing mechanism. Microorganisms have dedicated, specialized and sophisticated sensory systems. In *P. polycephalum*, chemotaxis [Durham and Ridgway, 1976; Kincaid and Mansour, 1978; Adamatzky, 2012] and phototaxis [Hato et al., 1976; Häder and Schreckenbach, 1984; Marwan, 2001] are prominent examples. Other, internal pathways are also realized in *P. polycephalum*, for example mitotic synchrony [Loidl and Sachsenmaier, 1982], or the activation of an AMPK pathway during glucose deprivation, which is described in this thesis for the first time (see chapter 5). Seemingly intelligent or even altruistic behavior can also be found in other, very simple organisms, for example the yeast *Saccharomyces cerevisiae*: It has been demonstrated that older cells undergo apoptosis when nutrients become scarce [Büttner et al., 2006]. The single-celled ciliate *Paramecium caudatum* might possibly be classically conditioned and trained in a discrimination learning task [Armus et al., 2006].

The multitude of models regarding the behavior and network formation of *P. polycephalum* provide quantitative and tunable statements about the observed phenomena [Marwan, 2010]. However, complex biological processes such as morphogenesis, growth and homeostasis are at their basis, many of which are completely unclear. All organisms can self-optimize in some way. Therefore, there exists some criticism of the minimal cognition concept, especially when it is ascribed to plants [Taiz et al., 2019] and even prokaryotes. An attempt to establish 'plant neurobiology' as a research field has been met by vehement disapproval [Rehm and Gradmann, 2010; Alpi et al., 2007], not least because of incorrect interpretations of measurements and outright artifacts. Good points have been made that consciousness needs a brain [Feinberg and Mallatt, 2016, 2018], and that cognition starts with nervous systems [Arnellos and Moreno, 2015]. However, supporters of a broader scope of cognition invoke that a 'brain-centric' dichotomy fails to provide an explanation for the behavioral complexities that can be found in brainless organisms [van Duijn et al., 2006]. They also argue that there seems to be a spectrum of cognitive abilities, with huge differences between, for example, nematodes, bacteria, starfish, ciliates and slime molds. Furthermore, processes which are deemed to be prerequisites for cognition, such as perception, memory, and action (behavioral

output), can be found in a wide variety of life forms. Therefore, if cognition is indeed a spectrum, slime molds and other protozoa are probably found at its low end and we should consider minimal cognition. However, below minimal cognition, there is a boundary which separates it from pure metabolic activity [Godfrey-Smith, 2016]. The author argues that cognition in the first place evolved to allow organisms to control their behavior, thus allowing them to cope with the complexity of their environment [Godfrey-Smith, 2001].

Activities such as perceiving and acting, decision making, learning and memory – which are all exhibited by *P. polycephalum* – fall within the domain of cognitive science when performed by humans. Although human behavior is not on the same level as that of slime molds, the goal here is to understand the basic principles employed in the responsible mechanisms. Focusing on simpler mechanisms employed in more primordial species can provide a basis for understanding the more complex mechanisms underlying human behavior regarded as cognitive.

1.8.2 Consciousness

While one can make a compelling point that intelligence and minimal cognition are present in *P. polycephalum*, the discussion of consciousness is much more difficult and verges on philosophy. While cognition can be thought of in terms of a spectrum or gradient, fading off into very simple manifestations as in bacteria, consciousness is more often thought of as a 'yes or no' matter [Godfrey-Smith, 2016]. Consciousness is often used synonymously with self-awareness, sentience or subjective experience. Therefore, self-awareness can be assumed to be the qualitative aspect of cognition [Godfrey-Smith, 2016]. It is unknown whether consciousness fades out in the same way that cognition does (from highly developed species such as humans down to single-celled organisms), but it can be speculated that cognitive complexity gives rise to sentience. Dehaene [2014] conjectures that within the broad spectrum of cognition, there is a subset of features and capacities which are relevant for consciousness, and that many cognitive processes have no subjectively experienced side. However, the question whether *P. polycephalum* possesses consciousness is as interesting as it is hard to answer. We will return to this subject in section 6.5.

P. polycephalum is about to take its place among established model organisms in behavioral science. Beekman and Latty [2015] pose the question whether the observed complex behavior of *P. polycephalum* could hint at fundamental processes underlying all decision making, and Vallverdú and coworkers have developed a minimal cognition framework for the slime mold Vallverdú et al. [2018]. Smith-Ferguson and Beekman [2019] even ask "Who needs a brain?" and argue that a brain is a biologically expensive organ to maintain. They state that even human decision making is governed by relatively simple behavioral rules. A compilation of models which aim to uncover physiological mechanisms behind the 'intelligent' behavior and which develop algorithms for solving

computational problems can be found in [Gao et al., 2018] and [Gao et al., 2019]. The involvement of the cytoskeleton with signaling pathways has been mentioned above (section 1.7.2 and [Bray, 2001]). In *P. polycephalum*, the actin cytoskeleton is crucial for locomotion, but its role as a network for transducing, transmitting and processing information is also under investigation [Mayne et al., 2015]. The cytoskeleton can also carry epigenetic information [Bray, 2001].

With an abundance of theories about the origin of minimal cognition, intelligence and consciousness, it is now time to investigate the physical, biological and biochemical basis for these concepts. First of all, we need to establish the nature and properties of the 'substrate' on which such computation takes place. In higher organisms, this would be the brain and nerve cells. An exceptional position is hereby occupied by social insects, flocks of birds and shoals of fish, which exhibit swarm intelligence [Kao and Couzin, 2019]. Similarly, groups of, for example, immune system cells or termite colonies can act together as 'liquid brains' [Solé et al., 2019; Piñero and Solé, 2019]. In *P. polycephalum*, the substrate of computation can be cytoplasm flow (see chapter 4 for details), the cytoskeleton (see chapter 3), and biochemical networks such as the primary oscillator (figure 2.3) and other cell signaling pathways. However, basic knowledge on fundamental properties of *P. polycephalum* is still scarce. A lot of seminal work on cell biology, molecular biology, and genetics is still to be done. *P. polycephalum* as a model system is much less well defined than other established species, because of the intermittent research history. Second, we need experiments to test intelligence, cognition and consciousness in the slime mold and other non-neural organisms. In behavioral neuroscience, cognitive mechanisms are often inferred from loss of function experiments [Silva, 2007]. Therefore, one approach could be to create mutant cell lines in which phototaxis or chemotaxis have been altered. Furthermore, since there is a great wealth of data and experimental connections between molecular, behavioral, cell biological and even cognitive data, as well as models, there is a need for tools to aid in the integration of research findings and in experiment planning [Silva and Müller, 2015].

It is striking that both cytoplasmic signaling pathways and the motile machinery are interconnected extensively. Cross-talk between signaling pathways and the cytoskeleton exists at every level. This becomes very evident in *P. polycephalum*, where the flow of endoplasm serves the dual purpose of locomotion and signal propagation. The pressure of the cytoplasm flow within a small, homogenous mesoplasmodium or the frontal, fan-shaped region of a macroplasmodium creates flow channels by breaking up the actin gel [Guy et al., 2011]. Stretching of the ectoplasm induces activation of contractile oscillations [Teplov, 2017], however, specific stretch receptors have not been found so far. It is speculated that stretching of the ectoplasm causes an increase in Ca^{2+} within the cell through mechanosensitive calcium channels.

The above-mentioned example also highlights the key role of underlying physical prin-

ciples such as fluid mechanics and soft matter physics of the cytoplasm for locomotion and cellular information processing. Like any other system, living organisms are subject to the laws of physics and can thus be examined with the conventional tools of physics. But in biology, there are also systems for which the traditional framework of physics does not provide appropriate theoretical and experimental models. Biological physics advances because new physical concepts and interactions are discovered within biology. Complex systems such as the slime mold have emergent properties, which develop from relatively simple interactions. Living organisms can be considered as self-organizing, active soft matter, which is out of equilibrium [Ornes, 2017]. In order to gain a complete picture and to unravel the detailed mechanisms of information processing and cognition, we need to characterize and model *P. polycephalum* on all levels starting at the bottom.

Chapter 2

Physarum polycephalum – a new take on a classic model system

Christina Oettmeier[1,3], Klaudia Brix[2], and Hans-Günther Döbereiner[1,3]

[1] Institute for Biophysics, University of Bremen,
Otto-Hahn-Allee 1, 28359 Bremen, Germany
[2] Jacobs University Bremen, Department of Life Sciences and Chemistry,
Campus Ring 1, 28759 Bremen, Germany
[3] Authors to whom any correspondence should be addressed.

2.1 Abstract

Physarum polycephalum, literally the "many-headed" slime mold, is a giant multinucleated but unicellular protist. Since the time of its first description, it has been the subject of a multitude of cell biological, biochemical, genetic, and lately physical studies. The enormous size of the cell, the easy method of *in vitro* cultivation, the unique life cycle and its highly visible internal cytoplasmic streaming have made it invaluable for investigations on cell cycle regulation, differentiation, cytoskeleton and locomotion. Research on *P. polycephalum* lost its prominent role when animal cell culture and genetic techniques became more advanced, thereby replacing the slime mold as a state-of-the-art model. However, research continued, driven by a small number of groups, resulting in full sequencing of the slime mold's genome, hence reviving interest in studying molecular processes that enable the astounding features of *P. polycephalum*. In recent years, research on *P. polycephalum* has again become cutting-edge. In 2000, Japanese researcher Toshiyuki Nakagaki performed a seminal experiment showing that the slime mold is able to find the shortest route through a maze. Ever since, smart problem-solving *P. polycephalum* has returned from the shadows and is nowadays back to center-stage when questions regarding the origins of intelligence and cognition are discussed. The basic mechanisms with which organisms perceive their environment,

integrate this information and make decisions based on this input are investigated. The aim is to find underlying universal mechanisms of decision making and awareness. If those mechanisms can be found in as primordial an organism as a slime mold, it could fundamentally change our perception of the nature and evolution of cognition.

2.2 *Physarum* and the physics of life

Many of the observed patterns in *P. polycephalum* are examples of emergence. They arise from basic chemical and physical processes, and there is great interest in deciphering the underlying processes which lead to the complex patterns of *P. polycephalum*'s locomotion and behavior (figure 2.1). A comprehensive and in-depth review of mechano-chemical

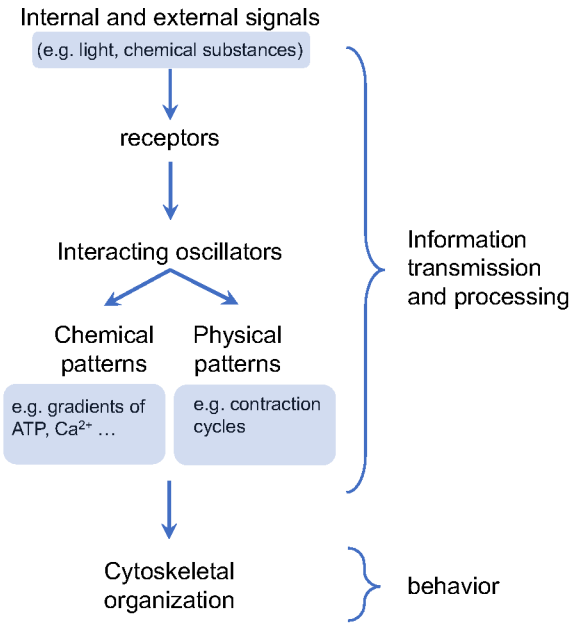

Figure 2.1: Emergence of behavior at different levels of organization.

models by Teplov, describing, for example, contractile phenomena and shuttle streaming, can be found in this issue [Teplov, 2017]. In higher organisms, many behavioral traits are attributed to a nervous system. One of the aims of physics research in *P. polycephalum* is to elucidate mechanisms of information processing coupled to network topology and morphology. Chemical as well as hydrodynamic oscillations create self-organized patterns throughout the giant cell, governing how the organism behaves. Oscillation patterns are related to environmental perception. In a more recent line of research, mechanisms are investigated by which emergent pattern formation processes could be used as a blueprint for unconventional computing [Jones, 2010]. This review focuses

on the biology of *P. polycephalum* and how biological background contributes to the construction of physical models.

2.3 A historical perspective – *Physarum polycephalum* comes of age

The acellular slime mold *P. polycephalum* is a model system that is interesting to biochemists, cell biologists, chemists, developmental biologists, geneticists and physicists alike. It was first described by von Schweinitz in 1822 [von Schweinitz, 1822]. Particularly in Japan, slime mold research has a long-standing tradition. The Japanese Emperor Hirohito, who reigned over Japan from 1926 to 1989, was fascinated by these unusual organisms. In 1935, he wrote, under an alias, a book devoted to slime molds found around his summer palace [Hattori, 1935]. Ever since, the research of slime molds in Japan has been considered a worthy and noble subject of study, and therefore a lot of research finds its origins there.

Since the 1960s, *P. polycephalum* has been used to investigate important and fundamental questions about how living organisms function, and it has recently reentered into the spotlights of biophysical and even psychological research, a lot of it being featured in this special issue. The unique ability to culture the slime mold *P. polycephalum* axenically (i.e., in pure culture) through every phase of its complex life cycle from haploid amoeba to the diploid vegetative stage (plasmodium) and back to gametes (spores) has made it an attractive model system for understanding the molecular mechanisms directing growth and development (figure 2.2). *P. polycephalum* has been instrumental in the study of cell differentiation (e.g. sporulation and the transition from amoeba to plasmodia) [Bailey, 1995, 1997], cell cycle regulation [Laffler and Tyson, 1986; Loidl and Eberharter, 1995; Jayasree et al., 2000], and DNA replication. Furthermore, its macroscopic size facilitates research on the cytoskeleton and locomotion [Kohama et al., 1993; Nakamura and Kohama, 1999], environmental sensing and response (photo- and chemotaxis) [Häder and Schreckenbach, 1984; Ueda et al., 1975]. Comprehensive reviews on the above topics were compiled by Aldrich & Daniel 1982 [Aldrich and Daniel, 1982a,b], Sauer [1982] and Burland et al. [1993a].

The high genetic stability of the slime mold's numerous nuclei, its synchronous mitotic cycle and its mechanism of DNA synthesis have inspired cancer researchers [Becker et al., 1963; Wright et al., 1984; Gorman et al., 1979], who tested antitumor compounds on it. *P. polycephalum* was a very helpful model organism for research before cell culture techniques and tissue engineering advanced. It could be grown axenically in large quantities [Brewer et al., 1964] of up to 100 liters, therefore providing enough material for biochemical analyses. Since a macroplasmodium is a coenocyte, all nuclei are clones of each other. This notion explains why molecular biologists value *P. polycephalum* so much, namely because it provides an extraordinary level of reproducibility. While

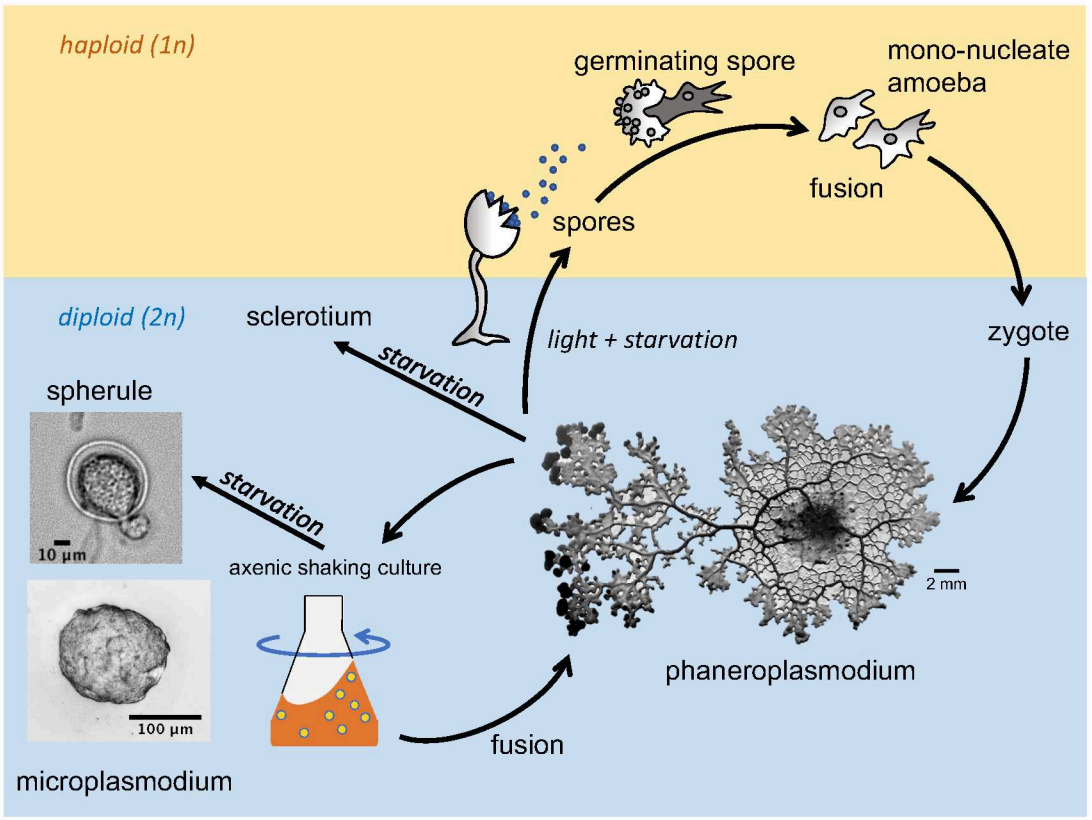

Figure 2.2: Life cycle of *P. polycephalum*. From the diploid vegetative form, the phanero- or macroplasmodium, smaller subunits can be generated by cultivating the slime mold in a liquid shaking culture. The resulting microplasmodia, when placed on a solid agar surface, can fuse and again give rise to a macroplasmodium. Two dormant stages, the spherule and the sclerotium, are induced by starvation. When starved and exposed to light, the macroplasmodium forms fruiting bodies. These sporangia then release spores which hatch into amoebae. When two haploid amoeba fuse, they form a diploid zygote which in turn grows into a large phaneroplasmodium.

research on *P. polycephalum* created new insight into the biology and physics of cells, progress in mammalian and bacterial cell culture in the 1970s and 80s soon exceeded it. For example, viruses could be replicated in infected human cells *in vitro*. Therefore, vaccines could be developed in large quantities using cell culture technologies. Furthermore, genetic engineering (recombinant DNA technology) advanced in the 1970s. For the first time, mammalian genes could be expressed in bacteria and soon after, genetically engineered animal cells were developed to produce more complex recombinant proteins, e.g. antibodies, for therapeutic and research purposes. A spectacular innovation was the production of recombinant human insulin, which was first marketed in the United States in 1982. Regarding these developments in molecular and cell biology, it is understandable that research on *P. polycephalum* took a back seat for a while.

Despite the lack of a nervous system or even neuronal network-like information processing structures, *P. polycephalum* can solve mazes [Nakagaki et al., 2000], geometrical puzzles [Nakagaki et al., 2004a] and features memorizing ability, both internally [Saigusa et al., 2008] and externally [Reid et al., 2012]. 'External memory', in this context, means the ability of the slime mold to recognize its own trail. A slime trace is left behind on the substrate, and when the organism encounters this slime deposit again, it avoids these already covered areas during foraging. Furthermore, it can make 'smart' decisions while distinguishing between different food sources [Reid et al., 2013]. When it comes to foraging, *P. polycephalum* can perform complex risk-management tasks, and considers different choices before making optimal decisions in taking the correct route [Dussutour et al., 2010; Latty and Beekman, 2010]. This hints to a rudimentary form of intelligence which is usually only ascribed to organisms having a higher level of neurological sophistication. Recent research has also included unconventional computing for path finding [Adamatzky, 2012; Shirakawa and Gunji, 2010] and even the control of robots by *P. polycephalum* [Jones et al., 2011]. A comprehensive review of the wide range of sensing and computing devices implemented with *P. polycephalum* is given by Adamatzky [2016].

The first to test *P. polycephalum*'s maze-solving abilities was the Japanese researcher Toshiyuki Nakagaki in the early 2000s [Nakagaki et al., 2000]. He allowed a plasmodium to cover an extensive labyrinth, before placing oat flakes at the entry and the exit. The slime mold quickly rearranged its veins until only the most efficient path between the two food sources remained. This is an astounding feat for a brainless organism. In a subsequent experiment, Nakagaki and coworkers arranged the oat flakes into an approximation of the geography of Tokyo and its surrounding cities [Tero et al., 2010]. The plasmodium grew out from its origin at the initial food source, and progressively reached out for colonizing each of the surrounding food sources. The spreading network of tubes connected all hubs consisting of oat flakes and finally *P. polycephalum* managed to form a network of veins that was shaped very similar to the existing railway system, demonstrating again its ability to create cost-efficient networks in a self-organized fashion. In terms of the slime mold network, cost-efficiency means a low total length of

veins with yet a short average minimum distance between food sources. The experiment has since been repeated, simulating many man-made structures, ranging from highways [Adamatzky and Jones, 2010] to wireless sensor networks [Tsompanas et al., 2015]. As an alternative solution to Nakagaki's maze experiment, it has been demonstrated that *P. polycephalum* can also solve a maze in one pass, i.e. without previously exploring the whole area of a given maze [Adamatzky, 2012]. The prerequisite is only that a chemo-attractant is placed at the destination site. This flexibility in behavior highlights the slime mold's suitability as a substrate for biological computing. Biologically inspired, highly efficient algorithms can be extracted from observing the formations built by the slime mold. The design of a transportation network takes into account fault tolerance, i.e. the ability of the network to cope with disturbances and disconnections. This parameter, called robustness, involves among other factors redundant connections. The trade-off between robustness and cost-efficiency is a recurring problem in network design. Living creatures have optimized their transport networks (e.g. vascular systems of plants and animals, foraging and migration patterns) through evolution over millions of years. Therefore, solutions from nature can be helpful and inspiring to human design. *P. polycephalum*'s network can be described as the outcome of natural biological computation, creating a robust and efficient transport network.

2.4 Neither a plant, nor belonging to fungi or animals – amoebozoa are special

Research on *P. polycephalum* is as versatile as the organism itself. The fact that the slime mold's sporangia look so much like the fruiting bodies of fungi have led to their early inclusion into the fungal kingdom. Furthermore, *P. polycephalum* feeds on organic material from e.g. decomposing plants, emulating a saprophytic lifestyle typical for fungi. However, slime molds are neither plants, nor animals or fungi, but have certain traits in common with all of these groups. By way of example, under non-favorable environmental conditions, *P. polycephalum* forms a sclerotium, an inactive dormant state that can be reversed and reactivated by adding water and nutrients. Sclerotia formation allows *P. polycephalum* to survive in a dormant state for several years. The robust walls of the sclerotium contain cellulose [Ogawa et al., 2010], a molecular feature of plants.

The pigments which give *P. polycephalum* its exquisite yellow color seem to be unique to the organism. So far, several pigments have been identified [Gray, 1955; Wormington and Weaver, 1976; Eisenbarth and Steffan, 2000]. Some of them serve as photoreceptors. *P. polycephalum* responds to UV and visible light by exerting negative phototaxis and light-induced morphogenesis (sporulation of starving plasmodia). Light sensing is mediated by phytochromes, and several such blue and UV light perceiving molecules feed information into signal transduction pathways, thus controlling basic cellular functions [Marwan, 2001]. Hence, the physiology of *P. polycephalum*'s photo-sensing shares motifs from both plants and animals; phytochromes and blue light receptors play a role in

higher plant development, whereas the light-induced sporulation pathways and negative phototactic motility responses are found in animal cells as well.

Furthermore, the numerous mitochondria, evolutionary understood as endosymbionts, are of the tubular type, which is typically found in fungi and other protozoa [Daniel and Järlfors, 1972]. In addition, mitochondrial fission follows a synchronized cycle [Kawano, 1991] – like nuclear divisions. The mitochondrial genome has been completely sequenced [Takano et al., 2001], revealing extensive RNA editing and biparental inheritance of mitochondria, which otherwise only occurs in some yeasts and fungi.

In the past, scientists curious to learn more about the huge and fast moving giant amoeboid organism *P. polycephalum* sent it to space [Block et al., 1986], coincidentally aboard the last successful mission of the space shuttle "Challenger". A few years later, the German astronaut Ulf Merbold performed experiments with *P. polycephalum* in space again [Block et al., 1994]. The goal of these experiments was to determine *P. polycephalum*'s ability to react to gravity (graviresponse). Down on Earth, another bench-marking demonstration was performed in the 1990s at the University of Bonn in Germany. In honor of Karl-Ernst Wohlfarth-Bottermann, then the Director of the University's Institute of Cytology and Micromorphology, the slime mold was grown on oat flakes laid out in a W-shaped filter paper-covered device (see Figure 1a in [Stockem and Brix, 1994]). It was at about this time that research on *P. polycephalum* spread from Japan to Europe and the Americas. The W-shaped specimen covered a surface area of $5.5\,\mathrm{m}^2$ at the end of the experiment and weighed approximately 3 kg, which earned it the title of largest single cell ever grown, worth a lasting entry into the Guinness Book of Records in 1989 [Hausmann and Stiemerling, 1997]. The 3 kg of biomass were used for subsequent biochemical experiments, in support of research efforts towards understanding the molecules enabling *P. polycephalum*'s astonishingly fast, precise, and decisive movement, that is, by a rhythmic shuttle streaming with a periodicity in the minutes-range.

From an evolutionary and taxonomic perspective, slime molds still offer challenges. *P. polycephalum* is a member of the myxogastria, which are characterized by the formation of syncytial plasmodia (i.e. plasmodia composed of a single cell). They are linked by common evolutionary ancestry to cellular slime molds, with *Dictyostelium discoideum* being the most prominent model organism among them. *Myxogastria* and *Dictyostelia* differ in several important aspects. The vegetative state of *D. discoideum* is a haploid solitary feeding stage. Sexual reproduction is preceded by aggregation and subsequent fusion of the cells (for reviews on *D. discoideum*, see [Romeralo et al., 2012] and [Li and Purugganan, 2011]). In contrast, the vegetative state of *P. polycephalum* is a large coenocyte with diploid nuclei, which differentiates into fruiting bodies producing haploid spores. The phenotypic characteristics of such fruiting bodies have been the main tool of classification in myxogastria. So far, agreement with evolutionary reconstruction is

based upon DNA sequence data [Fiore-Donno et al., 2008, 2010]. At the finer resolution of relatedness between species and genera, traditional systematics began to falter. Molecular evidence even blurred the concept of genera by providing evidence that the genus *Physarum* is not uniform, with *Badhamia utricularis* as a close relative of *P. polycephalum* [Nandipati et al., 2012]. Sampling of *B. utricularis* globally, for subsequent tests to understand geographic diversification, revealed this species as emerging from at least two different "cryptic" species [Aguilar et al., 2014]. It is likely that such cryptic diversity will be found in other widespread genera as well.

The ability of *D. discoideum* to produce viable offspring from cross breeding of different genotypes of established lab strains is narrow [Faix et al., 2004]. These limitations explain the complications occurring when strain-crossing experiments with cellular slime molds were performed. On the other hand, hybridizing different strains is well possible among *P. polycephalum*, thereby facilitating the generation and analysis of numerous mutants [Dee, 1982; Cooke and Dee, 1974]. Since a few years, transformation of *D. discoideum* with plasmid DNA is possible [Gaudet et al., 2007], but this technique has not been realized so far for *P. polycephalum*. Hence, it is still not possible to use classic means of genetic modification on *P. polycephalum*, hindering transient transfection or stable transduction experiments. There is, however, hope to establish state-of-the-art genome editing systems for genetic manipulation of *P. polycephalum*. Such experiments will be instructive with regard to overcoming the robustness of *P. polycephalum* to genetic manipulation, or, in other words, in understanding its impressive genetic stability.

Despite some limitations for experimental work with *P. polycephalum*, genome sequencing has been achieved [Glöckner et al., 2008]. The slime mold's genome is comprised of 188 million nucleotides, encoding 34,000 genes, which is over 50 percent more than the human genome has. The genome of *P. polycephalum* revealed unexpected insights into early evolution of eukaryotes such as an astonishingly early emergence of tyrosine kinase-mediated signaling [Schaap et al., 2015]. This pathway, previously considered important for the developing multicellularity in animals, has apparently been lost in the genomes of fungi and other amoebozoa such as *D. discoideum* [Eichinger et al., 2005].

Slime molds, in particular *P. polycephalum*, have been grown in laboratories around the world for many decades. The question therefore arises to what extent such strains maintained differences due to inbreeding, similar to phenomena observed in yeasts [Gu et al., 2005]. Adaptation was made responsible for easy cultivability of *P. polycephalum* amoebae on simple media [McCullough and Dee, 1976]. However, and forward-looking, it would be interesting to find out how quickly strains diverge upon continuous subculturing of plasmodia. In light of its long history as an *in vitro*-cultured giant amoeba featuring high genetic stability as such, *P. polycephalum* would be a good candidate as model organism in studies on microevolution.

2.5 Laying of the cornerstone: Locomotion – function follows structure

The foundations for many more recent discoveries were established decades ago. In particular, studies on the locomotion machinery and the cytoskeleton of *P. polycephalum*, which enable its characteristic oscillations, provide an important basis for establishing the acellular slime mold as a model organism.

One of the most prominent features of *P. polycephalum* is its motility. Since the organism is so big, its internal movements are easily visible, even with the naked eye. Shuttle streaming, i.e. the movement of endoplasm (fluid cytoplasm) through veins and the conversion from endo- to ectoplasm (gel-like rigid cytoplasm) in certain zones was one of the first phenomena to be described. Shuttle streaming has been discovered early on [Kamiya, 1950, 1960]. At first, the origins of the contraction-relaxation cycles were not clear. Contractile fibrils were identified [Wohlfarth-Bottermann, 1962], and soon a correlation between the fibrillary structures and the motive force generator driving the shuttle streaming was established [Wohlfarth-Bottermann, 1963, 1964; Porter et al., 1965; Nagai and Kamiya, 1966; Nagai and Kato, 1975; Rhea, 1966; Usui, 1971]. It became clear soon after that the filaments consisted of F-actin and that the motor protein was myosin [Nachmias et al., 1970]. Once this was established, the search for an underlying biochemical oscillator began which would explain the regular and rhythmic contraction-relaxation cycles of *P. polycephalum*'s acto-myosin system. Simultaneously, the ultrastructure was investigated further. The research efforts were focused on uncovering the components of the cytoskeleton of *P. polycephalum* in order to compare the rapidly emerging knowledge with data gained from other model organisms used in cell biology. Many groups [Wohlfarth-Bottermann and Fleischer, 1976; Wohlfarth-Bottermann, 1979, 1977; Brix and Stockem, 1987, 1989; Brix et al., 1987a] contributed extensively to this topic during the late 1970s and 1980s. The research endeavor proved right in fulfilling its promises for the future, as we now understand how actin and myosin interact with each other to bring about the cytoplasmic shuttle streaming that is so unique and special for *P. polycephalum* [Kamiya, 1981].

As a next step, the giant plasmodial network had to be miniaturized. At first, this might seem trivial, but reproducibly creating smaller units of the phaneroplasmodia remains a difficult task. Depending on the research question at hand, either isolated endoplasmatic drops, isolated actomyosin threads or microplasmodia can be used.

Particularly for light and electron microscopic investigations and biochemical experiments, it was necessary and useful to develop smaller models of *P. polycephalum*. When a vein is punctured, the endoplasm pours out due to the high intracellular pressure and forms so-called protoplasmic drops [Wohlfarth-Bottermann, 1965; Achenbach et al., 1979]. These can be taken off the strands after a couple of minutes for

further analysis. Characteristic for protoplasmic drops is the rapid creation of new plasma membrane and the formation of invaginations and vacuoles within 10 to 15 min. If the protoplasmic drops are incubated in a caffeine-containing medium, they will form spheres enclosed in a plasma membrane without any invaginations, producing so-called caffeine droplets [Sato et al., 1981; Kukulies and Stockem, 1985; Brix et al., 1987b]. Actomyosin threads can be generated by squeezing out the endoplasm into water [Baranowski and Wohlfarth-Bottermann, 1982]. These threads enable *in vitro* studies of actin and myosin over several contraction and relaxation cycles, and were useful in analyzing molecular events in cell motility, e.g. the role of ATP [Matsumura et al., 1980].

Alternatively, *P. polycephalum* can be maintained in constantly agitated axenic cultures, whereby shear forces create so-called microplasmodia [Goodman, 1980; Gawlitta et al., 1980]. This system is more reproducible than cutting off pieces from a macroplasmodium, because a macroplasmodium is not homogenous. There are chemical gradients, and cell organelles might not be distributed evenly. A great number of microplasmodia can be produced from one single macroplasmodium put into a shaking liquid culture. Shear forces tear the plasmodium apart, and after one or two days, equally sized microplasmodia appear. Their size is dependent upon the shaking speed. Microplasmodia, because they float freely in nutrient medium, have an actin network different from that of macroplasmodia grown on a solid substrate [Brix et al., 1987a]. From the investigations of microplasmodia from shaking cultures, insights into the formation of early networks could be gleaned. When microplasmodia are plated upon a solid agar surface, they fuse locally and give rise to a connected network *via* a percolation transition [Fessel et al., 2012, 2015]. The shape of the networks is strongly dependent on environmental parameters, e.g. softness of substrate, nutrient and repellent concentrations [Takamatsu et al., 2009].

Undisputed, the interactions between actin and myosin, specifically in the cortical cytoskeleton beneath the plasma membrane, are responsible for the relaxation-contraction cycles observed in macro- and microplasmodia of *P. polycephalum* (e.g. [Brix and Stockem, 1989; Brix et al., 1987a]). However, the search for the biochemical or primary oscillator is still ongoing. While it is highly likely that biochemical processes lie at the heart of the notional oscillator, it is also possible that hydrodynamic interactions alone account for the observed oscillations [Teplov et al., 1991]. This notion is reflected by some physical models, see section 2.6. Genetically encoded cellular rhythms are generated by complex interactions among macromolecules like cytoskeletal proteins, ions and metabolites. Such biochemical oscillators control every aspect of cell physiology and encompass signaling, motility and development. An example of an inherently oscillatory process is glycolysis. In *P. polycephalum*, the inhibition of glycolysis leads to a significant change in the oscillation period [Korohoda et al., 1983]. The comprehensive oscillatory system of cytoskeletal elements and biochemical pathways is, however, intricate and involves many parameters (figure 2.3). Energy metabolism, mitochondria and calcium

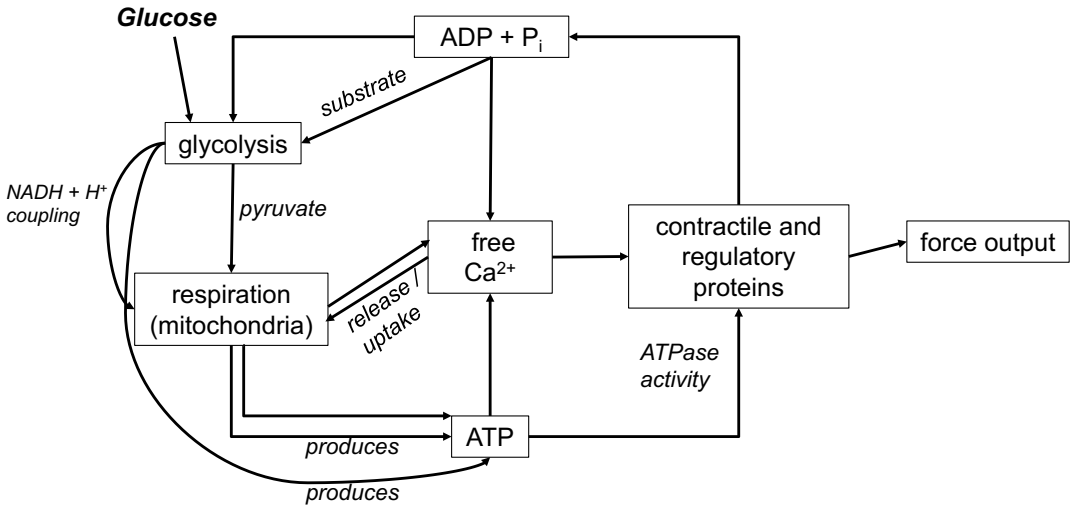

Figure 2.3: Proposed oscillatory network (modified after [Korohoda et al., 1983]). Model of the physiological oscillator governing rhythmic contractile phenomena.

ions are involved, as well as the contractile elements of the cytoskeleton, and their molecular regulators. It is this interplay that creates the observable force output.

Involved in the interaction between actin and myosin are calcium ions, since *P. polycephalum* myosin binds calcium, and becomes inhibited by high concentrations [Kawamichi et al., 2007; Nakamura and Kohama, 1999]. Thus, it was postulated that the contraction mechanism is unlike that in e.g. muscle cells, where calcium is strictly required for the interactions between myosin and actin molecules, but resembles that in plants (e.g. the alga *Chara*) and other lower eukaryotes, where the two proteins also interact in the absence of calcium. However, this interaction (binding and dissociation) and its inhibition might well be dependent on varying concentrations of free calcium ions. It is certain, however, that calcium plays a prominent role in the contraction-relaxation cycle. Evidence for a calcium binding site on the light chain of myosin has been found [Farkas et al., 2003]. Calcium oscillations have been described frequently in *P. polycephalum* (e.g. [Ridgway and Durham, 1976; Yoshimoto et al., 1981; Yoshimoto and Kamiya, 1982]). This underlines the importance of calcium (as Ca^{2+}) as ubiquitous second messenger with wide-ranging physiological roles. These include the aforementioned muscle contraction, neuronal transmission processes, cellular motility and fertilization of egg cells. It is important in cell growth and proliferation, and equally essential for the rapid oscillating motion allowing *P. polycephalum* to move and make its decisions for survival.

2.6 Physical Models

Recognizing the regularities of oscillatory phenomena in *P. polycephalum* and in acknowledging the actomyosin system as the driving force, questions about the biochemical nature and the spatiotemporal self-organization of mechanochemical activity emerged. Modeling supports assessments of the physics of self-organization, self-sustained (or auto-) oscillations, cytoplasmic streaming, and lastly, amoeboid motility. The purpose of creating models is to understand in simpler, albeit more abstract, terms how and why cells oscillate and move about. Several models have been suggested, the earliest being the proposal that the cell cycle of *P. polycephalum* is driven by a relaxation oscillator [Kauffman and Wille, 1975; Tyson and Kauffman, 1975].

Rhythmic oscillations are locally very well coordinated along the plasmodial body, so that they collectively and sequentially produce a gradient of pressure. This gradient induces protoplasmic streaming towards the leading edge ('front') of the plasmodium. Interestingly, the slime mold uses peristalsis to drive internal cytoplasmic flows. Peristalsis is caused by a wave of cross-sectional contractions along a tube. Neighboring areas are more in phase than tubes that are further apart in the network, and when the wavelength of the peristaltic wave is of the order of the size of the network, regardless of overall network size, transport is optimized [Alim et al., 2013]. It is puzzling, though, how the slime mold can measure its own size and adjust the peristaltic wavelength accordingly. It is suspected that signaling molecules are involved, which are triggered by a stimulus (e.g. food). The signaling molecules then cause a feedback loop by increasing the local contraction amplitude, thereby generating enhanced cytoplasmic flow to propagate further into the network, where the process is repeated [Alim et al., 2017].

When it comes to modelling the observed oscillation patterns, opinions diverge. Two general schools of thought are pointed out, namely a biochemically centered explanation, and another, based on mechanochemical oscillations. A prominent example of a calcium-driven mechanism was postulated by Smith and Saldana [1992]. In short, their model explains shuttle streaming in the veins of *P. polycephalum* to depend on phosphorylation-dephosphorylation cycles on the motor protein myosin. In this model, relaxation and contraction cycles are believed to be mainly driven by the exchange of calcium between the cytosol and intracellular storage compartments (like the endoplasmatic reticulum and the mitochondrial matrix). Later, this model was modified by taking flow and deformation into account [Radszuweit et al., 2010]. Other models were put forward early on, which focused on the chemical aspects of the oscillator. In spite of its unknown nature, coupled phase-oscillator models are mentioned consistently [Miyake et al., 1993; Takahashi et al., 1997; Takamatsu et al., 1997]. A reaction-diffusion-advection model was also postulated [Nakagaki et al., 1999], which considers diffusion as well as advection of the endoplasm.

Another set of models focuses on the assumption that spatial coordination can be achieved by mechanical interactions between different regions (e.g. [Matveeva et al., 2010b]). V.A. Teplov developed a model according to which self-excited mechanochemical oscillations occur when the external load exceeds a critical value [Teplov, 2010]. The activation of mechanical stress-induced membrane-bound receptor proteins (which are typically found in other cellular systems) and the subsequent activation of intracellular messengers, which then trigger the cytoskeleton, are central to this model. The advantage of this particular model in mechanistically explaining the shuttle streaming of the giant *P. polycephalum* is given by its validity for large-sized systems. Diffusion and convection are not limiting factors, but mechanical, i.e. hydrodynamical connections, play the dominant role. The hypothesis is that local positive feedback between deformation and contraction of the contractile apparatus exists. Thus, hydrodynamic interaction alone, between different regions of the strand via the streaming endoplasm, is capable of inducing the observed characteristic contractile behavior [Teplov et al., 1991]. In this latter aspect, earlier hypotheses also took hydro-dynamical changes into consideration in explaining periodic contraction-relaxation cycles of miniature models derived from *P. polycephalum* [Kukulies and Stockem, 1985].

However, the truth may lie between both classes of models. For example, a reaction-diffusion based model [Yamada et al., 2007] focuses on biochemical processes but takes into account hydrodynamic flow effects. Other chemo-mechanical models have also been constructed [Akahane et al., 1999]. The viscoelasticity and stiffness of the cytoplasm are important features that were integrated into more recently proposed models [Kobayashi et al., 2006; Rieu et al., 2015]. Based on experiments with migrating fragments of *P. polycephalum*, a model has been costructed which includes forces from the viscous endoplasm, a poro-elastic, contractile cytoskeleton and adhesive interactions with the substrate [Lewis et al., 2015]. The coordinated influences of these factors seem to be responsible for the observed locomotion. In addition, the extensive system of plasma membrane invaginations of plasmodial veins might allow for fine-tuned adjustments by means of localized surface extension and reduction.

As mentioned above, *P. polycephalum* exhibits intelligent characteristics, e.g. during foraging, where it is capable of solving the shortest path problem. The slime mold also has some form of memory. Given the absence of a nervous system, there has been considerable interdisciplinary interest in understanding the rules that govern its behavior. Memory, for example, can be modeled as a set of differential equations [Tachikawa, 2010]. It can, however, also be modeled as the response of a simple electronic circuit [Pershin et al., 2009]. The material properties of the slime mold, i.e. the elasticity of its membranes and cytoskeleton, and the fluid flow inside the veins, lend itself to the construction of an equivalent electrical circuit made up of passive elements such as resistors, capacitors and inductors. Together, they form a circuit which can 'learn' and

predict subsequent signals. A simplification, but it is an elegant one, which reduces the complexity of the biological system while still being useful in examining primitive intelligence.

2.7 The arts of *Physarum polycephalum*

BioArt is an artistic genre that emerged in the 1980s. It exploits the relationship between science and art by, for example, using living matter as a new medium. Unforeseen forms of beauty and understanding arise from scientific progress in biology and the life sciences, but also unexpected risks and ethical questions. BioArt takes up this ambivalence and materializes and visualizes it. The genre is varied. Historically, plants and animals have appeared in numerous works of art. In a long and ongoing process, humans have even influenced the evolution of plants and animals by selective breeding and domestication, creating e.g. ornamental flowers and various breeds of pets, selected and appreciated for their aesthetic value [Gessert, 2012]. Thus, the idea that organisms could be art is not new. Today, artists also work with bacteria, fungi, slime molds, and cell lines that have been genetically modified and only exist in laboratories. Such manipulations require collaborations with scientists and access to laboratories. By dealing with e.g. biotechnology, synthetic biology, genetics and biomedicine, BioArt can also serve as a way to communicate scientific developments to the public and to initiate ethical discussions. An overview and an introduction into BioArt is given by the book "Signs of Life: Bio Art and Beyond" by Eduardo Kac [Kac, 2007].

The beauty and fascination of *P. polycephalum*, this long-lived giant amoeba, has even inspired a growing number of artists who include the slime mold into their works of art and performances. The plasmodial network of *P. polycephalum* in itself is fascinating, and many scientific experiments, e.g. the observation of foraging patterns or network growth, possess a certain aesthetic quality. Therefore, it is not surprising that the slime mold has been embraced by the arts (figure 2.4). The slime mold has become a collaborator and performer in artistic endeavors. While growing inside, under and on sculptural art work, *P. polycephalum* is being used as a living material and an inspiration alike. Questions that interest researchers are also asked by artists, such as what can be learned from a primordial organism about decentralized cooperation and the limits of consciousness. By using living slime molds as art material, connections can be made between the different ways humans and non-sentient beings like the slime mold experience life. Or, in simpler terms: "How does the slime mold know what it knows? How do we know what we know?" [Wilk and Sutela, 2016].

The experiment "Being Slime Mold©", devised in 2013 by British artist Heather Barnett in collaboration with the journalist Daniel Grushkin, is a participatory experiment in which groups of people emulate the behavior of the slime mold by obeying simple rules. The 2014 documentary titled "The Creeping Garden" by Tim Grabham

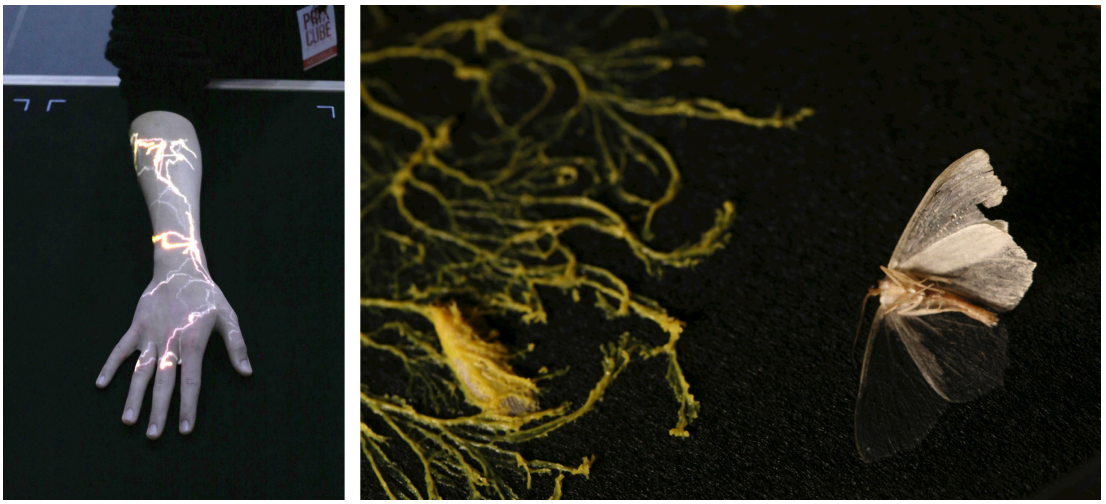

Figure 2.4: Left: "Bodymetries. Visitor at the installation at Prix Cube exhibition (2014)" by Theresa Schubert [2014]. Right: "Slime Mould Seeking Food" by Heather Barnett.

and Jasper Sharp shows that the growing, moving slime mold is aesthetically pleasing and very fascinating. German artist Theresa Schubert is also embracing the slime mold when creating pieces of art, for example by projecting its sophisticated network of veins onto human skin. Together with Andrew Adamatzky, they published the book "Experiencing the Unconventional: Science in Art" [Schubert and Adamatzky, 2015] which aims to bring together art, digital media projects, molecular biology and computer sciences, but also physics, chemistry, and robotic science. The slime mold is a unique organism, in that it inspires and extends into each and all of these areas. A fascinating workshop, Nodes & Networks [Barnett, 2015], has been designed by Heather Barnett around the First International *Physarum* Transport Networks Workshop (PhysNet), held as part of BICT (9^{th} Conference on Bio-Inspired Information and Communications Technologies) from December 3 – 5 2015 at Columbia University in New York City. An array of diverse individuals were discussing and creating interactions of arts and science. Amongst others, artists, physicists, a geneticist, an urban architect, a bee ecologist, an internet researcher, and a games designer, mingled for three days to come up with an *ad hoc* project in order to interact with the interested public on a Sunday. A write up of this adventure can be found in the August 2016 issue of SciArt Magazine [Kellhammer, 2016].

2.8 Conclusion

In summary, *P. polycephalum* is a versatile model organism that, despite decades of research, still holds some challenges in store. In particular, advancements in the subject of genetics will shed light onto the complicated processes of cell cycle regulation,

metabolism and signaling pathways. The complex behavior of *P. polycephalum* is currently another research focus. By studying how a brainless and rather simple organism navigates its environment and makes optimal decisions securing its survival, the broader question of an underlying universal mechanism of decision-making arises. The goal is not only to describe the behavioral pattern in response to environmental cues, but also how this information is perceived and processed within the slime mold. To answer these questions, the role of fluid flow and oscillations within the veins has to be investigated in order to get a detailed picture of network dynamics and motility. Present research on this fundamental topic is highly interdisciplinary and even extends to artificial intelligence and robotics. Furthermore, membrane-bound sensors and molecular signaling pathways need to be identified in order to complete our picture of the slime mold as a whole.

Chapter 3

Form follows function: ultrastructure of different morphotypes of *Physarum polycephalum*

Christina Oettmeier[1,2,3], Jonghyun Lee[1], and Hans-Günther Döbereiner[1,2,3]

[1] Institute for Biophysics, University of Bremen,
Otto-Hahn-Allee 1, 28359 Bremen, Germany
[2] Mechanobiology Institute, National University of Singapore, Singapore
[3] Authors to whom any correspondence should be addressed.

Supplementary material for this chapter is available online at `https://iopscience.iop.org/article/10.1088/1361-6463/aab147/data`. Further information can be found in the appendix (section 7.1).

3.1 Abstract

The multinucleate, unicellular slime mold *Physarum polycephalum* is a highly motile and morphologically diverse giant amoeba. Despite being brainless and lacking neurons, it exhibits 'smart' behavior. There is considerable interest in describing such traits and to investigate the underlying mechanochemical patterns which may hint at universal principles of behavior and decision-making. Furthermore, the slime mold's mechanism of locomotion is unique. It resembles amoeboid movement, but differs from the locomotion of other amoebae in many ways, e.g. in their much larger size and lack of lobopodia. These two aspects, behavior and locomotion, are linked by the cytoskeleton and the overall morphology of *P. polycephalum*. In this paper, we present a structural analysis of different growth forms (micro-, meso- and macroplasmodia) by transmission

electron microscopy (TEM), scanning electron microscopy (SEM), light microscopy, and fluorescence microscopy of F-actin. With these detailed investigations of cellular ultrastructure and morphology, we provide the basis for the analysis of, e.g., viscoelastic and rheological measurements. Our data also provide structural details for the many models that have been constructed for the understanding of locomotion. We conclude that morphological information is vital for the assessment and measurement of material properties.

3.2 Introduction

Physarum polycephalum is a unicellular but multi-nucleated protist. It is a coenocyte, i.e., a large cell with multiple nuclei which is the result of multiple nuclear divisions without accompanying cytokinesis. Cell organelles such as mitochondria, nuclei and food vacuoles move freely within the cytoplasm, which is enclosed by a plasma membrane. *P. polycephalum* does not possess many permanent structures, because the amoeboid cell is continuously changing its shape in adaptation to environmental factors and life cycle requirements. In addition, *P. polycephalum* is a highly motile organism, which utilizes directed cytoplasm flow to achieve locomotion.

P. polycephalum can take on many shapes and sizes, several of which are the subject of this study. Figure 3.1 gives an overview over the different morphotypes. The predominant growth form in nature is a **tubular vein network**. In its vegetative diploid state, the slime mold forms networks that can extend over square meters (figure 3.1 c). When the organism is cultivated in a liquid shaking culture, micrometer-sized **microplasmodia** are formed (figure 3.1 a). Microplasmodia can fuse with each other. During the sexual phase of *P. polycephalum*'s life cycle, haploid amoeba fuse to give rise to tiny diploid plasmodia. Diploid plasmodia can repeat this process, resulting in bigger diploid plasmodia. Fusing (diploid) microplasmodia mirror this sequence of fusion processes, but they belong in the vegetative phase of the life cycle. In between the micrometer-sized microplasmodia and the huge networks are millimeter-sized **mesoplasmodia** (figure 3.1 f). The ultrastructure of this growth form is described here for the first time.

A striking feature of *P. polycephalum* is its motility. Due to the organism's large size, its movements are easily visible. Especially the flow of endoplasm through veins (called shuttle streaming) and the regular oscillations can be observed with the naked eye. The cytoskeleton of *P. polycephalum* consists of several components and has different levels of organization, which vary between morphotypes. The most significant cytoskeletal element is the actomyosin system, because it is responsible for the contractile activity of the cell. Movement is caused by the interaction of actin and myosin, see e.g. [Kamiya, 1981; Nakamura and Kohama, 1999]. Different types of actin filaments can be found in *P. polycephalum*. All morphotypes have a membrane-bound filament

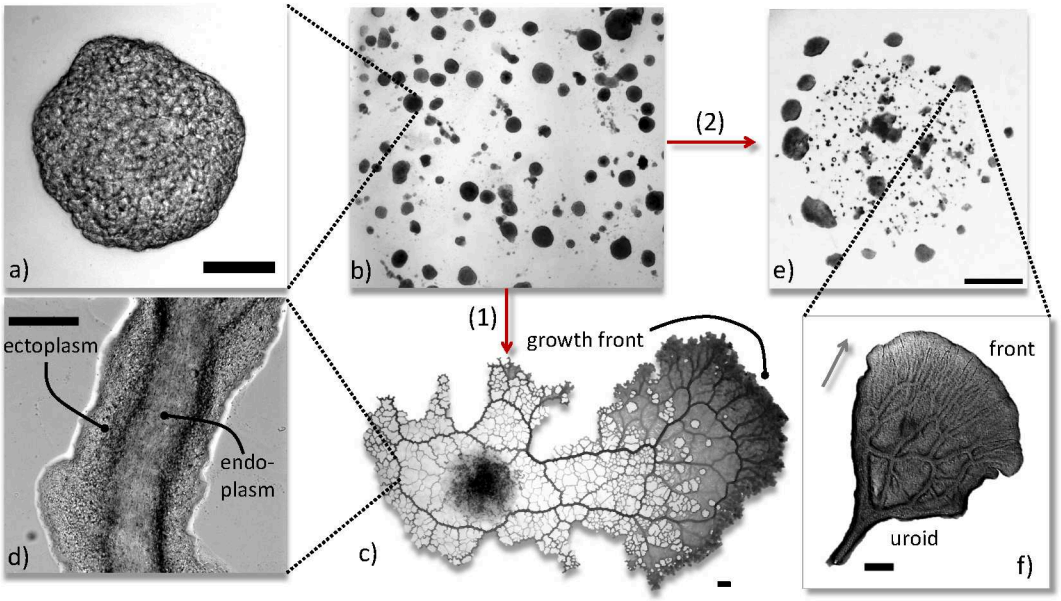

Figure 3.1: Variability of the diploid phase of *P. polycephalum*. a) Microplasmodium in liquid medium, scale bar = 100 µm. b) Microplasmodia plated onto an agar surface. Depending on the nutrient composition of the agar, the microplasmodia fuse and give rise to different growth patterns. (1) Under non-starvation conditions, the microplasmodia transition into a network. c) Macroplasmodial network formed under ideal nutritional conditions. The black area is inoculum residue from where microplasmodia were placed on the agar. In brightfield images, darker areas often correspond to a greater thickness. The network is thicker on its right side and has a pronounced growth front, which indicates movement to the right. However, this does not imply persistent movement to the right. Scale bar = 1000 µm. d) Detail of a vein. Stationary ecto- and flowing endoplasm are clearly visible. Scale bar = 100 µm. (2) When glucose is lacking from the medium, microplasmodia only fuse locally and give rise to mesoplasmodia. This is most probably a search pattern, because each single mesoplasmodium moves outwards from the initial patch on a straight trajectory for hours. e) Microplasmodia form mesoplasmodia. Scale bar = 3000 µm. f) Mesoplasmodium. This is a polarized cell which is differentiated into an anterior part (indicating the direction of movement) and a posterior part, also termed uroid. Scale bar = 250 µm. All images are of living, unstained slime mold and taken with a light microscope.

cortex, which is involved in motive force generation and serves to maintain intracellular pressure [Brix et al., 1987b; Gawlitta et al., 1980].

However, there are organizational differences between free-floating microplasmodia and substrate-attached forms, which have a more complicated microfilament system that is also involved in substrate adhesion. In meso-and macroplasmodia, the actin cytoskeleton is differentiated into a cortical and a fibrillar system [Brix and Stockem, 1987]. Both systems are made up of F-actin, but the cortical cytoskeleton remains attached to the plasma membrane, whereas the fibrillar system is rearranged often or lacking altogether, as in microplasmodia. The actin cytoskeleton is highly dynamic. Besides the motor protein myosin, many different proteins are involved in its dynamics. Profilin, for example, binds to monomeric actin and keeps over 50 percent of the cell's actin in the G-form without affecting the length distribution of actin filaments [Ozaki and Hatano, 1984]. Fragmin severs F-actin filaments and blocks the association of fragments by capping the ends [Hasegawa et al., 1980].

The cytoplasm of *P. polycephalum*'s macro- and mesoplasmodia is morphologically divided into ecto- and endoplasm. The solid ectoplasm (see figure 3.1 d) forms the walls of veins, through which the more liquid endoplasm flows. The different properties of endo- and ectoplasm are listed in table 3.1. Endoplasm flows passively through the veins

Table 3.1: Comparison of the properties of endo- and ectoplasm.

endoplasm	⇆	ectoplasm
no contraction		contractile
high G-actin content		high F-actin content
flowing		stationary
high plasticity		low plasticity
no pores		porous
low viscosity		high viscosity

due to hydrostatic pressure differences, which are brought about by rhythmic ectoplasmic contractions, i.e. actomyosin interactions. This differentiation into endo- and ectoplasm and the resulting internal flow is crucial for locomotion and shuttle streaming. However, endoplasm can be converted into ectoplasm and vice versa [Isenberg and Wohlfarth-Bottermann, 1976]. This phase transition can be caused by actin polymerization, but also by mechanical factors like flow-induced pressure [Guy et al., 2011]. Pressure increases the actin depolymerization rate and turns solid ectoplasm into fluid endoplasm.

What has sparked recent and renewed interest in slime molds is their seemingly 'intelligent' behavior. *P. polycephalum* has been shown to solve mazes [Nakagaki et al., 2000], connect multiple food sources *via* the mathematically shortest pathway [Nakagaki et al., 2004a], and tackle the traveling salesman problem [Zhu et al., 2013]. Furthermore, the

slime mold makes decisions, evaluates food sources based on their nutrient conditions [Dussutour et al., 2010], and possesses a memory [Reid et al., 2013; Saigusa et al., 2008; Reid et al., 2012]. These features are usually associated with life-forms which have a higher degree of information-processing sophistication, e.g. which possess brains or neuronal structures. Nonetheless, much of the slime mold's behavior is similar to that of higher organisms. The underlying functions are not neuron-based, but are emergent phenomena, resulting from mechanochemical processes on the tubular network.

The basic physiochemical processes which lead to the complex patterns of *P. polycephalum*'s locomotion and behavior are intimately linked to the cytoskeleton. An example is the processing of chemotactic stimuli: When a plasmodium encounters a chemoattractant, the local oscillation frequency increases. The whole organism then moves towards this area of higher frequency. In contrast, the plasmodium moves away from repellents, which locally decrease the frequency [Durham and Ridgway, 1976]. It has further been speculated that the cytoskeleton is a sensory-motor data network and facilitates the apparently intelligent behavior of the slime mold [Mayne et al., 2015]. Another observation that links the cytoskeleton to the perception and procession of external signals is phototaxis. Some photoreceptors trigger signal transduction pathways which target the cytoskeleton. This results in a change of streaming periodicity, cell shape and movement direction [Marwan, 2001].

Ultrastructural investigations are essential for the understanding of *P. polycephalum* as a biological material. There are several TEM studies which precede the present work [Daniel and Järlfors, 1972; Brix et al., 1987a; Rhea, 1966], but to our knowledge, there has not been an investigation of the slime mold's surface with SEM before, except for spherules [Chet and Kislev, 1973]. Both the contraction and behavioral patterns have their origin in morphological changes. In the absence of neuronal structures, endo- and ectoplasm and the cytoskeleton are not only merely structural support, but form a dynamic information-processing system capable of organizing cell movement, growth, and behavior.

This article aims to describe the ultrastructure and morphology of different growth forms of *P. polycephalum*. Besides macro- and microplasmodia, we investigate mesoplasmodia [Lee et al., 2018], a motile growth form which has not been previously described. The importance and influence of the morphology and internal structure of *P. polycephalum* for investigation techniques such as microindentation and the construction of physical models is discussed.

3.3 Material and Methods

3.3.1 Cultivation of different *P. polycephalum* growth forms

We used the *P. polycephalum* strain WT33[a] [Marwan and Starostzik, 2002]x LU898 [Kawano et al., 1987] which was kindly provided by W. Marwan. Macroplasmodia were grown on semi-defined medium (SDM) agar (1.7 %) modified after references [Daniel and Rusch, 1961] and [McCullough and Dee, 1976], at 24 °C. Hemin ($0.01\,\mathrm{g\,l^{-1}}$) has to be present in the medium as well [Daniel et al., 1962]. The glucose concentration was $10\,\mathrm{g\,l^{-1}}$.

Microplasmodia were created by transferring macroplasmodia into liquid growth medium at 24 °C in an incubated shaker. Torn apart by shear forces, the macroplasmodium gives rise to multiple small units, whose size is determined by the shaking speed. Spherical as well as dumbbell-shaped forms can be obtained and their size ranges from 100-400 µm in diameter.

Mesoplasmodia are generated under nutrient-depleted conditions [Lee et al., 2018]. To create this growth pattern, microplasmodia were kept in liquid shaking culture until they had depleted the medium of glucose, which occured after roughly 3 days. This was confirmed by testing the medium daily with a glucose monitoring strip test (Combur-Test, Roche). The microplasmodia were then taken out of the liquid culture and plated onto agar containing glucose-deficient SDM, where they form aggregates and fuse with each other. After about three hours, the first migrating units leave the initial patch and move radially outwards.

3.3.2 Fluorescence staining and microinjection

For the imaging of F-actin, micro-, meso- and macroplasmodia were stained with the selective F-actin stain rhodamine phalloidin (Biotium). The dye was dissolved in PBS (phosphate-buffered saline) without Ca/Mg (PAA) to obtain a final concentration of 22 µM. Micro- and macroplasmodia were microinjected with rhodamine phalloidin (2.3 nl, Nanoject 2, Drummond Scientific Company). Imaging was then performed using a Zeiss Axio Observer.Z1. An Axio-Cam MRm was employed for image acquisition in conjunction with Zeiss AxioVision Software. For fluorescence imaging, samples were illuminated with a Zeiss HXP120 mercury lamp, a 556 nm BrightLine HC filter (AHF Analysetechnik) and a Zeiss 76 HE reflector filter set. Mesoplasmodia were first fixed with cold TEM fixative and left in the fridge for 10 min. They were then stained with the same rhodamine phalloidin solution (22 µM) used for microinjection, to which we added 1 µl of Triton X 100 in order to render the membrane permeable. Mesoplasmodia were then left to stain for 15 min in the fridge. Fluorescence imaging for the fixed specimens was performed as described above.

[a] In the original publication, an incorrect strain name was given.

3.3.3 Brightfield microscopy

Live cell imaging (e.g. supplementary material S1 and S3, available online (`stacks.iop.org/JPhysD/51/134006/mmedia`)) was performed using a Zeiss Axio Oberver.Z1 equipped with a Zeiss incubation system consisting of a Heating Unit XL S and a Temp Module S. All observations were carried out at a temperature of 24 °C. A Zeiss Achro Plan 10x with a numerical aperture of 0.25 was used with a 1.6x optovar lens.

3.3.4 EM and light microscopic imaging of semi-thin sections

Microplasmodia were transferred into a fixative (80 mM KCl, 50 mM sodium cacodylate, pH 7.2, 20 mM NaCl, 2.5 % glutaraldehyde). The fixation was carried out for at least 30 minutes on ice. Macro- and mesoplasmodia were fixated together with the agar they were grown on. The agar was then cut into blocks the size of a few square millimetres with a scalpel. After the glutaraldehyde treatment, samples were washed three times for 5 min each in 50 mM sodium cacodylate buffer (pH 7.2).

For post-fixation and contrast enhancement of both microplasmodia and the agar blocks with the plasmodia on top, an osmium tetroxide solution (2 % OsO_4 in sodium cacodylate buffer) was used. Samples in solution were kept on ice for 60 min. After post-fixation, samples were washed thoroughly with double-distilled water. For a higher contrast, samples were then left for 12 hours at 4 °C in the dark in a 0.5 % aqueous uranyl acetate solution. After fixing and contrasting, all water had to be removed from the tissue samples in order to replace it with a solvent (in this case ethanol) that is miscible with the embedding medium. The dehydration process was accomplished by passing the tissues through a series of increasing ethanol concentrations. First they were treated with 30 % ethanol for 30 min, whereby the ethanol was exchanged after 15 minutes. This procedure was repeated for 50 %, 70 % , 90 % and 100 % ethanol. An extra step was performed with 100 % ethanol, dehydrated with a molecular sieve (15 min).

Prior to cutting ultra- or semithin sections, the specimens had to be embedded in resin. Embedding was performed with glycid ether 100 after the method described by Luft [1961]. The ethanol was replaced with the embedding medium in a descending alcohol series: First the samples were infiltrated for 15 min with a mixture of 100 % ethanol and glycid ether at a ratio of 3:1, then at a 1:1 ratio for 15 min and finally at a 1:3 ratio for 15 min. The ethanol-resin mixture was carefully removed and the last step was infiltration of the tissue with a pure glycid ether mixture for a total of 45 min, whereby the glycid ether was replaced twice after 15 min each. After the glycid ether was removed for the last time, 1.5 % of the accelerator DMP-30 was added to the mixture of glycid ether at a ratio of 3:7. The samples were then left to polymerize in a vacuum oven at 60 °C for 2 to 3 days.

Semi- and ultrathin cutting was performed with a Reichert-Jung Ultracut E micro-

tome. Semi-thin sections were cut to a thickness of ∼100 nm, ultra-thin sections to 40 - 60 nm. Semi-thin sections were mounted onto glass slides and stained with toluidine blue solution (0.5 % toluidine blue, 0.5 % borax) prior to imaging with a light microscope (Zeiss Axio Oberver.Z1). Ultra-thin sections were placed onto copper TEM grids. TEM micoscopy was carried out on a Zeiss EM900, equipped with a water-cooled frametransfer-CCD-camera (TRS). Images were acquired using a PC with the software 'ImageSP' (TRS).

SEM images were taken with a JCM-5000 NeoScope Table Top SEM (JEOL). The difficulty in preparing the samples for SEM microscopy laid in the removal of the extracellular mucus layer. Microplasmodia and detached veins were first centrifuged gently at 250 g, then fixed in 4 % PFA (paraformaldehyde) dissolved in PBS. They were then washed two times with PBS and centrifuged again. The dehydration process was accomplished by passing the samples through a series of increasing alcohol concentrations, starting with a 15 % ethanol solution. They were then transferred sequentially to 25 %, 50 %, 75 %, and 90 % ethanol for about an hour each. Samples were stored in the refrigerator over night in 100 % ethanol. They were finally mounted onto glass slides and dried at 40 °C, then sputter-coated with gold.

3.3.5 Disruption of cortex with latrunculin A

For the experiment as shown in figure 3.6, microplasmodia were taken from the liquid shaking culture and pipetted into a 35 mm diameter glass-bottom cell imaging dish. The microplasmodia were covered with liquid growth medium and allowed to sink to the bottom of the imaging dish. We used latrunculin A (Sigma-Aldrich; CAS number 76343-93-6), dissolved in DMSO (dimethyl sulfoxide). The working solution was diluted to 10 µmol latrunculin A with growth medium. Controls were performed beforehand with different concentrations of DMSO to rule out any effects of DMSO on the normal movement of microplasmodia. A concentration of 10 µmol DMSO had no effect on the normal movement of microplasmodia, and therefore it could be used as a solvent for latrunculin A. Latrunculin A disrupts the polymerization of G-actin into filaments, and irreversibly destroys actin fibres. The untreated microplasmodia were filmed for up to an hour before a quantity of 300 µl latrunculin A was added to the imaging dish.

3.3.6 Quantitative pore analysis from SEM images

The surface of *P. polycephalum* is characterized by many invaginations and pores. Their size and distribution does not appear random, but rather seems to form a uniform, evenly spaced spatial pattern. In order to obtain quantitative data about the size and distribution of the pores riddling the slime mold's surface, SEM images of microplasmodia and veins were analyzed with the open-source software FIJI [Schindelin et al., 2012]. First, images were smoothed with a Gaussian convolution filter (radius = 1). The images were then scaled and a semi-automated segmentation of the pores was performed

using the Blow/Lasso Tool. For the resulting objects, area, centroid coordinates and circularity C (according to equation 3.1) were measured.

$$C = 4\pi \frac{[area]}{[perimeter]^2} \tag{3.1}$$

C = 1 indicates a perfect circle, values approaching zero indicate an increasingly elongated shape. For average pore areas, only pores with a circularity above 0.85 were used, thereby excluding pores distorted by their location on a curved surface, i.e. pores on the sides of round structures which would appear flattened. Figure 3.2 a) shows 'accepted' pores (orange outlines) with C > 0.85 and 'rejected' pores (cyan outlines) with C < 0.85. As a next step, the plugin ND (nearest distance) [Haeri and Haeri, 2015] was used to obtain the average distances (equation 3.2) between pores.

$$d = \sqrt{(Y_2 - Y_1)^2 + (X_2 - X_1)^2} - (r_1 + r_2) \tag{3.2}$$

Circles with radii r were fitted on each pore according to its centroid coordinates (X, Y). d is the spacing between a pair of pores (see figure 3.2 b). The distances of each pore with all the other pores were computed, and depending on the coordination number of interest, the average of the distances was calculated. In the densest 2-dimensional hexagonal packing, the coordination number (number of neighboring circles) is 6. We chose a coordination number of 3, because the pores were not densely packed. For the calculation of average distance between pores, all pores were included, regardless of their circularity.

3.4 Results

The recapitulation of our results is organized as follows: First, we report our findings on three features which are ubiquitous for all three morphotypes of *P. polycephalum*, namely i) cell surface pores which correspond to internal channel systems (section 3.4.1), ii) the submembrane actin cortex, and iii) the slime layer (section 3.4.3). Pores, i.e. openings on the surface of the slime mold, belong to the vast invagination system which, topologically, constitutes extracellular space. Next, the results of our ultrastructural investigations of the three morphotypes – microplasmodia, mesoplasmodia and macroplasmodia – are summarized. We further compare these growth forms to each other and discuss differences and similarities.

3.4.1 Quantitative analysis of surface pores

The slime mold has a porous, sponge-like internal structure with an elaborate channel system, connected to the surface via pores. These regularly spaced openings are well visible in SEM images (figure 3.3 a-d), whereas the porous internal structure can be seen in TEM images (figure 3.3 f-h). For completeness, we want to point out that these are mesoscopic pores with diameters 2 orders of magnitude larger than plasma membrane

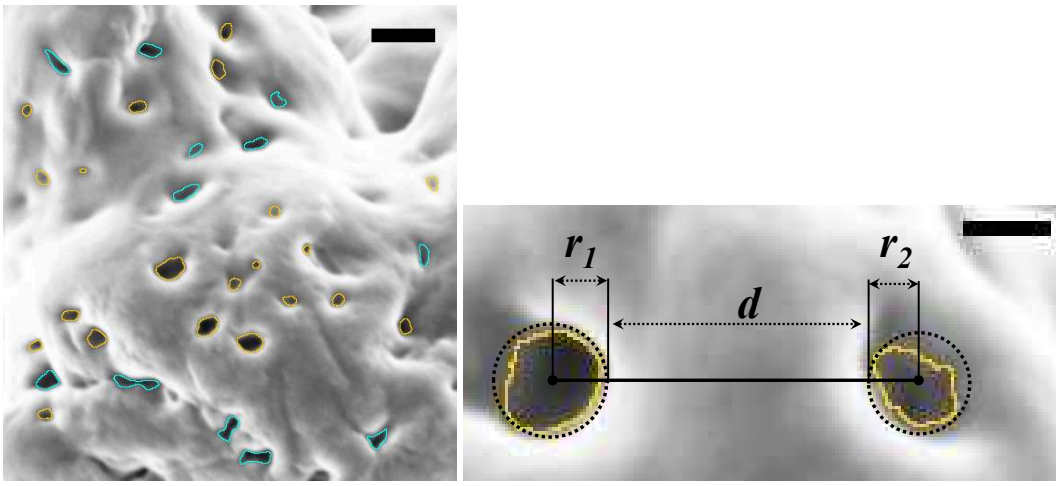

Figure 3.2: SEM images of the porous surface of microplasmodia. a) Segmented pores. Orange outline = pores with a circularity > 0.85. Cyan outline = circularity < 0.85. Scale bar = 5 µm. b) Schematic of distance calculation. Circles were fitted around two pores at the centroid coordinates. d = distance, r = radius. Scale bar = 5 µm.

pores (like e.g. in the nuclear membrane or in immune cells). Further, the topology of these systems is different. Whereas membrane pores are passages between the inside and the outside of the cell, the slime mold pores are gateways between the extracellular space and internal invaginations. Topologically, the latter corresponds to the intestinal tract of e.g. vertebrates. In total, the SEM images of 10 individual microplasmodia and 3 veins were used for the quantitative analysis of pore sizes and average distances. We found the average pore area to be $2.7 \pm 2.0\,\mu m^2$ (mean ± standard deviation) (n = 506 pores). A histogram of pore sizes can be found in figure 3.4 a, from which can be gleaned that the pore size is not normally distributed, in contrast to pore distance. Assuming a more or less circular perimeter, the pore diameter can be calculated as $2r = 2\sqrt{[area]/\pi}$. This gives an average pore diameter of $1.7 \pm 0.7\,\mu m$ (mean ± SD) (n = 506 pores). The most probable pore diameter is 1.1 µm. The pores on the surface of microplasmodia from shaking culture are more or less round, but pores on the surfaces of veins are oblong (see figures 3.3 c and d). This is reflected by their lower circularity, which was 0.74 ± 0.14 (mean ± SD)(n = 130 pores).

For the 10 examined microplasmodia, the nearest neighbor analysis data follows a seemingly normal distribution with a mean average distance between pores of $d = 7.3 \pm 3.03\,\mu m$ (n = 986 pores). A histogram of average distances can be found in figure 3.4 b. This means that pores are spaced apart by roughly 4 times their mean diameter. The relatively large error reflects some variability in the distribution of pores. However, the

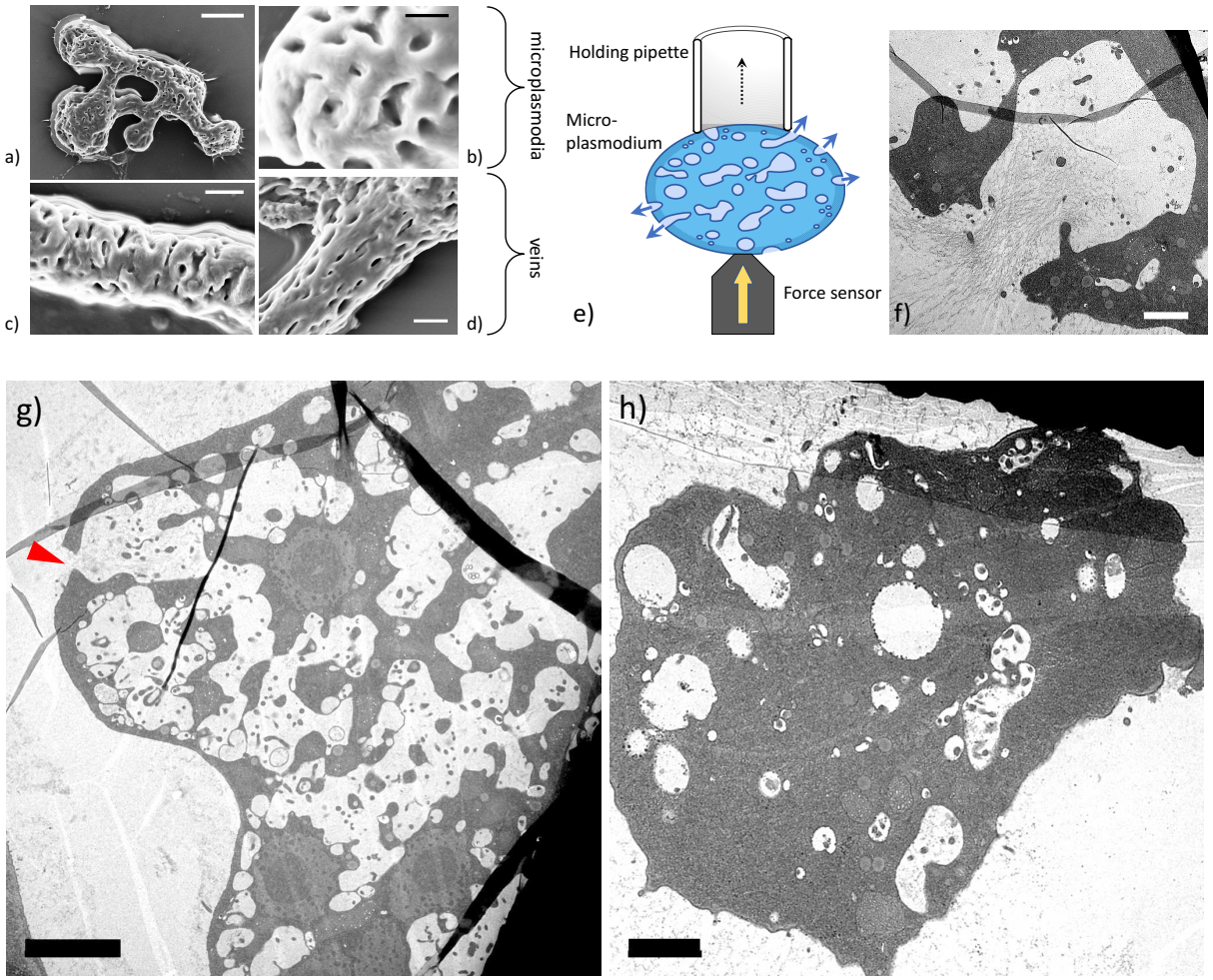

Figure 3.3: SEM images of microplasmodia (a,b) and veins (c,d). a) A larger microplasmodium which consists of several spheres connected by short tubes. Scale bar = 50 µm. b) Surface of a spherical microplasmodium. Scale bar = 5 µm. c) and d) Surfaces of veins. Scale bar = 10 µm. e) Schematic drawing of microindentation setup. A microplasmodium is sucked to a holding pipette and indented with a microforce-sensing probe. f) TEM image of a slime-filled vesicle opening to the outside of a microplasmodium and releasing slime. Extruding slime fibrils are visible. Scale bar = 2 µm. g) TEM image of a microplasmodium. Scale bar = 5 µm. h) TEM image of a small microplasmodium. Scale bar = 2 µm. Images g) and h) show the elaborate internal channel system of microplasmodia, which connects to the surface via pores (red arrow in g).

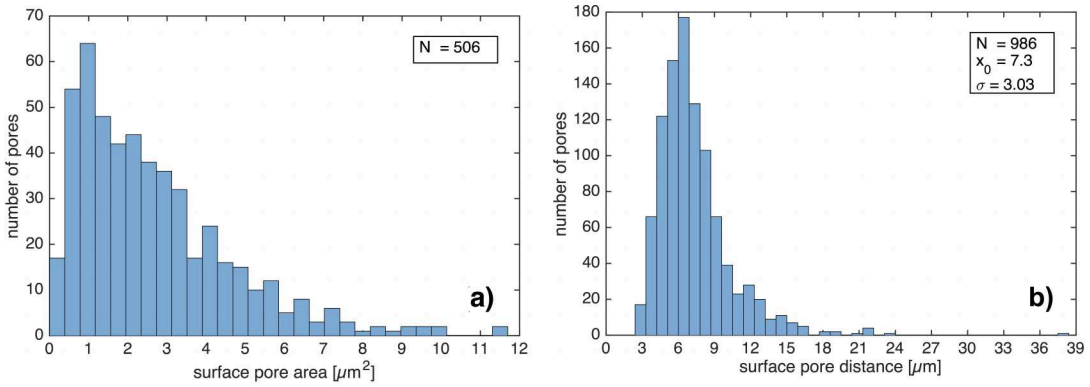

Figure 3.4: a) Histogram of surface pore area. Only pores with C > 0.85 were included, foregoing distorted pores at the sides. b) Histogram of distance between pores. Mean value $(x_0) = 7.3 \pm 3.03\,\mu m$.

standard error of the mean (S.E.M.) was only ± 0.1 µm, indicating a high measuring accuracy.

3.4.2 Cytoplasmic membrane invagination system

For an investigation of the internal channel system, we analyzed TEM images of ultra-thin sections. The invagination system [Gawlitta et al., 1980], lined with cell membrane, is connected to the cell surface via surface pores (see figure 3.3 f). Biologically, the spatial arrangement and size of pores has to be adjusted in order to provide transport of slime from the inside of the plasmodium to the exterior and vice versa. Furthermore, the invagination system provides an increase of surface area, which improves the exchange of substances across the membrane. Internal pores (see figure 3.3 g) contribute to the (macroscopic) permeability of the slime mold, i.e., the ability of a porous material to allow fluids to pass through it. We want to clarify that the term 'pore' in this context is used to indicate the fraction of void space in the material, i.e. akin to the porosity of a sponge. Permeability is related to the overall porosity of the material, but also to the shapes of the pores and their level of connectedness. Porosity can be measured from TEM images using the stereological method of point counting, based on Cavalieri's principle [Michel and Cruz-Orive, 1988]. According to Cavalieri's principle, volume fraction is equal to the area fraction, which can be obtained via point counting. Volume density, volume fraction (V_V) or porosity is the ratio between the volume of the structure and the volume of referent space.

$$V_V = \frac{\sum P_i}{\sum Q_i} \tag{3.3}$$

A grid is placed upon the image, and the number of points inside the pores (P_i) as well as all points of the structure (Q_i) are counted. In larger microplasmodia, porosity was

found to lie between 30 and 51 %, whereas small microplasmodia (such as shown in figure 3.3 h) have a porosity of only 9 to 16 %. However, unconnected pores impede fluid flow, regardless of their size. If the permeability coefficient k is known, Darcy's law governing the flow of fluids through porous media can be applied. This can be used to characterize the flow dynamics within the slime mold. Darcy permeability measurements can provide insights on the transport properties of nutrients, metabolites, and slime through the porous cell body of *P. polycephalum*.

TEM images of microplasmodia (figure 3.3 g and h), confirm that their internal structure is homogenous in that the pores are equally distributed throughout the microplasmodium. This is in contrast to meso- and macroplasmodia, where the porosity is characterized by a gradient from ecto- to endoplasm (Figure 3.9 c). This becomes especially obvious for vein cross-sections, where the flowing endoplasm is completely devoid of vacuoles and the surrounding ectoplasm of the tube wall has extensive external pores (figure 3.3 c and d) as well as internal invaginations (figure 3.11 a and b). Very small microplasmodia (figure 3.3 h) seem to have a reduced porosity as compared to larger microplasmodia (figure 3.3 g).

3.4.3 Cortex and slime layer

Like the surface pores, which constitute the openings of an extensive interconnected channel system, the cortex is found in every growth type of *P. polycephalum*, either substrate-bound or free floating. It is crucial for the generation of mechanical force and the maintenance of an intracellular overpressure relative to the exterior environment. The cortex is a membrane-associated layer, morphologically consisting exclusively of thin actin filaments [Kukulies et al., 1987]. Its thickness lies between 180 and 200 nm (figure 3.5 a). We could confirm the role of the cortex as a force-bearing cytoskeletal

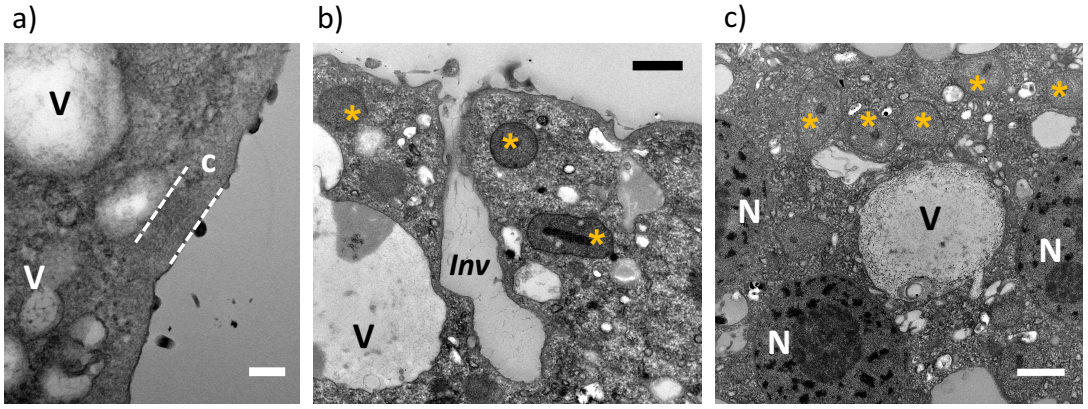

Figure 3.5: TEM images of the perimeter of microplasmodia. c = cortex; V = slime-filled vacuoles; Inv = invagination; ∗ = mitochondria; N = nuclei. a) Scale bar = 200 nm. b) Scale bar = 1000 nm. c) Scale bar = 1000 nm.

element by treating the plasmodium with latrunculin A. Latrunculin A, which severs the connections between actin filaments and also leads to their depolymerisation, caused an immediate dilation and structure loss of the cell (see figure 3.6). We used a concentration of 10 µM of latrunculin A. The intracellular pressure is very high, and the membrane

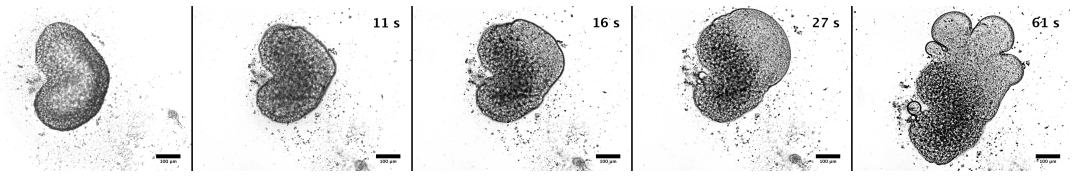

Figure 3.6: Time series of a microplasmodium treated with latrunculin A. Left image is taken before latrunculin A was added. Time stamps indicate seconds after addition of latrunculin A to the medium. Scale bar = 100 µm. The complete time series can be found online in the supplementary material (S1).

itself cannot contain this pressure. Thus, the cortex is not only necessary to keep the cell in shape, but also represents the major force generating system. In combination with the motor protein myosin, contractions of the cortex lead to rhythmic pulsations. Additionally, the cortex in the ectoplasm of a larger plasmodium orchestrates the constriction of the veins and thus the shuttle streaming. On top of the membrane lies an extensive slime layer, consisting of mucopolysaccharides [Wolf et al., 1981]. The slime is composed of an acidic polysaccharide consisting of galactose and sulfate; and trace amounts of rhamnose are present [McCormick et al., 1970]. Furthermore, the slime contains glycoproteins and enzymes [Morita and Nishi, 1991]. Slime covers the entire cell surface, including the invagination system and the internal channels and pores. Its function is to provide protection against harmful influences from the surrounding environment and to prevent dehydration. Furthermore, slime trails left on the substrate behind a migrating plasmodium can be considered an 'external memory' [Reid et al., 2012]. The slime is continuously produced in the upper layer of the ectoplasm, close to the membrane. From our images, it appears as though a more aqueous phase is also present. However, this is just a speculation and deserves further investigation. The slime appears as a filamentous layer on top of the plasma membrane. Wolf et al. [1981] have measured the diameter of such slime filaments in freeze-etched samples, which was between 5 and 10 nm. The length of the mucous filaments is difficult to analyze because the slime layer is sensitive to chemical fixation and resin embedding. Slime-filled vesicles are numerous (figure 3.5). After being filled with mucus, slime-filled vesicles move towards the plasma membrane, fuse with it and release the slime (figure 3.5 and figure 3.3 f), see also [Sesaki and Ogihara, 1997]. Slime mucopolysaccharides are clearly visible in TEM and show up as thin fibres in parallel orientation to the plasma membrane. The slime layer acts as a selective barrier for all kinds of substances, e.g. particles, dyes and other compounds. This poses a difficulty for staining protocols, making microinjection a necessity to achieve dye uptake. Staining of *P. polycephalum* with dyes that would normally be taken up through the plasma membranes of other cells has proven to be

unfeasible. We propose that the slime layer forms a barrier to diffusion. The barrier appears to be the glycoprotein sheath that surrounds the plasmodium. A similar phenomenon has been reported for the cellular slime mold *Dictyostelium discoideum* [Farnsworth and Loomis, 1974]. The authors deduce that the slime sheath surrounding *D. discoideum* is involved in a mechanism that gives the cells information concerning their position. They state that the cell may not be biochemically differentiated into an anterior and posterior end (e.g. with regard to substance or receptor gradients), but the slime layer has a different thickness at the anterior end and thus enables the diffusion of substances into the cell. It acts as a barrier to the diffusion of compounds at the other cell pole. This interesting mechanism is worth further investigation, especially with regard to the fact that the molecular nature of cell surface receptors in *P. polycephalum* remains unexplored. A slime diffusion barrier seems to be a suitable method for this organism to regulate the transport and sensing of compounds.

Furthermore, the slime cover has to be taken into consideration when discussing microindentation data. Upon compression, liquid medium and slime are reversibly forced from the pores (figure 3.3 e) and will likely re-enter the channels and invaginations when the structure is relaxed. This process will contribute greatly to the relaxation spectrum of the slime mold [Fessel et al., 2017]. The mechanical response of a poroelastic material such as the slime mold to applied loads is time-dependent, and this time dependence has an intrinsic length scale associated with the pore size of the material. This has been investigated for other poroelastic biological tissues such as hydrated bone and cartilage [Oyen et al., 2012].

3.4.4 Microplasmodia

Microplasmodia (figure 3.1 a and figure 3.7) are disconnected, spherical growth forms that are formed when macroplasmodia are cultivated in a liquid shaking culture [Bernitt et al., 2010]. This particular growth form does not occur in nature and is adapted to submersion, but there are parallels to haploid amoeba which occur during the sexual reproduction part of the life cycle. The sub-membrane cortex is well developed, but there is no distinction between endo- and ectoplasm. Microplasmodia are not polarized, i.e. they have no anterior or posterior pole which is owed to the fact that they are not locomoting, but freely floating. Polarization only occurs when they adhere to a solid surface. Microplasmodial oscillations are very distinct and have been well documented [Bernitt et al., 2010]. Microplasmodia are porous and have a sponge-like internal structure (figure 3.7). Pores (figure 3.7 b), which are open to the external environment, and corresponding elaborate internal channels (figure 3.7 b) are filled with filamentous polysaccharides (slime) and extracellular fluid (medium), plus excretion products.

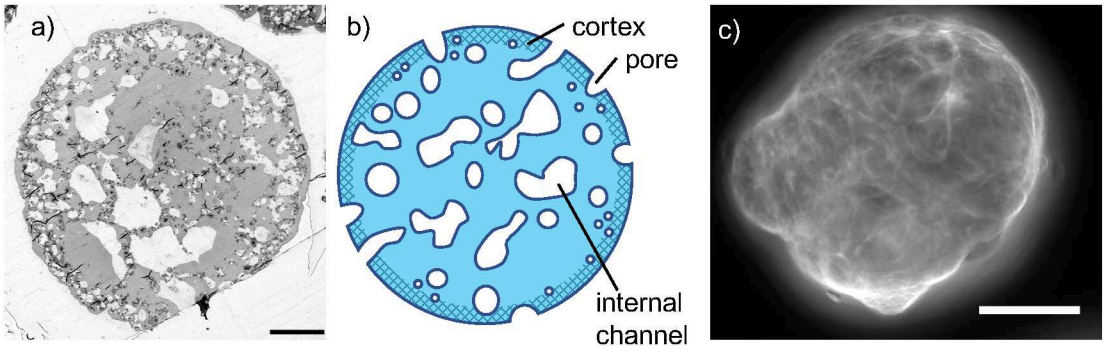

Figure 3.7: a) Semi-thin section of a microplasmodium. Scale bar = 50 µm. b) Schematic drawing of the internal structure of a microplasmodium. The thickness of the cortex is exaggerated. c) F-actin cortex (rhodamine phalloidin staining) of a microplasmodium. A Z-stack of this image can be found online in the supplementary material (S2).

3.4.5 Mesoplasmodia

We here describe the morphology and ultrastructure of a novel growth mode of *P. polycephalum*, which is induced by starvation [Lee et al., 2018]. Mesoplasmodia, as we are describing here, are not found in nature, because they result from the fusion of microplasmodia, which are in themselves a result of liquid shaking culture. Even though mesoplasmodia are artificially created, the very fact that they form functional structures provides a means to study their behavior. When microplasmodia are plated upon a solid agar surface, they fuse and give rise to a connected network via a percolation transition [Fessel et al., 2012, 2015]. However, when glucose is absent from the solid medium and when the microplasmodial culture is 'old' and has depleted its liquid growth medium of glucose, the microplasmodia do not form a network, but fuse into independent fragments which radially move away from the initial patch (figure 3.1 e and f). We use the term 'mesoplasmodia' in reference to their size, which lies in between microplasmodia and macroplasmodial networks. While microplasmodia are spherical and typically between 100 - 400 µm in diameter, mesoplasmodia are evenly thin and cover areas from 0.5 - 3 mm^2. Mesoplasmodia maintain their shapes and move on straight trajectories for hours. Because this morphotype is dedicated to migration, it serves as an excellent model for studying the locomotion of *P. polycephalum*. A time series of the front of a mesoplasmodium can be found online in the supplementary material (S3).

In contrast to microplasmodia, mesoplasmodia are polarized cells with a morphologically distinct anterior (front) and posterior (uroid) pole (figure 3.8 a). Actin fibrils are asymmetrically distributed along the anterior-posterior axis of the mesoplasmodium (figure 3.8), with longer and more pronounced fibers at the uroid and shorter, less ordered fibers near the front. At the uroid, as can be seen in figure 3.8 d, the actin fibers seem to extend outside of the plasma membrane. We speculate that they are

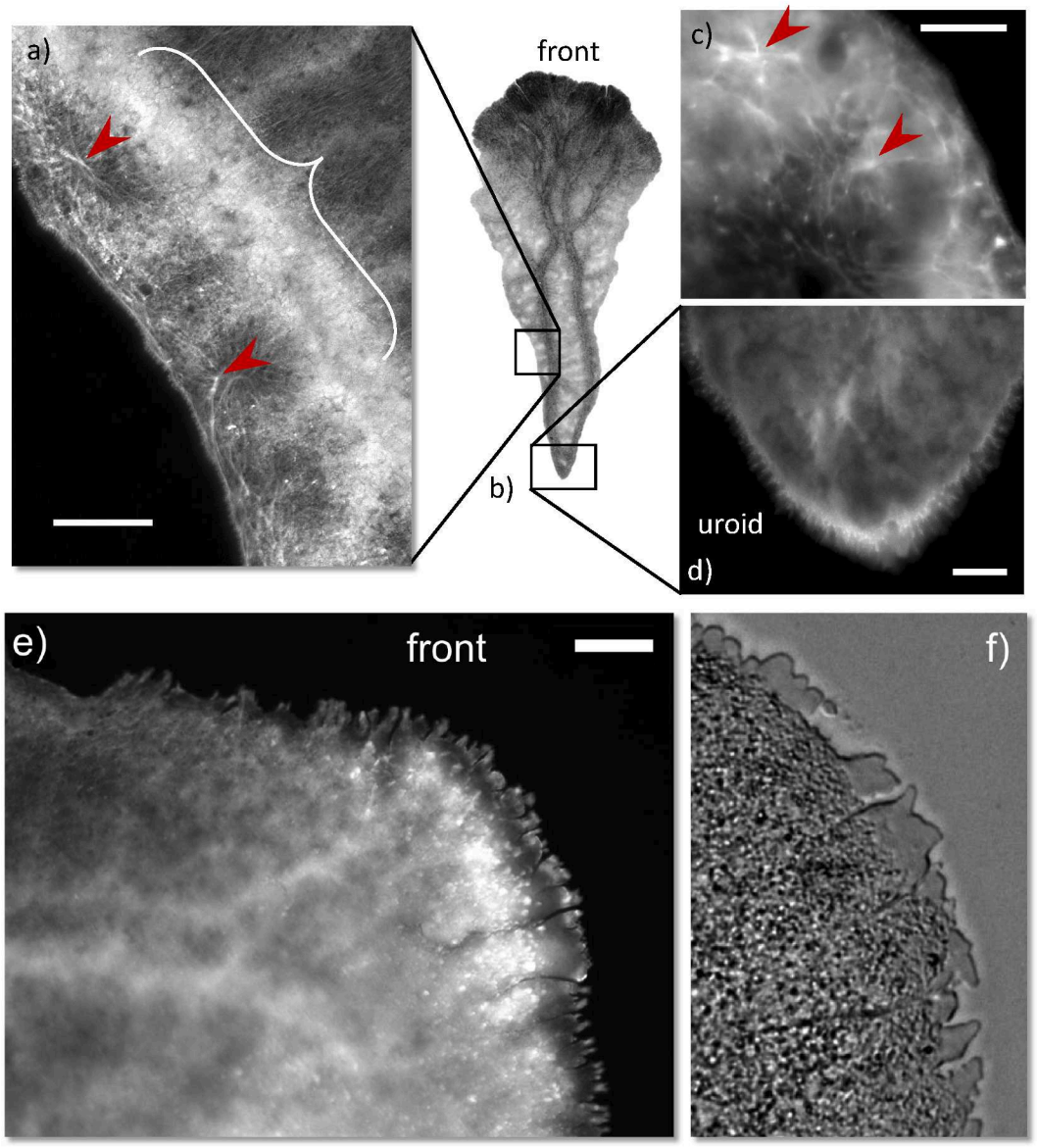

Figure 3.8: Fibrillar actin structures in *P. polycephalum* mesoplasmodia. a) Lateral F-actin lattice, consisting of star-shaped actin formations. Scale bar = 100 µm. An internal vein runs diagonally through the image (indicated by white bracket), higher fluorescence intensity indicates a high F-actin content. Red arrows = prominent actin asters. b) Typical migrating mesoplasmodium with differentiation into front and uroid (bright-field image). (a,c,d,e) Fluorescence imaging (rhodamine phalloidin staining). c) Example of actin asters (arrows) and long fibrils in the lateral section of mesoplasmodium. Scale bar = 50 µm. d) F-actin fibrils in the uroid of a satellite. Scale bar = 20 µm. e) At the front, longer F-actin filaments are lacking and filaments seem to end in foci. However, F-actin is present in the tips of blebs. Scale bar = 100 µm. f) Bright-field image of the front of a living mesoplasmodium. Blebs are clearly visible.

connected to adhesion points on the substrate, and are left behind by the slime mold as it crawls forward, thus leaving a trail of actin fibers. Actin structures in mesoplasmodia are varied and include actin asters (figure 3.8 a and c), which are here reported for the first time in *P. polycephalum*. A Z-stack of such actin structures can be found online in the supplementary material (S4). Actin asters are caused by the interaction of F-actin and a bundling protein. They are assumed to originate from changes in the mechanical stress of an active actin network, where the stress leads to the emergence of such ordered actin architectures [Fritzsche et al., 2017], and give stability and coherence to the actin cytoskeleton. Actin asters seem to appear in areas with high activity of motor proteins and high stresses [Kruse et al., 2004; Gowrishankar and Rao, 2016]. These self-organized filament structures influence cortical elasticity. Tuning the activity of actin nucleators (e.g. the Arp2/3 complex [Fritzsche et al., 2017] and myosin) to influence F-actin architecture could be a way for the slime mold to adjust macroscopic mechanical properties to physiological needs, e.g. cell shape during locomotion.

Furthermore, there is blebbing at the front of mesoplasmodia, the dynamics of which will be discussed in an upcoming publication. In figure 3.8 e, the front of a migrating mesoplasmodium is stained for F-actin. Each of the blebs seem to contain a thin layer of F-actin directly underlying the membrane, which is most likely due to the polymerization of G-actin during the blebbing process. A new submembrane cortex is formed.

Like the morphology of macroplasmodial veins, the cytoplasm of mesoplasmodia is also differentiated into endo- and ectoplasm. However, the transition is more gradual than in macroplasmodia. We cut several satellites perpendicular to their axis of movement. In this way, we obtained sequential slices providing information about the cross-sectional structure. The vertical creases of the frontal area, which are visible in both bright field (figure 3.9 a) and thin sections (figure 3.9 b), are oriented orthogonally to the front and are folds of the external membrane. They extend from the cell surface down to the substrate and represent membrane reservoirs. A similar mechanism has been found in motile CHO cells [Driscoll et al., 2015]. We speculate that these creases facilitate membrane extension in movement direction and are involved in blebbing. When inflowing endoplasm increases the pressure locally, the folds make it possible for the front to rapidly expand. Based on the analysis of spatiotemporal dynamics and ultrastructure data, we propose that the extending front of a mesoplasmodium represents a zone in which pressure-driven flow of endoplasm towards the frontal membrane breaks up the ectoplasm (figure 3.10). This highly dynamic process explains why internal flow channels can be observed in living mesoplasmodia, but not in TEM images: The transition between endo- and ectoplasm is driven by pressure generated in the back of the organism and not based on local morphological changes.

We propose that the front of mesoplasmodia is softer than other parts of its periphery, which is indicated by the formation of blebs at the leading edge, see figures 3.8 e and f.

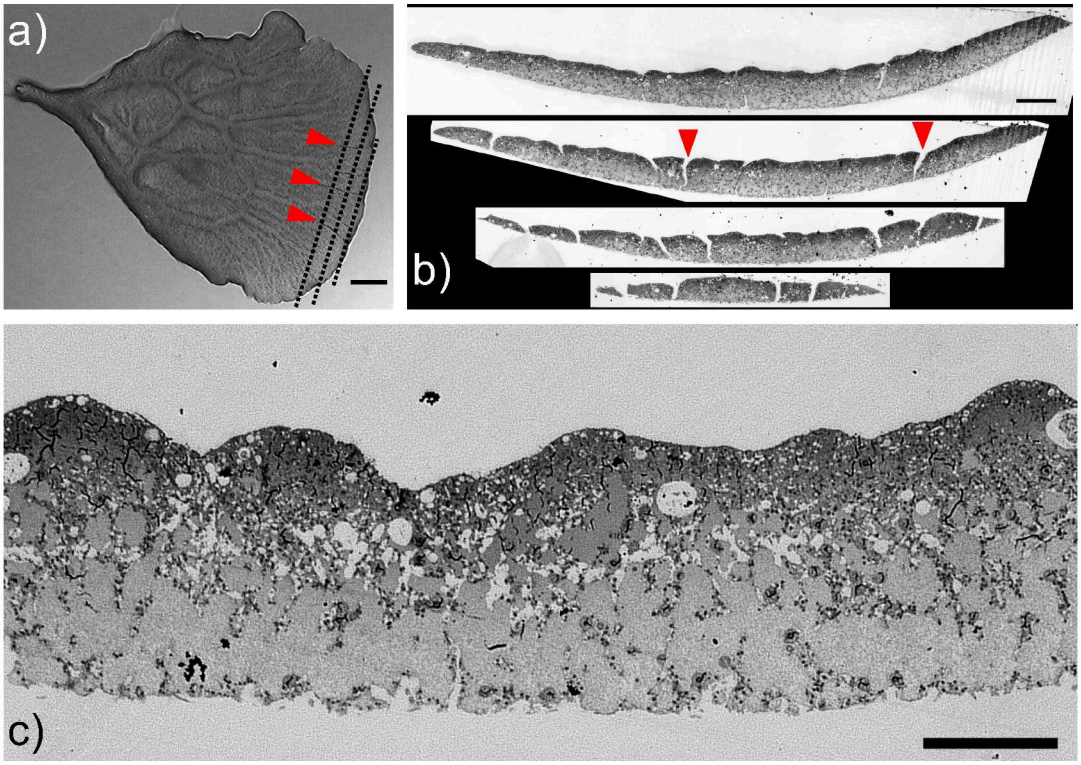

Figure 3.9: Vertical sections of a moving mesoplasmodium. a) Light microscopic image of living specimen. A well-developed internal vein network is visible. Dashed lines indicate the location and orientation of the semi-thin cuts, although the exact angle is unknown. Arrowheads = location of membrane creases. Scale bar = 200 µm. b) Sequential cuts. The curvature is likely to be an artefact from the cutting process. Arrowheads = membrane creases. Scale bar = 100 µm. c) Magnified detail from a vertical cut. The cytoplasm shows no signs of flow channels.The separation of the cytoplasm into endo- and ectoplasm, however, can be seen. Darker, more dense ectoplasm forms the top layer. Underneath is the less dense endoplasm. Scale bar = 50 µm.

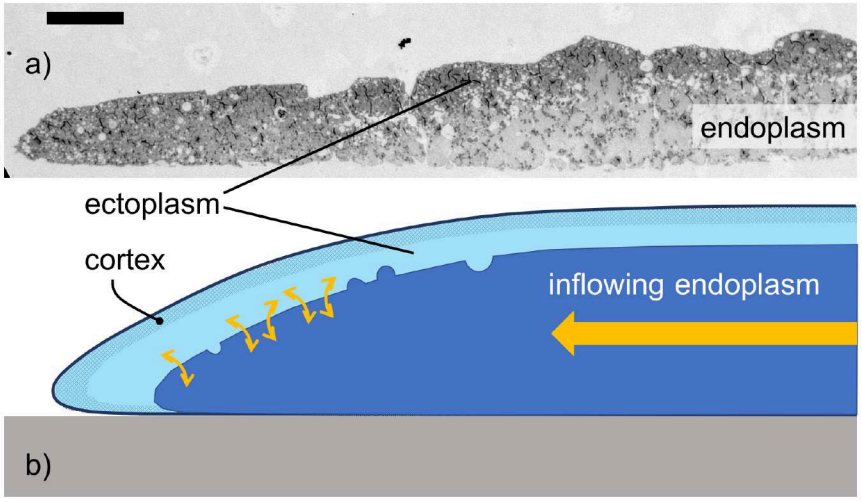

Figure 3.10: Vertical section of the front of a moving mesoplasmodium. a) Semi-thin section. Darker area on top = ectoplasm. Lighter area = endoplasm. Scale bar = 50 µm. b) Schematic drawing of endo- and ectoplasm dynamics during forward movement. The incoming endoplasm, following a pressure gradient, pushes against the frontal zone and breaks up the ectoplasm, which becomes fluid (yellow arrows). The cortex is so thin that it is not visible in the semi-thin section. Its dimension is exaggerated in the schematic drawing.

Due to the pressure-weakened ectoplasm and the less dense actin cortex in the front, the membrane yields by blebbing. This causes the protrusion of the front and the formation of new adhesion points. Similar structures have been observed by K. Brix and W. Stockem in adherent microplasmodia [Brix and Stockem, 1987].

There are many small delicate internal veins which transport endoplasm to the front. These veins are very dissimilar to the larger and much more pronounced external veins of macroplasmodia. The internal veins of mesoplasmodia do not represent continual morphological features, but represent the transition between endo- and ectoplasm. The smallest channels are ephemeral and often collapse or change their positions, whereas bigger veins towards the uroid of the mesoplasmodium are more stable and characterized by a diffuse meshwork of actin fibrils which surround them (figure 3.8 a, white bracket).

3.4.6 Macroplasmodia

This section focuses on the structure of macroplasmodia. Like mesoplasmodia, they are morphologically differentiated into growth fronts and veins. When grown under sufficient nutrient conditions, macroplasmodia consist of a sheet-like frontal part (figure 3.11 d) and tubular veins at the rear. However, unlike the veins in mesoplasmodia, which are more or less flow channels of more fluid endoplasm through more solid ectoplasm, the veins of a macroplasmodium are very efficient transport tubes. Their oscillations are organized

in a peristaltic wave to generate a highly efficient shuttle streaming throughout the whole cell body [Alim et al., 2013]. The actomyosin cytoskeleton is very well developed and features highly organized helical actin fibres (see figure 3.11 c) wound around the vein, which allows for powerful contraction. The macroplasmodial growth fronts are very similar to the fronts of mesoplasmodia, in that they are also differentiated into ecto- and endoplasm, although macroplasmodial growth fronts are much thicker (compare figures 3.10 and 3.11 d). Whereas mesoplasmodia are $\sim 100\,\mu m$ thick, macroplasmodial growth fronts measure $\sim 300\,\mu m$ and more in height. The morphological similarities hint at a functional analogy – both structures serve to advance the cell. Both front and tubular veins have a clear differentiation between endo- and ectoplasm (figure 3.11). The surface of the veins is covered in regularly spaced pores (figure 3.3 c and d). Both free-floating microplasmodia and the ectoplasm of substrate-bound veins have an overall porous structure. Those two 'tissues' are morphologically relatively similar and fulfill the same purpose: They generate contractile force. Using microplasmodia as a model system for the ectoplasm of extended network veins, e.g. in microindentation experiments, is thus a valid endeavor. Results from microplasmodia can be applied to the ectoplasm surrounding the veins. This is of interest with regard to investigating network dynamics such as peristalsis and shuttle streaming, because although the ectoplasm is crucial for force generation, it cannot be probed separately without the endoplasm.

3.5 Discussion

We first want to give a summary of our main findings.

1) We have identified and quantified plasma membrane pores from SEM images which correspond to internal channel systems. Pores are regularly spaced on the surface of all morphotypes of *P. polycephalum*. They have an average diameter of $1.72 \pm 0.66\,\mu m$ (n = 506 pores) and are evenly spaced apart on the cell surface, with an average distance of 4 times the pore diameter. The corresponding internal channel system was imaged by TEM. We found a high porosity of the ectoplasm, and no large vacuoles in flowing endoplasm whatsoever. Mesoplasmodia, a more transitionary morphotype with rapidly interchanging ecto- and endoplasm, had an intermediate porosity with less clear boundaries between the two cytoplasm types, but rather a gradient from the surface down to the substrate. Microplasmodia were uniformly porous, with larger microplasmodia having a higher pore volume than smaller ones.

2) We have, for the first time, described different actin structures in mesoplasmodia of *P. polycephalum*. The morphology of mesoplasmodia is dedicated to locomotion, and we have identified morphological features that can lead to an understanding of this locomotion type: The cortical actin layer with its actin asters, providing the basis for a high intercellular pressure and the creation of pressure gradients,

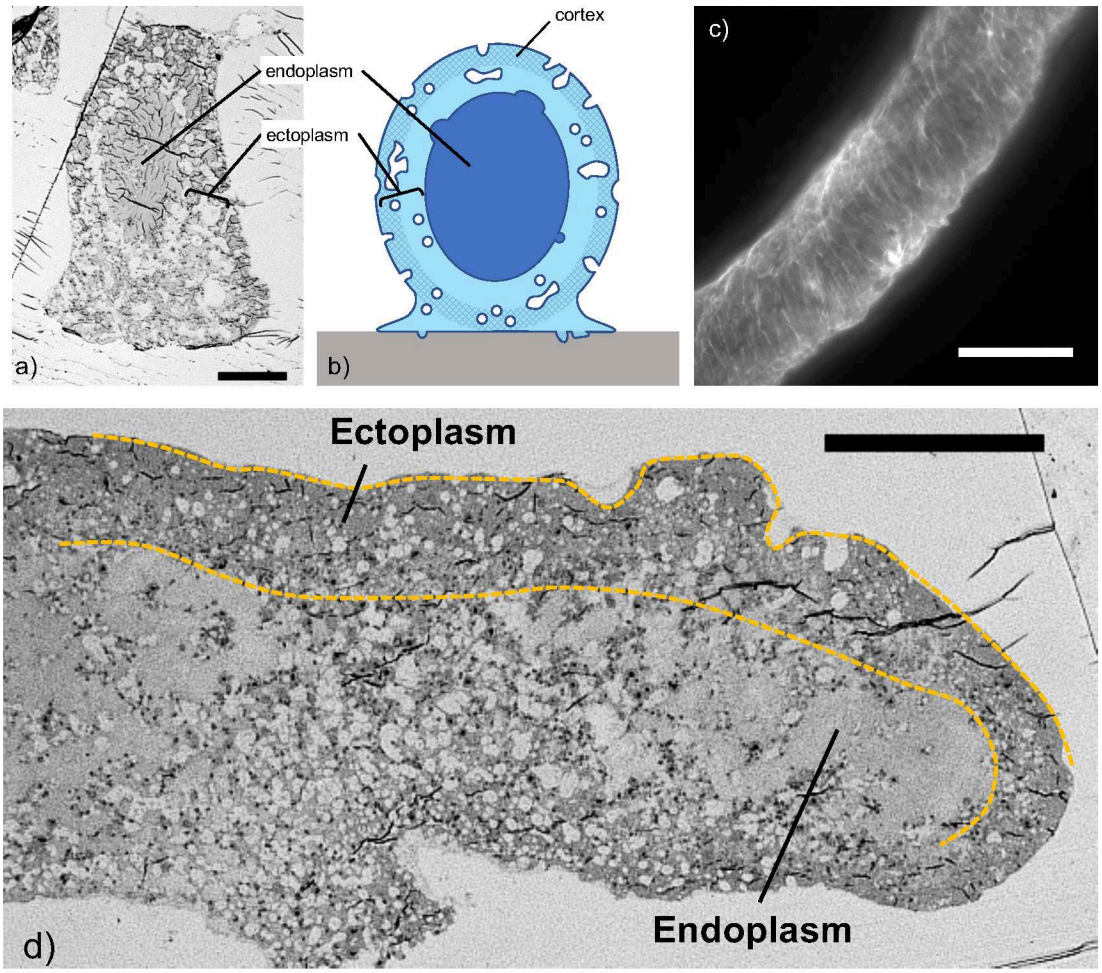

Figure 3.11: a) Semi-thin cross-section section of a vein. Scale bar = 50 µm. b) Corresponding sketch. c) Fibrillar actin cytoskeleton (rhodamine phalloidin staining) arranged helically around vein. Scale bar = 50 µm. A Z-stack of this image can be found online in the supplementary material (S5). d) Growth front of a macroplasmodium. Scale bar = 50 µm.

the actin 'trail' left on the substrate as an indicator of adhesion, and the process of blebbing.

3) We have investigated three different morphotypes, micro-, meso- and macroplasmodia, of which mesoplasmodia are a novel growth form which has not been previously described. These three morphotypes are not only different regarding their size, but, most importantly, they constitute adaptations to unique environmental conditions.

Next, we further compare these growth forms to each other and discuss differences and similarities. The dictum 'form follows function' means that the form of a body part or structure is related to its function. The form or shape of a structure within an organism is correlated to the purpose or function of that structure. We have investigated the underlying ultrastructures, and with that knowledge, we can attempt to identify mechanisms that regulate plasmodial form, and therefore function. Figure 3.12 gives an overview of the investigated morphotypes and highlights some of our findings. Microplasmodia, kept in liquid shaking culture, show no differentiation of the

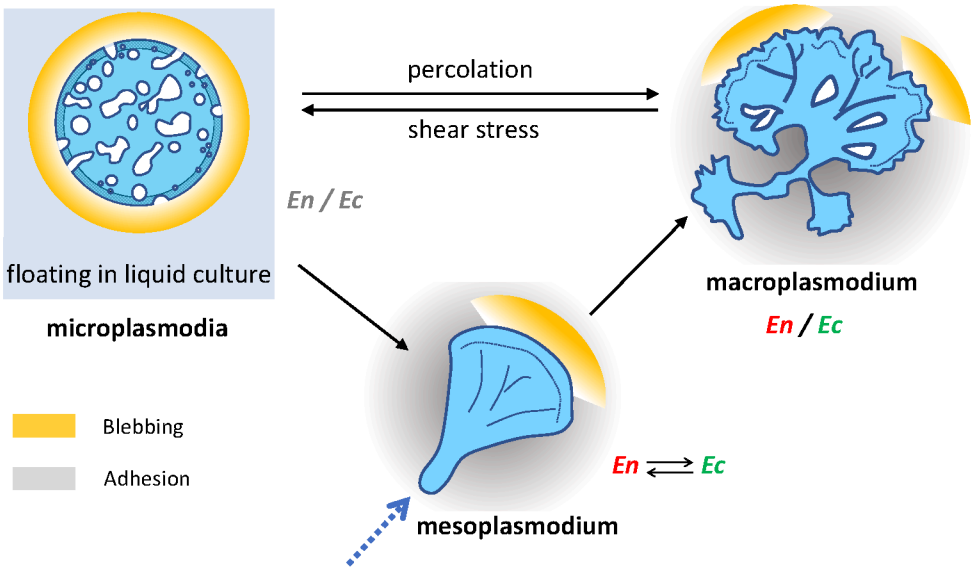

Figure 3.12: Schematic drawing of the three morphotypes of *P. polycephalum* investigated in this study. En = endoplasm, Ec = ectoplasm. Further explanation is provided in the text.

cytoplasm into ecto- and endoplasm. As described above, ecto- and endoplasm are just different states of cytoplasm. They can transform into each other, e.g. by mechanical force – a pressure increase causes actin depolymerization (ectoplasm → endoplasm), or by actin polymerization (endoplasm → ectoplasm). Furthermore, the proteins profilin and fragmin tip the cytoplasm balance in favor of the more fluid endoplasm, whereas

alpha-actinin and filamin are F-actin crosslinkers and stabilize the ectoplasm [Schaap et al., 2015]. Actin bundling proteins may provide nucleation points for asters [Itano and Hatano, 1991].

Microplasmodia are mostly spherical and, in order to enlarge their membrane surface (which is important for the exchange of substances and oxygen), they possess a large amount of invaginations. Their macroporous internal structure prevents a fast and unimpeded flow of cytoplasm on a large scale, as can be observed in macroplasmodia (shuttle streaming). Still, there is internal flow, but it is not the most prominent feature of microplasmodia. They are not polarized and have no substrate attachment, which is reflected by their ability to form blebs all along their periphery (yellow shaded area in figure 3.12).

The value of microplasmodia lies in their suitability as reproducible starting points for experiments. Unlike pieces cut off from macroplasmodia, microplasmodia are homogenous subunits. Macroplasmodial networks have uneven and unknown distributions of chemicals, organelles and other intracellular material. A fragment cut from a vein has a different composition than a fragment from the growth front. Also, the nucleus to cytoplasm (N/C)-ratio, or protein to DNA ratio, varies between cutouts. This ratio is important for the cell cycle control, because it determines whether mitosis will set in (when there is too much cytoplasm) or whether the cell will grow (when there are too many nuclei contained in too little cytoplasm). It is thus an internal cell size control [Sudbery and Grant, 1976].

Microplasmodia constitute the starting points for network growth and mesoplasmodium formation when provided with a solid surface. The migratory mesoplasmodia are triggered by starvation, thereby inducing pronounced locomotion. This is the function of mesoplasmodia, to provide optimal movement so that a search pattern can be executed. The structure of mesoplasmodia should therefore reflect the function of locomotion. Mesoplasmodia have some attachment to the substrate, and they are highly polarized, which could be achieved by chemical gradients within the cell. The front is softer, and blebbing occurs only there (yellow shaded area in figure 3.12). We found an asymmetry in shape and fibrillar distribution along the anterior–posterior axis of migrating mesoplasmodia which reflects the different functions that the uroid and front fulfill, respectively. A prerequisite for locomotion is the emergence of polarity. The uroid with its highly organized actin fibres provides the motive force which generates oscillating pressure gradients, which in turn push the frontal membrane outward. Endo- and ectoplasm reflects this highly dynamic growth form: Both types of cytoplasm are converted into each other at higher rates and faster timescales than in larger networks. It is highly likely that the events which lead to locomotion originate from structural asymmetries (e.g. softening of the frontal actomyosin cortex through an increase in pressure).

Mesoplasmodia and microplasmodia can turn into macroplasmodial networks. These networks have the highest temporal persistence and the most complex internal micro-anatomy, especially where external veins are concerned. Blebbing does never occur along the veins, but often at the growth fronts. These fan-shaped growth fronts appear and disappear along the periphery of the network, and indicate the direction into which the network expands. Ultrastructurally, growth fronts resemble mesoplasmodia. This is another example of our 'form follows function' hypothesis, since both mesoplasmodial fronts and macroplasmodial growth fronts are structures dedicated to forward movement and expansion.

While the micromorphology of *P. polycephalum* has been investigated before, many aspects still remain unexplored. The compilation of Z-stacks has allowed a detailed investigation of actin fibres, which has not been previously reported. We have peformed ultrastructural investigations on the biological model system we are currently working on. The exact culture conditions and the strain of *P. polycephalum* used for this study are known, which enhances the reproducibility of our research.

A multitude of mathematical and physical models aim to describe and predict the oscillatory patterns, contraction waves and the 'intelligent' behavior of *P. polycephalum*. In the sense that form follows function, some of the observed structures are surely linked to the versatile behavioral patterns of *P. polycephalum*. Emergence of this behavior is based on cytoskeletal organization. When describing *P. polycephalum* as viscoelastic [Kobayashi et al., 2006; Rieu et al., 2015] or poroelastic [Radszuweit et al., 2014] biological material, informations about the underlying structures are needed. Existing models mostly treat cells as a homogenous mass of cytoplasm, surrounded by a membrane. Both the internal channel system and the endo- and ectoplasm react differently to deformation than a homogenous mass of cytoplasm would. This has to be taken into account when assessing e.g. force measurements. Porosity needs to be taken into account for the design and analysis of microindentation experiments, because they affect the mechanical response: Upon compression, the internal channel system releases slime and extracellular fluid.

It remains astounding that a primordial organism like *P. polycephalum* with a low level of internal structural complexity can exhibit such a diversity of shapes and perform so many different tasks.

Morphological variability can be assessed from different points of view, one being genetics. The genome of *P. polycephalum* has been completely sequenced [Glöckner et al., 2008; Schaap et al., 2015], paving the way for research on gene expression and pathways. As in multicellular animals and plants, *P. polycephalum* exhibits cell differentiation, for example the occurrence of specialized cell types during the course of a life cycle. In response to environmental conditions that are sensed by specific receptors,

transcription factors are regulated, which leads to the differential expression of specific sets of genes encoding proteins that determine the morphology and ultimately the behavior of the slime mold [Werthmann and Marwan, 2017]. Thus, gene regulation is responsible for the observed variation of phenotypes.

However, another factor which is important for structure formation and morphology is based on the physical properties of the slime mold. As a huge amoeboid cell with few permanent structures, the slime mold does not need dedicated organelles to fulfill a multitude of functions. It appears that some complex behavior arises from simple hydrodynamic and biomechanical interactions. Our observation of actin stars and asters are an example of directed cytoskeleton self-organization. The slime mold is therefore an ideal model to study the basic functions of life and their intimate link to structure.

3.6 Acknowledgements

We thank Dr. Danny van Noort for his advice on SEM imaging, Prof. Dr. Reimer Stick for providing access to TEM, and the technicians Anja Bammann and Ute Helmboldt-Caesar for assistance with TEM imaging and cell preparations.

Chapter 4

A lumped parameter model of endoplasm flow in *Physarum polycephalum* explains migration and polarization-induced asymmetry during the onset of locomotion

Christina Oettmeier[1,2], Hans-Günther Döbereiner[1]

[1] Institute for Biophysics, University of Bremen,
Otto-Hahn-Allee 1, 28359 Bremen, Germany
[2] Author to whom any correspondence should be addressed.

Supplementary material for this chapter is available online at `https://journals.plos.org/plosone/article?id=10.1371/journal.pone.0215622#sec028` and in the appendix (section 7.2).

4.1 Abstract

The plasmodial slime mold *Physarum polycephalum* exhibits strong, periodic flow of cytoplasm through the veins of its network. In the special case of mesoplasmodia, a newly described starvation-induced, shape-constant morphotype, this periodic endoplasm streaming is the basis of locomotion. Furthermore, we presume that cytoplasm flow is also involved in signal transmission and signal processing. Mesoplasmodia motility resembles amoeboid locomotion. In contrast to other amoebae, however, mesoplasmodia move without extending pseudopods and retain a coherent, fan-shaped morphology

throughout their steady locomotion. Attaining sizes of up to $2\,\mathrm{mm}^2$, mesoplasmodia are also much bigger than other amoebae. We characterize this particular type of locomotion and identify patterns of movement. By using the analogy between pulsatile fluid flow through a network of elastic tubes and electrical circuits, we build a lumped model that explains observed fluid flow patterns. Essentially, the mesoplasmodium acts as a low-pass filter, permitting only low-frequency oscillations to propagate from back to front. This frequency selection serves to optimize flow and reduces power dissipation. Furthermore, we introduce a distributed element into the lumped model to explain cell polarization during the onset of chemotaxis: Biochemical cues (internal or external) lead to a local softening of the actin cortex, which in turn causes an increased flow of cytoplasm into that area and, thus, a net forward movement. We conclude that the internal actin-enclosed vein network gives the slime mold a high measure of control over fluid transport, especially by softening or hardening, which in turn leads to polarization and net movement.

4.2 Introduction

The acellular, multi-nucleated slime mold *P. polycephalum* can take on many shapes and sizes, depending on the mode of cultivation and various environmental parameters (e.g. nutrients, temperature, light). Typically, the slime mold forms large extended networks, characterized by a regular and vigorous flow of endoplasm (called shuttle streaming) through its veins. When placed in liquid shaking culture, shear forces tear the macroplasmodium apart and quasi-spherical, floating microplasmodia with diameters of a few hundred micrometers are produced. Regardless of shape and size, rhythmic oscillations of the cell periphery and the resulting flow of endoplasm are a characteristic feature of *P. polycephalum*. Cytoplasmic flow serves several purposes. First, it distributes nutrients, oxygen and cellular components throughout the cell body. Second, it is crucial for cell motility. In this work, we show that cytoplasmic flow is also a means of signal processing and distribution.

Rhythmic oscillations, caused by the contractile actomyosin cytoskeleton, are locally very well coordinated along the plasmodial body. They collectively and sequentially produce a pressure gradient, which induces protoplasmic streaming towards the leading edge ('front') of the plasmodium. In a stationary network, the flow through the network tubes is organized as a peristaltic wave, which is well-known [Baranowski and Wohlfarth-Bottermann, 1982] and has been elaborated on recently [Alim et al., 2013]. This peristaltic wave pattern leads to optimized transport. However, in migrating fragments of *P. polycephalum*, motility is achieved by the interplay of intracellular flow, adhesion, and traveling waves of contractile traction stresses [Lewis et al., 2015; Rieu et al., 2015]. Intracellular pressure gradients, caused by the actomyosin system, form the basis for this type of movement. Another prerequisite for migration is the polarization of the cell into an anterior (front) and a posterior end (uroid). This can be achieved by

the development of a chemical gradient, e.g. calcium, or by a softness gradient.

Heeding internal and external cues, *P. polycephalum* can adapt and alter its shape and size. For an overview of how the network morphology is influenced by chemicals and substrate softness, see [Takamatsu et al., 2009]. As we have shown before [Fessel et al., 2012], microplasmodia can form networks via a percolation transition when placed on a 2-dimensional agar surface. However, under starvation conditions, this transition does not occur. Instead, several disconnected, autonomous, millimeter-sized units form and migrate outward from the site of inoculation [Lee et al., 2018] (see figure 4.1 a). This

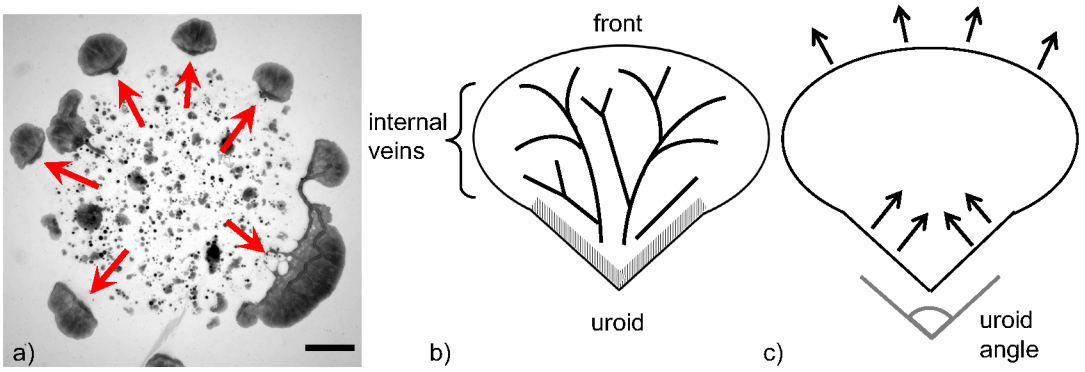

Figure 4.1: Mesoplasmodia migration pattern and schematic drawing. a) Mesoplasmodia emerging from microplasmodia plated on glucose-deficient agar. Image taken 7 hours after plating. Arrows indicate star-shaped migration pattern. Scale bar = 2 mm. b) and c) Schematic representation of a mesoplasmodium. b) The three most important regions involved in locomotion: the uroid (hatched area), internal veins, and front. An explanation is provided in the text. c) Proposed mechanism of the amoeboid locomotion employed by mesoplasmodia. Contractions are generated in the uroid, whose shape (uroid angle) influences locomotion speed. The front is pushed outwards passively by the flow.

new morphotype, which we termed mesoplasmodium (because its size places it between the micrometer-sized microplasmodium and the large macroplasmodium), is the focus of the present study. We establish it as a model system, because mesoplasmodia have a stable and defined morphology (for a schematic, see figure 4.1 b), a persistent shape, and move on straight trajectories for hours before they become stationary and once more transition into networks (a sketch of the locomotion pattern can be found in figure 4.1 c). Their ultrastructure has recently been described by us [Oettmeier et al., 2018]. The uroid (hatched area in figure 4.1 b) contains, apart from the ubiquitous cortex, specialized actin fibres which enable vigorous contractions. The uroid is morphologically different from the front. Internal veins transport flowing cytoplasm (endoplasm) through the more stationary ectoplasm. The veins have flexible boundaries and thus, pressure waves arrive at the front in an altered way, with a different frequency spectrum. The front lacks the organized actin fibres of the uroid and is thus softer than the back. As

we have described earlier [Oettmeier et al., 2018], blebbing at the front, an asymmetrical actin distribution throughout the cell, and the presence of actin asters in the uroid, but their absence in the frontal area, provide a strong argument for a softer front. Furthermore, as Lewis and coworkers have shown [Lewis and Guy, 2017], a softer front is a prerequisite for cell migration. In order to move forward, the cell needs to polarize and then establish a softness gradient. We were able to demonstrate this exact mechanism with our circuit model. If a symmetrical AC circuit, which is the equivalent of an unpolarized cell, suddenly becomes softer in one place (which is manifested as a local increase of electrical capacitance), there is a net current (i.e., the equivalent of net volumetric flow of endoplasm) which streams towards the softer area. It pushes the soft frontal membrane outwards. At the same time, the uroid keeps contracting rhythmically. Since the cytoplasm volume does not change, it follows that the bulk of cytoplasm is shifted towards the front, creating movement. As for a softening of the frontal actomyosin cortex during locomotion, this has been experimentally shown for *Dictyostelium discoideum*, a closely related cellular slime mold [Ramalingam et al., 2015]. Chemotaxis is a very prominent and important process in *P. polycephalum*. It is known that chemotactic receptors on the cell surface interact directly with the cytoskeleton in *D. discoideum* [Hall et al., 1989], affecting for example actin polymerization and pseudopod extension. In *P. polycephalum*, the nature of the chemotactic receptor(s) is still unknown, but it is very likely that the mechanism is similar.

P. polycephalum, like every other living organism, perceives its environment and reacts to it. In other terms, the plasmodium can be described as a cellular processor. The input variables are optical, chemical or mechanical cues. The slime mold processes this input, and, depending on the task at hand, creates an observable output. The output which is easiest to observe is mechanical in nature, i.e. shape, position and oscillations of the slime mold. Investigating how *P. polycephalum* processes and distributes information sheds light on basic emergent processes that lead to complex behavior in the absence of neuronal structures. We propose that the morphology and the physical properties of the slime mold and its (non-neuronal) information processing capacities are tightly interconnected. Computational processes are based on physically grounded dynamics (such as electrons moving through a circuit, or action potentials on neurons). As opposed to organisms with a brain as central processing and controlling unit, in the slime mold this 'brain' is its morphology. There is no particular location where memory or sensory input processing can be found; it is distributed throughout the entire body. The hydrodynamic network of *P. polycephalum* can thus be said to possess information processing capabilities. The oscillatory flow of cytoplasm is responsible for locomotion and signal processing, with the encoding of information being achieved by, e.g., frequency modulation.

After detailing the observed motility patterns, we use a hydrodynamic combined lumped-distributed model to describe and reproduce the cytoplasm flow of *P. polycephalum*.

The mechanism underlying the movement process of *P. polycephalum* is likened to the operation of an equivalent electrical circuit consisting of two basic passive electrical elements: resistor and capacitor. These models are usually lumped, meaning the equivalent circuits do not contain spatial information, which we aim to include in our model. Within the slime mold, a complex multitude of chemical and physical processes interacts to produce behavior, but the present analogy may nevertheless be very useful in better understanding the locomotion mechanism and signal processing capabilities of the slime mold.

4.3 Material and Methods

4.3.1 Cell culture and mesoplasmodium production

We used the strain WT33[a] [Marwan and Starostzik, 2002]x LU898 [Kawano et al., 1987] which was kindly provided by W. Marwan. Microplasmodia were grown in liquid shaking culture as described in [Bernitt et al., 2010]. After 6 days, the slime molds have depleted the medium of glucose, which was confirmed by a glucose monitoring strip test (Combur-Test, Roche). The microplasmodia were then taken out of the liquid culture and plated onto an agar plate containing glucose-deficient SDM-agar (prepared after [Daniel and Rusch, 1961] and modified by W. Marwan, personal communication). Once on the agar surface, microplasmodia form aggregates and fuse. At ~ 3 hours after plating, small plasmodia begin to leave the boundaries of the patch and move outwards in a star-shaped fashion. We call those autonomous, steadily migrating units mesoplasmodia. After approximately 10 hours, mesoplasmodia cease their straight, outward migration and transition into stationary networks in a topological transition creating numerous holes and handles. Directional persistence is evident for approximately 7 hours. All mesoplasmodia were observed and recorded within this seven-hour interval.

4.3.2 Image acquisition

Light microscopy of migrating mesoplasmodia was performed using a Zeiss Axiovert 25 equipped with a 5x Zeiss CP-Achromat with a numerical aperture of 0.12. For higher-resolution imaging of internal flow, a Zeiss Axio Oberver.Z1 was used. Bright field imaging was performed with a Zeiss Achro Plan 10x (numerical aperture 0.25). All experiments were carried out at room temperature.

4.3.3 Analysis of leading edge velocity

The analysis of the average leading edge velocity of mesoplasmodia was performed with the open-source software FIJI [Schindelin et al., 2012] and the Kymograph plugin written by J. Rietdorf and A. Seitz. Kymographs (schematic see figure 4.2) with a width of 1 pixel were generated on image sequences (stacks) of moving mesoplasmodia.

[a] In the original publication, an incorrect strain name was given.

Kymographs of the output stacks of optical flow analysis were also used to obtain flow velocities along internal veins.

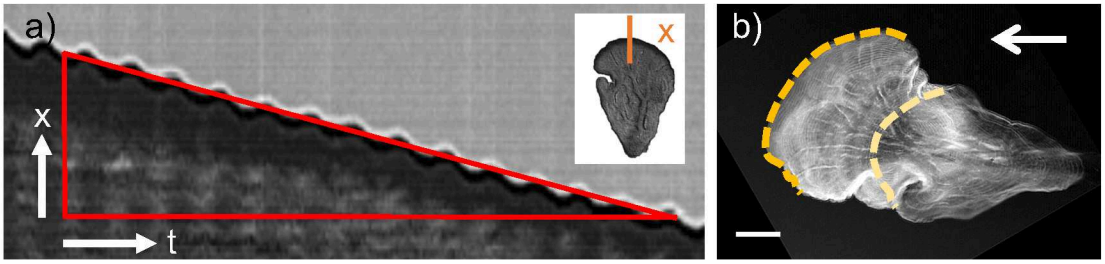

Figure 4.2: a) Kymograph of the growth front of a mesoplasmodium. x = spatial dimension, t = time. Inset: single frame of a time sequence. Kymograph is taken along orange line. b) Output image of a time series (standard deviation). Yellow dashed line = first frame of time series, orange dashed line = last frame. Scale bar = 20 µm. Arrow denotes direction of migration.

4.3.4 Optical flow analysis

We used the Horn-Schunck method of estimating optical flow [Horn and Schunck, 1981]. A detailed description of the method can be found in the appendix (7.2.1).

4.3.5 Time series analysis

Two-dimensional representations of time series were created using standard deviation in the z-dimension (time), resulting in a single output image for each image stack. The standard deviation of all images in a stack was calculated in FIJI. Each of the output image's pixels contains the standard deviation over all images in the stack at the particular pixel location. Areas with strongly fluctuating flow (high standard deviation) thus become visible and appear white, whereas areas with little flow variation have a low standard deviation and appear dark.

4.3.6 Contour detection

The detection of mesoplasmodium contours, based on the principles of active contour or 'snake' algorithms [Xu and Prince, 1998], was implemented in MATLAB2015b (The Mathworks) using custom-written routines by E. Bernitt [Bernitt, 2015].

4.4 Results and Discussion

4.4.1 Directional persistence and cell speed

We followed mesoplasmodia for several hours and analyzed their motion with respect to velocity, area, and shape (circularity f_{circ}) over time. These locomotion parameters are

given for six mesoplasmodia in the appendix (table 7.1). We found that mesoplasmodia migrate at constant speeds for up to 7 hours and maintain straight trajectories away from the original patch (see figure 4.1 a and figure 7.1 in the appendix). For unicellular eukaryotic cells, such behaviour is very uncommon. Usually, amoeba such as the cellular slime mold *D. discoideum* show directional persistence times of only ∼10 minutes in the absence of a stimulus [Li et al., 2008]. We measured migration speed during this phase of directional persistence as the velocity of the leading edge in direction of movement, which was obtained from kymographs (see figure 4.2 a). Mesoplasmodia travelled with an average of $6\,\mu m\,min^{-1}$ to $17\,\mu m\,min^{-1}$. Cell speeds show characteristic oscillations around their average values (see figure 4.3). Although a single mesoplasmodium main-

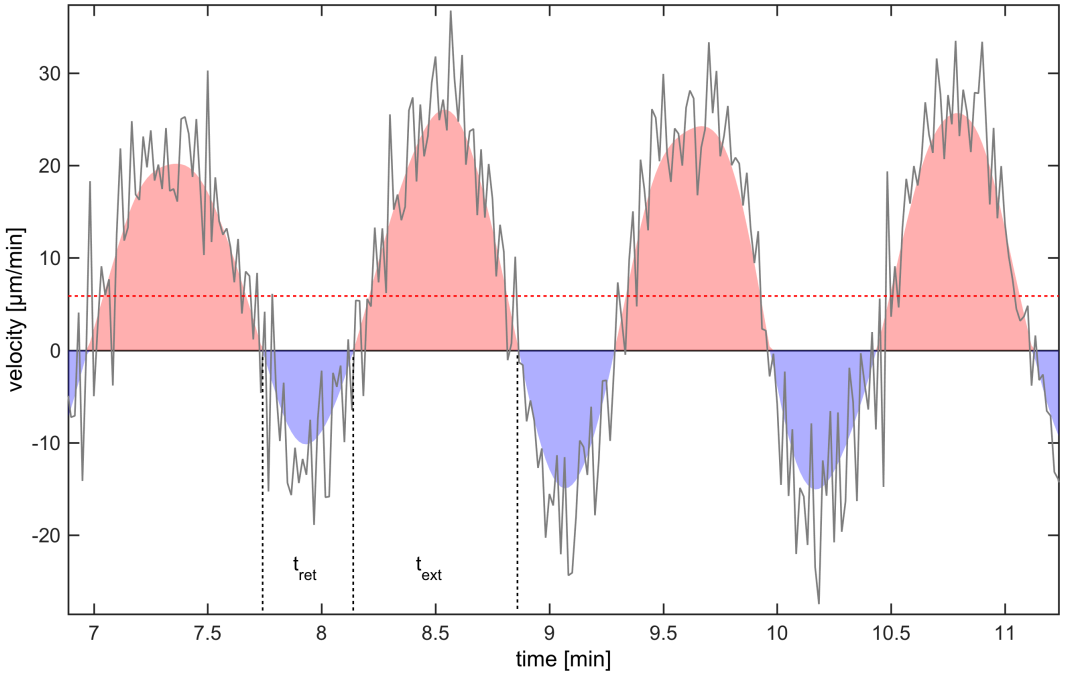

Figure 4.3: Movement speed of frontal membrane. Red dashed line = average velocity. Negative values = movement of cell contour towards center of mass. t_{ret} = membrane retraction time, t_{ext} = membrane extension time.

tains its shape during migration, mesoplasmodia differ in overall shape and size from each other. The general form is always the same, see figure 4.1, in that a front and a tail region are clearly distinguishable. Thus, even from looking at a single still frame, the direction of movement is always discernible. Independent of size, the tail region can be elongated (acute uroid angle) or oriented almost parallel to the front (obtuse uroid angle). Uroid angles for six mesoplasmodia can be found in the appendix (table 7.1).

Mesoplasmodial locomotion is characterized by a very long directional persistence

and a constant average cell speed, which fluctuates in a sinusoidal pattern. The mesoplasmodium achieves net forward movement by a long frontal membrane extension time (t_{ext}) and a short retraction time (t_{ret}), see figure 4.3. Extension time is the time over which the frontal membrane is expanded in direction of movement (calculated for an entire time series), and retraction time is the time span over which the membrane moves back towards the contour center. For all examined mesoplasmodia, the ratio of membrane extension to retraction time lies between 1.4 and 2.3. The overall area of a migrating mesoplasmodium oscillates regularly, with average periods of $T_{area} =$ 1.20 min. This parameter seems to be independent of size. The cell shape of migrating mesoplasmodia was assessed by the circularity factor f_{circ} which takes into account area A and perimeter P.

$$f_{circ} = \frac{4 \cdot \pi \cdot A}{P^2} \tag{4.1}$$

The circularity f_{circ} of a perfect circle is 1, whereas elongated cells assume values of <1. We found typical values of f_{circ} to lie between 0.84 and 0.92. The shape remains almost constant during migration (see figure 7.2 in the appendix), with regular fluctuations. Phases of high circularity roughly coincide with periods of slow locomotion (see figure 7.3 in the appendix).

4.4.2 Cell shape dynamics

So far, we have described the overall movement pattern and shape of mesoplasmodia. Next, we will investigate the dynamics of locomotion. Velocity charts reveal different patterns of membrane extension and retraction in the frontal zone and the uroid. Figure 4.4 shows the contour dynamics of an exemplary mesoplasmodium. As per our definiton, outward movement of the contours has a positive sign and is given the colour red in the velocity chart. Movement towards the contour center has a negative sign and is represented by blue colour. The oscillations of a mesoplasmodium are not homogenous along its contour, with the exception of the front. The frontal periphery expands and retracts evenly over its length (see figure 4.4 c). The uroid, however, shows a more versatile oscillation pattern (see figure 4.4 d). The occurrence of tilted lines of equal velocity indicates lateral waves moving along the contour (see figure 4.4 d). For microplasmodia, similar phenomena, i.e. lateral waves along the membrane and standing wave patterns, have been described by us [Bernitt et al., 2010]. Lateral waves also occur in other cell types, for example in T cells, mouse fibroblasts and *Drosophila* wing disk cells [Döbereiner et al., 2006]. The appearance of a common spatiotemporal pattern of membrane movement in a variety of cell types suggests an underlying universal pattern, most likely associated with actin. The front is also distinguished from the uroid by different oscillation frequencies. The back of a mesoplasmodium usually shows a higher frequency of oscillation than the front, see figure 4.5. Here, the back (figure 4.5 a) oscillates with a period of 1.20 min, and the front (figure 4.5 b) oscillates with a period of 2.40 min. Furthermore, the membrane velocities are higher in the back.

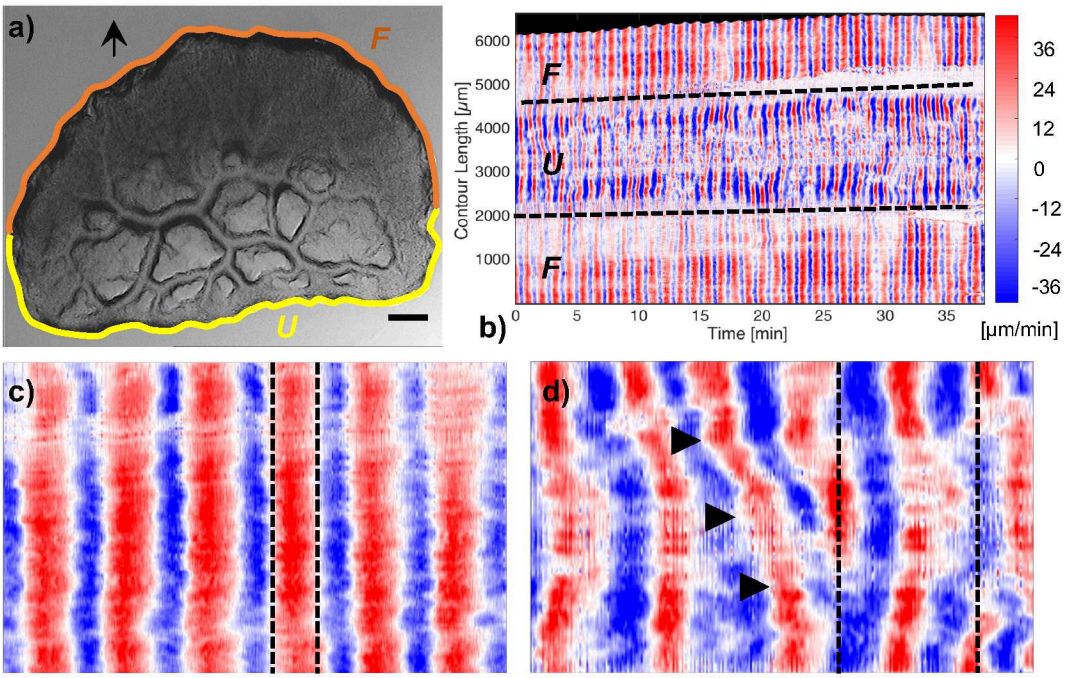

Figure 4.4: Contour dynamics. a) Still frame taken from a 40 minute recording of a mesoplasmodium with an obtuse angle. Scale bar = 200 µm. Arrow denotes the direction of movement. U = uroid, F = front. White arrowhead correponds to contour length 0 resp. 6000 µm in panel b). b) Velocity chart of same mesoplasmodium. Data was obtained as given in section 4.3.6. Dashed lines mark points on the contour where the uroid (U) transitions into the front (F). c) Magnified detail of the front shows uniform membrane extrusion and retraction. d) Magnified detail of uroid region shows simultaneous movements in opposite directions (dashed lines) and lateral wave phenomena (arrowheads).

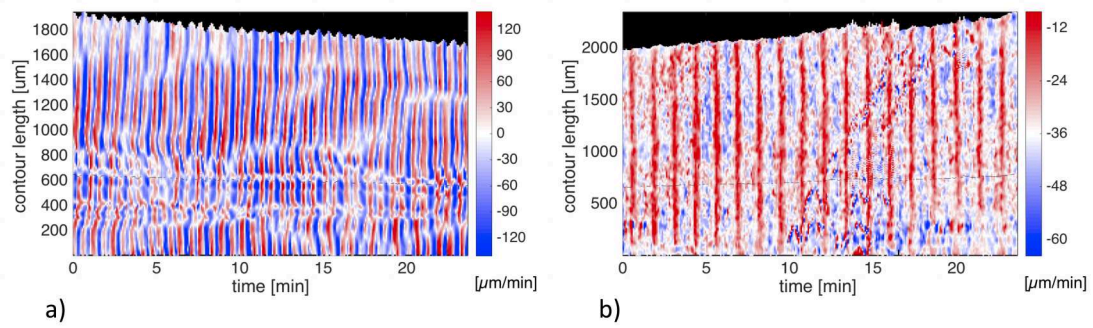

Figure 4.5: Frequency selection. a) Velocity chart of uroid of mesoplasmodium. b) Velocity chart of front. Data was obtained as given in section 4.3.6.

A video of this mesoplasmodium can be found online in the supplementary movie S1 (`https://doi.org/10.1371/journal.pone.0215622.s007`)[b].

4.4.3 Internal flow patterns

The analysis of the cell periphery shows very different oscillation patterns between front and uroid. Pressure differences caused by uroidal contractions lead to a propagation of waves from the back towards the front. We investigated the internal flow of endoplasm throughout the mesoplasmodium by means of optical flow analysis. Every examined mesoplasmodium showed the patterns described below, albeit at different levels of distinction. For the sake of clarity, we therefore chose to present data which best highlighted the observed behavior.

From the evaluation of time series (see section 4.3.5), it becomes evident that at least major veins are persistent over longer periods of time (up to hours) while the satellite moves forwards (see figure 4.6 a and c). Thus, the majority of veins is stationary in regard to the agar surface. In the frontal area, flow channels are more ephemeral. The veins are deconstructed as the uroid retracts, and newly formed at the expanding front. There are usually only two or three dominant veins, running parallel to the longitudinal axis, which are responsible for the bulk of the flow (veins traced in red in figure 4.6 a and c). Flow within the internal veins of a mesoplasmodium has a sinusoidal pattern, mirroring the extension-retraction pattern of the uroid's periphery. Performing cross-correlations of the velocity profiles throughout a vein from beginning (uroid) to end (front) show a gradually declining correlation coefficient (figure 4.6 b and d). This means that segments which are in close proximity to each other tend to have more similar flow patterns than segments that are further distant from each other. The self-similarity of the wave decreases along the longitudinal axis. Typical flow velocities in internal channels ranged from 5 to 100 $\mu m\,min^{-1}$, with highest flow velocities occurring in the middle of the mesoplasmodium. A remarkable phenomenon that originates in the uroid and propagates through the veins from back to front is a change in oscillation frequency. The resulting pattern (both high and low frequencies in the back, only low frequencies in the front) resembles an electronic low-pass filter. By performing a fast Fourier transform (FFT) on the oscillations, we obtained the dominant frequencies. Figure 4.7 shows different frequency spectra of uroid and frontal region. Frequency spectra for different regions of a dominant vein can be seen in figure 4.7 a. Segments closer to the uroid (blue) have a higher oscillation frequency that is absent in segments closer to the front (red). Whereas low frequencies are present in both uroid and front, higher frequencies are missing in the front. We show that, from back to front, a frequency selection takes place. Figure 4.7 b shows the comparison of frequencies present in the uroidal membrane (blue line) and the front (red line). The observed frequencies differ between individuals, but the mechanism of frequency

[b]The video is also archived by the University of Bremen together with this thesis.

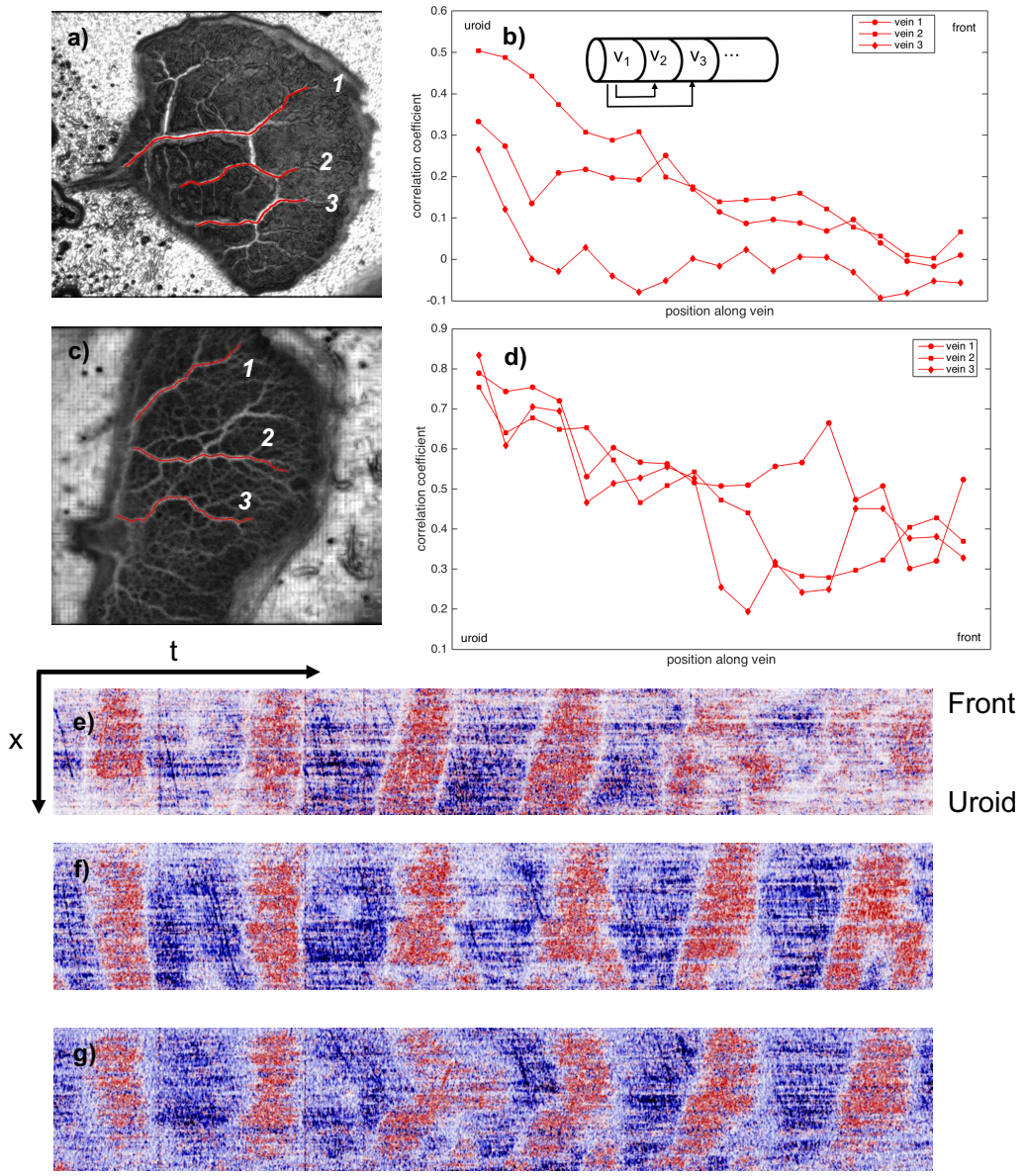

Figure 4.6: Flow pattern along veins. a) Satellite with acute uroid angle (time series over 7 min). Veins (red) run from uroid to front. b) Cross-correlation of flow velocities along the three veins. The velocity profile of the vein segment closest to the uroid is correlated with that of every subsequent segment along the vein (see inset). The correlation decreases slightly from back to front. c) and d) Similar analysis for satellite with obtuse angle. Time series over 14.5 min. e)-g) Kymographs (see method section 4.3.3) taken along three veins of the mesoplasmodium in c), denoted with numbers 4-6. x = spatial dimension (each vein is $\sim$ 800 µm long), t = time ($\sim$ 15 min). Bottom edge of each kymograph corresponds to vein area close to uroid; top edge is closest to the front. Along each vein, the transition from uroidal to frontal oscillation pattern (frequency selection) can be observed: The oscillation frequency is almost twice as high closest to the uroid as near the front.

selection is the same. To summarize this observation, we found that the oscillations

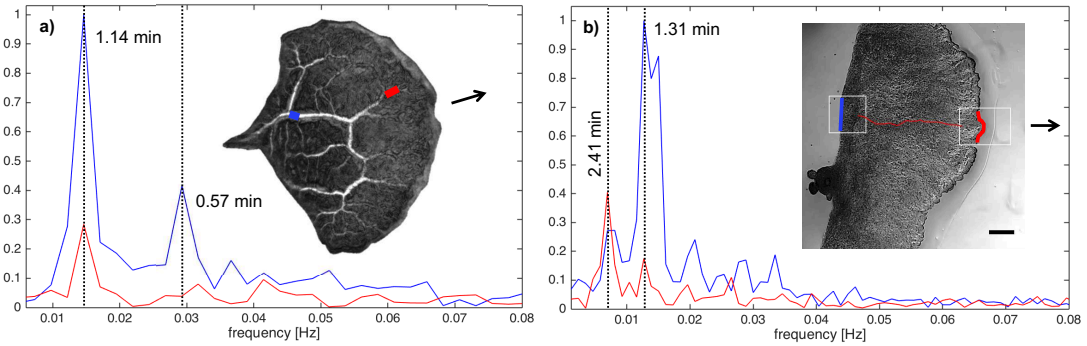

Figure 4.7: Fast Fourier transform (FFT) of mesoplasmodial oscillations. Examples of changing frequencies of endoplasm flow throughout a mesoplasmodium (a) and differences in the oscillation pattern between frontal and uroidal membrane (b). Arrows denote direction of movement. a) Data obtained from optical flow analysis. Blue denotes a segment in the back of the mesoplasmodium, red is a segment closer to the front. Whereas a frequency with a period of 1.14 min can be detected everywhere along the length of the vein (although getting less pronounced further away from the uroid), the higher frequency also present in the uroid (0.57 min) is filtered out towards the front. The mesoplasmodium as a whole shows area oscillations with a period of 0.62 min. b) Red = oscillations of the frontal membrane. Blue = oscillations of the uroidal membrane (see white boxes). Data obtained from kymographs.

of the uroid (periphery as well as internal flow) contain both high and low frequency components. As endoplasm flows towards the front, higher frequencies are filtered out along the way.

4.4.4 Lumped model of cytoplasm flow

We aim to provide a predictive model useful for the explanation of dynamic phenomena in slime mold. To this end, we develop a lumped parameter approach that allows us to analyze the behavior of mesoplasmodia with modest computational effort. Certain concepts in electrical circuits bear a strong similarity to fluid flow in networks of compliant tubes. Therefore, we can derive fundamental equations by applying electric circuit theory. Voltage in an electric system corresponds to pressure in a fluidic system, current to volumetric flow rate. In both fluidic and electric circuits, resistors and capacitors affect the flow of electrical current. Fluidic resistance is due to internal friction within the fluid. The fluidic equivalent to a capacitor lies in the elastic properties of the tube wall: An increase in pressure causes the elastic vein to expand and store fluid which it then releases, much like a capacitor stores and releases electric charge. The lumped parameter concept provides a tool to examine the dynamics of pulsatile flow in a mesoplasmodium as a whole. This modeling approach has been used extensively in hemodynamics [Zamir, 2000, 2016].

The slime mold's flow of cytoplasm follows complex patterns in space and time. At

the core of the ubiquitous relaxation-contraction cycles are the interactions between actin and myosin in the cortical cytoskeleton. However, the underlying primary (or biochemical) oscillator is still unknown. It may be founded in biochemical pathways [Korohoda et al., 1983], but could also be based on mechanochemical processes and / or mechanical interactions between different regions [Teplov, 2010]. We propose a model in which observed patterns are, in great parts, due to hydrodynamic processes without the need for biochemical signals. In the following, we will detail our lumped model and focus on the observed frequency selection phenomenon.

However, a challenge for the construction of a lumped model is that many parameters like cytoplasm density, viscosity and elasticity have to be known. Channel dimensions can be taken from microscopic images [Oettmeier et al., 2018], but rheological data for *P. polycephalum* are scarce [Fessel et al., 2017].

4.4.4.1 Reynolds number

To estimate what kind of flow regime is predominant in mesoplasmodia, we calculated the Reynolds number Re (equation 4.2)

$$Re = \frac{\rho_{cyto} \cdot v \cdot d}{\eta} \tag{4.2}$$

where ρ_{cyto} is the cytoplasm density, v the average flow velocity, d the typical diameter of a flow channel, and η the viscosity. The values we used for the calculations of Reynolds and Womersley numbers are given in Table 4.1. Average flow velocity shows some variation, depending on morphotype and position within the cell body. The mesoplasmodia which were the subject of this study showed, on average, a much lower flow speed, especially in the tiny flow channels in the frontal region. Flow through the large and well developed veins of macroplasmodia can reach up to $60\,000\,\mu m\,min^{-1}$, but this flow differs very much from the situation in mesoplasmodia, which are characterized by a much smaller cytoplasm volume, smaller size, and ultrastructure of the flow channels. Very often, the flow channels are simply constituted of faster-flowing endoplasm which is pushed through the more stationary cytoplasm surrounding it. This explains the much lower flow velocities. The calculated Reynolds number (2.37×10^{-8} – 4.75×10^{-8}), depending on flow velocity, is very low as compared to values at which flow is turbulent, thus we can assume smooth laminar flow which is dominated by viscosity. Therefore, endoplasmatic flow may be described by the equation for Poiseuille flow in a tube and, most importantly, inertial effects are negligible. In our considerations, we regard the endoplasm as an incompressible fluid, i.e., we take the density as a constant. However, cytoplasm is a non-Newtonian fluid.

4.4.4.2 Womersley number

The Womersley number α, which is dependent on the angular oscillation frequency ω, can be used to determine the flow profile. This dimensionless expression relates pulsatile

Table 4.1: Parameters used for the calculation of Re and α.

ρ_{cyto}	1120	$\mathrm{kg\,m^{-3}}$	[Sato et al., 1983a]
v	5 - 100	$\mu\mathrm{m\,min^{-1}}$	
d	70	µm	
η	0.275	$\mathrm{N\,s\,m^{-2}}$	[Sato et al., 1983b]
a	20	µm	

flow frequency to viscous effects. In a typical case for mesoplasmodia ($\omega = 0.08$ rad/s and radius $a = 20\,\mu\mathrm{m}$), the Womersley number α becomes

$$\alpha = a\left(\frac{\omega\rho_{cyto}}{\eta}\right)^{\frac{1}{2}} = 0.00036 \tag{4.3}$$

0.08 rad/s corresponds to an oscillation frequency of 0.013 Hz, which means a period of 1.31 min. For $\alpha \lesssim 2$, viscous forces tend to dominate the flow, and velocity profiles are parabolic in shape. The oscillations of the slime mold which are relevant to flow are well below 1 Hz, usually in the range of 0.007 to 0.02 Hz.

4.4.4.3 Model of an internal vein segment

The internal flow network of a mesoplasmodium is a fluidic network with deformable features. Each segment is a tube with a radius a_0 (see figure 4.8 a) and, theoretically, elastic walls. However, a peculiarity of mesoplasmodial internal veins is that they do not possess membranes to separate them from the surrounding ectoplasm [Oettmeier et al., 2018]. Rather, channels are created by pressure-driven flow [Guy et al., 2011]. In our model, we consider the vessels as compliant and able to expand in response to an inflow of endoplasm (see figure 4.8 a). Given the lack of a solid tube wall, they are also permeable. The lack of substantial walls and the permeability create a similar situation as in capillaries and venules in the blood circulatory system. Cytoplasm constantly leaves and enters the flow channel. This is denoted by R_2, an extra resistance added to the circuit to account for leakage through the sides of the vessel [Berger, 1993].

The circuit described above and depicted in figure 4.8 b) is known as a three-element Windkessel model and is widely used, especially in hemodynamics, to model e.g. coronary blood flow. The Windkessel effect helps in damping the fluctuation in fluid pressure during an oscillatory input. Fluctuations in pressure are attenuated or dampened, and the fluid flow becomes more constant. The basic relations of the Windkessel model can be derived from Navier-Stokes equations [Olufsen and Nadim, 2004]. We decided on the three-element Windkessel, because it provides one resistance to cytoplasm flow and a second one to simulate the permeability of flow channels. Thus, it represents the most important (experimentally accessible) parameters: resistance to flow, compliance of vessel 'walls', and loss of flow due to permeability. The four-element Windkessel

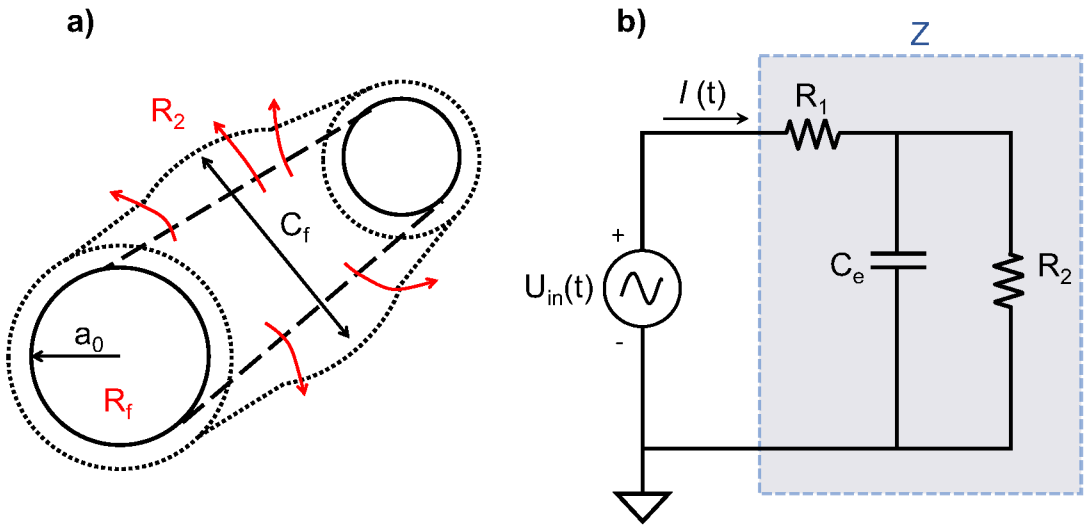

Figure 4.8: Schematic of a three-element Windkessel equivalent circuit. a) Schematic drawing of a tube segment of an internal vein. a_0 = radius, C_f = fluidic capacitance, R_f = fluidic resistance. R_2 = leakage due to permeable 'walls'. b) Schematic drawing of RC circuit. The blue box (denoted with Z) represents the impedance of one single 3-element Windkessel (see figure 4.9). $U_{in}(t)$ = input voltage signal, R_1 = resistance due to internal friction of the cytoplasm, R_2 = resistance due to leakage through vessel wall, C_e = electric capacitor, I = current.

includes an inductor. However, we ruled out inertance because the slime mold oscillates at very low frequencies.

The internal veins within a mesoplasmodium form a flow network of interconnected and branching pipes (see figure 4.9 a) through which endoplasm flows in a pulsatile flow pattern. Each of the more complicated branching tubes can be modeled as a different arrangement of simpler segments (see figure 4.9 b and c). Each letter Z in figure 4.9 c stands for the impedance of a single three-element Windkessel, i.e., each Z is a combination of two resistors and a capacitor. This representation highlights one of the advantages of the lumped model: For each Z, a circuit with individual elements can be employed and the parameters can be set according to measured data, for example radius and tube length. We chose the configuration of figure 4.9 c for our branching vein model because it corresponds to the typical conditions within a mesoplasmodium: The veins branch only in the final third of their length, towards the front. This is why we assign two 3-element Windkessels to the 'stem' of the Y and one 3-element Windkessel to each 'arm'.

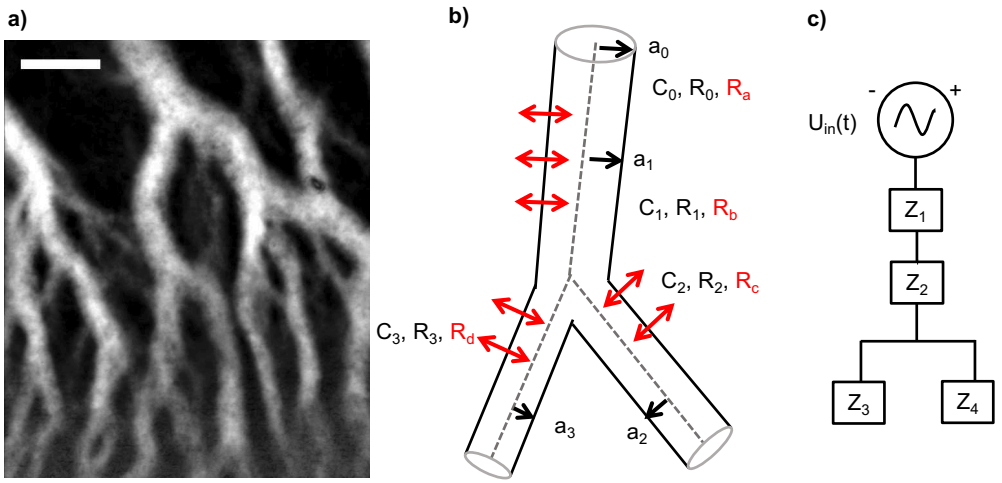

Figure 4.9: Modeling internal veins as an equivalent electrical circuit. a) Time series (standard deviation) of a mesoplasmodial internal vein network. Scale bar = 50 µm. b) Model of branching vein. Each branch has its own characteristic length, radius and resulting fluidic resistance and capacitance. c) The branching vein, drawn as an electrical circuit. It consists of 4 single 3-element Windkessels (Z1 - Z4).

4.4.4.4 Fluidic resistance

The resistance R for flow in a tube can be expressed in terms of properties of fluid (viscosity η) and tube (length l, radius a):

$$R_f = \frac{8\eta l}{\pi a^4} \tag{4.4}$$

4.4.4.5 Fluidic capacitance

Fluidic capacitance C_f represents the compliance of a tube, i.e., the elasticity of the channel 'walls'. Capacitance is equal to the change in volume divided by the change in pressure.

$$C_f = \frac{\Delta V}{\Delta p} \tag{4.5}$$

We follow the argumentation by Fibich and coworkers [Fibich et al., 1993], who constructed a model for blood flow in coronary capillaries. Capillary vessels in the human body can be compared to the internal flow channels in *P. polycephalum* because they share certain characteristics: Their length is comparable (~ 1 mm), and they have very thin and permeable walls. In a previous study [Skalak and Schmid-Schönbein, 1986], it was demonstrated that pressure changes in capillaries are linearly related to the strain, so that

$$\Delta p = E \cdot \varepsilon \tag{4.6}$$

where E is Young's modulus; and ε is the strain measure defined as

$$\varepsilon = \frac{1}{2}\left[\left(\frac{a(z,t)}{a_0}\right)^2 - 1\right] \tag{4.7}$$

$a(z,t)$ is the flow channel radius, and a_0 is the reference radius under zero transmural pressure. Fibich and coworkers define a normalized radius h as

$$h(z,t) = \frac{a(z,t)}{a_0} \tag{4.8}$$

Inserting h into equation 4.7, and from equation 4.6 it follows that h^2 can be regarded as a pressure:

$$h^2 = 1 + \frac{2\Delta p}{E} \tag{4.9}$$

The equation for the compliance

$$C_f = \frac{\partial V}{\partial P} = \frac{\partial}{\partial P}(\pi {a_0}^2 l) \tag{4.10}$$

reduces, with regard to equations 4.8 and 4.9, to

$$C_f = \frac{2\pi {a_0}^2 l}{E} \tag{4.11}$$

with E being Young's modulus, and a and l radius and length of the segment, respectively. The magnitude of C_f strongly depends on Young's modulus E. In our investigation of the ultrastructure of mesoplasmodia [Oettmeier et al., 2018], we have shown that the internal veins of mesoplasmodia (and also within the sheet-like growth fronts of macroplasmodia) are permeable and lack membranes. They are, however, surrounded by a regular F-actin meshwork. The calculated capacitance strongly relies upon the elastic modulus of the vessel 'wall', as can be seen in equation 4.11. We measured the Young's modulus of whole microplasmodia by indentation and found it to be in the range of 16.4 kPa [Fessel et al., 2017]. However, this is a bulk measurement which does not take into account local variations of the elasticity. We suggest that using the elastic modulus of a pure F-actin meshwork in the calculation of C_f gives a better representation of the actual condition of the internal veins. For a cross-linked actin network, values of Young's modulus were found to be ~ 5.2 kPa [Pujol et al., 2012], which is approximately three times smaller than what we measured in microplasmodia. Thus, we used $E = 5.2$ kPa for our calculations.

4.4.4.6 Impedance

We can now model a segment of internal flow channel as an electrical circuit, based on Ohm's law for alternating current (AC), which states that current equals voltage divided by impedance. In the equivalent fluid flow system, this relationship is

$$q = \frac{\Delta p}{[Impedance]} \tag{4.12}$$

Impedance (Z) is the opposition that a circuit presents to a current when a voltage is applied. Due to the fact that the shuttle streaming in the slime mold resembles an AC situation, the capacitor exhibits reactance (equivalent to resistance). Thus, its capacitive reactance varies with the applied frequency: Higher frequencies lead to a decrease in reactance.

The dynamics of cytoplasm flow in *P. polycephalum* are driven by pulsatile pressure waves generated by the actomyosin cortex. We therefore need to give the driving pressure gradient Δp the form of a cosine pressure source

$$\Delta p = \Delta p_0 cos\omega t \tag{4.13}$$

where Δp_0 is a constant (the amplitude of input pressure) and ω is the (angular) oscillation frequency. We want to obtain the steady state of the circuit. In steady state, the system has completely adjusted to the initial imposed conditions and no further change in flow rate pattern takes place. For further analysis of the fluid equivalent circuit, we used the freeware computer software LTSpice (Linear Technology Corporation), which implements a SPICE simulator of electronic circuits.

The complex impedance of a circuit as shown in figure 4.8 is

$$Z = (R_2 + R_1)\frac{1 + j\omega\tau_1}{1 + j\omega\tau_2} \tag{4.14}$$

with

$$\tau_1 = \frac{R_2 R_1}{R_2 + R_1}C \qquad \text{and} \qquad \tau_2 = R_2 C \tag{4.15}$$

τ_1 and τ_2 are time constants which give an indication of pressure decay. They are related as follows:

$$\tau_1 = \tau_2 \frac{R_1}{(R_2 + R_1)} \tag{4.16}$$

R_1 is the resistance of the vein segment to flow, and R_2 is the loss due to leakage. In contrast to R_1, which can be easily identified from equation 4.4, R_2 can not be obtained readily from image sequences. As described above, leakage is defined as R_2 [Berger, 1993], which is due to the complete absence of a vessel wall. R_2 accounts for the amount of cytoplasm lost laterally per unit length and can be interpreted as conductance, i.e., the inverse of an (unknown) resistance. In lymph nodes, which are very permeable vessels, the equivalent resistance is reported to be $\sim$ 100 times larger than that of non-filtrating lymph ducts [Margaris and Black, 2012]. We take a value for R_2 that is 50 times larger than R_1.

4.4.4.7 Cut-off frequency

By definition, the cut-off frequency of an electronic filter is the frequency at which the power output of this circuit has fallen to a given proportion of the power of the admitted

frequencies (also termed passband). This is usually at one half of the passband. The corresponding voltage ratio is at $\frac{1}{\sqrt{2}}$, or 3 dB. The transfer function of a 3-element Windkessel circuit is [Hauser et al., 2012]

$$H(s) = \frac{sR_2CR_1 + R_1 + R_2}{sR_2C + 1} \tag{4.17}$$

By setting the magnitude of the transfer function equal to $\frac{1}{\sqrt{2}}$, we obtain the cut-off frequency

$$f_c = \frac{\frac{R_1+R_2}{CR_1R_2}}{2\pi} \tag{4.18}$$

For the analysis of one short, unbranching vein segment as given in figure 4.8 a, we used an average vein radius of $a = 20\,\mu m$, and an average length of $l = 500\,\mu m$, as measured from images. From equations 4.4 and 4.5, we obtain the fluidic resistance $R_f = R_1 = 2.19 \times 10^{15}\,N\,s\,m^{-5}$ and the fluidic capacitance $C_f = 2.42 \times 10^{-16}\,m^5\,N^{-1}$. R_2 was set to 50 times R_1. Inserting these values into equation 4.18 gives a cut-off frequency of 0.31 Hz.

The same cut-off frequency can be obtained by modeling the circuit in LTSpice. For use in a circuit simulation program like LTSpice, fluidic values have to be converted into ohm and farad, respectively. The conversion of fluidic units to electrical analogue units can be found in the appendix (7.2.3). Table 4.2 gives the parameters for a single tube segment.

Table 4.2: Fluidic and corresponding electric characteristics of single tube segment.

$l = 500\,\mu m$	
$a = 20\,\mu m$	
$C_f = 2.42 \times 10^{-16}\,m^5\,N^{-1}$	$C_e = 0.053\,F$
$R_{1f} = 2.19 \times 10^{15}\,N\,s\,m^{-5}$	$R_{1e} = 10\,\Omega$
$R_{2f} = 1.09 \times 10^{17}\,N\,s\,m^{-5}$	$R_{2e} = 500\,\Omega$

4.4.4.8 Analytical solution of 3-element Windkessel model

Equation 4.14 can also be written as

$$Z = R_1 + \frac{R_2}{1 + (j\omega R_2C)} \tag{4.19}$$

This complex impedance has a real part (Z_{real}) and an imaginary part (Z_{im}):

$$Z_{real} = R_1 + \frac{R_2}{1 + (\omega^2 {R_2}^2 C^2)} \tag{4.20}$$

$$Z_{im} = \frac{{R_2}^2 C\omega}{1 + (\omega^2 {R_2}^2 C^2)} \tag{4.21}$$

From these equations, the magnitude of the impedance ($|Z|$), i.e., the ratio of the voltage difference amplitude to the current amplitude, and the phase angle (θ) between voltage and current can be obtained.

$$|Z| = \sqrt{{Z_{real}}^2 + {Z_{im}}^2} \tag{4.22}$$

$$\theta = \arctan\left(\frac{Z_{im}}{Z_{real}}\right) \text{ in radians} \tag{4.23}$$

The analytical solution for a 3-element Windkessel as shown in figure 4.8, i.e. for a single, non-branching internal vein segment, is as follows. We begin with a driving pressure drop, as was introduced in equation 4.13. Its complex form is

$$\Delta p(t) = \Delta p_0 e^{i\omega t} \tag{4.24}$$

The equation for flow rate is, as given by equation 4.12,

$$q(t) = \frac{\Delta p(t)}{Z} \tag{4.25}$$

or, to use the concept of reactance, we get the complex flow rate

$$q(t) = \frac{\Delta p_0 e^{i\omega t}}{Z_{real} + Z_{im}} \tag{4.26}$$

The imaginary part Z_{im} of the complex impedance is also termed reactance. The real part of equation 4.24 is a cosine function:

$$\Delta p(t) = \Re\{\Delta p_0 e^{i\omega t}\} \tag{4.27}$$

$$= \Delta p_0 \cos\, \omega t \tag{4.28}$$

Therefore, the flow rate corresponding to this pressure drop is the real part of the complex flow rate of equation 4.26:

$$q(t) = \Re\left\{\frac{\Delta p_0 e^{i\omega t}}{Z_{real} + Z_{im}}\right\} \tag{4.29}$$

$$= \Delta p_0 \Re\left\{\frac{(\cos\, \omega t + i\, \sin\, \omega t)(Z_{real} - Z_{im})}{{Z_{real}}^2 + {Z_{im}}^2}\right\} \tag{4.30}$$

$$= \Delta p_0 \left\{\frac{Z_{real}\, \cos\, \omega t + Z_{im}\, \sin\, \omega t}{{Z_{real}}^2 + {Z_{im}}^2}\right\} \tag{4.31}$$

which, using trigonometric identities, equals

$$q(t) = \frac{\Delta p_0}{\sqrt{{Z_{real}}^2 + {Z_{im}}^2}}\, \cos\, (\omega t - \theta) \tag{4.32}$$

$$= \frac{\Delta p_0}{|Z|}\, \cos\, (\omega t - \theta) \tag{4.33}$$

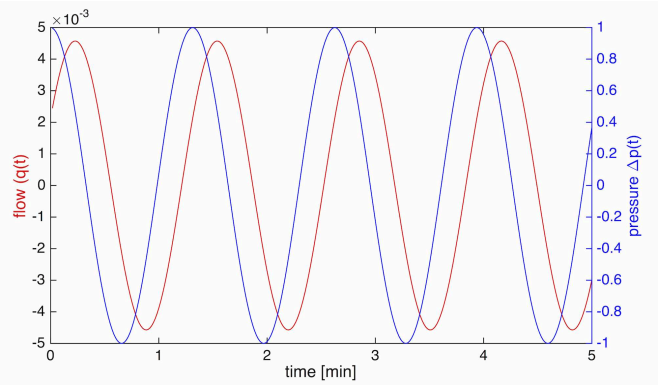

Figure 4.10: Phase difference between pressure and flow. Pressure ($\Delta p(t)$) and flow rate ($q(t)$). Flow lags $\theta = 62°$ behind the pressure wave.

with phase angle θ as given in equation 4.23. θ can also be obtained from the LTSpice simulated circuit. In figure 4.10, the relationship between pressure (equation 4.28) and flow (equation 4.33) is shown. To further elucidate the nature of impedance and phase angle, we can discuss the limiting behavior of these equations. If $C = 0$, Z_{im} becomes 0 and Z_{real} becomes $R_1 + R_2$. This means that $\theta = 0$, i.e. there is no phase difference between flow and pressure. Equation 4.32 would then become

$$q(t) = \frac{\Delta p_0}{\sqrt{(R_1 + R_2)^2}} \cos(\omega t) \tag{4.34}$$

indicating a purely resistive circuit. If $R_1 = 0$, Z_{im} remains unaffected and $Z_{real} = \frac{R_2}{1+(\omega^2 R_2^2 C^2)}$. Thus, the flow would not differ much. However, if $R_2 = 0$, $Z_{im} = 0$ and $Z_{real} = R_1$. This results in $\theta = 0$, and $q(t) = \frac{\Delta p_0}{\sqrt{R_1^2}} \cos(\omega t)$, i.e. a circuit that is also purely defined by resistance.

4.4.4.9 Dimensionless parameters

It is also possible to characterize the relationship between pressure and flow wave in the 3 element Windkessel model using the two dimensionless parameters $\tilde{r} = \frac{R_1}{R_2}$ and $\tilde{c} = CR_2\omega$, and the term $\frac{1}{R_2}$ [Brown, 2012]. Expressed in these terms of interest, the flow then becomes

$$q_{rel} = \left(\frac{\left(\frac{1}{R_2}(\tilde{r}+1) + \frac{1}{R_2}\tilde{r}\tilde{c}^2 \right) \Delta p_0}{(\tilde{r}+1)^2 + \tilde{r}^2\tilde{c}^2} \right) \cos(\omega t - \theta_{rel}) \tag{4.35}$$

The parameter $\frac{1}{R_2}$ acts as a scaling factor for the flow. To simplify things further, we introduce the dimensionless flow $\tilde{q}$.

$$\tilde{q} = \frac{qR_2}{\Delta p_0} = \frac{\tilde{r}+1+\tilde{r}\tilde{c}^2}{(\tilde{r}+1)^2 + \tilde{r}^2\tilde{c}^2} \cos(\omega t - \theta_{rel}) \tag{4.36}$$

The relative phase shift θ_{rel} between pressure and flow can also be expressed in terms of dimensionless parameters and then reads as follows:

$$\theta_{rel} = \arctan\left(\frac{\tilde{c}}{(\tilde{r}+1)+\tilde{r}\tilde{c}^2}\right) \tag{4.37}$$

Another factor that can be assessed is power dissipation (W), which has a steady and an oscillatory part [Berger et al., 1995]. The steady part is the product of mean pressure and mean flow and takes on very small values, hence it is disregarded in the following. The oscillatory power dissipation over one oscillation period is given as

$$W = \frac{1}{2}Q^2|Z|\cos\theta \tag{4.38}$$

where Q is the amplitude of q_{rel} (equation 4.35). Figure 4.11 shows how phase angle θ_{rel}, flow amplitude, power dissipation and impedance vary with $\tilde{r}$ and $\tilde{c}$. θ_{rel} has

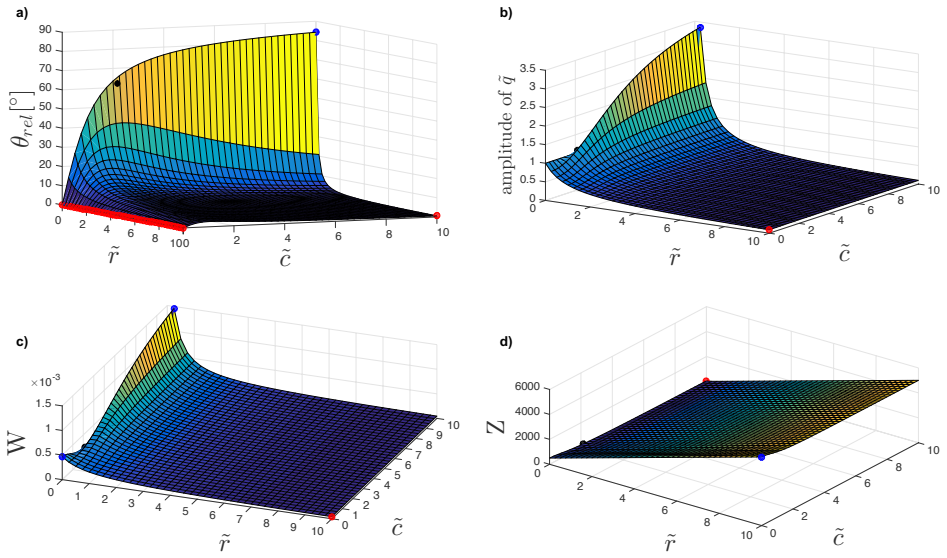

Figure 4.11: Dependence of phase angle, flow amplitude, power dissipation and impedance on the dimensionless parameters $\tilde{r}$ and $\tilde{c}$. Illustration of how θ_{rel} (a), amplitude of the flow $\tilde{q}$ (b), power dissipation W (c), and impedance Z (d) vary with the dimensionless parameters $\tilde{r}$ and $\tilde{c}$. Red dots = local minima, blue dots = local maxima, black dots = corresponding values for calculated $\tilde{r}$ and $\tilde{c}$.

a maximum at 84.3°, when $\tilde{r}$ is zero and $\tilde{c}$ is maximal. The effect of an increasing ratio of $\tilde{r}$ is the reduction of the phase angle between pressure and flow (figure 4.11 a). However, the effect is most pronounced for small $\tilde{r}$. For one vein segment (and one characteristic oscillation frequency), $\tilde{r}$ is 0.02 and $\tilde{c}$ is ~ 2. An increasing ratio of $\frac{R_1}{R_2}$

leads to a reduced amplitude of the flow wave (figure 4.11 b). As $\tilde{r}$ becomes small and $\tilde{c}$ becomes large, there is a peak in the amplitude of the flow. Thus, we can state that the flow rate increases with the vessel compliance. A higher elasticity, in combination with low-frequency pulsatile flow, leads to an enhanced flow rate. This has been established [Zamir, 2000; San and Staples, 2012].

In a mesoplasmodium, the uroid generates sinusoidal pressure waves with different oscillation frequencies, but we observe net forward flow of cytoplasm (see figure 4.3). Thus, when simulating equivalent electric circuits, we model this by superimposing a DC signal over the AC signal. This grants net forward flow without necessitating diodes (electrical) or valves (biological).

The forward migration of mesoplasmodia is based on myosin II-driven rhythmic back-and-forth oscillations of the actin cytoskeleton. These contractions drive the observed cytoplasm flow along the longitudinal axis of the amoeba. The entire locomotion process is far from completely understood, but an asymmetry of the cell in terms of a softness gradient [Lewis and Guy, 2017] seems to play a big role, as well as substrate adhesion [Rieu et al., 2015; Matsumoto et al., 2008] and the transition from endo- to ectoplasm and vice versa.

Kirchhoff's current law (KCL) states that charge cannot accumulate at the nodes of a circuit. In fluid dynamics, that means that the amount of fluid which flows into one end of a pipe equals the outflow. Continuing with our analogy that the elastic tube walls act like capacitors, we have to take into consideration that capacitance C affects the total volume of the tube. Therefore, the flow rate at the entrance of the tube may not be the same as that at the exit, because some of the flow may inflate the tube upon entering it, thus reducing the output; and some of the exit flow may result from a part of the vessel deflating. We therefore have to take retrograde flow of endoplasm into account. This means that forward flow through the internal veins enters the frontal region, then bounces off the membrane and transforms into backwards flow.

The LTSpice schematic of the single tube (a single 3-element Windkessel) is given in figure 4.12 a. An AC analysis results in a Bode plot (see figure 4.12 b), and at the -3 dB mark, the cut-off frequency f_c can be read off. It can also be determined via equation 4.18. Both methods give $f_c = 0.31$ Hz (corresponding to an oscillation with T = 3.26 s). Therefore, a single tube segment does act as a low-pass filter, but only at frequencies way above what we observe in slime mold mesoplasmodia.

A slight lag between the voltage at node 1 and node 2 (see figure 4.12 a) can be observed. Node 1 represents the input voltage (U_1), whereas at node 2, the voltage as influenced by the circuit's components can be extracted (U_2). The phase angle between both voltage signals is $\phi_{U_1U_2} = 2.4°$. This means that along the vein segment (we

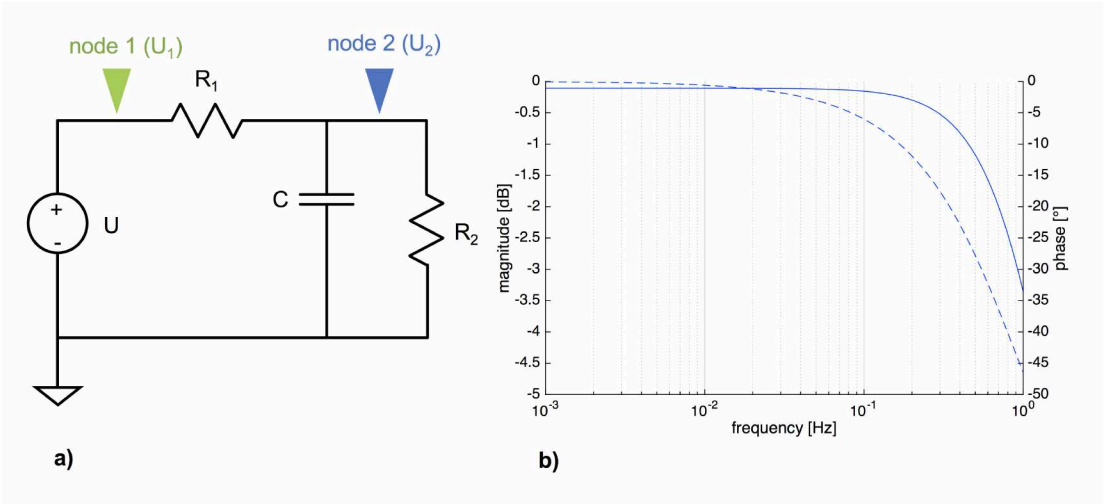

Figure 4.12: LTSpice schematic and resulting Bode plot of a three-element Windkessel. a) Schematic of 3-element Windkessel. U = voltage source, R_1, R_2 = resistors, C = capacitor. Green arrow = node 1, blue arrow = node 2. b) Bode plot of the circuit, taken at node 2. The cut-off frequency can be obtained mathematically, or it can be found from the Bode plot at the frequency where the gain falls below - 3 dB.

assumed a length of 500 µm), the voltage (pressure) signal is slightly delayed. This delay of the pressure wave along the tube is a feature of a distributed model, in which spatial dimension does play a role. Furthermore, when flow is occurring in an elastic tube, the local change of pressure propagates like a wave crest down the tube. In a rigid tube, a local change of pressure would occur instantaneously everywhere within the tube.

In summary, we find that a single tube section of internal vein can not account for the observed frequency selection, although it acts as a low-pass filter. Pressure precedes the flow by 62°, and along the length of the segment, the pressure wave is slightly delayed between the entrance and the exit of the tube.

4.4.4.10 Analysis of four coupled segments

Since one single 3-element Windkessel (3WK) model was not sufficient to describe the dynamics within the mesoplasmodium, we constructed a branching vein model as shown in figure 4.9 c. The corresponding LTSpice circuit is given in figure 4.13. The model circuit consists of four 3WK elements, branching in a Y-shaped fashion. The respective values were the same as in the single 3WK model (see table 4.2). The arrangement of figure 4.13 is a filter cascade, connecting multiple low-pass filters. An AC analysis reveals different cutoff-frequencies throughout the circuit, as given by the three different traces (green, blue, red) in figure 4.13. f_c of position 3 (red), the end point of the branching structure, was found to be 0.033 Hz, which is in accordance with our data

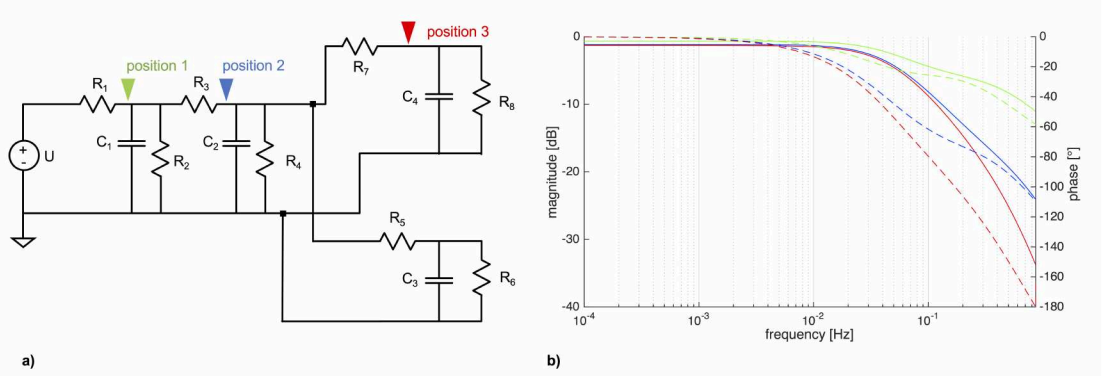

Figure 4.13: LTSpice schematic and resulting Bode plot of four three-element Windkessel. a) LTSpice schematic of four cascaded 3WK elements. U = voltage source, R = resistor, C = capacitor. b) Bode plots obtained at positions 1 (green), 2 (blue), and 3 (red). The more segments are added, the steeper does the filter cutoff become. Solid lines = magnitude [dB], dashed lines = phase [°].

(see figure 4.7). This frequency is ten times lower than that of one single 3WK element. f_c of position 1 (green) was 0.058 Hz, and f_c of position 2 (blue) was 0.036 Hz. Thus, the further the distance from the uroid (the input signal) and the further along the filter cascade, the better does the Y arrangement reflect the real situation within the slime mold. In other words, the length of the internal vein plays a major role in the low-pass filtering process. This explains why very small mesoplasmodia do not exhibit frequency selection.

Within the branched four 3WK model, flow and pressure wave do not occur simultaneously. Rather, pressure (voltage) leads the flow (current), see figure 4.14. The phase difference between input pressure and flow at position 3 is $\theta \approx 127°$. Along the Y-shaped cascade, the voltage (i.e. pressure wave) is slightly delayed. This can be seen in figure 4.14 b. We found a phase angle of $\phi \approx 18°$ between the input voltage signal and voltage at position 3 (red arrow in figure 4.13). Figure 4.15 shows flow velocity measurements at two different positions along an internal vein. It becomes obvious that the flow waves lag between positions, more specifically, that the flow occurs first closer to the uroid and then travels towards the front.

4.4.5 Modeling chemotaxis

Our Y-shaped filter cascade works very well to describe the dynamics within a moving mesoplasmodium. However, our lumped model can also be adapted and used to explain how a slime mold starts to migrate in one particular direction, or how it could change its direction. This again introduces a spatial (or distributed) component to the otherwise lumped model. To model asymmetry introduced by polarization and (chemotactic) migration, we arranged two 3WK symmetrically side by side, with a voltage source as

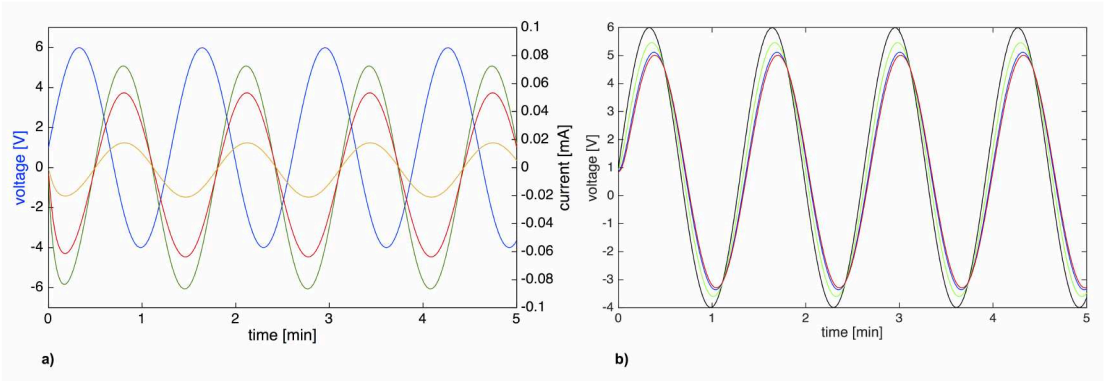

Figure 4.14: Input voltage and currents at three different positions; voltage at different positions. a) Input voltage (blue curve) and current through R_1 (green curve), R_3 (red curve), and R_7 (orange curve), respectively. b) Voltage measured at positions 1 (green), 2 (blue), and 3 (red). Input voltage = black curve.

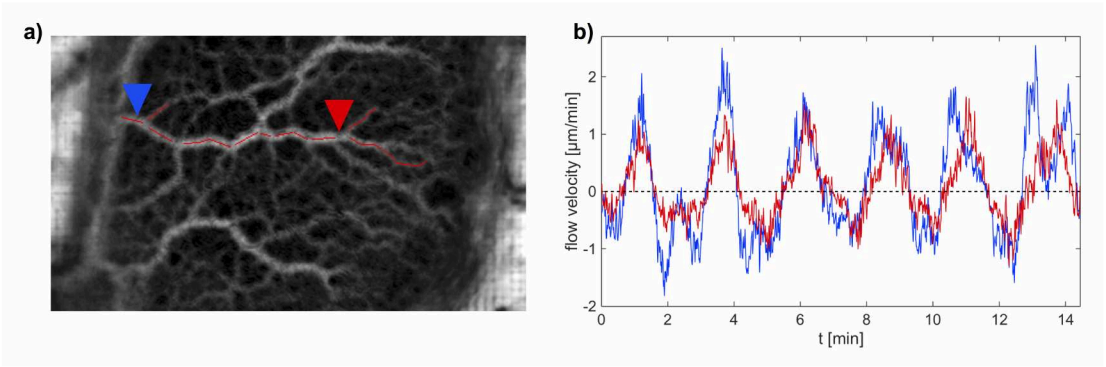

Figure 4.15: Flow velocity at different positions along a vein. a) Time series (standard deviation) of a mesoplasmodium with a major vein highlighted in red. Blue and red arrowheads denote positions at which internal flow was measured. b) Flow velocity at the two indictated positons in a) along a forward moving mesoplasmodium.

oscillating driving pressure (without DC offset) in the middle (see figure 4.16). This circuit is symmetrical, meaning the same impedance is present on both sides. The current which flows through the entire right side of the circuit can be obtained by measuring it at R_1, and for the entire left side, at R_3, respectively.

4.4.5.1 Case 1: Stationary microplasmodium

In the first case, we want to consider a stationary, non-migrating microplasmodium. It is not motionless, because it exhibits rhythmic oscillations [Bernitt et al., 2010]. However, the cell is unpolarized. The actin cortex which surrounds the whole microplasmodium and which lies directly underneath the plasma membrane is homogenous [Oettmeier

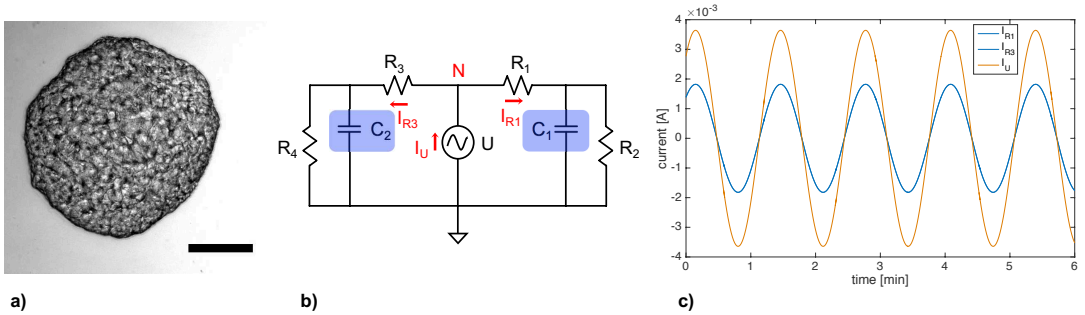

Figure 4.16: Case 1: Stationary, unpolarized microplasmodium. a) Stationary, unpolarized microplasmodium. Scale bar = 100 µm. b) Symmetrical model circuit for an oscillating but stationary microplasmodium. C = capacitors, R = resistors, U = voltage source, I = current, N = node. c) Current flowing through the right side as taken at R_1 and R_3 (blue) and the voltage source (I_U, orange).

et al., 2018]. This condition is represented by the circuit as shown in figure 4.16, with the resistors and capacitors on both sides set to the same values, respectively. The AC voltage source represents the rhythmic contraction-relaxation pattern which is the basis of the pressure waves. At node N, according to Kirchhoff's current law (KCL), the sum of currents flowing into the node equals the sum of currents flowing out of the node, i.e. $I_U = I_{R1} + I_{R2}$. This circuit arrangement can best be compared to a valve that connects two identical balloons. Because the balloons are the same, the inflow (I_U) splits up evenly into two flows to the right (I_{R1}) and the left (I_{R3}). Figure 4.16 c shows I_{R1} and I_{R3}, which have the exact same phase and amplitude because of the circuit's symmetry. Since both currents are flowing out of the node, their direction is also identical. Averaged over 5 oscillation periods, I_U gives an average current of almost zero (9.85×10^{-6} A). In the slime mold, the total volume of cytoplasm remains constant, and thus KCL also applies to the fluidic system. Because there is no difference in elasticity, each side receives the same amount of cytoplasm. This is equivalent to a stationary, oscillating plasmodium.

4.4.5.2 Case 2: Cell polarity: introducing asymmetry

In the second case, we discuss polarization and subsequent start of migration. We argue that the onset of locomotion is due to the development of an elasticity gradient throughout the cell. It is known that the front of a migrating plasmodium is softer than the back. Local softening of the actin cortex plays a big role in the amoeboid movement of *P. polycephalum* [Lewis et al., 2015; Lewis and Guy, 2017]. The ultrastructural analysis of a migrating mesoplasmodium also shows a denser, more organized actin cortex in the back and a weaker cortex in the front [Oettmeier et al., 2018]. A strong actin cortex in the trailing edge and a soft actin cortex at the leading edge are also a requirement for locomotion in *D. discoideum* [Ramalingam et al., 2015]. The ubiquitous

oscillations are always present (as represented by the AC voltage source in figure 4.17), but the mesoplasmodium is now polarized and subsequently moves. The components

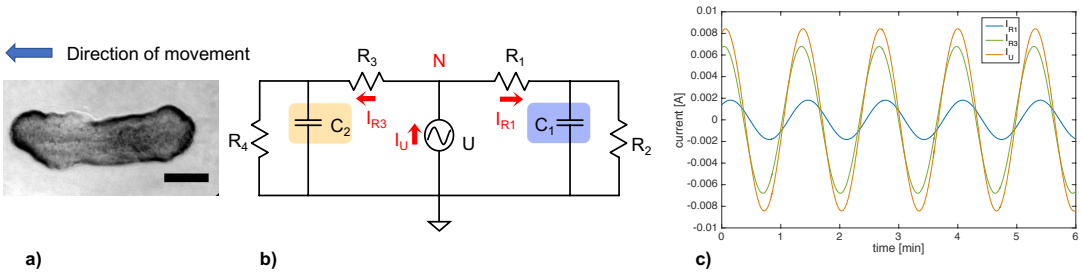

Figure 4.17: Case 2: Polarized, migrating plasmodium. a) Migrating, polarized microplasmodium. Scale bar = 50 µm. b) Symmetrical model circuit for a motile microplasmodium. C = capacitors, R = resistors, U = voltage source, I = current. c) Current flowing through the right side as taken at R_1 (blue) and the left side as taken at R_3 (green), and current flowing through the voltage source (I_U, orange).

of importance in the equivalent circuit are the capacitors. C_2 was set to five times C_1, which corresponds to a higher elasticity at the front. Due to the higher capacitance, the reactance of capacitor C_2 is reduced and the current increases in the left side of the circuit. In an electric capacitor, the larger the capacitance, the more charge has to flow to build up a particular voltage, and the higher the resulting current will be. Returning to the aforementioned example of a valve connecting two balloons, we now have the situation of the left balloon being five times softer than the right balloon. Thus, due to the smaller resistance, the inflow (I_U) splits up into a low flow to the right (I_{R1}) and an enhanced flow to the left (I_{R3}). In terms of fluidics, this means a higher flow rate towards the left side of the circuit. Averaged over 5 oscillation periods, I_U gives an average current of 3.09×10^{-4} A, which is $\sim$ 30 times more than in the stationary case. Increasing the capacitance of the left capacitor (C_2) to five times that of C_1 (right side) also results in a current through the left side (I_{R3}) which is fifty times higher than I_{R1}.

To verify this outcome, we calculated the volumetric flow rates in a migrating mesoplasmodium (see figure 4.18 a). As mentioned before, both the volume and the shape of a mesoplasmodium remain constant over the time scale of observation. Also, mesoplasmodia travel on straight trajectories. Thus, by overlaying the image at the start of a time sequence with the last image in the stack, we obtain the solid red area in figure 4.18 a. This is the area which is accumulated during the time interval of interest. Assuming a constant height of 100 µm, we obtain a volumetric flow rate of $Q_{total} = 9.8 \times 10^5\,\mu m^3\,min^{-1}$. Q_{total} corresponds to I_U. Next, we measured the flow rate in the back of the mesoplasmodium, which is the equivalent to I_{R1}, i.e., the flow through the right side of the circuit. The red diamonds in figure 4.18 a show the points at which flow was measured. We calculated the volumetric flow rate as follows (equation 4.39) to obtain the flow for each vein from the flow velocity v, which was obtained

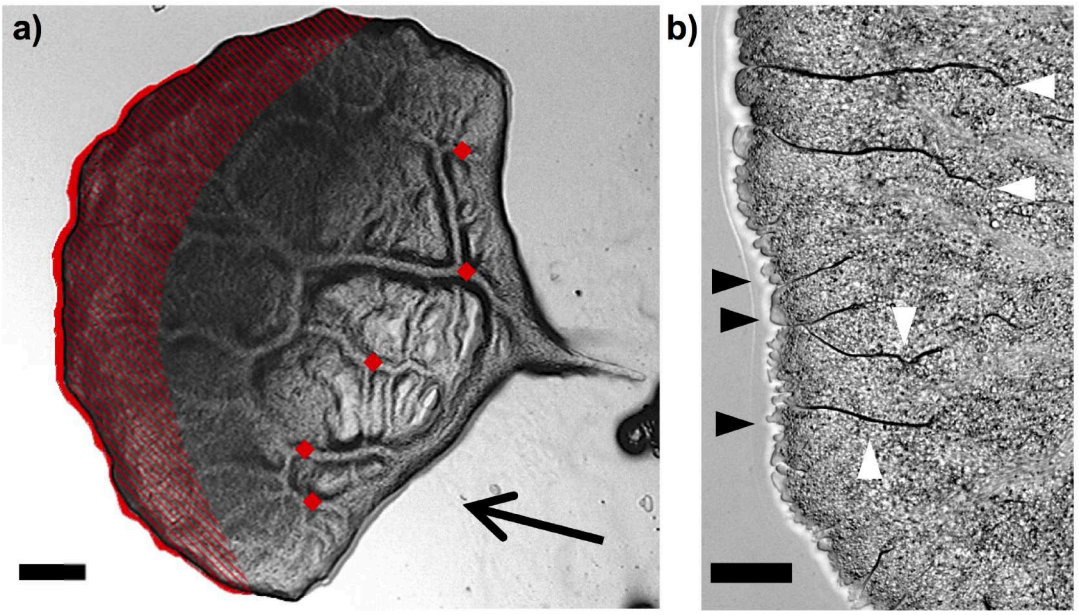

Figure 4.18: Volumetric flow rates and micromorphology in a migrating mesoplasmodium. a) Migrating mesoplasmodium. Scale bar = 200 µm. Overlay of two images taken at an interval of ~ 3 min. From the solid red area, we calculated the overall volumetric flow rate (which corresponds to I_U). Red diamonds designate points on main internal veins at which flow rates were measured and which correspond to I_{R1}. Hatched area indicates frontal sheet. b) Higher resolution of the front of a migrating mesoplasmodium. Scale bar = 50 µm. White arrows point to membrane folds, black arrows to blebs.

from optical flow analysis, and the cross-sectional areas A of the veins, assuming a radius of $a = 20\,\mu\text{m}$.

$$Q = vA \tag{4.39}$$

Most of the flow in the uroidal region passes through those veins. The sum of the flows amounts to $Q_{back} = 2.8 \times 10^4\,\mu\text{m}^3\,\text{min}^{-1}$. By applying KCL, we find the flow rate through the frontal area as $Q_{front} = Q_{total} - Q_{back} = 9.5 \times 10^5\,\mu\text{m}^3\,\text{min}^{-1}$. Q_{front} corresponds to I_{R3}, the flow through the left side of the circuit. Q_{front} is ~ 30 times larger than Q_{back}, which is in good agreement with the electric circuit model (where $I_{R3} = 30 \times I_{R1}$).

At this point, the interdependence between ultrastructure and flow needs to be briefly discussed. For a more detailed investigation, see [Oettmeier et al., 2018]. As can be seen in figure 4.18 b, the frontal area of the mesoplasmodium (hatched area in figure 4.18 a) possesses many deep folds and creases which most likely represent a membrane reservoir. Like inflating a wrinkled balloon, when cytoplasm flows into this area, the membrane easily yields. Furthermore, blebbing can be observed along

the whole front. Other effects at play in the frontal sheet are height fluctuations and gel-sol transitions. All of these processes have their own dynamics and will affect the flow.

In summary, we propose a mechanism which, induced by a chemotactic signal transduction (or internal cues), leads to a local softening of the actin cortex at the site of the chemoattractant stimulus. The capacitance of the vessels increases, which, in turn, enhances the flow in the affected vessels. A correlation between more elastic vessels and enhanced volumetric flow has also been shown to occur in blood vessels [Guo and Fu, 2012]. This leads to an increased mass transport towards the left side (see figure 4.17) and less flow towards the right, so that the slime mold would effectively move to the right.

4.5 Conclusion and Outlook

Recently, *P. polycephalum* has become the focus of research on the fundamental mechanisms of cognition and decision-making (for a review, see [Vallverdú et al., 2018]). The question of how the slime mold processes information in the absence of a nervous system is still unanswered. For its apparent reminiscential capabilities, a model based on memristors has been put forward [Pershin et al., 2009]. The selection of frequencies is an example of hydrodynamic information processing. We speculate that cytoplasm flow is a means for the slime mold to transmit information throughout its cell body, and to process this information so that an observable change in behavior takes place. The input signal, e.g., a chemotactic stimulus, could cause a change in the oscillation pattern which is then transmitted through the entire organism. On the other hand, based on internal cues (e.g. the cell cycle or nutritional status), the slime mold could control, globally or locally, the radius and stiffness of its veins via the actin cytoskeleton. This would change the fluidic properties (resistance, capacitance), and thus the flow. The internal flow pattern, in turn, changes the morphology and behavior of the organism.

To our knowledge, no previous modeling has been done using the lumped parameter approach presented here. As of late, several models regarding the mechanical properties of *P. polycephalum* and their implications for pattern formation and oscillations have been proposed. By integrating experimental data into a quantitative framework, these models can shed light on the spatio-temporal coordination of cell motility. Some variables are hard to measure experimentally, which is a strong motivation for the use of physical models, including our lumped model. Under this premise, various models have been constructed. Viscoelastic or poroelastic models were able to reproduce many experimentally observed movement patterns, for example [Alonso et al., 2016, 2017; Radszuweit et al., 2014]. Zhang et al. [2017] have also measured endoplasm velocity, but have extended their measurements to include traction stress and calcium. They found that asymmetric spatio-temporal patterns of endoplasmic flow lead to a higher migration speed than purely symmetrical patterns, a result that is in accordance to our findings. However,

most of those models rely on accurate biological data, e.g. biochemical processes and calcium dynamics, which are still not very well understood in *P. polycephalum*. An advantage of our model is that it does not require a great deal of biological detail, e.g. the dynamics and quantitative rates of chemical reactions. As we learn more about the inner workings of the slime mold, such detail can be used to amend and expand our model.

We present an efficient and fast way in which signals can be processed without the necessity for complicated biochemical signal transduction pathways. Our model explains how *P. polycephalum*'s complex behavior is based on intracellular cytoplasm flow. Furthermore, local softening of the actin cortex can account for an increased flow towards that area and a subsequent introduction of asymmetry, so that locomotion can be initiated.

Chapter 5

Mitochondrial numbers increase during glucose deprivation in the slime mold *Physarum polycephalum*

Christina Oettmeier[1,3], Hans-Günther Döbereiner[2]

[1] Institut für Biophysik, Universität Bremen, NW1 Raum N4260, Otto-Hahn-Allee 1, 28359 Bremen, Germany
[2] Institut für Biophysik, Universität Bremen, NW1 Raum O4040, Postfach 330440, 28334 Bremen, Germany
[3] Author to whom any correspondence should be addressed.

Supplementary material for this chapter is available online at `https://link.springer.com/article/10.1007/s00709-019-01410-1#SupplementaryMaterial`. Further information can be found in the appendix (section 7.3).

5.1 Abstract

Glucose deprivation in the slime mold *Physarum polycephalum* leads to a specific morphotype, a highly motile mesoplasmodium. We investigated the ultrastructure of both meso- and non-starved plasmodia and found significantly increased numbers of mitochondria in glucose-deprived mesoplasmodia. The volume of individual mitochondria was the same in both growth forms. We conjecture that the number of mitochondria correlates with the metabolic state of the cell: When glucose is absent, the slime mold is forced to switch to different metabolic pathways, which occur inside mitochondria. Furthermore, a catabolic cue (such as AMP-activated protein kinase (AMPK)) could stimulate mitochondrial biogenesis.

5.2 Introduction

The giant unicellular slime mold *Physarum polycephalum* grows into transport networks (termed macroplasmodia) which can reach sizes of up to square meters [Stockem and Brix, 1994]. Under certain nutritional conditions, i.e., a lack of glucose in the solid agar medium, and when the culture has reached a certain age, a special foraging pattern can be observed. Instead of forming a coherent network from isolated fragments, the slime mold aggregates into independent, unconnected units (termed mesoplasmodia), which then move in a straight trajectory away from their point of origin [Lee et al., 2018]. Mesoplasmodia are well suited as models to study the mechanism of the slime mold's locomotion [Oettmeier and Döbereiner, 2019a], because they move for hours in straight trajectories and keep a constant shape. The movement of those autonomous foraging units is comparatively fast, reaching speeds of up to $17\,\mu m\,min^{-1}$.

Slime molds exhibit characteristic continuous rhythmic oscillations, orchestrated by the cytoskeletal proteins actin and myosin. A detailed description of the ultrastructure can be found in [Oettmeier et al., 2018]. These vigorous and perpetual contractions, which are the basis for locomotion in *P. polycephalum* [Oettmeier and Döbereiner, 2019a], require a lot of energy in the form of ATP, which is supplied by glycolysis and oxidative phosphorylation in mitochondria. Glycolysis takes place in the cytoplasm and seems to be intensely operated by the slime mold [Sauer, 1982].

P. polycephalum possesses mitochondria with tubular cristae. The ultrastructure of eumycetozoan mitochondria is unique and characteristic for slime molds [Dykstra, 1977], but their function is the same as in any other eukaryotic organism. Mitochondria in *P. polycephalum* are isolated and spherical or lenticular (see figure 5.1). Our observation of the shape conform to earlier findings [Daniel and Järlfors, 1972; Sauer, 1982]. Mitochondria do not form networks, because the vigorous intracellular flow within the amoeboid cell body is constantly moving them around. A video of this can be found in the supplementary material (S1 a and S1 b; `https://link.springer.com/article/10.1007/s00709-019-01410-1#SupplementaryMaterial`). An elaborate mitochondrial network (as for example in budding yeast), would not be feasible due to the dynamic nature of the cytoplasm. Furthermore, it has been demonstrated that the slime mold's mitochondria can migrate within the cell [Kuroiwa and Takahashi, 1978] in response to culture conditions: they moved towards the periphery of the cell when a liquid shaking culture was left unstirred for a few hours. This migration is reversible; when the microplasmodia were agitated, they dispersed evenly again. Apart from the characteristic tubular cristae, the mitochondria possess mitochondrial DNA (mtDNA), which is packaged into the electron-dense mitochondrial nucleoid (see figure 5.1 a), along with many proteins [Itoh et al., 2011]. The complete mitochondrial genome has been sequenced [Takano et al., 2001].

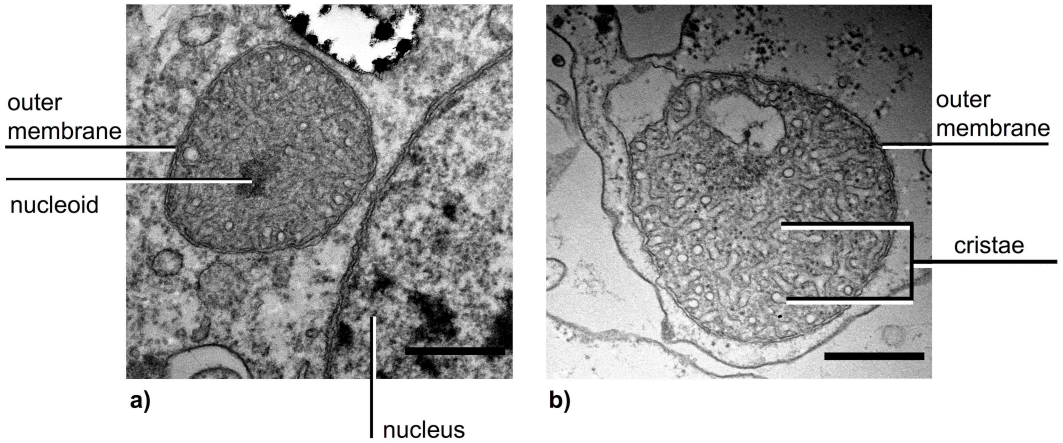

Figure 5.1: a) Mitochondrium of a starved mesoplasmodium. b) Mitochondrium within an unstarved plasmodium of *P. polycephalum*. Scale bars = 0.5 µm.

Mitochondria perform many important biological functions. Most important is the production of ATP through oxidative phosphorylation, but they also play a role in the pronounced and well-described oscillations of the slime mold: mitochondria store and release calcium [Nations et al., 1989; Achenbach et al., 1984], thereby forming a crucial component of the biochemical oscillator. The nature and localization of this pacemaker of the contraction-relaxation cycle poses one of the most interesting problems regarding the dynamic processes of the non-muscle contractile system in *P. polycephalum*. Although the exact mechanism remains unknown, it is clear that mitochondria and the processes taking place within them are integral parts [Satoh et al., 1982; Korohoda et al., 1983]. Inhibiting glycolysis or respiration leads to changes in the pattern and frequency of the oscillations.

When sufficient glucose is present in the medium, glycolysis takes place in the cytosol, producing two molecules of ATP and two molecules of NADH per molecule of glucose. Furthermore, it produces two molecules of pyruvate which are then transported into the mitochondria to enter the citric acid cycle. Electrons from the glycolysis and citric acid cycle are then being transferred by NADH and $FADH_2$ to the electron transport chain, ultimately driving oxidative phosphorylation and producing more ATP (more than 30 molecules per molecule of glucose). Citric acid cycle and oxidative phosphorylation take place across the inner membrane and cristae of the mitochondria. When glucose is absent from the medium, *P. polycephalum* immediately starts to use its abundant stores of glycogen in a process termed glycogenolysis [Nader and Becker, 1983]. The glycogen polymer is broken down by the enzyme glycogen phosphorylase, releasing glucose, which can then be used in glycolysis. Besides glucose (and other carbohydrates), the slime

mold is also able to catabolize proteins [Goodman and Beck, 1974] and lipids [Poulos and Thompson, 1971]. If given a choice, *P. polycephalum* seems to prefer a diet that contains equal ratios of proteins and carbohydrates, or a ratio of two times more proteins than carbohydrates [Dussutour et al., 2010].

Usually, when microplasmodia of *P. polycephalum* are cultivated in a growth medium that lacks nutrients (but contains salts to maintain pH), inactive cyst-like stages are formed after a certain time [Hüttermann, 1973]. These spherules also occur when a shaking culture of microplasmodia depletes its liquid medium of nutrients. Depending on the starting conditions (temperature, culture volume, nutrient concentrations, shaking speed), glucose is depleted after 2.5 [Nader and Becker, 1983] to 4 days [Lee et al., 2018]. In this study, we used the same conditions as described by Lee et al. [2018], which means that microplasmodia reach their maximum biomass after 3 to 4 days and turn into spherules after ~ 7 days after inoculation, if left in their shaking culture. However, when microplasmodia from a 6 day old culture are plated onto an agar plate lacking glucose, they will form the aforementioned mesoplasmodia which then begin to move outward from the inoculation centre. For about 9 hours, the mesoplasmodia migrate on straight trajectories without much changing their shape or showing an increase in biomass. Our samples were taken from mesoplasmodia in the middle of the migration period. After this motile phase, at around 10 hours after initial plating, the mesoplasmodia reach a pause state in which migration is ceased. After this pause, mesoplasmodia either transition into static networks, continue to migrate, or move in a different pattern.

As observed in skeletal muscle cells, an elevated energy demand (e.g. through exercise) increases mitochondrial volume density [Lundby and Jacobs, 2016]. Similarly, myocardial hypertrophy [Wiesner et al., 1994], changes in neuronal activity [Liu and Wong-Riley, 1995], and other metabolic challenges lead to an increase in mitochondrial biogenesis. Therefore, many cells are capable of adjusting their mitochondria to a change of energy demand, requiring that they possess an appropriate intracellular energy sensor. Since mitochondria are so important for both energy metabolism and the primary oscillator, we compared, in the present study, the mitochondria of glucose-deprived mesoplasmodia and non-starved plasmodia. We found a significantly increased number of mitochondria in glucose-deprived mesoplasmodia. We hypothesize that mitochondrial biogenesis is stimulated in *P. polycephalum* mesoplasmodia grown in the absence of glucose, probably in order to compensate for the reduced supply of glycolytic ATP and pyruvate.

5.3 Material and Methods

5.3.1 Microplasmodia culture

We used the strain WT33 [Marwan and Starostzik, 2002]x LU898 [Kawano et al., 1987], which was kindly provided by Prof. Dr. Wolfgang Marwan (Universität Magdeburg). Microplasmodia were grown in a liquid growth medium (see table 5.1 and table 5.2).

Table 5.1: Liquid growth medium for microplasmodia.

Ingredient	amount (for 1 l.)
Bacto tryptone	10 g
Yeast extract	1.5 g
D(+) glucose monohydrate	11 g
Anhydrous citric acid	3.54 g
Iron(II)sulfate heptahydrate	0.084 g
Calcium chloride dihydrate	0.6 g
Potassium dihydrogen phosphate	2 g
100 x MMZ solution	10 ml
Fill up to 1 l with MilliQ water	
pH adjusted to 4.6 with 4 N NaOH	

Table 5.2: 100 x MMZ solution.

Ingredient	amount (for 1 l.)
Magnesium sulfate heptahydrate	60 g
Manganese(II)chloride dihydrate	6 g
Zinc sulfate heptahydrate	3.4 g

The cultures were grown at a constant temperature of 24 °C and rotation speed (180 rpm) in the dark. Torn apart by shear forces, multiple small and spherical units are produced, whose size is determined by the shaking speed. Fresh microplasmodia cultures were prepared by taking 2 ml of the previous culture at day 3 to 4, centrifuging gently and discarding the supernatant. The pellet was then transferred into new liquid medium.

5.3.2 Mesoplasmodia

To create mesoplasmodia, microplasmodia from a 6 day old liquid culture were centrifuged, the supernantant discarded, and they were resuspended briefly with MilliQ water. Microplasmodia were then transferred onto a semi-defined medium (SDM) agar plate lacking glucose (see table 5.3). *P. polycephalum* requires hemin to grow [Daniel et al.,

Table 5.3: 2 x SDM-agar without glucose.

Ingredient	amount (for 1 l.)
Bacto soytone	20 g
Anhydrous citric acid	7.08 g
Iron(II)chloride tetrahydrate	0.078 g
D(+) biotin	0.01 g
Thiamin hydrochloride	0.08 g
Potassium dihydrogen phosphate solution, $80\,g\,l^{-1}$	50 ml
Calcium chloride dihydrate solution, $41.2\,g\,l^{-1}$	50 ml
Magnesium sulfate heptahydrate solution, $24\,g\,l^{-1}$	50 ml
EDTA disodium salt dihydrate solution, $9.2\,g\,l^{-1}$	50 ml
Zinc sulfate heptahydrate solution, $136\,g\,l^{-1}$	0.5 ml
Fill up to 1 l with MilliQ water pH adjusted to 4.6 with 4N NaOH	
Agar	17 g
Dissolve in MilliQ water, then autoclave	500 ml
Add 2 x SDM medium	500 ml
Add hemin solution, $0.5\,g\,l^{-1}$	10 ml
Pour into Petri dishes.	

1962]. However, hemin is poorly soluble in water. Therefore, it needs to be dissolved in 1 N NaOH first. This solution can then be mixed with MilliQ water to achieve the desired final concentration. SDM agar contains an additional 20 g of D(+) glucose per liter when used to grow typical macroplasmodial networks. On the glucose-deficient agar, the microplasmodia form aggregates and fuse with each other. After about three hours, the first migrating units leave the initial patch and move radially outwards.

5.3.3 Transmission electron microscopy (TEM)

Macro- and mesoplasmodia growing on an agar surface were submerged with a fixative (80 mM KCl, 50 mM sodium cacodylate, pH 7.2, 20 mM NaCl, 2.5% glutaraldehyde). The fixation was carried out for at least 30 minutes on ice. Plasmodia were fixed together with the agar they were growing on, which was then cut into blocks the size of a few square millimetres with a scalpel. Post-fixation and contrast enhancement was carried out in 2 % OsO_4 on ice for 60 min. After post-fixation, the samples were washed thoroughly with double-distilled water. Samples were then left to contrast for 12 hours at 4 °C in the dark in 0.5 % uranyl acetate. Uranyl acetate helps to increase the contrast as well as the stability of the fine structures of the cell. After fixing and contrasting, the samples were dehydrated by passing them through a series of increasing ethanol concentrations. First they were treated with 30 % ethanol for 30 min, whereby

the ethanol was exchanged after 15 minutes. This procedure was repeated for 50 %, 70 % , 90 % and 100 % ethanol. An extra step was performed with 100 % ethanol, dehydrated with a molecular sieve (15 min).

Next, the specimens were embedded in resin. Embedding was performed with glycid ether 100 [Luft, 1961]. The ethanol was replaced in a descending alcohol series with the glycid ether 100. The glycid ether solutions A and B were mixed at a ratio 3:7 (A:B). A descending alcohol series was prepared as follows at room temperature: First the samples were infiltrated for 15 min with a mixture of 100 % ethanol and glycid ether A+B at a ration of 3:1, then at a 1:1 ratio for 15 min and finally at a 1:3 ratio for 15 min. The ethanol-resin mixture was carefully removed and the last step was infiltration of the tissue with a pure glycid ether (A+B) mixture for a total of 45 min, whereby the glycid ether was replaced twice after 15 min each. After the glycid ether was removed for the last time, the accelerator DMP-30 was added to the mixture. The samples were then left to polymerize in a vacuum oven at 60 °C for 2 to 3 days. Ultra-thin cutting (40 - 60 nm) was performed with a Reichert-Jung Ultracut E microtome. TEM was carried out on a Zeiss EM 900, equipped with a water-cooled frame-transfer-CCD-camera (TRS). Images were acquired using a PC with the software 'ImageSP' (TRS).

5.3.4 Stereological measurements

Stereology is defined as a set of mathematical methods which relate parameters defining three-dimensional structures to measurements obtained from two-dimensional sections. In other words, one can estimate higher-dimensional information from lower-dimensional samples. The advantage of evaluating thin sections with stereology is that it yields quantitative morphological data. Geometric properties of structures (e.g. mitochondria) embedded in a referent space (e.g. cytoplasm) can be estimated by studying the intersection of these structures with a probe. Probes are points, lines or grids which are being superimposed onto the section (image). A prerequisite for stereology is that samples must be uniform, isotropic, and random (UIR); this means that the orientation of the cut surface and the position of the embedded specimen must be random, as well as the positioning of probes. We use the following stereological relationships:

5.3.4.1 Volume density V_V

Volume density (V_V) or volume fraction is the ratio between the volume of the structure and the volume of the referent space (equation 5.1). The probes used are points. A point grid is superimposed onto the TEM image and mitochondria are counted which coincide with the probes (see figure 5.2 a). By doing a point count on an image (i), we obtain the number of points which fall onto mitochondria (P_i) and the number of points in the referent space (i.e. cytoplasm, Q_i).

$$V_V = \frac{\sum P_i}{\sum Q_i} \tag{5.1}$$

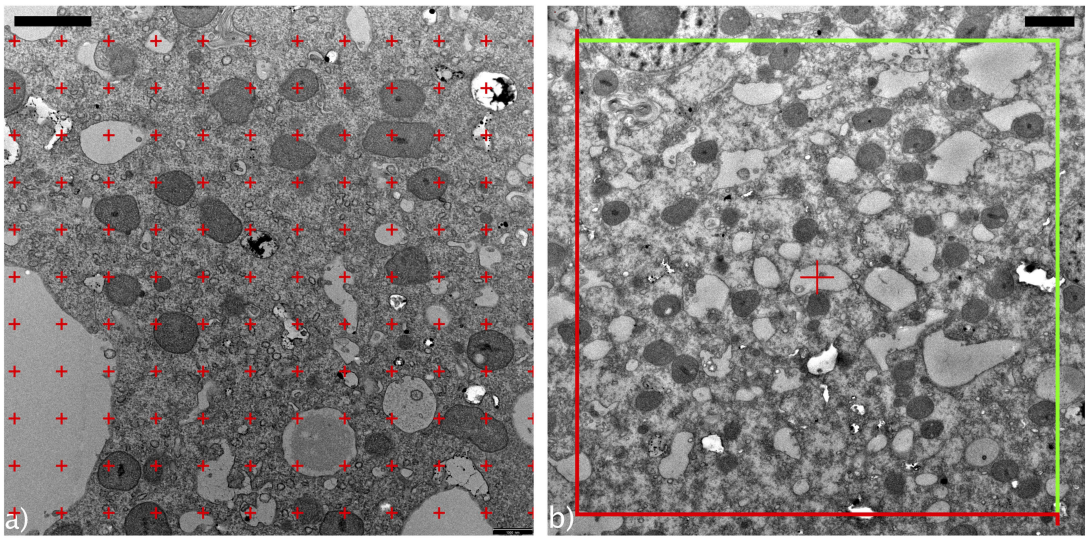

Figure 5.2: a) Random offset grid. The number of points (red crosses) which fall on mitochondria are counted (P_i), as well as the number of points which fall onto the referent volume (cytoplasm, Q_i). This takes into account the relatively high porosity of the slime mold's cytoplasm. Scale bar = 2 µm. b) Counting frame. Green line = inclusion line, red line = exclusion line. Scale bar = 2 µm.

The volume density states which percentage of the cytoplasm is occupied by mitochondria. FIJI provides grids with random offset. Depending on magnification, the area per point was chosen to lie between 1 and 5 μm^2 (110 - 361 points per image).

5.3.4.2 Numerical density N_V

Numerical density (N_V) is the number of structures per volume of the referent space (i.e., number of mitochondria per unit volume of cytoplasm). In this case, the probes are volumes. Since the mitochondria of *P. polycephalum* are ellipsoid in shape and of similar sizes, we can use the method proposed by Weibel and Gomez [1962]. First, using a counting frame (a macro [Mironov, 2014] implemented in FIJI), the number of structures per unit area (N_A) is computed (see figure 5.2 b). Following stereological rules, a mitochondrion is only counted if it lies entirely within the counting frame or if it touches a green inclusion line. It is not counted if it intersects a red exclusion line. Second, we need to calculate ϵ, i.e. the ratio of short (a) to long semi-axis (b) (equation 5.2):

$$\epsilon = \frac{a}{b} \tag{5.2}$$

Here, ϵ is approximately 0.86, indicating a slightly prolate ellipsoid ($\epsilon < 1$). For each ϵ, the corresponding shape factor β has to be obtained from literature [Weibel and Gomez, 1962]. In our case, β is 1.4. For a perfect sphere, $\epsilon = 1$ and $\beta = 1.38$. The numerical

density (N_V) can now be calculated using equation 5.3.

$$N_V = \left(\frac{1}{\beta}\right) \frac{{N_A}^{\frac{3}{4}}}{{V_V}^{\frac{1}{2}}} \tag{5.3}$$

5.3.4.3 Mean mitochondrial volume $\bar{V}$

The mean volume of mitochondria can be calculated from V_V and N_V using equation 5.4 [Cruz-Orive and Weibel, 1990]:

$$\bar{V} = \frac{V_V}{N_V} \tag{5.4}$$

5.3.5 Autofluorescence

Autofluorescence imaging of microplasmodia was performed using a Zeiss Axio Oberver.Z1 equipped with a Zeiss incubation system consisting of Heating Unit XL S and Temp Module S. Imaging was carried out at 24 °C. A Zeiss Plan Apochromat 40x with a numerical aperture of 0.95 was used, and images were taken by a Zeiss Axio-Cam MRm. Microplasmodia were plated onto Petri dishes with thin glass bottoms. They were illuminated at a wavelength of 380 nm with a Zeiss HXP 120 mercury lamp, of which the UV filter was removed. We used a 79000 ET FURA 2 Hybrid filter set (Chroma) and a Zeiss 76 HE reflector filter set.

5.4 Results

5.4.1 Volume fraction, number density and mean volume

We compared TEM images of three specimens each of glucose-deprived mesoplasmodia and non-starved plasmodia. On average, mitochondria in unstarved plasmodia occupy ~ 4 % of the cytoplasm volume, but ~ 9 % in starved mesoplasmodia (figure 5.3). The results for the numerical density V_V are similar: Unstarved plasmodia contain ~ 0.035 mitochondria per µm^3, whereas starved mesoplasmodia contain ~ 0.08 mitochondria per µm^3. There are approximately twice as many mitochondria per unit volume of cytoplasm in mesoplasmodia than in unstarved plasmodia. Both the results for V_V and N_V show statistically highly significant differences as confirmed by two-sample T-tests (both $p < 0.001$). The mean mitochondrial volume, however, does not vary between starved and unstarved plasmodia (see figure 5.4).

5.4.2 Autofluorescence

When living plasmodia are illuminated with wavelengths in the range of 340 to 380 nm, they show pronounced autofluorescence with an emission wavelength of around 460 nm. A base autofluorescence is detectable in the cytoplasm, as well as brightly fluorescing

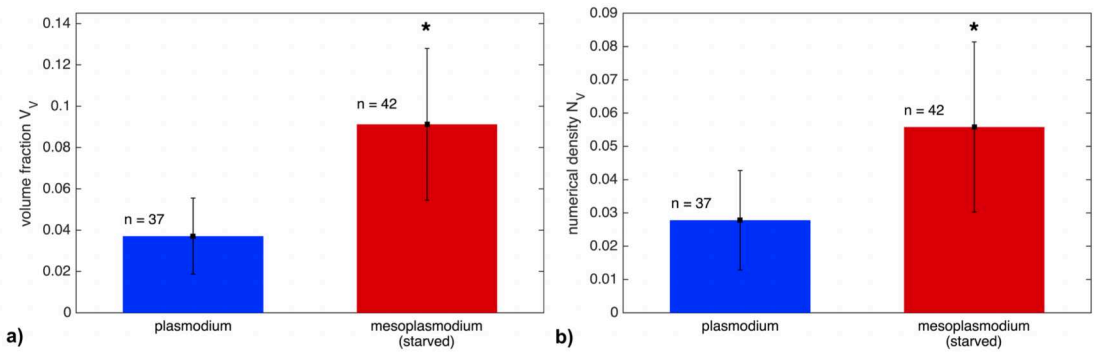

Figure 5.3: a) Volume fraction V_V of mitochondria in unstarved (blue) and starved (red) slime mold. Starved mesoplasmodia contain a significantly higher volume fraction of mitochondria ($p < 0.001$) than unstarved specimens. b) Numerical density N_V [μm^{-3}] of mitochondria in unstarved and starved slime mold. Again, the difference is statistically significant ($p < 0.001$). Error bars = standard deviation σ.

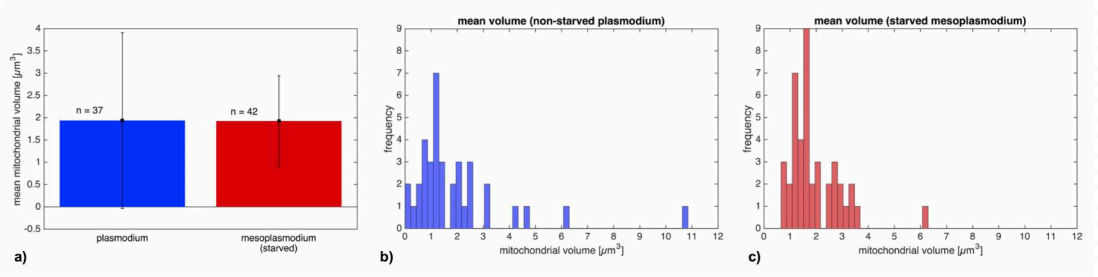

Figure 5.4: a) Mean mitochondrial volume of unstarved (blue) and starved (red) slime mold. Error bars = standard deviation σ. b) Histogram of mitochondrial volume (unstarved plasmodium) c) Histogram of mitochondrial volume (starved mesoplasmodium).

spots (see figure 5.5 b). We deduce that these spots are mitochondria. This conclusion is based on the presence of NAD and its reduced form, NADH, in both mitochondria and cytoplasm. NADH strongly absorbs ultraviolet light, with an emission peak at 460 nm. In small amounts, NADH is produced during glycolysis, which explains the low fluorescence of the cytoplasm. However, the largest share of the cell's NADH is found inside the mitochondria [Ince et al., 1992], accounting for the strong autofluorescence. The autofluorescence data also confirms our stereological finding that mitochondria do not form networks, but are rather isolated organelles (see supplementary video S1 b). NADH autofluorescence can be used to assess intracellular pH [Ogikubo et al., 2011], monitor mitochondrial toxicity [Rodrigues et al., 2011], and can generally give insight into the energy metabolism [Bartolomé and Abramov, 2015; Evans et al., 2005; Mayevsky and Rogatsky, 2007]. However, in *P. polycephalum*, this autofluorescence can cause problems when short-wavelength calcium-staining dyes, such as Fura 2, are used. A video of a living microplasmodium exhibiting autofluorescence (Video S1 b) and the

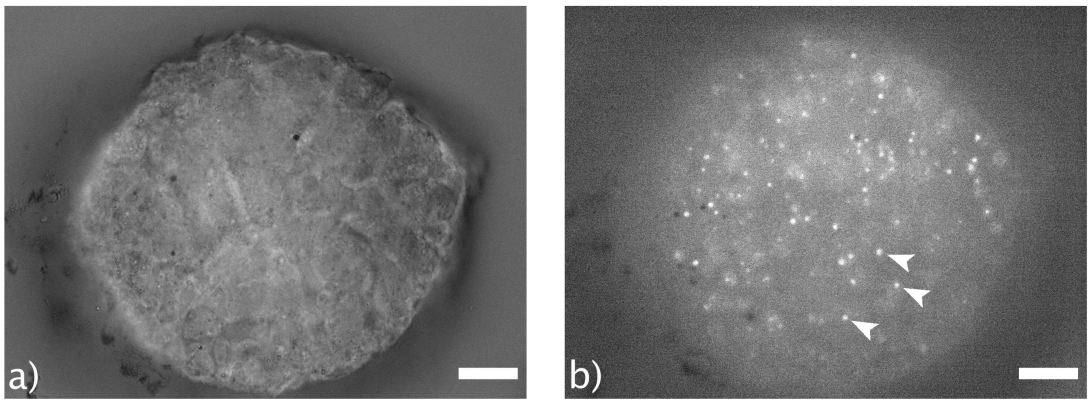

Figure 5.5: a) Bright field image of a microplasmodium from a shaking culture. b) Fluorescence image. The same microplasmodium was illuminated with 380 nm wavelength light. Arrow heads point to mitochondria. Scale bars = 25 µm.

same microplasmodium at bright field illumination (Video S1 a) can be found in the supplementary material.

5.5 Discussion

Our results show that under glucose-deprived conditions, the number of mitochondria is significantly increased. Their volume does not differ between glucose-deprived and unstarved plasmodia, indicating that this is not an instance of fragmentation. In contrast, in mouse embryonic fibroblasts, glucose depletion leads to increased mitochondrial fragmentation [Rambold et al., 2011]. Likewise, in yeast, glucose deprivation under aerobic conditions leads to a fragmentation of mitochondria into many small units [Visser et al., 1995]. However, how cells respond in detail to glucose withdrawal is not well studied, and results are controversial [Song and Hwang, 2019; Wappler et al., 2013]. In cancer cells, for example, glucose deprivation causes cell death [Iurlaro et al., 2017]. However, the ability to reprogram the energy metabolism is a hallmark of cancer [Hanahan and Weinberg, 2011]. In other cell types, viability is not significantly affected [Jelluma et al., 2006]. It seems that there is a great variability in the response to glucose depletion, depending also on cofactors like a simultaneous lack of oxygen. For example, after a non-lethal phase of both oxygen and glucose depletion, an increase in mitochondrial biogenesis in neurons was observed [Wappler et al., 2013].

Apart from fragmentation, mitochondrial morphology can be affected by the metabolic state of the cell. Starved amoeba of the species *Chaos carolinense* exhibited highly organized special membrane structures within their mitochondria [Chong et al., 2018]. During starvation-induced autophagy, mitochondria can increase in size and become elongated in shape, which optimizes ATP production and spares them from being

digested [Blackstone and Chang, 2011]. In other words, stress can affect mitochondrial morphology. Our results show no difference in morphology between glucose-deprived and non-starved plasmodia. A difference to the studies cited above, however, is that apart from a lack of glucose, the medium contained a source of protein (see table 5.3). Soytone is an enzymatic digest of soybean meal, it contains peptides, amino acids, vitamins and complex carbohydrates. Those are alternative energy sources that the slime mold can metabolize, and therefore, neither the increase in number nor the morphology are related to stress.

Our results show that mitochondrial biogenesis is stimulated in *P. polycephalum* grown in the absence of glucose, probably in order to compensate for the diminished supply of glycolytic ATP and pyruvate. We speculate that the number of mitochondria correlates to the metabolic state of the cell (see figure 5.6). The increase in mitochondrial numbers

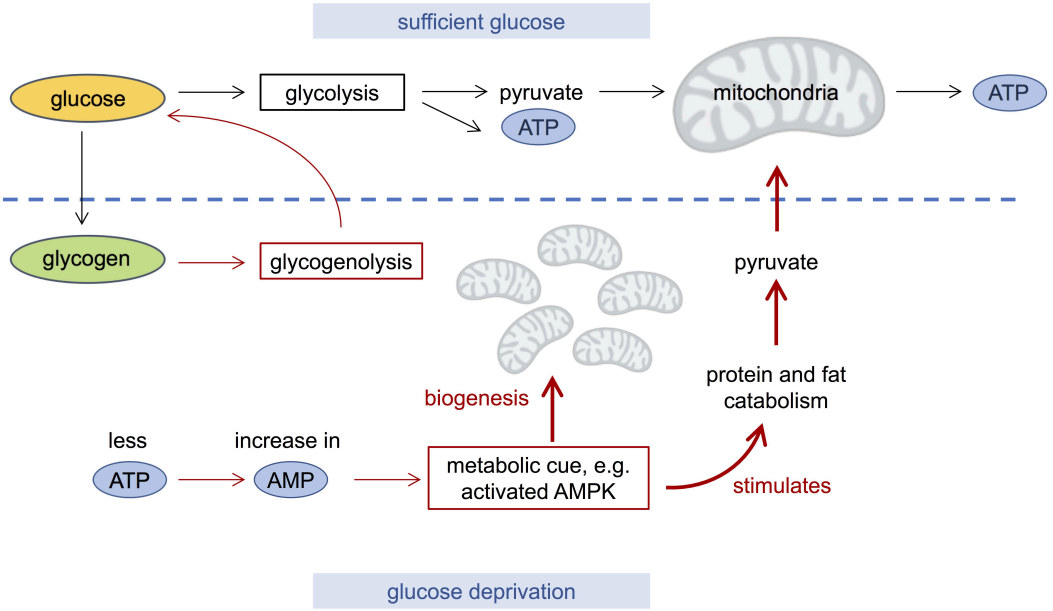

Figure 5.6: Proposed metabolic control of mitochondrial number. Explanation is given in the text.

leads to a higher ATP production. In conditions where glucose is abundant (upper panel in figure 5.6), glucose is converted to ATP and pyruvate via glycolysis. At the same time, the slime mold stores surplus energy in the form of glycogen [Goodman and Rusch, 1969; Nader and Becker, 1983]. Pyruvate is then transported into the mitochondria, where it enters the citric acid cycle, and during oxidative phosphorylation, more ATP is produced. This seems to be the preferred metabolic pathway when sufficient glucose is present. However, when glucose is withdrawn (lower panel in figure 5.6), different

metabolic pathways are taken. First, *P. polycephalum* uses up its glycogen storages. Glycogenolysis releases glucose from glycogen, which then enters glycolysis. Nader and Becker [1983] have measured that after the glucose in the growth medium was depleted, glycogen stores within microplasmodia lasted for a period of $\sim$ 5.5 days until it ran out. As soon as exogenous glucose is consumed or removed, glycogen is degraded.

Another pathway during glucose depletion starts with lower levels of ATP in the cell, with a simultaneous increase in AMP. This is a metabolic cue, which leads to the activation of AMP-activated protein kinase (AMPK). This enzyme belongs to a highly conserved protein family with orthologs in yeast (*Saccharomyces cerevisiae* (SNF1)) [Hedbacker and Carlson, 2008], in other fungi, in plants (SnRK1) [Margalha et al., 2016], and in *Dictyostelium discoideum* [Bokko et al., 2007], a member of the amoebozoa group of organisms to which *Physarum* also belongs. Several AMPK orthologs are encoded in the *P. polycephalum* genome [Schaap et al., 2015] and are expressed in starving, sporulation-competent plasmodia [Glöckner and Marwan, 2017]. AMPK plays a role in cellular energy homeostasis. When ATP levels lower, AMPK activation stimulates, among other processes, fatty acid oxidation and mitochondrial biogenesis [Mihaylova and Shaw, 2011; Song and Hwang, 2019]. Furthermore, AMPK enhances protein catabolism [He et al., 2017]. AMPK is an intracellular energy status sensor and key regulator of mitochondrial biogenesis. When activated by low ATP levels, AMPK triggers a metabolic switch, decreasing the activity of anabolic pathways and enhancing catabolic processes to restore the energy balance.

In summary, we propose that an imbalance between energy requirement and energy supply (deprivation of glucose) regulates mitochondrial biogenesis. By withdrawing glucose from the culture medium, we forced the slime mold to be exclusively dependent on mitochondrial ATP production. As a result, mitochondrial biogenesis was increased and we found a very high number of mitochondria. Additionally, mesoplasmodia are migrating fast and far in search for food, and this locomotion is also very energy-consuming. To compensate for a lack of glycolytic ATP, mitochondrial numbers are increased. Our findings highlight the importance of the AMPK-like metabolic switch in *P. polycephalum*. This pathway has not yet been confirmed for glucose-deprived mesoplasmodia, but appears to be a very likely candidate to explain our observations. A closer investigation of this sophisticated system of energy metabolism adaptation is needed in order to get a more complete understanding of how *P. polycephalum* manages homeostasis in the face of nutritional challenges.

5.6 Acknowledgement

We would especially like to thank Prof. Dr. Wolfgang Marwan for kindly providing us with strains of *P. polycephalum*, and for comments regarding the AMPK pathway, which greatly improved the manuscript. We are grateful to Prof. Dr. Reimer Stick and

Ute Helmboldt-Caesar for providing expertise and access to the TEM. We thank Anja Bammann and John Lee for experimental assistance.

Chapter 6

Summary and Conclusion

6.1 Synopsis and outlook

In chapter 2, we sum up the current and past state of research on *P. polycephalum*, because much of it is highly interdisciplinary and therefore not easily accessible: Research on the slime mold covers network research, genetics, cell biology, fluidics, and even extends to artificial intelligence and robotics. Furthermore, we endeavor to further establish the slime mold as a model system. We gather the relevant information and sort it into a coherent view of the 'state of the art'. This helps to identify further research topics, but also gaps in our current knowledge of the system: It becomes clear, for example, that advancements in the field of genetics will shed light onto the complicated processes of cell cycle regulation, membrane-bound receptors, metabolism and signaling pathways. Other examples for such uncharted territory can be found in the assumptions made by several current models: The model of Alim et al. [2017] is based on a hypothetical signaling molecule advected by fluid flows and hypothetical receptors. The signaling molecule can be speculated to be calcium, but so far, there has been no success in measuring or quantifying this. Calcium has long been speculated to play a major role in the locomotion of *P. polycephalum*, but it is difficult to get exact measures of its dynamics. Teplov [2010] constructs a mathematical model of the longitudinal dynamics of a vein of *P. polycephalum*, and speculates on the existence of a stretch receptor. This is proposed to be triggered by an extension of the vein, causing in turn an influx of calcium which then controls the contraction of the strand. In all probability, these models are correct in their assumptions. They also coincide with experimental findings. However, the exact molecular mechanisms and receptors and pathways involved are completely unclear and unknown at this point.

The identification of such gaps in our knowledge is important and very helpful because it provides a framework for future research. The objective is threefold: Firstly, an improvement of existing techniques and protocols (for example calcium imaging) is needed. Secondly, the invention of new techniques (for example the use of methods on

the mesoscopic scale, such as hemodynamic models) is called for. Thirdly, the stage is set for the discovery of more new physical concepts and interactions. One common theme at the intersection of physics and biology is intercellular interaction and information transfer at the scale of molecules, cells, individual organisms and even groups of individuals. Specific interactions and information transfer are ubiquitous at all levels of biological organization. Physics can provide quantitative ideas and tools to further the understanding of living matter. There even is a "physics of information" [Bais and Farmer, 2008], which is the title of a chapter published in the book "Philosophy of Information" [Adriaans and van Benthem, 2008]. Another topic is the theory of dynamical systems, which is valuable for understanding the behavior of nonlinear systems, with living organisms being the epitome of nonlinear phenomena. Dynamics play a crucial role in living systems, especially rhythmic events like the cell cycle, locomotion and neural oscillations.

Research on the fundamental, underlying mechanisms that cause the complex behavior of *P. polycephalum* is crucial, so that we can forgo purely phenomenological, descriptive models. The remarkably rich phenomenology of the behavior of *P. polycephalum*, especially during foraging and food-based decision making, has been described [Latty and Beekman, 2009, 2010, 2011a; Beekman and Latty, 2015]. However, it is desirable to go beyond the observations and on to the underlying mechanisms. Transforming observational studies into models of dynamics and causal mechanisms poses new challenges and requires stronger integration of theoretical, computational and experimental frameworks. This thesis aims to integrate findings from cell biology to achieve an understanding of behavior.

In chapter 3 we have, for the first time, described in detail three morphotypes of *P. polycephalum* (micro-, macro- and mesoplasmodium). Further, we have identified and quantified pores in the outward plasma membrane which correspond to internal channel systems. This was done for all three morphotypes of *P. polycephalum*. The corresponding internal channel system was imaged by TEM. Our findings have subsequently proven to be useful for the construction of poroelastic models ([Kulawiak et al., 2018; Zhang et al., 2019; Westendorf et al., 2018; Kulawiak et al., 2019]). Ultrastructural findings are very important for such models, since they provide a biological, quantifiable basis. When describing *P. polycephalum* as viscoelastic or poroelastic biological material, informations about the underlying structures are needed. Further, we have described different actin structures in mesoplasmodia, which can lead to an understanding of this locomotion type: We have visualized the cortical actin layer with its actin asters, which provides the basis for a high intercellular pressure and the creation of pressure gradients. The ultrastructural investigations also showed that the growth fronts of a network resemble mesoplasmodia. This probably is not surprising, since both mesoplasmodia and macroplasmodial growth fronts are structures dedicated to forward movement and expansion. However, it plays a role in how those structures are interpreted and modeled. The slime mold is a huge amoeboid cell with few permanent structures. It appears that some

complex behavior arises from simple hydrodynamic and biomechanical interactions, as the observed actin stars and asters, which are an example of cytoskeletal self-organization.

While investigating oscillation patterns (chapter 4), it became clear that the rhythmic cytoplasmic flows do not only serve to create an effective intracellular transport, but also play a role in cell migration. Furthermore, we found evidence of hydrodynamic information processing, i.e. the selection of frequencies. Cytoplasmic flow is a means for the slime mold to transmit information throughout its cell body. Our proposed lumped parameter model is the first of its kind to address both locomotion and information processing, presenting an efficient and fast way in which signals can be processed without the necessity of complicated biochemical signal transduction pathways. The model explains how intracellular cytoplasm flow underlies *P. polycephalum*'s complex behavior. Furthermore, it describes how asymmetry can be introduced to a previously unpolarized, stationary plasmodium through local softening of the actin cortex. The increased flow towards that area and a subsequent cell polarization initiates locomotion.

6.2 Network of networks

The introduction (chapter 1) poses several questions, which reflect current research topics. The answers include the dynamics of intracellular fluid flow, metabolism, organelles such as mitochondria, genetics and the actin cytoskeleton, which each account for complex and emergent output (behavior). Each of those are components of networks, as illustrated in figure 1.2. One network includes signaling molecules and cytoskeletal proteins, another is the metabolic network and yet another the genetic and epigenetic regulatory network. The slime mold is an integrated network of interconnected and interacting systems, each representing a separate network of its own. The behavior and processes within one physiological system, or network, can affect the dynamics of all other systems in this network of networks which is *P. polycephalum*. The term "network of networks" [Kenett et al., 2015b] illustrates that processes taking place in one network might significantly affect what is happening in many other networks. A special issue on networks of networks has been published [Kenett et al., 2015a] and contains a wealth of papers, ranging from brain science to game theory to epidemic dynamics. The authors of the introductory article [Kenett et al., 2015b] compare the introduction of coupling into networks with the introduction of particle interactions in statistical physics: The study of individual particles leads to the understanding of the properties of a gas, but to understand a liquid or a solid, the interactions between particles need to be known as well. In the same way that particle interactions helped to understand such sumptuous phenomena as phase transitions, it can be expected that an analysis of the interconnected networks of *P. polycephalum* will yield insight into its dynamics, behavior and emergent properties. Results from network biology indicate that cellular networks are governed by universal laws, meaning that some features of molecular interaction networks can also be found in other complex systems, such as

human society or the internet [Barabási and Oltvai, 2004].

6.2.1 The example of mitochondria

Mitochondria are an example for the above-mentioned 'network of networks' in *P. polycephalum*. The most prominent function of mitochondria is to provide energy in the form of ATP through respiration. Furthermore, they are major Ca^{2+} stores [Nations et al., 1989; Achenbach et al., 1984] and participate in the synthesis of several cellular components such as phospholipids (in conjunction with the endoplasmatic reticulum (ER)) [Mejia and Hatch, 2016]. In addition to the ER, there is cross-talk between mitochondria and other organelles as well, particularly lysosomes and peroxisomes [Diogo et al., 2018]. Mitochondria are also involved in many other processes central to cellular function, including cell growth and differentiation, cell cycle control and even plasmodial longevity [Nakagawa et al., 1998].

Interestingly, there is also a strong connection between mitochondria and the cytoskeleton. In many cells, mitochondria move along microtubules (in mammalian cells) or actin fibres (in plants and fungi) [Anesti and Scorrano, 2006]. However, mitochondria themselves can also influence actin-related cell functions. Since mitochondria produce ATP, cell stiffness and contraction also depend on their ATP production [Bartolák-Suki et al., 2017]. Overall cell mechanical functions such as stiffness and contractility are thus influenced at least in part by the relationship between cortical actin and mitochondrial structure. Furthermore, mitochondria are also involved in the primary oscillator of *P. polycephalum*: Time-keeping of the contractional rhythm is related primarily to oscillations of mitochondrial activity and resulting oscillating cytosolic calcium concentrations [Satoh et al., 1982, 1984].

The role of mitochondria as regulators of signal transduction becomes more and more apparent: They can communicate their biosynthetic and bioenergetics fitness to the rest of the cell and thus have signaling functions which go beyond the purely metabolic ones [Chandel, 2014]. This seems smart, because it prevents cells from becoming committed to a biological process (i.e., growth, differentiation) without the ability of the mitochondria to meet the metabolic needs in terms of energy provision. Additionally, as is discussed in chapter 5, we propose that low levels of ATP in the cell are a metabolic cue for the activation of the AMPK pathway: among other processes, fatty acid oxidation and mitochondrial biogenesis are triggered. When the slime mold is deprived of glucose, it is thus forced to depend on mitochondrial ATP production, and forgo glycolysis (after the glycogen stores are used up). Another aspect is mitochondrial reactive oxygen species (ROS) signaling. During oxidative phosphorylation, mitochondria utilize oxygen to generate ATP, but in the process, also produce ROS. ROS are products of oxidative metabolism, created by one-electron transfers from a redox donor to molecular oxygen (O_2). This generates superoxide radical anions (O_2^-), which can be transformed into, for example, hydrogen peroxide (H_2O_2) or hydroxyl radicals ($OH^\cdot$). While they can

have detrimental effects, and have initially been regarded as toxic byproducts of aerobic metabolism, ROS are now also recognized as important signaling molecules [Shadel and Horvath, 2015]. ROS signaling is rapid and specific; involving and integrating homeostasis, metabolism, protein kinase networks and many other different signaling pathways [Mittler et al., 2011]. Most importantly, ROS affect the actin cytoskeleton. Actin and other cytoskeletal proteins are sensitive to ROS, and therefore, redox regulation is an important modulator of the actin cytoskeleton with multiple different effects on cellular form and function [Wilson et al., 2016]. ROS can (reversibly and irreversibly) oxidate proteins. S-nitrosylation is such a reversible oxidative modification of cysteine, and plays an important role in cell migration and cytoskeleton remodeling. Furthermore, many signaling molecules (including receptor tyrosine kinases (RTKs), which are very abundant in *P. polycephalum*) possess redox-sensitive cysteine residues. Lastly, actin itself is susceptible to ROS, as well as actin-binding proteins [Xu et al., 2017]. Thus, mitochondria are at the crossroads of energy metabolism, cytoskeletal dynamics and information processing, and can have a direct impact on the actin cytoskeleton.

A very interesting approach to an information processing mechanism is proposed by Hickey and Noriega [2008]. They formulate an information processing model based on cell structure and mitochondrial redox signaling. In regard to *P. polycephalum*'s maze-solving ability, they postulate that the macroplasmodium locally senses a food source, which is then taken up. As the slime mold digests the nutrients, local mitochondria are stimulated and release ROS. ROS, in turn, is a signal which can dilate the local veins, due to actin filament reorganization and other processes as described above. The vein dilatation leads to an increased cytoplasmic flow, causing an increased transport of food and ROS into the neighboring areas, and generally increasing endoplasm flow towards the locally stimulated area. This represents a computation goal based on positive feedback. Interestingly, a similar mechanism has been identified in the colonial hydroids *Podocoryna carnea* and *Eirene viridula* [Blackstone et al., 2005]: moderate levels of ROS in stolon tips of the colony trigger outward growth and inhibit branching, acting as a kind of growth factor. However, a certain variability of phenotypes was found, and speculated to depend on the particular spatial and temporal patterns of ROS formation within the colony. Thus, ROS signaling and mitochondrial redox regulation may play a role in both uni- and multicellular organisms.

The model of Hickey and Noriega [2008] corresponds very well to our own findings (see chapter 4): In our lumped parameter model, we conjecture that biochemical cues lead to a local softening of the actin cortex, which in turn causes an increased flow of cytoplasm and, thus, a net forward movement. Mitochondria and the cytoskeleton, two different levels of the 'network of networks', interact to achieve a complex behavioral process: the evaluation of the slime mold's internal nutritional status, assessment of external food availability, and the subsequent decision to migrate; either chemotactically towards a known food source or as a foraging pattern away from an already depleted area.

6.3 Convergent evolution of cognition

P. polycephalum is capable of distinguishing between 'self' and 'non-self' [Masui et al., 2018]. This process is termed allorecognition and was introduced in section 1.8.1. It is likely that allorecognition evolved independently multiple times during the history of life [Grosberg and Plachetzki, 2010]. Thus, it represents a fundamental example of convergent evolution of a behavioral phenotype. The idea that complex behaviors are also subject to recurrent evolution, both within closely related and across distant taxa, is relatively new [York and Fernald, 2017]. It is very probable that natural selection acts on several biological pathways which are unique to behavioral traits, for example the form and function of nervous systems, but also sensory-motor coupling.

Phagocytosis, the incorporation of foreign material into the cell, is another universal mechanism which is used by many primordial life forms such as protozoans to ingest food. Phagocytosis is also involved in the immune response of higher organisms. However, there are great differences between the sophisticated components of the human immune system (e.g. the presence of lymphocytes and immunoglobulin) and that of lower invertebrates [Bayne, 1990], where such specialized cells and structures are often absent. Instead, there is such a diversity of different phagocytotic mechanisms, which are often unique to a particular taxon, that convergent evolution seems plausible [Stuart and Ezekowitz, 2008]. This observation is not limited to phagocytosis and allorecognition, but extends to other areas of physiology as well.

Therefore, it is conceivable that cognition has evolved in the same way. Convergent evolution implies that the same end result – cognition – occurred independently several times throughout the history of life. Different mechanisms are employed by neural and non-neural organisms to achieve the same goal. van Duijn et al. [2006] propose that minimal cognition is immanent in sensorimotor systems, i.e. the integration of the sensory system and the motile machinery. This function is quintessentially realized in nervous systems, but analogous mechanisms exist in unicellular eukaryotes and even in bacteria. Thus, cognition is not restricted to nervous systems, but may be a universal feature of life [Keijzer, 2017]. Even the evolution of complex brains is considered convergent: The brains of highly intelligent octopi and primates have evolved independently, although from a common ancestor [Hirth and Reichert, 2007; Roth, 2015]. Regarding habituation, a very ancient form of learning, available molecular evidence suggests that it evolved independently in very different species, such as protists, plants and neural organisms [van Duijn, 2017]. *P. polycephalum* is also capable of habituation [Boisseau et al., 2016; Vogel et al., 2016]. Different life forms seem to have arrived at the same adaptive solution, because of the benefits of possessing such a mechanism.

However, certain parallels and similarities can be detected between the cognition in neural and non-neural organisms. Sufficiently complex information-processing struc-

tures need to be present. In the brain, anatomical and functional connectivity plays a big role. In the slime mold, interacting networks of cellular signaling and the motile machinery fulfill a roughly analogue function. However, the overall cognitive complexity of *P. polycephalum* is by no means equivalent to that of a brain. On the spectrum of minimal cognition, the slime mold and other protozoa are probably at its low end. Still, there are some similarities between slime molds and synaptic connections in the brain. The interconnected macroplasmodial transport network, for example, exhibits distinct oscillation patterns which are intimately linked to behavior. The oscillation patterns show great variability in frequency, amplitude and response to stimuli, and could be involved in memory and minimal cognition. It needs to be investigated whether they are truly analogous to information processing mechanisms or just the reaction of coupled oscillators to a periodic external signal.

The concept of convergent evolution puts cognition into perspective: The fact that similar features evolved independently shows that the evolution of mind was probably not a historical accident, but that, instead, cognitive traits are a replicable feature within the evolutionary process [Powell et al., 2017].

6.4 From cell biology to complex behavior

The connections between the different chapters of this thesis become obvious now. In the lumped parameter model (chapter 4), we have proposed a mechanism for locomotion which, induced by a chemotactic signal transduction (or internal cues), leads to a local softening of the actin cortex at the site of the chemoattractant stimulus. As described above, the softening of the actin cortex can also be achieved by mitochondria-mediated ROS signaling as response to a particular nutrient situation, for example the deprivation of glucose, which is in turn responsible for the amazing migration of mesoplasmodia. The role of mitochondria in information processing becomes clear, as well as the role of fluid dynamic-based information processing. The actin cytoskeleton shows a great variability between the different morphotypes of *P. polycephalum*, as can be gleaned from chapter 3, and shows a rich spectrum of oscillation patterns. Investigating how the resulting fluid flows shape organisms across a wide range of length scales will shed light on intracellular transport phenomena, but also locomotion and self-organization. Furthermore, it leads to the hypothesis that fluid flow can be used by *P. polycephalum* to process and distribute information, making the cytoplasm and the cell body in itself the substrate for information processing. This in turn provides an alternative model to neuron-based information processing which is completely decentralized and self-organized. As a further research topic, the complex behavior of *P. polycephalum* is currently in focus. By studying how a non-neural unicellular organism navigates its environment and makes optimal decisions securing its survival, the broader question of an underlying universal mechanism of decision-making arises.

6.5 Consciousness revisited

As mentioned in section 1.8.2, consciousness is often thought of as a 'yes or no' trait [Godfrey-Smith, 2016]. It is believed that the communication of neurons with each other in the brain leads to consciousness, the exact mechanism, however, remains unclear. General anesthesia causes loss of consciousness, probably involving a phase transition in the brain [Zhou et al., 2015]. The authors modeled how a small reduction in information transfer between neurons can cause a sudden loss of consciousness. This implies, on the other hand, that a sudden increase in connectivity, complexity and information transfer can give rise to consciousness in a percolation transition. This is an example for a strongly mechanistic view of consciousness, as held, for example, by Craver [2007] and Badcock et al. [2019]. Craver [2007] describes how mechanisms are organized to produce phenomena of interest, and emphasizes the importance of mechanisms for the understanding of consciousness.

Viewing the slime mold as a highly complex and interconnected network of networks brings us closer in understanding consciousness. According to the Integrated Information Theory (IIT) of consciousness, developed by Tononi and coworkers [Tononi et al., 2016], consciousness arises within any sufficiently complex, information-processing system. This implies that all animals, from amoeba to earthworms up to humans, are conscious. Very briefly, IIT assigns to any complex system, for example a brain, a number (Φ) which denotes how integrated a system is. Φ is considered a measure of consciousness, i.e. the higher the number, the higher the amount of consciousness. The degree and extent of the causal interactions and connections within the system give rise to behavior and other emergent phenomena. The theory aligns with the discussion of cognition, which was addressed in the introduction (chapter 1), in that consciousness, like cognition, is a spectrum. At the lower end are simple, sparsely connected systems. The higher the complexities, connections and interactions, the more conscious the system. At first glance, the consciousness spectrum proposed by IIT seems to contradict the phase transition view of consciousness as described above. However, a compromise may be that the probability of a phase transition to consciousness increases with increasing Φ: The higher the complexities, connections and interactions, the more probable it is for a system to become conscious.

P. polycephalum is an amazingly complex system, with rich signaling pathways and the ability to perceive and react to its environment. In the absence of neurons, the substrate for the integration and computation of information is the whole of its cell body. Slime molds are probably not conscious in a way that humans are, but they definitely have a Φ that differs significantly from zero.

Chapter 7

Appendix

7.1 Supplementary material for chapter 3

The supplementary data for chapter 3 consists of five video files. They can be accessed at the website of the journal (Journal of Physics D: Applied Physics) `https://iopscience.iop.org/article/10.1088/1361-6463/aab147/data`. Furthermore, the video files are archived by the University of Bremen (FB 1) together with this thesis.

7.2 Supplementary material for chapter 4

7.2.1 Optical flow analysis

The calculation of the optical flow, the apparent movement of particles in image sequences, is used to analyze where and when endoplasm is flowing in order to gain a better understanding of the internal veins and their role in the locomotion of *P. polycephalum* mesoplasmodia. We utilized particles which are naturally flowing within the internal veins of the slime mold to calculate flow speed. The advantage of this method is that no foreign particles have to be inserted. Prior to the optical flow analysis, image sequences were smoothed by a Gaussian filter in order to remove noise. Optical flow is based on calculating the motion of particles between two frames.The result is a vector field. A brightness constraint is implied, assuming that a particle at position (x, y, t) with an intensity of $I(x, y, t)$ moves by Δx and Δy in sequential images (Δt), but that the overall brightness remains constant (equation 7.1)

$$I(x, y, t) = I(x + \Delta x, y + \Delta y, t + \Delta t) \tag{7.1}$$

which is the same as

$$I_x \cdot u + I_y \cdot v + I_t = 0 \tag{7.2}$$

Using partial derivatives and assuming small particle movements from one frame to the next, equation (7.1) can be developed to (equation 7.3)

$$\frac{\partial I}{\partial x}V_x + \frac{\partial I}{\partial y}V_y + \frac{\partial I}{\partial t} = 0 \tag{7.3}$$

This, however, is not enough to calculate the velocity components u and v since they are both unknowns, making it an ill-posed problem. Additional constraints are necessary. We used the method first described by Horn and Schunck [Horn and Schunck, 1981], whereby a smoothness constraint is introduced to obtain the optical flow components. It is assumed that the change in the vector field is supposed to be minimal and that the objects move coherently through the frames. Taking into account both equation (7.1) and the smoothness constraint (second term in equation 7.4), an energy functional (equation 7.4) can be proposed which then has to be minimized.

$$E(u,v) = \iint [(I_x u + I_y v + I_t)^2 + \alpha(|\nabla u|^2 + |\nabla v|^2)]dxdy \tag{7.4}$$

α, a global regularization constant, has to be chosen according to the data quality, i.e. image intensities, type of motion and the amount of noise affecting the image sequence [Ng and Solo, 1997]. For our experiments, a value of $\alpha = 1$ was chosen. Equation 7.4 is now solved for the vectors u and v using the Jacobi method [Bronštejn and Semendyayev, 2013], and the vectors are scaled in space and time accordingly. The analysis of the optical flow was performed using the software MATLAB2015b (The Mathworks) with the Image Processing Toolbox. Obtaining a vector field with scaled flow velocities v_{flow} was done using equation 7.5.

$$v_{flow} = \sqrt{u^2 + v^2} \cdot sgn(u) \tag{7.5}$$

This is permissible because forward moving mesoplasmodia do not deviate from a straight path, and major veins run mostly parallel to the direction of movement. The cytoplasm flow responsible for locomotion is back and forth, i.e. parallel to the axis of motion. Therefore, flow in the direction perpendicular to the direction of movement can be neglected.

The resulting vector field was stored as an image, with every pixel containing v_{flow} at that pixel's location. The standard deviation of all images in a stack was calculated (Z-projection) in FIJI. Each of the output image's pixels contains the standard deviation over all images in the stack at the particular pixel location. Areas with strongly fluctuating flow thus become visible (high standard deviation), whereas areas with little flow variation have a low standard deviation and appear dark. From a Z-projection, the location of a vein was obtained as a segmented line. Along this vein, a kymograph was performed. The kymograph contains the flow velocities along the vein.

7.2.2 Locomotion parameters for six mesoplasmodia

Mean locomotion speed as gathered from kymographs, uroid half angle, area covered by mesoplasmodium, circularity, period of area oscillations, and ratio of membrane extension to retraction time.

Table 7.1: Locomotion parameter of several satellites. $\bar{v}_{kymo}$ = Mean locomotion speed as gathered from kymographs. θ = uroid half angle. $area$ = area covered by satellite. f_{circ}= circularity. T_{area} = period of area oscillations. $\frac{t_{ext}}{t_{ret}}$ = ratio of membrane extension to retraction time.

$\bar{v}_{kymo}$ [µm min^{-1}]	θ [°]	$area$ [mm^2]	f_{circ}	T_{area} [min]	$\frac{t_{ext}}{t_{ret}}$
8.94 ± 0.22	26.07 ± 1.70	0.33 ± 0.02	0.84	1.20	1.4
9.14 ± 1.26	55.61 ± 5.18	1.92 ± 0.01	0.86	0.63	1.4
11.66 ± 0.66	20.99 ± 0.47	1.93 ± 0.03	0.63	1.35	2.3
16.72 ± 0.49	25.94 ± 2.48	1.53 ± 0.01	0.84	1.09	1.6
5.73 ± 0.19	63.75 ± 9.75	0.19 ± 0.00	0.92	1.34	1.7
5.96 ± 0.18	81.31 ± 5.08	2.79 ± 0.08	0.84	1.23	1.6

Trajectories of four mesoplasmodia

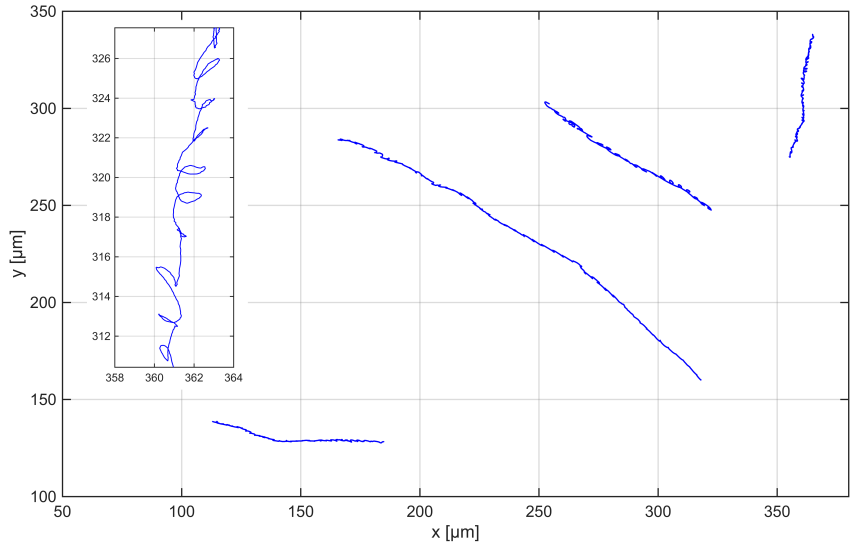

Figure 7.1: Trajectories of the center of mass of four migrating mesoplasmodia. A straight path is maintained for hours. Inset: Magnification of a detail of a trajectory. The centre of mass of a mesoplasmodium moves along a cycloid path.

Circularity over time

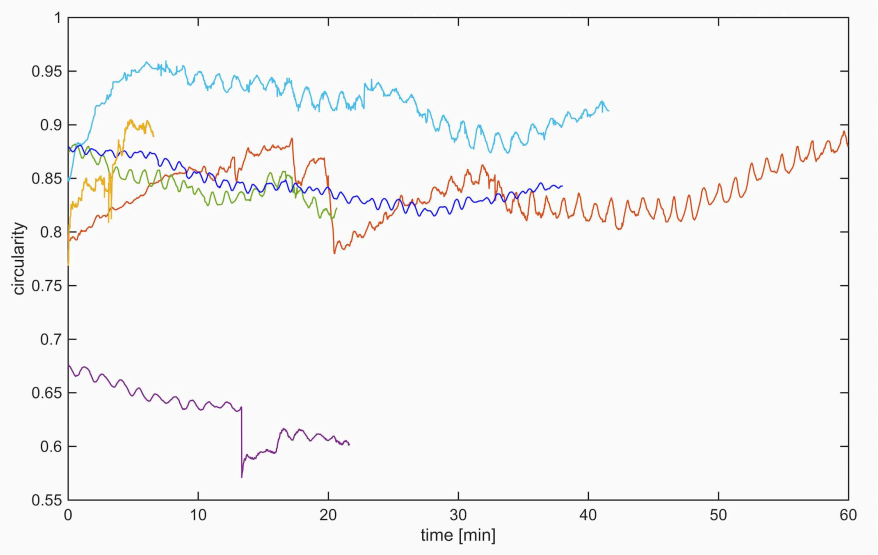

Figure 7.2: Circularity f_{circ} over time for six mesoplasmodia. Abrupt drops correspond to mesoplasmodia which developed holes, thus biasing the ratio of area over perimeter.

Circularity and frontal membrane velocity over time

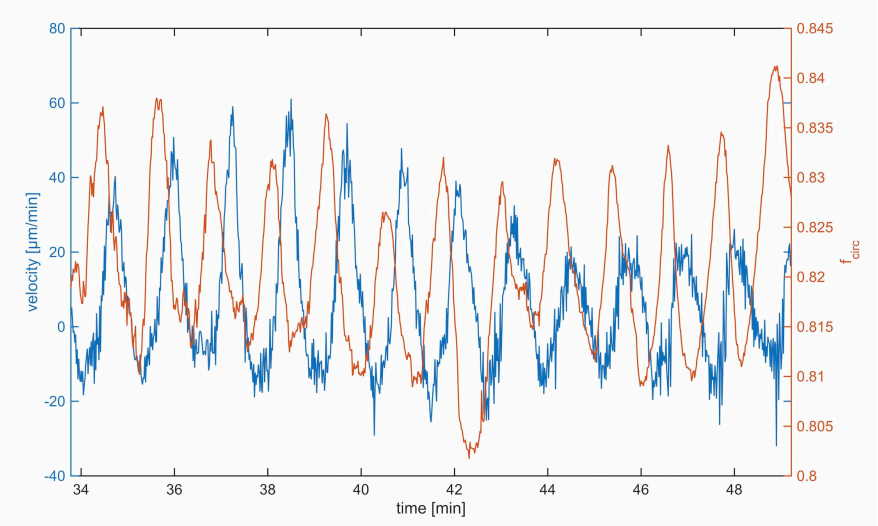

Figure 7.3: Phases of high circularity correspond to a slowing of locomotion.

7.2.3 Conversion of fluidic to electric units.

For use in a circuit simulation program like LTSpice, fluidic values have to be converted into ohm and farad, respectively. The conversion of fluidic units to electrical analogue units was done as follows: To obtain meaningful electronic capacitances and resistances (C_e and R_e, respectively), we introduce the following equations and definitions.

$$R_f = R_0 R_e \tag{7.6}$$
$$C_f = C_0 C_e \tag{7.7}$$
$$t_f = t_0 t_e \tag{7.8}$$
$$t_0 \stackrel{!}{=} 1 \tag{7.9}$$
$$R_{1e} \stackrel{!}{=} 10\ \Omega \tag{7.10}$$
$$R_{2e} \stackrel{!}{=} 800\ \Omega \tag{7.11}$$

We arbitrarily set the electric resistance R_{1e} to 10 Ω, and $R_{2e} = 800\ \Omega$ and keep the time scales identical. We now have to find the equivalent electric capacitance C_e. Both the fluidic and the electric system are equivalent and coupled via time ($t_e = t_f$), thus we can write

$$R_f C_f = R_e C_e \tag{7.12}$$
$$(R_0 R_e)(C_0 C_e) = R_e C_e \tag{7.13}$$
$$C_0 = \frac{R_e}{R_f} \tag{7.14}$$
$$R_f = R_{1f} + R_{2f} \tag{7.15}$$
$$R_e = R_{1e} + R_{2e} \tag{7.16}$$

C_0 can then be reintroduced into equation (7.7), and the equation can be solved for C_e:

$$C_e = \frac{C_f}{C_0} \tag{7.17}$$
$$= \frac{C_f(R_{1f} + R_{2f})}{(R_{1e} + R_{2e})} \tag{7.18}$$
$$= 0.053\ \text{F} \tag{7.19}$$

The capacitance thus becomes 0.053 F. These values were calculated for one single tube segment. As mentioned above, the time constant τ remains the same, in the electrical as well as in the fluidic system.

7.3 Supplementary material for chapter 5

The supplementary data for chapter 5 consists of two video files. They can be accessed at the website of the journal (Protoplasma) `https://link.springer.com/article/10.1007/s00709-019-01410-1#SupplementaryMaterial`. Furthermore, the video files are archived by the University of Bremen (FB 1) together with this thesis.

7.4 Authorship attribution statement

This cumulative thesis contains four papers published in the following peer-reviewed journals.

Chapter 2 is published as

> Oettmeier, C., Brix, K., & Döbereiner, H.-G. (2017).
> *Physarum polycephalum*—A new take on a classic model system.
> Journal of Physics D: Applied Physics, 50(41), 413001.
> DOI: `https://doi.org/10.1088/1361-6463/aa8699`

Contribution of doctoral candidate to publication Oettmeier et al. [2017]:

(i) Wrote the manuscript and led the successful publication process to *Journal of Physics D: Applied Physics*

(ii) Researched and compiled literature

Chapter 3 is published as

> Oettmeier, C., Lee, J., & Döbereiner, H.-G. (2018).
> Form follows function: ultrastructure of different morphotypes of *Physarum polycephalum*.
> Journal of Physics D: Applied Physics, 51(13), 134006.
> DOI: `https://doi.org/10.1088/1361-6463/aab147`

Contribution of doctoral candidate to publication Oettmeier et al. [2018]:

(i) Wrote the manuscript and led the successful publication process to *Journal of Physics D: Applied Physics*

(ii) Developed the research design

(iii) Performed the experiments (Fluorescence and brightfield imaging, microinjection, TEM, SEM)

(iv) Analyzed and interpreted the data

(v) Researched and compiled literature

Chapter 4 is published as

> Oettmeier, C. & Döbereiner, H.-G. (2019).
> A lumped parameter model of endoplasm flow in *Physarum polycephalum* explains migration and polarization-induced asymmetry during the onset of locomotion.
> PloS one, 14(4), e0215622.
> DOI: `https://doi.org/10.1371/journal.pone.0215622`

Contribution of doctoral candidate to publication Oettmeier and Döbereiner [2019a]:

(i) Wrote the manuscript and led the successful publication process to *PloS one*

(ii) Conceptualized and developed the research design

(iii) Performed the experiments (image acquisition)

(iv) Created and implemented the lumped parameter model

(v) Analyzed and interpreted the data

(vi) Researched and compiled literature

Chapter 5 is published as

> Oettmeier, C. & Döbereiner, H.-G. (2019).
> Mitochondrial numbers increase during glucose deprivation in the slime mold *Physarum polycephalum*.
> Protoplasma, 1-9.
> DOI: `https://doi.org/10.1007/s00709-019-01410-1`

Contribution of doctoral candidate to publication Oettmeier and Döbereiner [2019b]:

(i) Wrote the manuscript and led the successful publication process to *Protoplasma*

(ii) Developed the research design

(iii) Performed the experiments (TEM, autofluorescence microscopy)

(iv) Analyzed and interpreted the data

(v) Researched and compiled literature

Chapter 8

Bibliography

Achenbach, F., Achenbach, U., and Kessler, D. (1984). Calcium Binding Sites in Plasmodia of *Physarum polycephalum* as Revealed by the Pyroantimonate Technique. *J. Histochem. Cytochem.*, 32(11):1177–1184.

Achenbach, F., Achenbach, U., and Wohlfarth-Bottermann, K. E. (1979). Plasmalemma invaginations, contraction and locomotion in normal and caffeine-treated protoplasmic drops of *Physarum*. *Eur. J. Cell Biol.*, 20(1):12–23.

Adamatzky, A. (2012). Slime mold solves maze in one pass, assisted by gradient of chemo-attractants. *IEEE Trans. Nanobiosci.*, 11(2):131–134.

Adamatzky, A. (2015). Slime mould processors, logic gates and sensors. *Philos. Trans. A Math. Phys. Eng. Sci.*, 373(2046):20140216.

Adamatzky, A., editor (2016). *Advances in Physarum machines: Sensing and computing with slime mould*, volume 21. Springer International Publishing.

Adamatzky, A. (2019). A brief history of liquid computers. *Philos. Trans. R. Soc. Lond., B, Biol. Sci.*, 374(1774):20180372.

Adamatzky, A. and Jones, J. (2010). Road planning with slime mould: If *Physarum* built motorways it would route M6/M74 through Newcastle. *Int. J. Bifurcation Chaos*, 20(10):3065–3084.

Adriaans, P. and van Benthem, J., editors (2008). *Philosophy of Information*, volume 8 of *Handbook of the Philosophy of Science*. North-Holland, Amsterdam.

Aguilar, M., Fiore-Donno, A., Lado, C., and Cavalier-Smith, T. (2014). Using environmental niche models to test the 'everything is everywhere' hypothesis for *Badhamia*. *ISME Journal*, 8:737–745.

Akahane, T., Miyake, Y., and Yamaguchi, Y. (1999). Flexibility and consistency in adaptation of *Physarum* - chemo-mechanical coupling model of pattern formation in taxis. *IEEE SMC '99 Conference Proceedings*, pages 401–406.

Akita, D., Kunita, I., Fricker, M. D., Kuroda, S., Sato, K., and Nakagaki, T. (2017). Experimental models for Murray's law. *J. Phys. D: Appl. Phys.*, 50(2):024001.

Aldrich, H. C. and Daniel, J. W., editors (1982a). *Cell Biology of Physarum and Didymium (Organisms, Nucleus, and Cell Cycle)*, volume I. Academic Press.

Aldrich, H. C. and Daniel, J. W., editors (1982b). *Cell Biology of Physarum and Didymium (Differentiation, Metabolism, and Methodology)*, volume II. Academic Press.

Alim, K., Amselem, G., Peaudecerf, F., Brenner, M. P., and Pringle, A. (2013). Random network peristalsis in *Physarum polycephalum* organizes fluid flows across an individual. *Proc. Natl. Acad. Sci. U.S.A.*, 110(33):13306–13311.

Alim, K., Andrew, N., Pringle, A., and Brenner, M. P. (2017). Mechanism of signal propagation in *Physarum polycephalum*. *Proc. Natl. Acad. Sci. U.S.A.*, 114(20):5136–5141.

Allen, R. D. and Allen, N. S. (1978). Cytoplasmic streaming in amoeboid movement. *Annu. Rev. Biophys. Bioeng.*, 7:469–495.

Alonso, S., Radszuweit, M., Engel, H., and Bär, M. (2017). Mechanochemical pattern formation in simple models of active viscoelastic fluids and solids. *J. Phys. D: Appl. Phys.*, 50(43):434004.

Alonso, S., Strachauer, U., Radszuweit, M., Bär, M., and Hauser, M. J. (2016). Oscillations and uniaxial mechanochemical waves in a model of an active poroelastic medium: Application to deformation patterns in protoplasmic droplets of *Physarum polycephalum*. *Physica D*, 318-319:58–69.

Alpi, A., Amrhein, N., Bertl, A., Blatt, M. R., Blumwald, E., Cervone, F., Dainty, J., De Michelis, M. I., Epstein, E., Galston, A. W., Goldsmith, M. H. M., Hawes, C., Hell, R., Hetherington, A., Hofte, H., Juergens, G., Leaver, C. J., Moroni, A., Murphy, A., Oparka, K., Perata, P., Quader, H., Rausch, T., Ritzenthaler, C., Rivetta, A., Robinson, D. G., Sanders, D., Scheres, B., Schumacher, K., Sentenac, H., Slayman, C. L., Soave, C., Somerville, C., Taiz, L., Thiel, G., and Wagner, R. (2007). Plant neurobiology: no brain, no gain? *Trends Plant Sci.*, 12(4):135–136.

Álvarez-González, B., Meili, R., Bastounis, E., Firtel, R., Lasheras, J., and delÁlamo, J. (2015). Three-dimensional balance of cortical tension and axial contractility enables fast amoeboid migration. *Biophys. J.*, 108(4):821 – 832.

Anesti, V. and Scorrano, L. (2006). The relationship between mitochondrial shape and functionand the cytoskeleton. *Biochim. Biophys. Acta*, 1757:692–699.

Armus, H. L., Montgomery, A. R., and Jellison, J. L. (2006). Discrimination learning in paramecia (*P. caudatum*). *The Psychological Record*, 56(4):489–498.

Arnellos, A. and Moreno, A. (2015). Multicellular agency: an organizational view. *Biology & Philosophy*, 30(3):333–357.

Avsievich, T., Frolov, S., and Proskurin, S. (2017). Interrelation between respiratory and contractile activity of *Physarum polycephalum. J. Phys. D: Appl. Phys.*, 50(22):224003.

Badcock, P. B., Friston, K. J., Ramstead, M. J. D., Ploeger, A., and Hohwy, J. (2019). The hierarchically mechanistic mind: an evolutionary systems theory of the human brain, cognition, and behavior. *Cogn. Affect. Behav. Neurosci.*, pages 1–33.

Bailey, J. (1995). Plasmodium development in the myxomycete *Physarum polycephalum*: genetic control and cellular events. *Microbiology*, 141:2355–2365.

Bailey, J. (1997). Building a plasmodium: development in the acellular slime mould *Physarum polycephalum. BioEssays*, 19(11):985–992.

Bais, F. A. and Farmer, J. D. (2008). The physics of information. In Adriaans, P. and van Benthem, J., editors, *Philosophy of Information*, Handbook of the Philosophy of Science, pages 609 – 683. North-Holland, Amsterdam.

Baldauf, S. L. (1999). A search for the origins of animals and fungi: Comparing and combining molecular data. *Am. Nat.*, 154(S4):178–188.

Baldauf, S. L. and Doolittle, W. F. (1997). Origin and evolution of the slime molds (Mycetozoa). *Proc. Natl. Acad. Sci. U.S.A.*, 94:12007–12012.

Baluška, F. and Reber, A. (2019). Sentience and consciousness in single cells: How the first minds emerged in unicellular species. *BioEssays*, 41(3):1800229.

Barabási, A. and Oltvai, Z. N. (2004). Network biology: understanding the cell's functional organization. *Nat. Rev. Genet.*, 5(2):101–113.

Baranowski, Z. and Wohlfarth-Bottermann, K. (1982). Endoplasmic veins from plasmodia of *Physarum polycephalum*: a new strand model defined age, structure, and behavior. *Eur. J. Cell Biol.*, 27(1):1–9.

Barbey, A. K. (2018). Network neuroscience theory of human intelligence. *Trends Cogn. Sci.*, 22(1):8–20.

Barnett, H. (2015). Nodes and networks: the city as superorganism. `https://heatherbarnett.co.uk/work/nodes-and-networks/`.

Bartolomé, F. and Abramov, A. Y. (2015). Measurement of mitochondrial NADH and FAD autofluorescence in live cells. *Methods Mol. Biol.*, 1264:263–270.

Bartolák-Suki, E., Imsirovic, J., Nishibori, Y., Krishnan, R., and Suki, B. (2017). Regulation of mitochondrial structure and dynamics by the cytoskeleton and mechanical factors. *Int. J. Mol. Sci.*, 18(8):1812.

Bayne, C. J. (1990). Phygocytosis and non-self recognition in invertebrates. *BioScience*, 40(10):723–731.

Bayne, T., Brainard, D., Byrne, R. W., Chittka, L., Clayton, N., Heyes, C., Mather, J., Ölveczky, B., Shadlen, M., Suddendorf, T., and Webb, B. (2019). What is cognition? *Curr. Biol.*, 29(13):R608–R615.

Becker, J., Daniel, J., and Rusch, H. (1963). Growth inibition of *Physarum polycephalum* for the evaluation of chemotherapeutic agents. *Cancer Res.*, 23:1910–1929.

Beekman, M. and Latty, T. (2015). Brainless but multi-headed: decision-making by the acellular slime mould *Physarum polycephalum*. *J. Mol. Biol.*, 427(23):3734–3743.

Berger, D. S., Li, J. K., and Noordergraaf, A. (1995). Arterial wave propagation phenomena, ventricular work, and power dissipation. *Ann. Biomed. Eng.*, 23(6):804–11.

Berger, S. (1993). Flow in large blood vessels. In Cheer, A. and Van Dam, C. P., editors, *Fluid dynamics in biology*, volume 141 of *Contemporary Mathematics*. American Mathematical Soc.

Bernitt, E. (2015). *The dynamics of dorsal actin waves*. PhD thesis, University of Bremen.

Bernitt, E., Oettmeier, C., and Döbereiner, H.-G. (2010). Microplasmodia dynamics of *Physarum polycephalum*. *IFMBE Proceedings*, 31:1133–1136.

Beylina, S. I., Matveeva, N. B., Priezzhev, A. V., Romanenko, Y. M., Sukhorukov, A. P., and Teplov, V. A. (1984). Plasmodium of the myxomycete *Physarum polycephalum* as an autowave self-organizing system. In Krinsky, V. I., editor, *Self-Organization Autowaves and Structures Far from Equilibrium*, pages 218–221, Berlin, Heidelberg. Springer Berlin Heidelberg.

Blackstone, C. and Chang, C. (2011). Mitochondria unite to survive. *Nat. Cell Biol.*, 13(5):521–522.

Blackstone, N. W., Bivins, M. J., Cherry, K. S., Fletcher, R. E., and Geddes, G. C. (2005). Redox signaling in colonial hydroids: many pathways for peroxide. *J. Exp. Biol.*, 208(2):383–390.

Blätke, M. A., Heiner, M., and Marwan, W. (2012). Predicting phenotype from genotype through automatically composed petri nets. In Gilbert, D. and Heiner, M., editors, *Computational Methods in Systems Biology*, pages 87–106, Berlin, Heidelberg. Springer Berlin Heidelberg.

Block, I., Briegleb, W., Sobick, V., and Wohlfarth-Bottermann, K. (1986). Confirmation of gravisensitivity in the slime mold *Physarum polycephalum* under near weightlessness. *Adv. Space Res.*, 6(12):143–150.

Block, I., Wolke, A., and Briegleb, W. (1994). Gravitational response of the slime mold *Physarum*. *Adv. Space Res.*, 14(8):21–34.

Boisseau, R. P., Vogel, D., and Dussutour, A. (2016). Habituation in non-neural organisms: evidence from slime moulds. *Proc. R. Soc. London, Ser. B*, 283(1829):20160446.

Bokko, P. B., Francione, L., Bandala-Sanchez, E., Ahmed, A. U., Annesley, S. J., Huang, X., Khurana, T., Kimmel, A. R., and Fisher, P. R. (2007). Diverse cytopathologies in mitochondrial disease are caused by AMP-activated protein kinase signaling. *Mol. Biol. Cell*, 18(5):1874–1886.

Boussard, A., Delescluse, J., Pérez-Escudero, A., and Dussutour, A. (2019). Memory inception and preservation in slime moulds: the quest for a common mechanism. *Philos. Trans. R. Soc. London, Ser. B*, 374(1774):20180368.

Bray, D. (2001). *Cell Movements: From Molecules to Motility*. Garland Publishing, second edition.

Brewer, E., Kuraishi, S., Garver, J., and Strong, F. (1964). Mass culture of a slime mold, *Physarum polycephalum*. *Appl. Microbiol.*, 12(2):161–164.

Brix, K., Kukulies, J., and Stockem, W. (1987a). Studies on microplasmodia of *Physarum polycephalum*. V. Correlation of Cell Surface Morphology, Microfilament Organization and Motile Activity. *Protoplasma*, 137:156–167.

Brix, K. and Stockem, W. (1987). Studies on microplasmodia of *Physarum polycephalum*. VII. adhesion-dependent changes in the organization of the fibrillar actin system. *Cell Biol. Int. Rep.*, 11(7):529–536.

Brix, K. and Stockem, W. (1989). Functional analysis of actin fibrils in *Physarum polycephalum*. a morphological and quantitative study. *Cell Tissue Res.*, 257(1):115–122.

Brix, K., Stockem, W., and Kukulies, J. (1987b). Chemically induced changes in the morphology, dynamic activity and cytoskeletal organization of *Physarum* cell fragments. *Cell Biol. Int. Rep.*, 11(11):803–811.

Bronštejn, I. N. and Semendyayev, K. A. (2013). *Handbook of mathematics.* Springer Science & Business Media., 3 edition.

Brown, A. G. (2012). *Patient-specific local and systemic haemodynamics in the presence of a left ventricular assist device*. PhD thesis, University of Sheffield.

Bundschuh, R., Altmüller, J., Becker, C., Nürnberg, P., and Gott, J. M. (2011). Complete characterization of the edited transcriptome of the mitochondrion of *Physarum polycephalum* using deep sequencing of RNA. *Nucleic Acids Res.*, 39(14):6044–6055.

Burland, T., Solnica-Krezel, L., Bailey, J., Cunningham, D., and Dove, W. (1993a). Patterns of inheritance, development and the mitotic cycle in the protist *Physarum polycephalum*. *Adv. Microb. Physiol.*, 35:1–69.

Burland, T. G., Bailey, J., Pallotta, D., and Dove, W. F. (1993b). Stable, selectable, integrative DNA transformation in *Physarum*. *Gene*, 132(2):207–212.

Burnet, F. (1971). "Self-recognition" in colonial marine forms and flowering plants in relation to the evolution of immunity. *Nature*, 232(5308):230–235.

Büttner, S., Eisenberg, T., Herker, E., Carmona-Gutierrez, D., Kroemer, G., and Madeo, F. (2006). Why yeast cells can undergo apoptosis: death in times of peace, love, and war. *J. Cell Biol.*, 175(17101700):521–525.

Calvo, P. and Baluška, F. (2015). Conditions for minimal intelligence across eukaryota: a cognitive science perspective. *Front. Psychol.*, 6:1329.

Chandel, N. S. (2014). Mitochondria as signaling organelles. *BMC Biol.*, 12(1):34.

Chet, I. and Kislev, N. (1973). Scanning electron microscopy of spherules of *Physarum polycephalum*. *Tissue Cell*, 5(4):545–551.

Chong, K., Almsherqi, Z. A., Shen, H., and Deng, Y. (2018). Cubic membrane formation supports cell survival of amoeba *Chaos* under starvation-induced stress. *Protoplasma*, 255(2):517–525.

Cooke, D. and Dee, J. (1974). Methods for the isolation and analysis of plasmodial mutants in *Physarum polycephalum*. *Genet. Res.*, 24(2):175–187.

Craver, C. F. (2007). *Explaining the Brain: Mechanisms and the mosaic unity of neuroscience*. Oxford University Press.

Cruz-Orive, L. M. and Weibel, E. R. (1990). Recent stereological methods for cell biology: a brief survey. *Am. J. Physiol.*, 258((4 Pt 1)):L148–L156.

Daniel, J. W. and Järlfors, U. (1972). Plasmodial ultrastructure of the myxomycete *Physarum polycephalum*. *Tissue Cell*, 4(1):15–36.

Daniel, J. W., Kelley, J., and Rusch, H. P. (1962). Hematin-requiring plasmodial myxomycete. *J. Bacteriol.*, 84:1104–1110.

Daniel, J. W. and Rusch, H. P. (1961). The pure culture of *Physarum polycephalum* on a partially defined soluble medium. *J. Gen. Microbiol.*, 25:47–59.

De la Fuente, I. M. (2015). Elements of the cellular metabolic structure. *Front. Mol. Biosci.*, 2(16).

Dee, J. (1982). Genetics of *Physarum polycephalum*. In Aldrich, H. and Daniel, J., editors, *Cell Biology of Physarum and Didymium*, volume I, pages 211–251. Academic Press Inc.

Dehaene, S. (2014). *Consciousness and the brain: deciphering how the brain codes our thoughts*. Viking Press.

Diogo, C. V., Yambire, K. F., Mosquera, L. F., F., T. B., and Raimundo, N. (2018). Mitochondrial adventures at the organelle society. *Biochem. Biophys. Res. Commun.*, 500(1):87–93. Mitochondrial Dynamics.

Dirnberger, M. and Mehlhorn, K. (2017). Characterizing networks formed by *P. polycephalum*. *J. Phys. D: Appl. Phys.*, 50(22):224002.

Driscoll, M. K., Losert, W., Jacobson, K., and Kapustina, M. (2015). Spatiotemporal relationships between the cell shape and the actomyosin cortex of periodically protruding cells. *Cytoskeleton*, 72(6):268–281.

Durham, A. C. and Ridgway, E. B. (1976). Control of chemotaxis in *Physarum polycephalum*. *J. Cell Biol.*, 69(1):218–223.

Dussutour, A., Latty, T., Beekman, M., and Simpson, S. J. (2010). Amoeboid organism solves complex nutritional challenges. *Proc. Natl. Acad. Sci. U.S.A.*, 107(10):4607–4611.

Dykstra, M. J. (1977). The possible phylogenetic significance of mitochondrial configurations in the acrasid cellular slime molds with reference to members of the Eumycetozoa and fungi. *Mycologia*, 69(3):579–591.

Döbereiner, H.-G., Dubin-Thaler, B. J., Hofman, J. M., Xenias, H. S., Sims, T. N., Giannone, G., Dustin, M. L., Wiggins, C. H., and Sheetz, M. P. (2006). Lateral membrane waves constitute a universal dynamic pattern of motile cells. *Phys. Rev. Lett.*, 97:038102.

Eichinger, L., Pachebat, J. A., Glockner, G., Rajandream, M.-A., Sucgang, R., Berriman, M., Song, J., Olsen, R., Szafranski, K., Xu, Q., Tunggal, B., Kummerfeld, S., Madera, M., Konfortov, B. A., Rivero, F., Bankier, A. T., Lehmann, R., Hamlin, N., Davies, R., Gaudet, P., Fey, P., Pilcher, K., Chen, G., Saunders, D., Sodergren, E., Davis, P.,

Kerhornou, A., Nie, X., Hall, N., Anjard, C., Hemphill, L., Bason, N., Farbrother, P., Desany, B., Just, E., Morio, T., Rost, R., Churcher, C., Cooper, J., Haydock, S., van Driessche, N., Cronin, A., Goodhead, I., Muzny, D., Mourier, T., Pain, A., Lu, M., Harper, D., Lindsay, R., Hauser, H., James, K., Quiles, M., Madan Babu, M., Saito, T., Buchrieser, C., Wardroper, A., Felder, M., Thangavelu, M., Johnson, D., Knights, A., Loulseged, H., Mungall, K., Oliver, K., Price, C., Quail, M. A., Urushihara, H., Hernandez, J., Rabbinowitsch, E., Steffen, D., Sanders, M., Ma, J., Kohara, Y., Sharp, S., Simmonds, M., Spiegler, S., Tivey, A., Sugano, S., White, B., Walker, D., Woodward, J., Winckler, T., Tanaka, Y., Shaulsky, G., Schleicher, M., Weinstock, G., Rosenthal, A., Cox, E. C., Chisholm, R. L., Gibbs, R., Loomis, W. F., Platzer, M., Kay, R. R., Williams, J., Dear, P. H., Noegel, A. A., Barrell, B., and Kuspa, A. (2005). The genome of the social amoeba *Dictyostelium discoideum*. *Nature*, 435(7038):43–57.

Eisenbarth, S. and Steffan, B. (2000). Structure and Biosynthesis of Chrysophysarin A, a Plasmodial Pigment from the Slime Mould *Physarum polycephalum* (Myxomycetes). *Tetrahedron*, 56:363–365.

Ermakov, V. and Priezzhev, A. (1984). Wave regimes of the contractile activity of the strands of myxomycete plasmodium *Physarum* and their connection with the transport of the protoplasm. *Biophysics*, 29:106–112.

Evans, N., Gnudi, L., Rolinski, O., Birch, D., and Pickup, J. (2005). Glucose-dependent changes in NAD(P)H-related fluorescence lifetime of adipocytes and fibroblasts in vitro: Potential for non-invasive glucose sensing in diabetes mellitus. *J. Photochem. Photobiol., B*, 80:122–129.

Faix, J., Kreppel, L., Shaulsky, G., Schleicher, M., and Kimmel., A. (2004). A rapid and efficient method to generate multiple gene disruptions in *Dictyostelium discoideum* using a single selectable marker and the cre-*loxP* system. *Nucleic Acids Res.*, 32(19):e143.

Farkas, L., Málnási-Csizmadia, A., Nakamura, A., Kohama, K., and Nyitray, L. (2003). Localization and Characterization of the Inhibitory Ca^{2+}-binding Site of *Physarum polycephalum* Myosin II. *J. Biol. Chem.*, 278(30):27399–27405.

Farnsworth, P. A. and Loomis, W. F. (1974). A barrier to diffusion in pseudoplasmodia of *Dictyostelium discoideum*. *Dev. Biol.*, 41(1):77 – 83.

Feinberg, T. E. and Mallatt, J. (2016). The nature of primary consciousness. a new synthesis. *Conscious. Cogn.*, 43:113–127.

Feinberg, T. E. and Mallatt, J. M. (2018). *Consciousness Demystified*. The MIT Press.

Fessel, A., Oettmeier, C., Bernitt, E., Gauthier, N. C., and Döbereiner, H.-G. (2012). *Physarum polycephalum* percolation as a paradigm for topological phase transitions in transportation networks. *Phys. Rev. Lett.*, 109:078103.

Fessel, A., Oettmeier, C., and Döbereiner, H.-G. (2015). Structuring precedes extension in percolating *Physarum polycephalum* networks. *Nano Commun. Netw.*, 6(3):87–95. Special Issue on Biological Information and Communication Technology.

Fessel, A., Oettmeier, C., Wechsler, K., and Döbereiner, H.-G. (2017). Indentation analysis of active viscoelastic microplasmodia of *P. polycephalum*. *J. Phys. D: Appl. Phys.*, 51(2):024005.

Fibich, G., Lanir, Y., and Liron, N. (1993). Mathematical model of blood flow in a coronary capillary. *Am. J. Physiol.*, 265(5):H1829–H1840. PMID: 8238597.

Fiore-Donno, A., Meyer, M., Baldauf, S., and Pawlowski, J. (2008). Evolution of dark-spored myxomycetes (slime-molds): Molecules versus morphology. *Mol. Phylogenet. Evol.*, 46:878–889.

Fiore-Donno, A., Nikolaev, S., Nelson, M., Pawlowski, J., Cavalier-Smith, T., and Baldauf, S. (2010). Deep phylogeny and evolution of slime moulds (mycetozoa). *Protist*, 161:55–70.

Fletcher, D. A. and Mullins, R. D. (2010). Cell mechanics and the cytoskeleton. *Nature*, 463(7280):485–492.

Ford, B. J. (2017). Cellular intelligence: Microphenomenology and the realities of being. *Prog. Biophys. Mol. Biol.*, 131:273–287.

Foster, R., editor (2017). *Convergent minds: the evolution of cognitive complexity in nature*, volume 7(3) of *Interface Focus*. The Royal Society Publishing.

Fritzsche, M., Li, D., Colin-York, H., Chang, V. T., Moeendarbary, E., Felce, J. H., Sezgin, E., Charras, G., Betzig, E., and Eggeling, C. (2017). Self-organizing actin patterns shape membrane architecture but not cell mechanics. *Nat. Commun.*, 8:14347.

Fuerstman, M. J., Deschatelets, P., Kane, R., Schwartz, A., Kenis, P. J. A., Deutch, J. M., and Whitesides, G. M. (2003). Solving mazes using microfluidic networks. *Langmuir*, 19(11):4714–4722.

Fukui, Y. (2002). Mechanistics of amoeboid locomotion: signal to forces. *Cell Biol. Int.*, 26(11):933–944.

Gao, C., Liu, C., Schenz, D., Li, X., Zhang, Z., Jusup, M., Wang, Z., Beekman, M., and Nakagaki, T. (2018). Does being multi-headed make you better at solving problems? a survey of physarum-based models and computations. *Phys. Life Rev.*

Gao, C., Liu, C., Schenz, D., Li, X., Zhang, Z., Jusup, M., Wang, Z., Beekman, M., and Nakagaki, T. (2019). Physarum inspires research beyond biomimetic algorithms: Reply to comments on "does being multi-headed make you better at solving problems?". *Phys. Life Rev.*

Gaudet, P., Pilcher, K., Fey, P., and Chisholm, R. (2007). Transformation of *Dictyostelium discoideum* with plasmid DNA. *Nat. Protoc.*, 2(6):1317–1324.

Gawlitta, W., Wolf, K. V., Hoffmann, H.-U., and Stockem, W. (1980). Studies on microplasmodia of *Physarum polycephalum*. I. Classification and Locomotion Behavior. *Cell Tissue Res.*, 209:71–86.

Gessert, G. (2012). *Green Light: Toward an art of evolution*. MIT Press.

Gibbs, K. A., Urbanowski, M. L., and Greenberg, E. P. (2008). Genetic determinants of self identity and social recognition in bacteria. *Science*, 321(5886):256–259.

Ginsburg, S. and Jablonka, E. (2008). Epigenetic learning in non-neural organisms. *J. Biosci.*, 34(4):633–646.

Glöckner, G., Golderer, G., Werner-Felmayer, G., Meyer, S., and Marwan, W. (2008). A first glimpse at the transcriptome of *Physarum polycephalum*. *BMC Genomics*, 9:6.

Glöckner, G. and Marwan, W. (2017). Transcriptome reprogramming during developmental switching in *Physarum polycephalum* involves extensive remodeling of intracellular signaling networks. *Sci. Rep.*, 7(1):12304.

Godfrey-Smith, P. (2001). Environmental complexity and the evolution of cognition. In Sternberg, R. J. and Kaufman, J. C., editors, *The Evolution of Intelligence*, pages 223–251. Psychology Press.

Godfrey-Smith, P. (2016). Individuality, subjectivity, and minimal cognition. *Biology & Philosophy*, 31(6):775–796.

Goodman, E. and Rusch, H. (1969). Glycogen in *Physarum polycephalum*. *Experientia*, 25(6):580.

Goodman, E. M. (1980). *Physarum polycephalum*: A review of a model system using a structure-function approach. *Int. Rev. Cytol.*, 63:1–58.

Goodman, E. M. and Beck, T. (1974). Metabolism during differentiation in the slime mold *Physarum polycephalum*. *Can. J. Microbiol.*, 20:107–11.

Gorman, J., Dove, W., and Shaibe, E. (1979). Mutations affecting the initiation of plasmodial development in *Physarum polycephalum*. *Dev. Genet.*, 1:47–60.

Gowrishankar, K. and Rao, M. (2016). Nonequilibrium phase transitions, fluctuations and correlations in an active contractile polar fluid. *Soft Matter*, 12:2040–2046.

Gray, W. D. (1955). Riboflavin synthesis in cultures of *Physarum polycephalum*. *Ohio J. Sci.*, 55(4):212–214.

Grebecki, A. (1994). Membrane and cytoskeleton flow in motile cells with emphasis on the contribution of free-living amoebae. *Int. Rev. Cytol.*, 148:37–80.

Grebecki, A. and Cieslawska, M. (1978). Plasmodium of *Physarum polycephalum* as a synchronous contractile system. *Cytobiologie*, 17(2):335–342.

Grice, L. F. and Degnan, B. M. (2017). Transcriptomic profiling of the allorecognition response to grafting in the demosponge *Amphimedon queenslandica*. *Mar. Drugs*, 15(5):136.

Grosberg, R. and Plachetzki, D. (2010). Marine invertebrates: Genetics of colony recognition. In Breed, M. D. and Moore, J., editors, *Encyclopedia of Animal Behavior*, pages 381–388. Academic Press, Oxford.

Gu, Z., David, L., Petrov, D., Jones, T., Davis, R., and Steinmetz, L. (2005). Elevated evolutionary rates in the laboratory strain of *Saccharomyces cerevisiae*. *Proc. Natl. Acad. Sci. U.S.A.*, 102(4):1092–1097.

Guo, P. and Fu, B. M. (2012). Effect of wall compliance and permeability on blood-flow rate in counter-current microvessels formed from anastomosis during tumor-induced angiogenesis. *J. Biomech. Eng.*, 134(4):041003.

Guy, R. D., Nakagaki, T., and Wright, G. B. (2011). Flow-induced channel formation in the cytoplasm of motile cells. *Phys. Rev. E: Stat., Nonlinear, Soft Matter Phys.*, 84:016310.

Haeri, M. and Haeri, M. (2015). Imagej plugin for analysis of porous scaffolds used in tissue engineering. *J. Open Res. Softw.*, 3(1):e1.

Haindl, M. and Holler, E. (2005). Use of the giant multinucleate plasmodium of *Physarum polycephalum* to study RNA interference in the myxomycete. *Anal. Biochem.*, 342(2):194 – 199.

Hall, A. L., Warren, V., and Condeelis, J. (1989). Transduction of the chemotactic signal to the actin cytoskeleton of *Dictyostelium discoideum*. *Dev. Biol.*, 136:517–25.

Hanahan, D. and Weinberg, R. A. (2011). Hallmarks of cancer: the next generation. *Cell*, 144(5):646–674.

Hasegawa, T., Takahashi, S., Hayashi, H., and Hatano, S. (1980). Fragmin: a calcium ion sensitive regulatory factor on the formation of actin filaments. *Biochemistry*, 19:2677–83.

Hato, M., Ueda, T., Kurihara, K., and Kobatake, Y. (1976). Phototaxis in true slime mold *Physarum polycephalum*. *Cell Struct. Funct.*, 1:269–278.

Hattori, H. (1935). *Myxomycetes of the Nasu District*. Tokyo, 1st and 2nd edition, 1935, 1964 edition.

Hauser, J., Parák, J., Ložek, M., and Havlík, J. (2012). System analyze of the Windkessel models. In *BioDat Conference on Advanced Methods of Biological Data and Signal Processing*.

Hausmann, K. and Stiemerling, R. (1997). In Memoriam: Karl-Ernst Wohlfarth-Bottermann (1923-1997). *Eur. J. Protistol.*, 33:452–459.

He, L., Zhou, X., Huang, N., Li, H., Tian, J., Li, T., Yao, K., Nyachoti, C. M., Kim, S. W., and Yin, Y. (2017). AMPK regulation of glucose, lipid and protein metabolism: mechanisms and nutritional significance. *Curr. Protein Pept. Sci.*, 18(6):562–570.

Hedbacker, K. and Carlson, M. (2008). SNF1/AMPK pathways in yeast. *Front. Biosci.*, 13:2408–20.

Henderson, I. R., Shindo, C., and Dean, C. (2003). The need for winter in the switch to flowering. *Annu. Rev. Genet.*, 37(1):371–392. PMID: 14616066.

Hickey, D. and Noriega, L. (2008). Relationship between structure and information processing in *Physarum polycephalum*. *Int. J. Model. Ident. Control*, 4(4):348–356.

Hirth, F. and Reichert, H. (2007). Basic nervous system types: One or many? In Kaas, J. H., editor, *Evolution of Nervous Systems*, pages 55 – 72. Academic Press, Oxford.

Horn, B. K. and Schunck, B. G. (1981). Determining optical flow. *Artif. Intell.*, 17:185–203.

Houbraken, M., Demeyer, S., Staessens, D., Audenaert, P., Colle, D., and Pickavet, M. (2012). Fault tolerant network design inspired by *Physarum polycephalum*. *Nat. Comput.*, 12(2):277–289.

Häder, D.-P. and Schreckenbach, T. (1984). Phototactic orientation in plasmodia of the acellular slime mold, *Physarum polycephalum*. *Plant Cell Physiol.*, 25(1):55–61.

Hütt, M., Kaiser, M., and Hilgetag, C. C. (2014). Perspective: network-guided pattern formation of neural dynamics. *Philos. Trans. R. Soc. London, Ser. B*, 369(1653):20130522.

Hüttermann, A. (1973). Biochemical events during spherule formation of *Physarum polycephalum*. *Ber. Dtsch. Bot. Ges.*, 86(1–4):55–76.

Iima, M., Kori, H., and Nakagaki, T. (2017). Studies of the phase gradient at the boundary of the phase diffusion equation, motivated by peculiar wave patterns of rhythmic contraction in the amoeboid movement of *Physarum polycephalum*. *J. Phys. D: Appl. Phys.*, 50(15):154004.

Ince, C., Coremans, J. M. C. C., and Bruining, H. A. (1992). In vivo NADH fluorescence. In Erdmann, W. and Bruley, D. F., editors, *Oxygen Transport to Tissue XIV*, volume 317 of *Advances in Experimental Medicine and Biology*, pages 277–296. Springer US, Boston, MA.

Isenberg, G. and Wohlfarth-Bottermann, K. E. (1976). Transformation of cytoplasmic actin importance for the organization of the contractile gel reticulnm and the contraction — relaxation cycle of cytoplasmic actomyosin. *Cell Tissue Res.*, 173(4):495–528.

Itano, N. and Hatano, S. (1991). F-actin bundling protein from *Physarum polycephalum*: Purification and its capacity for co-bundling of actin filaments and microtubules. *Cell Motil.*, 19(4):244–254.

Itoh, K., Izumi, A., Mori, T., Dohmae, N., Yui, R., Maeda-Sano, K., Shirai, Y., Kanaoka, M. M., Kuroiwa, T., Higashiyama, T., Sugita, M., Murakami-Murofushi, K., Kawano, S., and Sasaki, N. (2011). DNA packaging proteins Glom and Glom2 coordinately organize the mitochondrial nucleoid of *Physarum polycephalum*. *Mitochondrion*, 11:575–86.

Iurlaro, R., Püschel, F., Léon-Annicchiarico, C. L., O'Connor, H., Martin, S. J., Palou-Gramón, D., Lucendo, E., and Muñoz-Pinedo, C. (2017). Glucose deprivation induces ATF4-mediated apoptosis through TRAIL death receptors. *Mol. Cell. Biol.*, 37(10):e00479–16.

Jayasree, P. R., Kumar, P. R. M., and Nair, R. V. (2000). The plasmodia of *Physarum polycephalum*, an elegant system to demonstrate the importance of genome integrity in traversing the g2/m checkpoint of the cell cycle. *Curr. Sci.*, 78(9):1127–1130.

Jelluma, N., Yang, X., Stokoe, D., Evan, G. I., Dansen, T. B., and Haas-Kogan, D. A. (2006). Glucose withdrawal induces oxidative stress followed by apoptosis in glioblastoma cells but not in normal human astrocytes. *Mol. Cancer Res.*, 4(5):319–330.

Jones, J. (2010). Characteristics of pattern formation and evolution in approximations of *Physarum* transport networks. *Artif. Life*, 16(2):127–153.

Jones, J., Tsuda, S., and Adamatzky, A. (2011). *Towards Physarum Robots*, pages 215–251. Springer Berlin Heidelberg, Berlin, Heidelberg.

Kac, E., editor (2007). *Signs of Life: Bio Art and Beyond*. MIT Press.

Kalyanasundaram, I. (2004). Morphological Diversity in the Myxomycetes. *Syst. Geogr. Pl.*, 74(2):231–237.

Kamiya, N. (1950). The rate of protoplasmic flow in the myxomycete plasmodium i. *Cytologia*, 15:183–193.

Kamiya, N. (1960). Physics and chemistry of protoplasmic streaming. *Annu. Rev. Plant Physiol.*, 11:323–340.

Kamiya, N. (1981). Physical and chemical basis of cytoplasmic streaming. *Annu. Rev. Plant Phys.*, 32:205–236.

Kao, A. B. and Couzin, I. D. (2019). Modular structure within groups causes information loss but can improve decision accuracy. *Philos. Trans. R. Soc. London, Ser. B*, 374:20180378.

Kauffman, S. and Wille, J. J. (1975). The mitotic oscillator in *Physarum polycephalum*. *J. Theor. Biol.*, 55:47–93.

Kawamichi, H., Zhang, Y., Hino, M., Nakamura, A., Tanaka, H., Farkas, L., Nyitray, L., and Kohama, K. (2007). Calcium inhibition of *Physarum* myosin as examined by the recombinant heavy mero-myosin. *Adv. Exp. Med. Biol.*, 592:265–272.

Kawano, S. (1991). The life cycle of mitochondria in the true slime mould, *Physarum polycephalum*. *Bot. Mag. Tokyo*, 104:97–113.

Kawano, S., Anderson, R., Nanba, T., and Kuroiwa, T. (1987). Polymorphism and Uniparental Inheritance of Mitochondrial DNA in *Physarum polycephalum*. *J. Gen. Microbiol.*, 133:3175–3182.

Keijzer, F. A. (2017). Evolutionary convergence and biologically embodied cognition. *J. R. Soc. Interface Focus*, 7(3):20160123.

Kellhammer, O. (2016). Nodes and networks. What slime mold can show us about collective behavior and city living. *SciArt in America*.

Kenett, D. Y., Perc, M., and Boccaletti, S., editors (2015a). *Networks of Networks*, volume 80 of *Chaos, Solitons & Fractals*.

Kenett, D. Y., Perc, M., and Boccaletti, S. (2015b). Networks of networks – an introduction. *Chaos, Solitons & Fractals*, 80:1–6.

Kessler, D., Eisenlohr, L., Lathwell, M., Huang, J., Taylor, H., Godfrey, S., and Spady, M. (1980). Physarum Myosin Light Chain Binds Calcium. *Cell Motil.*, 1:63–71.

Kincaid, R. L. and Mansour, T. E. (1978). Measurement of Chemotaxis in the Slime Mold *Physarum polycephalum*. *Exp. Cell Res.*, 116:365–375.

Kobayashi, R., Tero, A., and Nakagaki, T. (2006). Mathematical model for rhythmic protoplasmic movement in the true slime mold. *J. Math. Biol.*, 53(2):273–286.

Kohama, K., Li-Hong, Y., and Nakamura, A. (1993). Calcium-binding proteins that are involved in the calcium inhibition of the actomyosin system of a lower eukaryote, *Physarum polycephalum*. *Biomed. Res.*, 14:57–62.

Korohoda, W., Shraideh, Z., Baranowski, Z., and Wohlfarth-Bottermann, K. (1983). Energy metabolic regulation of oscillatory contraction activity in *Physarum polycephalum*. *Cell Tissue Res.*, 231:675–691.

Kruse, K., Joanny, J. F., Jülicher, F., Prost, J., and Sekimoto, K. (2004). Asters, vortices, and rotating spirals in active gels of polar filaments. *Phys. Rev. Lett.*, 92:078101.

Kukulies, J., Brix, K., and Stockem, W. (1987). Studies on microplasmodia of *Physarum polycephalum*. VI. Functional analysis of a cortical and fibrillar actin system by use of fluorescent-analog cytochemistry. *Cell Tissue Res.*, 250:125–134.

Kukulies, J. and Stockem, W. (1985). Function of the microfilament system in living cell fragments of *Physarum polycephalum* as revealed by microinjection of fluorescent analogs. *Cell Tissue Res.*, 242(2):323–332.

Kulawiak, D. A., Löber, J., Bär, M., and Engel, H. (2018). Oscillatory motion of a droplet in an active poroelastic two-phase model. *J. Phys. D: Appl. Phys.*, 52(1):014004.

Kulawiak, D. A., Löber, J., Bär, M., and Engel, H. (2019). Active poroelastic two-phase model for the motion of *Physarum* microplasmodia. *PLoS One*, 14(8):e0217447.

Kuroda, R. and Kuroda, H. (1982). Relation of cytoplasmic calcium to contractility in *Physarum polycephalum*. *J. Cell Sci.*, 53:37–48.

Kuroda, S., Takagi, S., Nakagaki, T., and Ueda, T. (2015). Allometry in *Physarum* plasmodium during free locomotion: size versus shape, speed and rhythm. *J. Exp. Biol.*, 218(23):3729–3738.

Kuroiwa, T. and Takahashi, K. (1978). Induction of mitochondrial migration in the slime mold *Physarum polycephalum*. *Plant Cell Physiol.*, 19(8):1561–1564.

Laffler, T. G. and Tyson, J. J. (1986). *The Physarum Cell Cycle*, pages 79–109. Springer New York, Boston, MA.

Latty, T. and Beekman, M. (2009). Food quality affects search strategy in the acellular slime mould, *Physarum polycephalum*. *Behav. Ecol.*, 20:1160–1167.

Latty, T. and Beekman, M. (2010). Food quality and the risk of light exposure affect patch-choice decisions in the slime mold *Physarum polycephalum*. *Ecology*, 91(1):22–27.

Latty, T. and Beekman, M. (2011a). Irrational decision-making in an amoeboid organism: transitivity and context-dependent preferences. *Proc. R. Soc. London, Ser. B*, 278:307–312.

Latty, T. and Beekman, M. (2011b). Speed-accuracy trade-offs during foraging decisions in the acellular slime mold *Physarum polycephalum*. *Proc. R. Soc. B*, 278:539–545.

Lee, J., Oettmeier, C., and Döbereiner, H.-G. (2018). A novel growth mode of *Physarum polycephalum* during starvation. *J. Phys. D: Appl. Phys.*, 51(24):244002.

Leontyev, D. V. and Schnittler, M. (2017). Chapter 3 - the phylogeny of myxomycetes. In Stephenson, S. L. and Rojas, C., editors, *Myxomycetes*, pages 83–106. Academic Press.

Leontyev, D. V., Schnittler, M., Stephenson, S. L., Novozhilov, Y. K., and Shchepin, O. N. (2019). Towards a phylogenetic classification of the myxomycetes. *Phytotaxa*, 399(3):209–238.

Levenson, J. M. and Sweatt, J. D. (2005). Epigenetic mechanisms in memory formation. *Nat. Rev. Neurosci.*, 6(2):108–118.

Lewis, O. L. and Guy, R. D. (2017). Analysis of peristaltic waves and their role in migrating *Physarum* plasmodia. *J. Phys. D: Appl. Phys.*, 50(28):284001.

Lewis, O. L., Zhang, S., Guy, R. D., and del Álamo, J. C. (2015). Coordination of contractility, adhesion and flow in migrating *Physarum* amoebae. *J. R. Soc. Interface*, 12(106):20141359.

Li, L., Nørrelykke, S., and Cox, E. (2008). Persistent cell motion in the absence of external signals: a search strategy for eukaryotic cells. *PLoS One*, 3(5):e2093.

Li, S. and Purugganan, M. (2011). The cooperative amoeba: *Dictyostelium* as a model for social evolution. *Trends Genet.*, 27(2):48–54.

Liu, S. and Wong-Riley, M. (1995). Disproportionate regulation of nuclear- and mitochondrial-encoded cytochrome oxidase subunit proteins by functional activity in neurons. *Neuroscience*, 67(1):197 – 210.

Liu, Y., Gao, C., and Zhang, Z. (2019). Simulating transport networks with a *Physarum* foraging model. *IEEE Access*, 7:23725–23739.

Loidl, P. and Eberharter, A. (1995). Nuclear matrix and the cell cycle. *Int. Rev. Cytol.*, 162B:377–403.

Loidl, P. and Sachsenmaier, W. (1982). Control of mitotic synchrony in *Physarum polycephalum*. phase shifting by fusion of heterophasic plasmodia contradicts a limit cycle oscillator model. *Eur. J. Cell Biol.*, 28:175–179.

Luft, J. H. (1961). Improvements in epoxy resin embedding methods. *J. Biophys. Biochem. Cytol.*, 9(2):409–414.

Lundby, C. and Jacobs, R. A. (2016). Adaptations of skeletal muscle mitochondria to exercise training. *Exp. Physiol.*, 101:17–22.

Lundqvist, M., Herman, P., Warden, M. R., Brincat, S. L., and Miller, E. K. (2018). Gamma and beta bursts during working memory readout suggest roles in its volitional control. *Nat. Commun.*, 9(1):394.

Lyon, P. (2006). The biogenic approach to cognition. *Cogn. Process.*, 7:11–29.

Lyon, P. (2015). The cognitive cell: bacterial behavior reconsidered. *Front. Microbiol.*, 6:264.

Lämmermann, T. and Sixt, M. (2009). Mechanical modes of 'amoeboid' cell migration. *Curr. Opin. Cell Biol.*, 21:636–644.

Marbach, S., Alim, K., Andrew, N., Pringle, A., and Brenner, M. P. (2016). Pruning to increase taylor dispersion in *Physarum polycephalum* networks. *Phys. Rev. Lett.*, 117:178103.

Margalha, L., Valerio, C., and Baena-González, E. (2016). Plant SnRK1 kinases: structure, regulation, and function. *Exp. Suppl.*, 107:403–438.

Margaris, K. N. and Black, R. A. (2012). Modelling the lymphatic system: challenges and opportunities. *J. R. Soc. Interface*, 9(69):601–612.

Marwan, W. (2001). Chapter 20: Photomovement and photomorphogenesis in *Physarum polycephalum*: targeting of cytoskeleton and gene expression by light. In Häder, D.-P. and Breure, A., editors, *Photomovement*, volume 1 of *Comprehensive Series in Photosciences*, pages 561–587. Elsevier.

Marwan, W. (2010). Amoeba-Inspired Network Design. *Science*, 327:419–420.

Marwan, W. and Starostzik, C. (2002). The Sequence of Regulatory Events in the Sporulation Control Network of *Physarum polycephalum* Analysed by Time-resolved Somatic Complementation of Mutants. *Protist*, 153(4):391–400.

Marwan, W., Wagler, A., and Weismantel, R. (2011). Petri nets as a framework for the reconstruction and analysis of signal transduction pathways and regulatory networks. *Nat. Comput.*, 10(2):639–654.

Masui, M., Satoh, S., and Seto, K. (2018). Allorecognition behavior of slime mold plasmodium—*Physarum rigidum* slime sheath-mediated self-extension model. *J. Phys. D: Appl. Phys.*, 51(28):284001.

Materna, S. C. and Marwan, W. (2005). Estimating the number of plasmids taken up by a eukaryotic cell during transfection and evidence that antisense RNA abolishes gene expression in *Physarum polycephalum*. *FEMS Microbiology Letters*, 243(1):29–35.

Matsumoto, K., Takagi, S., and Nakagaki, T. (2008). Locomotive mechanism of *Physarum* plasmodia based on spatiotemporal analysis of protoplasmic streaming. *Biophys. J.*, 94(7):2492–2504.

Matsumura, F., Yoshimoto, Y., and Kamiya, N. (1980). Tension generation by actomyosin thread from a non-muscle system. *Nature*, 285(5761):169–171.

Matveeva, N., Beylina, S., Klyueva, A., and Teplov, V. (2014). Involvement of phosphatidylinositol 4,5-bisphosphate binding proteins in the generation of contractile oscillations in the *Physarum polycephalum* plasmodium. *Biophysics*, 59(5):758–763.

Matveeva, N., Beylina, S., and Teplov, V. (2008). The role of phosphoinositide-3-kinase in the control of shape and directional movement of the *Physarum polycephalum* plasmodium. *Biophysics*, 53(6):533–538.

Matveeva, N., Morozov, M., Nezvetsky, A., Orlova, T., Teplov, V., and Beylina, S. (2010a). Involvement of extracellular cAMP-specific phosphodiesterase in the control of motile activity of *Physarum polycephalum* plasmodium. *Biophysics*, 55(6):982.

Matveeva, N., Teplov, V., and Beylina, S. (2010b). Suppression of the autooscillatory contractile activity of *Physarum polycephalum* plasmodium by the inhibitor of the IP_3-induced Ca^{2+} release, 2-aminoethoxydiphenyl borate. *Biochemistry (Moscow) Supplement Series A: Membrane and Cell Biology*, 4(1):70–76.

Matveeva, N., Teplov, V., and Beylina, S. (2012a). Coupling of phospholipase C and PI3K/PTEN signaling pathways in *Physarum polycephalum*: The action of U73122 on motile and autooscillatory activity of plasmodium. *Biochemistry (Moscow) Supplement Series A: Membrane and Cell Biology*, 6(3):255–264.

Matveeva, N., Teplov, V., Nezvetsky, A., Orlova, T., and Beylina, S. (2012b). Involvement of cyclic adenosine monophosphate in the control of motile behavior of *Physarum polycephalum* plasmodium. *Biophysics*, 57(5):832–839.

Mayevsky, A. and Rogatsky, G. G. (2007). Mitochondrial function in vivo evaluated by NADH fluorescence: from animal models to human studies. *Am. J. Physiol., Cell Physiol.*, 292:C615–C640.

Mayne, R., Adamatzky, A., and Jones, J. (2015). On the role of the plasmodial cytoskeleton in facilitating intelligent behavior in slime mold *Physarum polycephalum*. *Commun. Integr. Biol.*, 8(4):e1059007.

Mazzolai, B. and Mattoli, V. (2016). Robotics: Generation soft. *Nature*, 536(7617):400–401.

McCormick, J. J., Blomquist, J. C., and Rusch, H. P. (1970). Isolation and Characterization of an Extracellular Polysaccharide from *Physarum polycephalum*. *J. Bacteriol.*, 104(3):1110–1118.

McCullough, C. H. and Dee, J. (1976). Defined and semi-defined media for the growth of amoebae of *Physarum polycephalum*. *J. Gen. Microbiol.*, 95(1):151–158.

McKitrick, T. R. and Tomaso, A. W. D. (2010). Molecular mechanisms of allorecognition in a basal chordate. *Semin. Immunol.*, 22(1):34 – 38. Evolution of innate and adaptive immune recognition structures.

Mejia, E. M. and Hatch, G. M. (2016). Mitochondrial phospholipids: role in mitochondrial function. *J. Bioenerg. Biomembr.*, 48(2):99–112.

Michel, R. P. and Cruz-Orive, L. M. (1988). Application of the Cavalieri principle and vertical sections method to lung: estimation of volume and pleural surface area. *J. Microsc.*, 150:117–36.

Mihaylova, M. M. and Shaw, R. J. (2011). The AMPK signalling pathway coordinates cell growth, autophagy and metabolism. *Nat. Cell Biol.*, 13(9):1016–1023.

Miller, D., Padmanabhan, R., and Sarcar, S. N. (2017). Chapter 4 - genomics and gene expression in myxomycetes. In Stephenson, S. L. and Rojas, C., editors, *Myxomycetes*, pages 107–143. Academic Press.

Mironov, A. (2014). Unbiased frames. Version 1.0. `https://imagej.nih.gov/ij/macros/Unbiased_Frames.txt`.

Mitchison, T. J. and Cramer, L. P. (1996). Actin-based cell motility and cell locomotion. *Cell*, 84(3):371–379.

Mittler, R., Vanderauwera, S., Suzuki, N., Miller, G., Tognetti, V. B., Vandepoele, K., Gollery, M., Shulaev, V., and Van Breusegem, F. (2011). ROS signaling: the new wave? *Trends Plant Sci.*, 16(6):300–309.

Miyake, Y., Yamaguchi, Y., Masafumi, Y., and Shimizu, H. (1993). Environment-dependent self-organization of positional information in coupled nonlinear oscillator system–a new principle of real-time coordinative control in biological distributed system. *IEICE Trans. Fundam. Electron. Commun. Comput. Sci.*, 76(5):780–785.

Mogilner, A. and Manhart, A. (2018). Intracellular fluid mechanics: coupling cytoplasmic flow with active cytoskeletal gel. *Annu. Rev. Fluid Mech.*, 50:347–370.

Morita, M. and Nishi, A. (1991). Glycoproteins and enzymes associated with the plasmodial membrane and slime layer of *Physarum polycephalum*. *J. Gen. Appl. Microbiol.*, 37(1):93–109.

Nachmias, V., Huxley, H., and Kessler, D. (1970). Electron microscope observations on actomyosin and actin preparations from *Physarum polycephalum*, and on their interaction with heavy meromyosin subfragment i from muscle myosin. *J. Mol. Biol.*, 50(1):83–90.

Nachmias, V. T. and Ingram, W. C. (1970). Actomyosin from Physarum polycephalum: electron microscopy of myosin-enriched preparations. *Science*, 170(959):743–745.

Nader, W. F. and Becker, J.-U. (1983). Regulation of Glycogen Metabolism and Glycogen Phosphorylase in *Physarum polycephalum*. *J. Gen. Microbiol.*, 129:2481–2487.

Nagai, R. and Kamiya, N. (1966). Movement of the myxomycete plasmodium. ii. electron microscopic studies on fibrillar structures in the plasmodium. *Proc. Jpn. Acad.*, 42(8):934–939.

Nagai, R. and Kato, T. (1975). Cytoplasmic filaments and their assembly into bundles in *Physarum plasmodium*. *Protoplasma*, 86(1):141–158.

Nakagaki, T., Kobayashi, R., Nishiura, Y., and Ueda, T. (2004a). Obtaining multiple separate food sources: behavioural intelligence in the *Physarum* plasmodium. *Proc. R. Soc. Lond. B Biol. Sci.*, 271(1554):2305–2310.

Nakagaki, T., Yamada, H., and Hara, M. (2004b). Smart network solutions in an amoeboid organism. *Biophys. Chem.*, 107(1):1–5.

Nakagaki, T., Yamada, H., and Ito, M. (1999). Reaction–diffusion–advection model for pattern formation of rhythmic contraction in a giant amoeboid cell of the *Physarum* plasmodium. *J. Theor. Biol.*, 197(4):497 – 506.

Nakagaki, T., Yamada, H., and Ágota Tóth (2000). Intelligence: Maze-solving by an amoeboid organism. *Nature*, 407:470.

Nakagawa, C. C., Jones, E. P., and Miller, D. L. (1998). Mitochondrial DNA rearrangements associated with mF plasmid integration and plasmodial longevity in *Physarum polycephalum*. *Curr. Genet.*, 33(3):178–187.

Nakamura, A. and Kohama, K. (1999). Calcium regulation of the actin-myosin interaction of *Physarum polycephalum*. *Int. Rev. Cytol.*, 191:53–98.

Nandipati, S., Haugli, K., Coucheron, D., Haskins, E., and Johansen, S. (2012). Polyphyletic origin of the genus *Physarum* (Physarales, Myxomycetes) revealed by nuclear rDNA mini-chromosome analysis and group I intron synapomorphy. *BMC Evol. Biol.*, 12:166.

Naoz, M., Manor, U., Sakaguchi, H., Kachar, B., and Gov, N. S. (2008). Protein localization by actin treadmilling and molecular motors regulates stereocilia shape and treadmilling rate. *Biophys. J.*, 95(12):5706–5718.

Nations, C., Allison, V. F., Aldrich, H. C., and Allen, R. G. (1989). Biological oxidation and the mobilization of mitochondrial calcium during the differentiation of *Physarum polycephalum*. *J. Cell. Physiol.*, 140(2):311–316.

Natsume, K., Miyake, Y., Yano, M., and Shimizu, H. (1992). Development of spatiotemporal pattern of Ca^{2+} on the chemotactic behaviour of *Physarum* plasmodium. *Protoplasma*, 166:55–60.

Ng, L. and Solo, V. (1997). A data-driven method for choosing smoothing parameters in optical flow problems. In *Proceedings 1997 International Conference on Image Processing, ICIP'97, Santa Barbara, California, USA, October 26-29, 1997*, pages 360–363.

Ntinas, V., Vourkas, I., Sirakoulis, G., and Adamatzky, A. (2017). Modeling *Physarum* space exploration using memristors. *J. Phys. D: Appl. Phys.*, 50(17):174004.

Oettmeier, C., Brix, K., and Döbereiner, H.-G. (2017). *Physarum polycephalum* - a new take on a classic model system. *J. Phys. D: Appl. Phys.*, 50(41):413001.

Oettmeier, C. and Döbereiner, H.-G. (2019a). A lumped parameter model of endoplasm flow in *Physarum polycephalum* explains migration and polarization-induced asymmetry during the onset of locomotion. *PLoS One*, 14(4):e0215622.

Oettmeier, C. and Döbereiner, H.-G. (2019b). Mitochondrial numbers increase during glucose deprivationin the slime mold *Physarum polycephalum*. *Protoplasma*, pages 1–9.

Oettmeier, C., Lee, J., and Döbereiner, H.-G. (2018). Form follows function: Ultrastructure of different morphotypes of *Physarum polycephalum*. *J. Phys. D: Appl. Phys.*, 51(13):134006.

Ogawa, K., Sato, M., Ashihara, H., and Kaneko., T. (2010). Evidence for deposition of cellulose prior to dark-starvation treatment during spherulation in *Physarum* microplasmodia. *Cytologia*, 75(4):397–407.

Ogikubo, S., Nakabayashi, T., Adachi, T., Islam, M. S., Yoshizawa, T., Kinjo, M., and Ohta, N. (2011). Intracellular pH sensing using autofluorescence lifetime microscopy. *J. Phys. Chem. B*, 115(34):10385–10390.

Oh, K. W., Lee, K., Ahn, B., and Furlani, E. P. (2012). Design of pressure-driven microfluidic networks using electric circuit analogy. *Lab Chip*, 12:515–45.

Ohl, C., Brix, K., and Stockem, W. (1991). Studies on microplasmodia of *Physarum polycephalum*. Quantitative analysis of contractile activities and microfilament organization. *Cell Tissue Res.*, 264:283–291.

Olufsen, M. S. and Nadim, A. (2004). On deriving lumped models for blood flow and pressure in the systemic arteries. *Math. Biosci. Eng.*, 1(1):61–80.

Onoda, M., Ueki, T., Tamate, R., Shibayama, M., and Yoshida, R. (2017). Amoeba-like self-oscillating polymeric fluids with autonomous sol-gel transition. *Nat. Commun.*, 8:15862.

Ornes, S. (2017). Core concept: How nonequilibrium thermodynamics speaks to the mystery of life. *Proc. Natl. Acad. Sci. U.S.A.*, 114(3):423–424.

Oyen, M. L., Shean, T. A., Strange, D. G., and Galli, M. (2012). Size effects in indentation of hydrated biological tissues. *J. Mater. Res.*, 27(1):245–255.

Ozaki, K. and Hatano, S. (1984). Mechanism of regulation of actin polymerization by *Physarum* profilin. *J. Cell Biol.*, 98:1919–1925.

Paluch, E. K. and Raz, E. (2013). The role and regulation of blebs in cell migration. *Curr. Opin. Cell Biol.*, 25:582–90.

Perkins, T. J. and Swain, P. S. (2009). Strategies for cellular decision-making. *Mol. Syst. Biol.*, 5(1):326.

Pershin, Y. V., Fontaine, S. L., and Ventra, M. D. (2009). Memristive model of amoeba learning. *Phys. Rev. E: Stat., Nonlinear, Soft Matter Phys.*, 80(2 Pt 1):021926.

Piñero, J. and Solé, R. (2019). Statistical physics of liquid brains. *Philos. Trans. R. Soc. Lond., B, Biol. Sci.*, 374:20180376.

Pollard, T. D. and Cooper, J. A. (2009). Actin, a central player in cell shape and movement. *Science*, 326(5957):1208–1212.

Porter, K., Kawakami, N., and Ledbetter, M. (1965). Structural basis of streaming in *Physarum polycephalum*. *J. Cell Biol.*, 27(2):A78.

Poulos, A. and Thompson, G. A. (1971). Ether-containing lipids of the slime mold, *Physarum polycephalum*: II. Rates of biosynthesis. *Lipids*, 6(7):470–474.

Powell, R., Mikhalevich, I., Logan, C., and Clayton, N. S. (2017). Convergent minds: the evolution of cognitive complexity in nature. *Interface Focus*, 7(3):20170029.

Pujol, T., du Roure, O., Fermigier, M., and Heuvingh, J. (2012). Impact of branching on the elasticity of actin networks. *Proc. Natl. Acad. Sci. U.S.A.*, 109(26):10364–10369.

Radszuweit, M., Engel, H., and Bär, M. (2010). A model for oscillations and pattern formation in protoplasmic droplets of Physarum polycephalum. *Eur. Phys. J. Special Topics*, 191:159–172.

Radszuweit, M., Engel, H., and Bär, M. (2014). An active poroelastic model for mechanochemical patterns in protoplasmic droplets of *Physarum polycephalum*. *PLoS One*, 9(6):e99220.

Ramalingam, N., Franke, C., Jaschinski, E., Winterhoff, M., Lu, Y., Brühmann, S., Junemann, A., Meier, H., Noegel, A. A., Weber, I., Zhao, H., Merkel, R., Schleicher, M., and Faix, J. (2015). A resilient formin-derived cortical actin meshwork in the rear drives actomyosin-based motility in 2d confinement. *Nat. Commun.*, 6:8496.

Rambold, A. S., Kostelecky, B., Elia, N., and Lippincott-Schwartz, J. (2011). Tubular network formation protects mitochondria from autophagosomal degradation during nutrient starvation. *Proc. Natl. Acad. Sci. U.S.A.*, 108(25):10190–10195.

Rehm, H. and Gradmann, D. (2010). Intelligent plants or stupid studies. *Lab Times*, 3:30–32.

Reid, C. R., Beekman, M., Latty, T., and Dussutour, A. (2013). Amoeboid organism uses extracellular secretions to make smart foraging decisions. *Behav. Ecol.*, 24(4):812–818.

Reid, C. R., Latty, T., Dussutour, A., and Beekman, M. (2012). Slime mold uses an externalized spatial "memory" to navigate in complex environments. *Proc. Natl. Acad. Sci. U.S.A.*

Rhea, R. (1966). Electron microscopic observations on the slime mold *Physarum polycephalum* with specific reference to fibrillar structures. *J. Ultrastruct. Res.*, 15(3):349–379.

Ridgway, E. B. and Durham, A. C. (1976). Oscillations of calcium ion concentrations in physarum polycephalum. *J. Cell Biol.*, 69:223–226.

Rieu, J.-P., Delanoe-Ayari, H., Takagi, S., Tanaka, Y., and Nakagaki, T. (2015). Periodic traction in migrating large amoeba of *Physarum polycephalum*. *J. R. Soc. Interface*, 12:20150099.

Rieu, J.-P., Saito, T., Delanoe-Ayari, H., Sawada, Y., and Kay, R. R. (2009). Migration of *Dictyostelium* Slugs: Anterior-like Cells May Provide the Motive Force for the Prespore Zone. *Cell Motil. Cytoskel.*, 66:1073–1086.

Rinkevich, B. (2004). Allorecognition and xenorecognition in reef corals: a decade of interactions. *Hydrobiologia*, 530(1–3):443–450.

Rodrigues, R. M., Macko, P., Palosaari, T., and Whelan, M. P. (2011). Autofluorescence microscopy: a non-destructive tool to monitor mitochondrial toxicity. *Toxicol. Lett.*, 206(3):281–288.

Romeralo, M., Escalante, R., and Baldauf., S. (2012). Evolution and diversity of dictyostelid social amoebae. *Protist*, 163(3):27–343.

Roth, G. (2015). Convergent evolution of complex brains and high intelligence. *Philos. Trans. R. Soc. Lond. B. Biol. Sci.*, 370(26554042):20150049.

Rätzel, V. and Marwan, W. (2015). Gene expression kinetics in individual plasmodial cells reveal alternative programs of differential regulation during commitment and differentiation. *Dev. Growth Differ.*, 57:408–420.

Sachsenmaier, W., Remy, U., and Plattner-Schobel, R. (1972). Initiation of synchronous mitosis in *Physarum polycephalum*. *Exp. Cell Res.*, 73:41–48.

Saigusa, T., Tero, A., Nakagaki, T., and Kuramoto, Y. (2008). Amoebae anticipate periodic events. *Phys. Rev. Lett.*, 100(1):018101–1–4.

San, O. and Staples, A. E. (2012). Dynamics of pulsatile flows through elastic microtubes. *Int. J. Appl. Mech.*, 4(1):1250006.

Santarnecchi, E. and Rossi, S. (2016). Advances in the neuroscience of intelligence: from brain connectivity to brain perturbation. *Span. J. Psychol.*, 19(e94):1–7.

Sanz, C., Rodríguez-Romero, J., Idnurm, A., Christie, J. M., Heitman, J., Corrochano, L. M., and Eslava, A. P. (2009). Phycomyces madb interacts with mada to form the primary photoreceptor complex for fungal phototropism. *Proc. Natl. Acad. Sci. U.S.A.*, 106(17):7095–7100.

Sato, H., Hatano, S., and Sato, Y. (1981). Contractility and protoplasmic streaming preserved in artificially induced plasmodial fragments, the 'caffeine drops'. *Protoplasma*, 109(1):187–208.

Sato, M., Wong, T. Z., and Allen, R. D. (1983a). Rheological properties of living cytoplasm: endoplasm of *Physarum* plasmodium. *J. Cell Biol.*, 97(4):1089–1097.

Sato, M., Wong, T. Z., and Allen, R. D. (1983b). Preliminary rheological investigation of living *Physarum* endoplasm. In Earnshaw, J. C. and Steer, M. W., editors, *The Application of Laser Light Scattering to the Study of Biological Motion. NATO Advanced Science Institutes Series A*, volume 59, pages 389–402. Springer US, Boston, MA.

Satoh, H., Ueda, T., and Kobatake, Y. (1982). Primary oscillator of contractional rhythm in the plasmodium of *Physarum polycephalum*: Role of mitochondria. *Cell Struct. Funct.*, 7:275–283.

Satoh, H., Ueda, T., and Kobatake, Y. (1984). Rhythmic contraction in the plasmodium of the myxomycete *Physarum polycephalum* in relation to the mitochondrial function. *Cell Struct. Funct.*, 9:37–44.

Sauer, H. W. (1982). *Developmental Biology of Physarum*. Cambridge University Press.

Schaap, P., Barrantes, I., Minx, P., Sasaki, N., Anderson, R. W., Benard, M., Biggar, K. K., Buchler, N. E., Bundschuh, R., Chen, X., Fronick, C., Fulton, L., Golderer, G., Jahn, N., Knoop, V., Landweber, L. F., Maric, C., Miller, D., Noegel, A. A., Peace, R., Pierron, G., Sasaki, T., Schallenberg-Rudinger, M., Schleicher, M., Singh, R., Spaller, T., Storey, K. B., Suzuki, T., Tomlinson, C., Tyson, J. J., Warren, W. C., Werner, E. R., Werner-Felmayer, G., Wilson, R. K., Winckler, T., Gott, J. M., Glockner, G., and Marwan, W. (2015). The *Physarum polycephalum* genome reveals extensive use of prokaryotic two-component and metazoan-type tyrosine kinase signaling. *Genome Biol. Evol.*, 8(1):109–125.

Schenz, D., Shima, Y., Kuroda, S., Nakagaki, T., and Ueda, K.-I. (2017). A mathematical model for adaptive vein formation during exploratory migration of *Physarum polycephalum*: routing while scouting. *J. Phys. D: Appl. Phys.*, 50(43):434001.

Schindelin, J., Arganda-Carreras, I., Frise, E., Kaynig, V., Longair, M., Pietzsch, T., Preibisch, S., Rueden, C., Saalfeld, S., Schmid, B., Tinevez, J.-Y., White, D. J., Hartenstein, V., Eliceiri, K., Tomancak, P., and Cardona, A. (2012). Fiji: an open-source platform for biological-image analysis. *Nat. Methods*, 9(7):676–682.

Schnittler, M., Dagamac, N. H. A., and Novozhilov, Y. K. (2017). Chapter 9 - biogeographical patterns in myxomycetes. In Stephenson, S. L. and Rojas, C., editors, *Myxomycetes*, pages 299 – 331. Academic Press.

Schubert, T. (2014). Bodymetries. `http://theresaschubert.com/arts-experiments/art/bodymetries-mapping-the-human-body-through-amorphous-intelligence/#images-videos`.

Schubert, T. and Adamatzky, A. (2015). *Experiencing the Unconventional: Science in Art*. World Scientific.

Sesaki, H. and Ogihara, S. (1997). Secretion of slime, the extracellular matrix of the plasmodium, as visualized with a fluorescent probe and its correlation with locomotion on the substratum. *Cell Struct. Funct.*, 22(2):279–289.

Shadel, G. S. and Horvath, T. L. (2015). Mitochondrial ROS signaling in organismal homeostasis. *Cell*, 163(3):560–569.

Shirakawa, T. and Gunji, Y. (2010). Computation of voronoi diagram and collision-free path using the plasmodium of *Physarum polycephalum*. *Int. J. Unconv. Comput.*, 6(2):79–88.

Shirakawa, T., Niizato, T., Sato, H., and Ohno, R. (2019). Biased Lévy-walk pattern in the exploratory behavior of the *Physarum* plasmodium. *Biosystems*, page 103985.

Silva, A. J. (2007). The science of research: The principles underlying the discovery of cognitive and other biological mechanisms. *J. Physiol. Paris*, 101(4-6):203–213.

Silva, A. J. and Müller, K.-R. (2015). The need for novel informatics tools for integrating and planning research in molecular and cellular cognition. *Learn. Mem.*, 22(9):494–498.

Skalak, T. C. and Schmid-Schönbein, G. W. (1986). Viscoelastic properties of microvessels in rat spinotrapezius muscle. *J. Biomech. Eng.*, 108(3):193–200.

Smith, D. A. and Saldana, R. (1992). Model of the Ca^{2+} oscillator for shuttle streaming in *Physarum polycephalum*. *Biophys. J.*, 61(2):368–380.

Smith-Ferguson, J. and Beekman, M. (2019). Who needs a brain? Slime moulds, behavioural ecology and minimal cognition. *Adaptive Behavior*, page 1059712319826537.

Smith-Ferguson, J., Reid, C. R., Latty, T., and Beekman, M. (2017). Hänsel, Gretel and the slime mould—how an external spatial memory aids navigation in complex environments. *J. Phys. D: Appl. Phys.*, 50(41):414003.

Solé, R., Moses, M., and Forrest, S. (2019). Liquid brains, solid brains. *Philos. Trans. R. Soc. Lond., B, Biol. Sci.*, 374:20190040.

Song, S. B. and Hwang, E. S. (2019). A rise in ATP, ROS, and mitochondrial content upon glucose withdrawal correlates with a dysregulated mitochondria turnover mediated by the activation of the protein deacetylase SIRT1. *Cells*, 8(1):11.

Stephenson, S. L. and Rojas, C., editors (2017). *Myxomycetes: Biology, Systematics, Biogeography and Ecology*. Academic Press.

Stockem, W. and Brix, K. (1994). Analysis of Microfilament Organization and Contractile Activities in *Physarum*. *Int. Rev. Cytol.*, 149:145–215.

Strychalski, W., Copos, C. A., Lewis, O. L., and D.Guy, R. (2015). A poroelastic immersed boundary method with applications to cell biology. *J. Comput. Phys.*, 282:77–97.

Stuart, L. and Ezekowitz, R. (2008). Phagocytosis and comparative innate immunity: learning on the fly. *Nat. Rev. Immunol.*, 8(2):131.

Sudbery, P. E. and Grant, W. D. (1976). The control of mitosis in *Physarum polycephalum*: the effect of delaying mitosis and evidence for the operation of the control mechanism in the absence of growth. *J. Cell Sci.*, 22:59–65.

Sujatha, A., Balaji, S., Devi, R., and Marwan, W. (2005). Isolation of *Physarum polycephalum* plasmodial mutants altered in sporulation by chemical mutagenesis of flagellates. *Eur. J. Protistol.*, 41:19–27.

Tachikawa, M. (2010). A mathematical model for period-memorizing behavior in *Physarum* plasmodium. *J. Theor. Biol.*, 263(4):449–454.

Taiz, L., Alkon, D., Draguhn, A., Murphy, A., Blatt, M., Hawes, C., Thiel, G., and Robinson, D. G. (2019). Plants neither possess nor require consciousness. *Trends Plant Sci.*

Takagi, S. and Ueda, T. (2010). Annihilation and creation of rotating waves by a local light pulse in a protoplasmic droplet of the *Physarum* plasmodium. *Physica D: Nonlinear Phenomena*, 239(11):873 – 878. Emergent Phenomena in Spatially Distributed Systems.

Takahashi, K., Takamatsu, A., Hu, Z. S., and Tsuchiya, Y. (1997). Asymmetry in the self-sustained oscillation of *Physarum* plasmodial strands. *Protoplasma*, 197(1):132–135.

Takamatsu, A., Gomi, T., Endo, T., Hirai, T., and Sasaki, T. (2017). Energy-saving with low dimensional network in *Physarum* plasmodium. *J. Phys. D: Appl. Phys.*, 50(15):154003.

Takamatsu, A., Takaba, E., and Takizawa, G. (2009). Environment-dependent morphology in plasmodium of true slime mold *Physarum polycephalum* and a network growth model. *J. Theor. Biol.*, 256(1):29–44.

Takamatsu, A., Takahashi, K., Nagao, M., and Tsuchiya, Y. (1997). Frequency coupling model for dynamics of responses to stimuli in plasmodium of *Physarum polycephalum*. *J. Phys. Soc. Jpn.*, 66(6):1638–1646.

Takano, H., T.Abe, Sakurai, R., Moriyama, Y., Miyazawa, Y., Nozaki, H., Kawano, S., Sasaki, N., and Kuroiwa, T. (2001). The complete DNA sequence of the mitochondrial genome of *Physarum polycephalum*. *Mol. Gen. Genet.*, 264:539–545.

Teplov, V., Romanovsky, Y., and Latushkin, O. (1991). A continuum model of contraction waves and protoplasm streaming in strands of *Physarum* plasmodium. *Biosystems*, 24:269–289.

Teplov, V. A. (2010). Cytomechanics of oscillatory contractions. modeling the longitudinal dynamics of *Physarum polycephalum* protoplasmic strands. *Biophysics*, 55(6):987–995.

Teplov, V. A. (2017). Role of mechanics in the appearance of oscillatory instability and standing waves of the mechanochemical activity in the *Physarum polycephalum* plasmodium. *J. Phys. D: Appl. Phys.*, 50(21):213002.

Tero, A., Takagi, S., Saigusa, T., Ito, K., Bebber, D. P., Fricker, M. D., Yumiki, K., Kobayashi, R., and Nakagaki, T. (2010). Rules for Biologically Inspired Adaptive Network Design. *Science*, 327:439.

Thiriet, C. (2018). Nuclear dynamics at specific cell cycle stages in the slime mold *Physarum polycephalum*. In Lavelle, C. and Victor, J.-M., editors, *Nuclear Architecture and Dynamics*, volume 2 of *Translational Epigenetics*, pages 557 – 567. Academic Press, Boston.

Tononi, G., Boly, M., Massimi, M., and Koch, C. (2016). Integrated information theory: from consciousness to its physical substrate. *Nat. Rev. Neurosci.*, 17:450–461.

Tsompanas, M.-A. I., Mayne, R., Sirakoulis, G. C., and Adamatzky, A. I. (2015). A cellular automata bioinspired algorithm designing data trees in wireless sensor networks. *Int. J. Distrib. Sens. Netw.*, 11(6).

Turnbull, L., Hütt, M., Ioannides, A. A., Kininmonth, S., Poeppl, R., Tockner, K., Bracken, L. J., Keesstra, S., Liu, L., Masselink, R., and Parsons, A. J. (2018).

Connectivity and complex systems: learning from a multi-disciplinary perspective. *Appl. Netw. Sci.*, 3(1):11.

Tyson, J. and Kauffman, S. (1975). Control of mitosis by a continuous biochemical oscillation: Synchronization; spatially inhomogeneous oscillations. *J. Math. Biol.*, 1(4):289–310.

Ueda, T., Matsumoto, K., Akitaya, T., and Kobatake, Y. (1986). Spatial and Temporal Organization of Intracellular Adenine Nucleotides and Cyclic Nucleotides in Relation to Rhythmic Motility in *Physarum* Plasmodium. *Exp. Cell Res.*, 162:486–494.

Ueda, T., Terayama, K., Kurihara, K., and Kobatake, Y. (1975). Threshold phenomena in chemoreception and taxis in slime mold *Physarum polycephalum*. *J. Gen. Physiol.*, 65(2):223–234.

Umedachi, T., Idei, R., Ito, K., and Ishiguro, A. (2013). True-slime-mould-inspired hydrostatically coupled oscillator system exhibiting versatile behaviours. *Bioinspiration & Biomimetics*, 8(3):035001.

Usui, N. (1971). Fibrillar differentiation in a microplasmodium of the slime mold *Physarum polycephalum*. *Dev. Growth Differ.*, 13(4):241–255.

Vallverdú, J., Castro, O., Mayne, R., Talanov, M., Levin, M., Baluška, F., Gunji, Y., Dussutour, A., Zenil, H., and Adamatzky, A. (2018). Slime mould: The fundamental mechanisms of biological cognition. *Biosystems*, 165:57–70.

van Duijn, M. (2017). Phylogenetic origins of biological cognition: convergent patterns in the early evolution of learning. *J. R. Soc. Interface*, 7(3):20160158.

van Duijn, M., Keijzer, F., and Franken, D. (2006). Principles of minimal cognition: Casting cognition as sensorimotor coordination. *Adaptive Behavior*, 14(2):157–170.

Visser, W., van Spronsen, E. A., Nanninga, N., Pronk, J. T., Gijs Kuenen, J., and van Dijken, J. P. (1995). Effects of growth conditions on mitochondrial morphology in *Saccharomyces cerevisiae*. *Antonie van Leeuwenhoek*, 67(3):243–253.

Vogel, D. and Dussutour, A. (2016). Direct transfer of learned behaviour via cell fusion in non-neural organisms. *Proc. R. Soc. London, Ser. B*, 283(1845):20162382.

Vogel, D., Gautrais, J., Perna, A., Deneubourg, D. J. S. J., and Dussutour, A. (2016). Transition from isotropic to digitated growthmodulates network formation in *Physarum polycephalum*. *J. Phys. D: Appl. Phys.*, 50(1):014002.

von Schweinitz, L. D. (1822). Synopsis Fungorum. Supplement No. 382. *Naturforschende Gesellschaft in Leipzig*, page 63.

Walker, L. M., Hoppe, T., and Silliker, M. E. (2017). Chapter 5 - molecular techniques and current research approaches. In Stephenson, S. L. and Rojas, C., editors, *Myxomycetes*, pages 145–173. Academic Press.

Wappler, E. A., Institoris, A., Dutta, S., Katakam, P. V. G., and Busija, D. W. (2013). Mitochondrial dynamics associated with oxygen-glucose deprivation in rat primary neuronal cultures. *PLoS One*, 8(5):e63206.

Weibel, E. and Gomez, D. (1962). A principle for counting tissue structures on random sections. *J. Appl. Physiol.*, 17:343–348.

Werthmann, B. and Marwan, W. (2017). Developmental switching in *Physarum polycephalum*: Petri net analysis of single celltrajectories of gene expression indicates responsiveness and genetic plasticity of the waddington quasipotential landscape. *J. Phys. D: Appl. Phys.*, 50(46):464003.

Westendorf, C., Gruber, C., Schnitzer, K., Kraker, S., and Grube, M. (2018). Quantitative comparison of plasmodial migration and oscillatory properties across different slime molds. *J. Phys. D: Appl. Phys.*, 51(34):344001.

Whiting, J. G., Jones, J., Bull, L., Levin, M., and Adamatzky, A. (2016). Towards a *Physarum* learning chip. *Sci. Rep.*, 6:19948.

Wiesner, R., Aschenbrenner, V., Ruegg, J., and Zak, R. (1994). Coordination of nuclear and mitochondrial gene expression during the development of cardiac hypertrophy in rats. *Am. J. Physiol.*, 267:C229–C235.

Wilk, E. and Sutela, J. (2016). Slime intelligence. Rhizome Blog.

Wilson, C., Terman, J. R., González-Billault, C., and Ahmed, G. (2016). Actin filaments - a target for redox regulation. *Cytoskeleton*, 73:577–595.

Wissman, J., Dickey, M. D., and Majidi, C. (2017). Fieldcontrolled electrical switch with liquid metal. *Adv. Sci.*, 4(12).

Wohlfarth-Bottermann, K. (1962). Weitreichende, fibrilläre Protoplasmadifferenzierungen und ihre Bedeutung für die Protoplasmaströmung. I. Elektronenmikroskopischer Nachweis und Feinstruktur. *Protoplasma*, 54(4):514–539.

Wohlfarth-Bottermann, K. (1963). Weitreichende, fibrilläre Protoplasmadifferenzierungen und ihre Bedeutung für die Protoplasmaströmung. II. Lichtmikroskopische Darstellung. *Protoplasma*, 57(1):747–761.

Wohlfarth-Bottermann, K. (1964). Cell structures and their significance for ameboid movement. *Int. Rev. Cytol.*, 16:61–131.

Wohlfarth-Bottermann, K. (1977). Oscillating Contractions in Protoplasmic Strands of *Physarum*: Simultaneous Tensiometry of Longitudinal and Radial Rhythms, Periodicity Analysis and Temperature Dependence. *J. Exp. Biol.*, 67:49–59.

Wohlfarth-Bottermann, K. (1979). Oscillatory Contraction Activity in *Physarum*. *J. Exp. Biol.*, 81:15–32.

Wohlfarth-Bottermann, K. and Fleischer, M. (1976). Cycling aggregation patterns of cytoplasmic f-actin coordinated with oscillating tension force generation. *Cell Tissue Res.*, 165(3):327–344.

Wohlfarth-Bottermann, K. E. (1965). Weitreichende, fibrilläre Protoplasmadifferenzierungen und ihre Bedeutung für die Protoplasmaströmung. III. Entstehung und experimentell induzierbare Musterbildungen. *Wilhelm Roux Arch. Entwickl. Mech. Org.*, 156(4):371–403.

Wolf, K., Hoffmann, H.-U., and Stockem, W. (1981). Studies on microplasmodia of *Physarum polycephalum*: II. Fine Structure and Function of the Mucous Layer. *Protoplasma*, 107:345–359.

Wormington, W. M. and Weaver, R. F. (1976). Photoreceptor pigment that induces differentiation in the slime mold *Physarum polycephalum*. *Proc. Natl. Acad. Sci. U.S.A.*, 73(11):3896–3899.

Wright, M., Lacorre-Arescaldino, I., Macquet, J., and Daffé, M. (1984). Induction of polyploid nuclei in the plasmodium of *Physarum polycephalum* by platinum antitumor compounds. *Cancer Res.*, 2(44):777–783.

Xu, C. and Prince, J. (1998). Snakes, shapes, and gradient vector flow. *IEEE Trans. Image Processing*, 7(3):359–369.

Xu, Q., Huff, L. P., Fujii, M., and Griendling, K. K. (2017). Redox regulation of the actin cytoskeleton and its role in the vascular system. *Free Radical Biol. Med.*, 109:84–107.

Yamada, H., Nakagaki, T., Baker, R., and Maini, P. (2007). Dispersion relation in oscillatory reaction-diffusion systems with self-consistent flow in true slime mold. *J. Math. Biol.*, 54:745–760.

York, R. A. and Fernald, R. D. (2017). The repeated evolution of behavior. *Front. Ecol. Evol.*, 4:143.

Yoshimoto, Y. and Kamiya, N. (1982). Ca^{2+} oscillation in the homogenate of *Physarum* plasmodium. *Protoplasma*, 110(1):63–65.

Yoshimoto, Y., Matsumura, F., and Kamiya, N. (1981). Simultaneous Oscillations of Ca^{2+} Efflux and Tension Generation in the Permealized Plasmodial Strand of Physarum. *Cell Motil. Cytoskel.*, 1:433–443.

Zacharioudakis, I., Gligoris, T., and Tzamarias, D. (2007). A yeast catabolic enzyme controls transcriptional memory. *Curr. Biol.*, 17(23):2041–2046.

Zamir, M. (2000). *The physics of pulsatile flow*. Springer International Publishing.

Zamir, M. (2016). *Hemo-Dynamics*. Springer International Publishing.

Zhang, S., Guy, R. D., Lasheras, J. C., and del Álamo, J. C. (2017). Self-organized mechano-chemical dynamics in amoeboid locomotion of *Physarum* fragments. *J. Phys. D: Appl. Phys.*, 50(20):204004.

Zhang, S., Lasheras, J. C., and del Álamo, J. C. (2019). Symmetry breaking transition towards directional locomotion in *Physarum* microplasmodia. *bioRxiv*.

Zhou, D. W., Mowrey, D. D., Tang, P., and Xu, Y. (2015). Percolation model of sensory transmission and loss of consciousness under general anesthesia. *Phys. Rev. Lett.*, 115(10):108103.

Zhu, L., Aono, M., Kim, S.-J., and Hara, M. (2013). Amoeba-based computing for traveling salesman problem: long-term correlations between spatially separated individual cells of *Physarum polycephalum*. *Bio Systems*, 112:1–10.